

# Metabolic interactions between axons and Schwann cells of the mouse sciatic nerve

**Laura Rose Rich BSc (Hons), MRes, AFHEA**

Thesis submitted to the University of Nottingham  
for the degree of Doctor of Philosophy

September 2021

# Declaration

---

I declare that this thesis has been composed solely by myself and that it has not been submitted, in whole or in part, in any previous application for a degree under the supervision of Dr Angus Brown at the University of Nottingham with the following exceptions:

- Western blots in chapter 6 were performed with substantial help from Dr Maxine Fowler (University of Nottingham)
- Western blot for fructokinase in chapter 6 was previously published in my MRes thesis
- Immunohistochemistry confocal images in chapter 6 were acquired by Ian Ward (SLIM, University of Nottingham)

# Acknowledgments

---

First and foremost I would like to thank my supervisor Dr Angus Brown, I am extremely grateful for the opportunities he has provided me. Angus' extensive knowledge, guidance and belief in me has enabled me to develop into an independent and confident scientist. I now feel ready to take on my next challenge. I also wish to thank Dr Maxine Fowler, her knowledge and continuous support has allowed me gain excellent problem solving skills when it comes to immunohistochemistry! My thanks is also extended to Ian Ward for all his help with the confocal microscopy and the weekly trips down to stores with gas cylinders! I would also like to thank various academics in the Neuroscience department that have allowed me to be involved in teaching of undergraduate practical classes, these opportunities have been invaluable and enhanced my PhD experience.

Special thanks to my partner, Helena, for her unwavering support. I don't know what I would have done without your logical nature and emotional support. Finally, I would like to express my gratitude to my parents, without their encouragement and support I would never have got this far.

# Abbreviations

---

$\mu$	Population mean
1- $\alpha$	Confidence level
1- $\beta$	Power
2DG	2deoxyglucose
aCSF	Artificial cerebral spinal fluid
ALAT	Alanine aminotransferase
ALS	Amyotrophic lateral sclerosis
Ammonium	$\text{NH}_4^+$
AMPA	$\alpha$ -Amino-3-hydroxy-5-methyl-4-isoxazolepropionic acid
ANLSH	Astrocyte-neurone lactate shuttle hypothesis
APES	3-aminopropyltriethoxysilane
ATP	Adenosine triphosphate
AUC	Area under the curve
$\text{BaCl}_2$	Barium chloride
BDNF	Brain derived neurotrophic factor
Bicarbonate	$\text{HCO}_3^-$
BSA	Bovine serum albumin
cAMP	Cyclic adenosine monophosphate
CAP	Compound action potential
CCB	Cytochalasin B
CIN	Cinnamate
CNS	Central nervous system
CPP	Conditioned placed preference
DAB	1,4-dideoxy-1,4-imino-D-arabinitol
DAPI	4',6-diamidino-2-phenylindole

DIDs	4,4'-Diisothiocyano-2,2'-stilbenedisulfonic acid
EAAT	Excitatory amino acid transporter
Erk	Extracellular signal-regulated kinase
EU	Experimental unit
$E_x$	Reversal potential
F	Faraday constant
FAD	Flavin adenine dinucleotide
$FADH_2$	Dihydroflavine-adenine dinucleotide
FK	Fructokinase
FRET	Forster Resonance Energy Transfer
GLUT	Glucose transporter
$H_0$	Null hypothesis
$H_1$	Alternative hypothesis
$H^+$	Proton
HCAR1	Hydroxycarboxylic acid receptor
HFCS	High fructose corn syrup
HFS	High frequency stimulation
HK	Hexokinase
IHC	Immunohistochemistry
$K^+$	Potassium
LDH	Lactate dehydrogenase
LTP	Long term potentiation
MCT	Monocarboxylate transporter
n	Sample number
$Na^+$	Sodium
NAD	Nicotinamide adenine dinucleotide
NADH	1,4-Dihydronicotinamide adenine dinucleotide
NBC	Sodium bicarbonate cotransporter

NC3R	National Centre for the Replacement, Refinement & Reduction of Animals in Research
NF 200	Neurofilament 200
NGS	Normal goat serum
NHS	National Health Service
NMDA	N-methyl-D-aspartate
NRS	Normal rabbit serum
OCT	Optimal cutting temperature compound
PAS	Periodic Acid-Schiff
PBS	Phosphate Buffered Saline
PDC	Pyruvate dehydrogenase complex
PFA	Paraformaldehyde
PFK	Phosphofructokinase
PGE <sub>2</sub>	Prostaglandin E <sub>2</sub>
PGT	Prostaglandin transporter
PKA	Protein kinase A
PNS	Peripheral nervous system
R	Gas constant
RCF	Relative centrifugal force
RIPA	Radioimmunoprecipitation assay
S <sup>2</sup> p	Pooled sample variance
sAC	Soluble adenylyl cyclase
SD	Standard deviation
SDS	Sodium dodecyl sulfate
SEM	Standard error of the mean
SF	Substrate free
SLIs	Schmidt-Lanterman Incisures
SN	Sciatic nerve
STZ	Streptozotocin
T	Temperature

TBS	Tris-buffered saline
TBST	Tris-buffered saline with Tween 20
TCA cycle	Tricarboxylic acid cycle
THA	DL-threo-P-hydroxyaspartate
TTX	Tetrodotoxin
VGCC	Voltage gated Ca <sup>2+</sup> channels
WB	Western Blot
X	Sample mean
Z	Valence
$\alpha$	Type 1 error, significance level
$\beta$	Type 2 error
$\sigma$	Standard deviation

# Table of Contents

---

Declaration .....	1
Acknowledgments .....	2
Abbreviations.....	3
Abstract .....	11
Chapter 1: Introduction .....	13 - 75
1.1 Cells of the nervous system .....	14
1.2 Energy metabolism.....	16
1.2.1 Glycolysis.....	18
1.2.2 The TCA cycle and electron transport chain .....	20
1.3 Nervous system energy metabolism .....	25
1.3.1 Glucose.....	29
1.3.2 Glycogen.....	33
1.3.3 Lactate .....	36
1.3.4 Physiological and pathophysiological importance .....	43
1.4 Axon-glia metabolic signalling .....	56
1.4.1 Glutamate .....	56
1.4.2 Ammonium.....	61
1.4.3 Potassium .....	63
1.5 Aim .....	74
Chapter 2: Methodology .....	76 - 93
2.1 Mice.....	77
2.1.1 Optic nerve dissection.....	77
2.1.2 Sciatic nerve dissection.....	78
2.2 Stimulus evoked CAP electrophysiology .....	80
2.2.1 Data analysis .....	81
2.3 Lactate biosensors .....	85
2.3.1 Data analysis .....	86
2.4 Western blot.....	88
2.5 Fluorescence immunohistochemistry .....	91
Chapter 3: A statistically validated method for recording the stimulus evoked CAP the reduces animal use.....	94 - 119

3.1 Introduction .....	95
3.1.1 Statistics theory .....	97
3.2 Methodology.....	105
3.2.1 Mice and tissue dissection .....	105
3.2.2 Stimulus evoked CAP electrophysiology.....	105
3.3 Results .....	109
3.3.1 HFS under substrate free conditions reduces the latency to failure of the mouse sciatic nerve A fibre CAP .....	109
3.3.2 Conditioning exposure reduces latency to failure of the mouse optic nerve CAP in subsequent substrate free conditions.....	111
3.4 Discussion.....	113
3.4.1 The role of glial cell glycogen in supporting axon conduction during insufficient energy substrate availability .....	113
3.4.2 Statistical acceptance .....	114
3.5 Conclusion .....	119
Chapter 4: Schwann cell metabolic support of A fibre conduction during high frequency stimulation in mouse sciatic nerve .....	120 - 148
4.1 Introduction .....	121
4.2 Methods .....	123
4.2.1 Mice and tissue dissection .....	123
4.2.2 Stimulus evoked CAP electrophysiology.....	123
4.2.3 Lactate biosensors .....	124
4.3 Results .....	128
4.3.1 The role of Schwann cell glycogen during substrate free conditions.....	128
4.3.2 Energy supply vs. demand.....	130
4.3.3 The role of lactate during HFS .....	132
4.3.4 Glycogen as a potential source of lactate .....	135
4.4 Discussion.....	141
4.4.1 The low metabolic rate of the sciatic nerve in the absence of energy substrate supply.....	141
4.4.2 Schwann cell metabolic support during increased firing of A fibres .....	142
4.5 Conclusion .....	147
Chapter 5: K <sup>+</sup> , a potential universal signal for axon-glia metabolic interactions .....	149 - 172
5.1 Introduction .....	150

5.2 Methods .....	154
5.2.1 Mice and tissue dissection .....	154
5.2.2 Stimulus evoked CAP electrophysiology.....	154
5.2.3 Lactate biosensors .....	155
5.3 Results .....	156
5.3.1 The relationship between extracellular K <sup>+</sup> and lactate concentration .....	156
5.3.2 The effect of extracellular K <sup>+</sup> on sciatic nerve A fibre conduction.....	158
5.3.3 The effect of stimulus frequency on the extracellular lactate concentration .....	159
5.3.4 The effect of BaCl <sub>2</sub> on the latency to A fibre CAP failure during substrate free conditions .....	162
5.4 Discussion.....	164
5.4.1 Lactate profile .....	164
5.4.2 Logarithmic relationship .....	167
5.4.3 Increased extracellular K <sup>+</sup> increased glycogen metabolism of Schwann cells .....	168
5.5 Conclusion .....	171
Chapter 6: The role of Schwann cells in fructose metabolism of the mouse sciatic nerve.....	173 - 201
6.1 Introduction .....	174
6.2 Methodology.....	179
6.2.1 Mice and tissue dissection .....	179
6.2.2 Western blot.....	179
6.2.3 Fluorescence Immunohistochemistry.....	180
6.2.4 Stimulus evoked CAP electrophysiology.....	186
6.3 Results .....	188
6.3.1 Fructokinase and GLUT5 are expressed within the mouse sciatic nerve .....	188
6.3.2 Fructokinase is only expressed by A fibres .....	189
6.3.3 GLUT5 is expressed by A fibres and Schwann cells.....	193
6.3.4 Higher concentrations of fructose maintain A fibre conduction during HFS.....	194
6.4 Discussion.....	196
6.4.1 Sciatic nerve fructokinase expression.....	196

6.4.2 Fructokinase and GLUT5 expression does not determine efficient metabolism of exogenously supplied fructose by the mouse sciatic nerve .....	196
6.4.3. Central vs. peripheral nervous system fructose metabolism .....	198
6.5 Conclusion .....	201
Chapter 7: Summary .....	202 - 208
7.1 The importance of Schwann cell derived lactate as an energy substrate for A fibres of the mouse sciatic nerve.....	203
7.2 The role of Schwann cells in fructose metabolism by the PNS	205
7.3 Future directions .....	206
7.3.1 Metabolic signals .....	206
7.3.2 Fructose metabolism of the sciatic nerve .....	207
Bibliography.....	209
Publications .....	229
Peer reviewed papers .....	229
Book Chapters .....	229
Reviews and Articles .....	229
Presentations at Conferences .....	230
Covid-19 impact statement.....	231

# Abstract

---

Astrocytes of the central nervous system (CNS) provide glycogen derived lactate to axons when energy substrate availability is low and when axons have an increased energy demand. Signals, including glutamate and  $K^+$ , released from axons communicate the need for metabolic support and trigger astrocyte lactate production. Whether similar metabolic interactions occur between axons and Schwann cells of the peripheral nervous system (PNS) is less well understood. The association of peripheral neuropathy with the metabolic disease diabetes makes the study of axon-Schwann cell metabolic interactions valuable. Myelinating Schwann cells possess glycogen and glycolytically metabolise this to lactate, which their associated axons, known as A fibres, benefit from as an energy substrate when glucose availability is reduced. The aim of this thesis was to use the mouse sciatic nerve to investigate the role of Schwann cells in providing lactate to A fibres during increased axonal activity and the ability of  $K^+$  to act as a metabolic signal. Fructose metabolism of the mouse sciatic nerve was also investigated.

Stimulus evoked compound action potential (CAP) electrophysiology was used to measure the conduction of, and lactate biosensors were used to record the lactate released from, the mouse sciatic nerve *ex vivo*. The method of stimulus evoked CAP electrophysiology was first adapted to record from paired, rather than single nerves, reducing the number of required animals whilst maintaining statistical power. Using this adapted method nerves were subjected to high frequency stimulation (HFS) to increase energy demand. A fibre conduction was maintained through increased glucose supply or Schwann cell derived lactate. The importance of Schwann cell lactate was evident by the loss and inability to maintain recovery of conduction when cinnamate (CIN), an inhibitor that prevents the shuttling of lactate from Schwann cells to

axons, was present under normoglycaemic conditions. These findings prompted investigations into  $K^+$  as a trigger of Schwann cell lactate production. Increasing the concentration of extracellular  $K^+$  increased the concentration of extracellular lactate, a relationship which was logarithmic in response to global changes in  $K^+$  within the artificial cerebrospinal fluid (aCSF), but not in response to local changes in  $K^+$  as the result of increasing stimulus frequency. This suggests the Schwann cell membrane potential influences lactate production. When fructose is supplied to the *ex vivo* sciatic nerve preparation, Schwann cells provide lactate to A fibres, with these axons unable to directly benefit from fructose. Using fluorescent immunohistochemistry, the expression of the fructose specific transporter, GLUT5, and the fructose metabolism specific enzyme, fructokinase, was not found to parallel these electrophysiology findings. With fructokinase expressed exclusively by A fibres and GLUT5 expressed by A fibres and myelinating Schwann cells. These molecular findings might reflect a neuroprotective strategy in which Schwann cells convert excess glucose to fructose via the polyol pathway, a pathway upregulated during diabetes. This fructose may then be shuttled to A fibres for metabolism via fructokinase.

These findings further our understanding of the metabolic role of Schwann cells and provide insight into the potential signal that enables metabolic communication between axons and Schwann cells.

# Chapter 1: Introduction

---

## 1.1 Cells of the nervous system

The importance of the brain to life fascinated physicians and scientists since antiquity (Finger, 2010). Although the Greeks (1500 - 300 BC) were considered the first to write about the brain (Finger, 2010), in the 1930's James Breasted completed the translation of the Edwin Smith Surgical Papyrus originating even further back in time from ancient Egypt (Breasted, 1930). Since the 'dawn of neurology' in 1600 BC, the revolution in microscopy techniques in the 19<sup>th</sup> century enabled scientists such as Purkyně to study the nervous system in greater detail (Finger, 2010). The pioneering work by Golgi, in the development of his silver stain, allowed him to describe the morphology of neural cells (Golgi, 1886; Finger, 2010). Unfortunately he was unable to differentiate the ends of dendrites and axons and therefore concluded that all the cells were interconnected (Finger, 2010). However, by the late 19<sup>th</sup> century, Cajal, using the Golgi stain applied to the nervous system of birds, revealed that nerve cells are single entities that do not fuse, but are separated by small gaps, a theory known as the neurone doctrine and now accepted as an accurate representation of the cellular composition of the brain (Cajal, 1888; Jones, 1994). Cajal also recognised that the nervous system comprised of individual glial cells (Cajal, 1888), in contrast to Virchow who, in 1856, originally assigned the name neuroglia to describe the interstitial substance between neurones rather than the cellular elements that constitute the substance (Virchow, 1856). It is now widely accepted that there are two main cell types that make up the nervous system: neurones and glia (Purves *et al.*, 2012). This alone however is an overgeneralisation. The brain comprises many subtypes of neurones and glial cells. The neurones share the common feature of electrochemical communication, the generation of action potentials along their axons to trigger the release of neurotransmitters at the synapse, which can act on receptors to stimulate the post-synaptic neurone (Bear *et al.*, 2007). However, the function of this communication is different for the different neuronal subtypes present in different areas of the brain e.g. certain

hippocampal neurones display particular firing patterns that encode spatial parameters associated to the organism's orientation and position (Hartley *et al.*, 2014).

Since their discovery in 1856 glia have been described as support cells; passive cells that are only present in the nervous system to provide structural support to neurones. However, it is now appreciated that there are many subtypes of glial cell present within the nervous system, all of which perform different roles. The main types of glia include astrocytes, oligodendrocytes, Schwann cells (all 3 are macroglia) and microglia. Briefly, astrocytes maintain the homeostasis of the extracellular environment of the central nervous system (CNS), oligodendrocytes and Schwann cells myelinate axons of the central and peripheral nervous system (PNS), respectively and microglia are the resident immune cells of the CNS (Bear *et al.*, 2007).

The presence of multiple different cell types in the brain is in contrast to other organs which tend to mainly comprise of repeated expression of the same cell type e.g. hepatocytes in the liver (Kmieć, 2001). This makes the brain unique and adds additional layers of complexity to its understanding. Although the brain is made up of a multitude of cell types, the different cells all share a common extracellular space. This extracellular space only equates to the 18-24% of the total adult brain volume and is highly dynamic (Nicholson & Syková, 1998), therefore changes in its composition and volume affects all surrounding cells. As a result, the extracellular space allows the neurones and glial cells to communicate with and influence one another.

An important aspect of physiology of communication between neurones and glia is energy metabolism. Originally thought to be self-regulating, it is now apparent that neurones require glial cells to regulate and distribute energy substrates particularly under increased energy demand conditions (Pellerin & Magistretti, 2013).

## 1.2 Energy metabolism

To understand the metabolic role of glial cells in the nervous system, whole body energy metabolism must be understood. Metabolism is a broad term to describe the biochemical processes used by cells of living organisms to acquire energy (Voet & Voet, 2011). Chemotrophs (including animals and humans) gain their energy, mainly in the form of adenosine triphosphate (ATP), via the oxidation of three classes of organic biomolecules: carbohydrates, lipids and proteins (Voet & Voet, 2011). Broadly, the metabolism of these compounds culminates in the formation of acetyl CoA (Voet & Voet, 2011; figure 1.1). These compounds are first broken down into their monomer units, before energy can be obtained from their metabolism; proteins into amino acids, lipids into fatty acids and glycerol, and carbohydrates into glucose (Voet & Voet, 2011). The focus for the rest of this section is on glucose since it is the obligatory energy substrate in many organisms (Voet & Voet, 2011).

Once glucose is produced from ingested complex carbohydrates, its concentration in the blood must be regulated to ensure optimum benefit to the body. The physiological range of the blood glucose concentration in humans is about 3.9mM (3.3-7.2mM; Röder *et al.*, 2016). Since these concentrations can fluctuate as the result of increased ingestion and metabolism to provide energy, the concentration of blood glucose must be tightly controlled to prevent prolonged exposure to excess or insufficient glucose. The antagonistic hormones, insulin and glucagon, released from islet cells of the pancreas play a key role in maintaining the homeostasis of blood glucose (Röder *et al.*, 2016). When blood glucose levels drop, e.g. during sleep, glucagon is released from  $\alpha$ -cells, which binds to glucagon receptors on the liver to promote glycogenolysis and gluconeogenesis (Röder *et al.*, 2016).

Glycogenolysis refers to the breakdown of glycogen, the storage form of glucose, to glucose whilst gluconeogenesis is the synthesis of glucose from non-carbohydrate precursors such as lactate (Voet & Voet, 2011). The glucose can then be released into the systemic

circulation thus raising the concentration of blood glucose. In contrast, in response to increased blood glucose insulin, released from the pancreatic  $\beta$ -cells, binds to insulin receptors on muscle and fat, promoting insulin-dependent uptake, via the insulin-sensitive glucose transporter 4 (GLUT4), into these cells facilitating two main goals, storage of glucose and reduction of blood glucose (Röder *et al.*, 2016). Thus, glucose is stored within these cells as glycogen for use later when blood glucose drops. In addition to the action of glucagon and insulin on peripheral organs, these two hormones are able to penetrate the blood brain barrier and act on their respective receptors, expressed throughout the CNS, contributing to the regulation of systemic glucose homeostasis (Havrankova *et al.*, 1978; Hoosein & Gurd, 1984). These hormones act on the hypothalamus, an area of the brain that is involved in glucose sensing and regulating peripheral metabolism (Abraham & Lam, 2016). Insulin acts on astrocytes in the hypothalamus, reducing appetite and food intake reflected in reduced blood glucose levels via increased uptake of glucose into the brain (García-Cáceres *et al.*, 2016). Interestingly, the action of glucagon in hypothalamic regions of the brain also reduces food intake as well as reduces liver glucose production, in contrast with the action of glucagon on peripheral organs (Abraham & Lam, 2016).

Chronic blood glucose elevations are the principal symptom of the heterogenous metabolic disorder, diabetes (Petersmann *et al.*, 2019). Type 1 diabetes results from an autoimmune response that attacks the  $\beta$ -cells preventing the pancreas from producing insulin, whilst type 2 diabetes can range from the result of inadequate production of insulin to insulin resistance (Petersmann *et al.*, 2019). The prevalence of diabetes in the UK between 2018-2019 was 4.9 million people, with 13.6 million people at increased risk of type 2 diabetes (Diabetes UK, 2021). The high blood glucose associated with diabetes causes neuropathy, with diabetes known to be the main cause of 50% of neuropathy cases (Stino & Smith, 2017). Peripheral neuropathy is the most common type of diabetic neuropathy, affecting one third to one

half of diabetic patients (NIDDK, 2021). The mechanism underlying this neuropathy is unclear, therefore research into understanding glucose metabolism within the peripheral nervous system, and particularly peripheral nerves, is a research area of prime importance.

The first stage of glucose specific metabolism is glycolysis (Nelson & Cox, 2009). The end product of glycolysis can then be oxidised to acetyl-CoA, the common metabolic intermediate of amino acids, fatty acids and glucose. Acetyl-CoA can then enter the second stage of energy metabolism known as the tricarboxylic acid cycle (TCA cycle; Nelson & Cox, 2009). Here acetyl-CoA is oxidised to CO<sub>2</sub> and energy released from this metabolism is stored in reduced electron carriers, NADH and FADH<sub>2</sub> (Nelson & Cox, 2009). Electrons, from the oxidation of NADH and FADH<sub>2</sub>, are then passed along the electron transport chain, the third stage of metabolism, ultimately producing O<sub>2</sub> and ATP (Nelson & Cox, 2009; figure 1.2).

### 1.2.1 Glycolysis

Glycolysis is a 10-step enzymatic pathway that occurs in the cell cytoplasm. Glucose uptake into cells is achieved by facilitated diffusion, which involves membrane bound transporters moving the energy substrate from a region of high to low concentration (Nakrani *et al.*, 2020). Glucose transporters (GLUTs) are uniport transporters that move glucose in either direction depending on the transmembrane concentration gradient and exist as many different isoforms (Gould & Holman, 1993). Cellular glucose is immediately phosphorylated to glucose-6-phosphate (Nakrani *et al.*, 2020). This forms the first step of glycolysis and is catalysed by the enzyme hexokinase (Voet & Voet, 2011). This is a key step since it is rate limiting and requires ATP (Berg *et al.*, 2002). At this point glucose-6-phosphate can proceed along the glycolytic pathway, or if present at high concentrations triggers glycogen synthase and ultimately storage as glycogen (Vijjar-Palasi & Guinovart, 1997; figure 1.2).

Glycolysis exists as two distinct phases (figure 1.2). The first phase refers to the first 5 enzyme reactions and is known as the preparatory phase, where glucose is destabilised and cleaved into two interconvertible three carbon molecules (Nelson & Cox, 2009). This is the energy (ATP) requiring phase of glycolysis, where the enzymes hexokinase and phosphofructokinase require a molecule of ATP each, and ultimately converts one molecule of the six carbon glucose to two molecules of the three carbon glyceraldehyde 3-phosphate (Nelson & Cox, 2009). These can then pass into the second phase of glycolysis, the payoff phase, where the three carbon molecules are oxidised to pyruvate (Nelson & Cox, 2009). In this phase 4 molecules of ATP and 2 molecules of NADH are produced. Altogether glycolysis produces 2 molecules of ATP, 2 NADH and 2 pyruvate from 1 glucose molecule (Nelson & Cox, 2009).

Although glycolysis is glucose specific, many other carbohydrates can enter the glycolytic pathways at different points once they have been converted into a glycolytic intermediate (Nelson & Cox, 2009). This allows energy to be obtained from carbohydrate sources other than glucose. For example the monosaccharide, fructose, can enter the glycolytic pathway via hexokinase which converts it to fructose-6-phosphate, or via fructokinase ultimately converting it to glyceraldehyde 3-phosphate (Nelson & Cox, 2009; figure 1.3). The use of fructose as an energy substrate results in the same net production of ATP as glucose.

Pyruvate is conventionally assigned as the end product of glycolysis, however there is evidence to suggest lactate is always the end product of glycolysis (Rogatzki *et al.*, 2015). A final enzyme reaction of glycolysis is the conversion of pyruvate to lactate via lactate dehydrogenase. This reaction enables the regeneration of Nicotinamide adenine dinucleotide (NAD) for subsequent glycolysis (Nelson & Cox, 2009). Traditionally the formation of pyruvate is described as aerobic glycolysis since the 1,4-Dihyronicotinamide adenine dinucleotide

(NADH) is reoxidised by transferring its electrons to O<sub>2</sub> in the electron transport chain, and pyruvate subsequently enters the TCA cycle and electron transport chain to form oxygen (Nelson & Cox, 2009).

Glycolysis resulting in lactate was described as anaerobic glycolysis since in the presence of insufficient oxygen NADH cannot be reoxidised by O<sub>2</sub> but instead is regenerated by lactate dehydrogenase, converting pyruvate to lactate (Nelson & Cox, 2009). The reaction performed by lactate dehydrogenase is reversible in that pyruvate can be converted to lactate, but lactate can also be converted to pyruvate (figure 1.2). Generally, this equilibrium tends to favour lactate production evident by the higher baseline intracellular concentration of lactate compared to pyruvate; in the brain the lactate to pyruvate ratio is ~20:1 (Rogatzki *et al.*, 2015). The view that glycolysis ending with lactate means subsequent energy is not derived from the TCA cycle or electron transport chain may also be redundant since lactate can enter the mitochondria via monocarboxylate transporters, where the TCA cycle and electron transport chain occur, and can be converted to pyruvate via lactate dehydrogenase for mitochondrial oxidation (Rogatzki *et al.*, 2015). This suggests lactate should be considered as a key end-product of glycolysis whether oxygen is present at sufficient concentrations or not.

### *1.2.2 The TCA cycle and electron transport chain*

For pyruvate to enter the second stage of metabolism, the TCA cycle, it must first be transported from the cytoplasm into the mitochondrial matrix via the mitochondrial pyruvate carrier (Bender & Martinou, 2016) and then oxidised to acetyl-CoA, a reaction that is catalysed by the pyruvate dehydrogenase complex and produces a molecule of NADH per pyruvate (Nelson & Cox, 2009). The TCA cycle occurs in the mitochondrial matrix and is a cyclical pathway consisting of 8 enzyme steps that oxidises the acetyl group of acetyl-CoA to 2 molecules of CO<sub>2</sub>, 1 ATP, 3 NADH and 1 Dihydroflavine-adenine dinucleotide (FADH<sub>2</sub>; Nelson & Cox, 2009; figure 1.2).

Thus far, glucose is completely oxidised to CO<sub>2</sub> and 10 molecules of NADH and 2 FADH<sub>2</sub> are produced. The electrons removed from glucose during glycolysis and the TCA cycle are stored in NADH and FADH<sub>2</sub> and are subsequently transferred to the electron transport chain (figure 1.2), located at the inner mitochondrial membrane (Voet & Voet, 2011). This involves the reoxidation of the 10 NADH and 2 FADH<sub>2</sub> molecules liberating electrons and protons (H<sup>+</sup>) (Voet & Voet, 2011). As the electrons are transported along the 4 complexes of the electron transport chain, H<sup>+</sup> are pumped from an area of high concentration in the mitochondrial matrix into the mitochondrial intermembrane space, an area of low concentration (Voet & Voet, 2011). Complex IV of the electron transport chain also reduces O<sub>2</sub> to H<sub>2</sub>O (Voet & Voet, 2011). The free energy stored in the H<sup>+</sup> gradient drives the synthesis of ATP via ATP synthase, altogether known as oxidative phosphorylation (Voet & Voet, 2011).

Overall, complete oxidation of glucose liberates 32 molecules of ATP, whilst glycolysis alone only produces 2 molecules of ATP per glucose (Voet & Voet, 2011; figure 1.2).

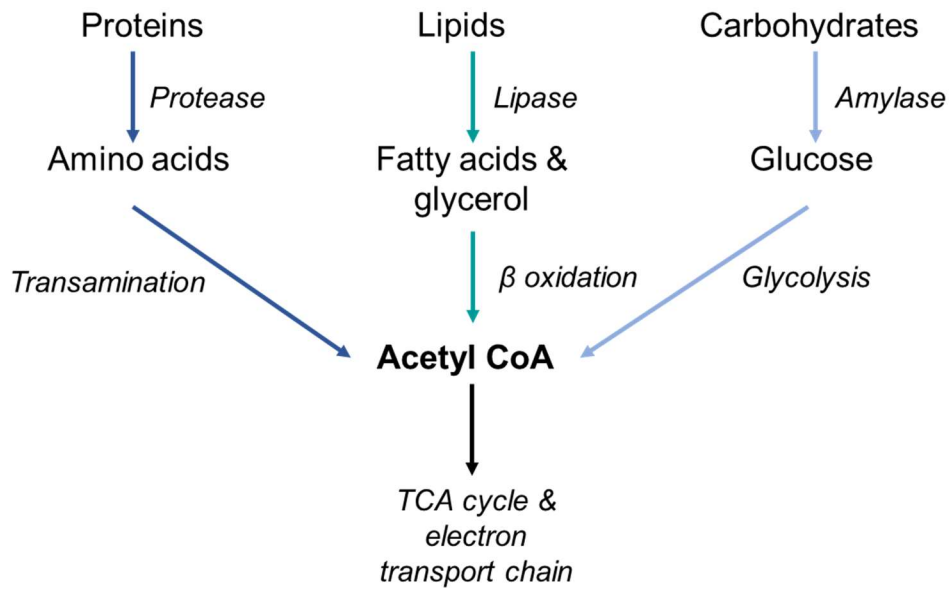


**Figure 1.1:** Energy metabolism. Ingested proteins, lipids and carbohydrates are broken down into their monomer units amino acids, fatty acids and glycerol, and glucose via protease, lipase and amylase enzymes, respectively. These monomer units are then metabolised via their specific pathways (transamination,  $\beta$  oxidation and glycolysis) to the common intermediate, acetyl CoA, which then continues along the common metabolic pathways, the TCA cycle and electron transport chain. (Voet & Voet, 2011).

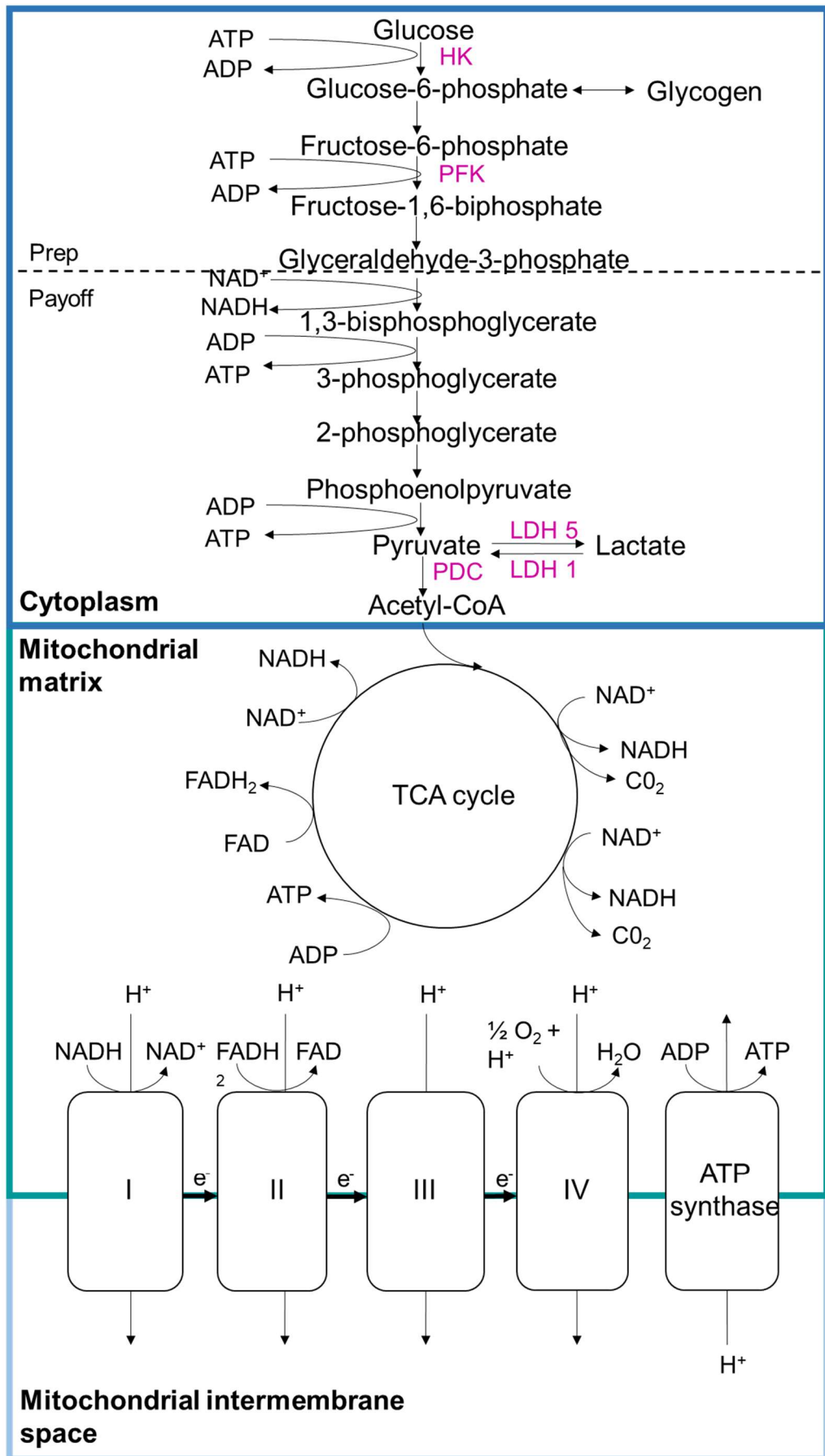


**Figure 1.2:** Glucose metabolism. Glycolysis occurs in the cytoplasm of the cell and involves both energy requiring (prep) and energy producing (payoff) phases. After fructose-1,6-biphosphate two of each compound is produced overall resulting in two molecules of pyruvate, two ATP and two NADH. Pyruvate can either be converted to lactate via lactate dehydrogenase (LDH) or transported into the matrix of the mitochondria and converted to acetyl-CoA via the pyruvate dehydrogenase complex (PDC). The key enzymes that limit the rate of glycolysis are hexokinase (HK) and phosphofructokinase (PFK), and when glucose is present in excess of demand it can be stored as glycogen. In the mitochondrial matrix acetyl-CoA enters the TCA cycle where it is completely oxidised to  $2\text{CO}_2$ , 1 ATP, 3 NADH and 1  $\text{FADH}_2$ .  $\text{H}^+$  from the reduction of NADH and  $\text{FADH}_2$ , formed during glycolysis and the TCA cycle, are pumped from the matrix into the intermembrane space by the four complexes of the electron transport chain, situated on the inner mitochondrial membrane, producing a  $\text{H}^+$  gradient used by ATP synthase to phosphorylate ADP to ATP. (Voet & Voet, 2011).

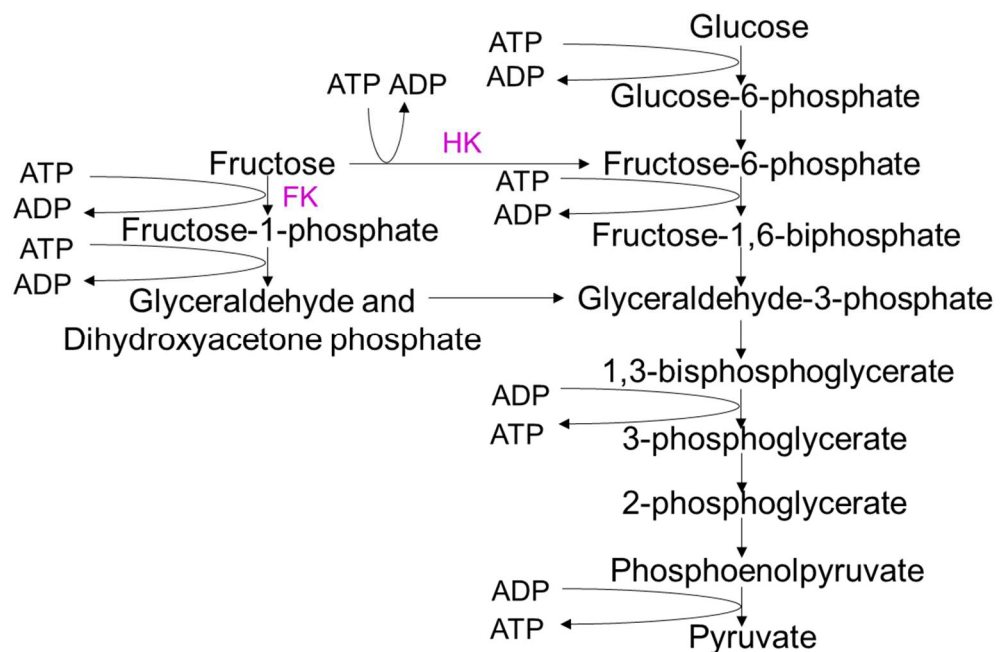


**Figure 1.3:** Fructose metabolism. Fructose enters the glycolytic pathway at the level of fructose-6-phosphate via hexokinase (HK) or glyceraldehyde-3-phosphate via fructokinase (FK). Fructose metabolism via either enzyme requires and produces the same number of ATP as glucose metabolism. (Nelson & Cox, 2009).

### 1.3 Nervous system energy metabolism

The brain has an extremely high demand for energy. Despite the adult brain only contributing 2% to the total body weight, the brain consumes 15-20% of the cardiac output (Williams & Leggett, 1989). This is even higher in the developing brain where the total brain glucose uptake to meet the daily energy requirement peaks at 43% (Kuzawa *et al.*, 2014). The requirement of cardiac output by the adult brain is high compared to other organs of the body e.g. the lungs and pancreas, but is comparable to other high energy demand organs including the muscle and gastrointestinal tract (Williams & Leggett, 1989). To ensure a sufficient supply of glucose to meet the brain's energy demand, an excess of glucose is supplied via the circulation to the brain (Dienel, 2019). These reasons, in addition to the onset of a coma within minutes when the blood supply to the brain is disrupted (Kabat & Anderson, 1943), reinforces the high energy requirement of the brain and the importance of studying nervous system energy metabolism.

The majority of the brain's energy is used by neurones to restore ion gradients that are disrupted as the result of electrical activity (Attwell & Laughlin, 2001). Since the basis of the brain's function is neuronal signalling, it might be considered illogical to assume neurones are solely responsible for maintaining their energy levels. The presence of different cell types in the brain has in fact enabled metabolic compartmentalisation and cooperation to evolve.

Since Golgi's discovery that glial cells, now known to be astrocytes, reside between and make contact with the vasculature of the brain and neurones, a considerable amount of research has highlighted the importance of astrocytes in controlling blood flow in the brain, and as metabolic communicators between the vasculature and neurones (Nortley & Attwell, 2017).

One of the first major studies highlighting the metabolic role of glial cells utilised the honeybee drone retina, which is comprised of photoreceptors (neurones) and outer pigment cells (glial cells)

(Tsacopoulos *et al.*, 1994). It was found that glucose is glycolytically metabolised to pyruvate, which is subsequently transaminated by the enzyme alanine aminotransferase (ALAT) to alanine within the glial cell (Tsacopoulos *et al.*, 1994). Alanine is then released into the extracellular space via a Na<sup>+</sup>-dependent mechanism into mitochondria enriched photoreceptors where it is transaminated back to pyruvate for metabolism within the TCA cycle (Tsacopoulos *et al.*, 1994; figure 1.4). An additional key finding of this study is the glycolytic nature of the glial cells whilst neurones appear to show a preference for mitochondrial oxidative metabolism. This metabolic compartmentalisation between glial cells and neurones has since been extended to mammalian astrocytes and neurones, supported by various genetic studies that have found; a) PFKFB3, a gene that encodes a glycolytic enzyme is expressed at a higher level by astrocytes than neurones (Herrero-Mendez *et al.*, 2009), b) astrocytes express isoform 5 of the lactate dehydrogenase (LDH) enzyme, which favours the conversion of pyruvate to lactate, whilst neurones express LDH1 which tends to oxidise lactate to pyruvate (Bittar *et al.*, 1996), c) the pyruvate dehydrogenase complex tends to be in its inactive (phosphorylated) form in astrocytes, while it tends to be present in its active (dephosphorylated) state in neurones (Halim *et al.*, 2010), d) the aspartate glutamate complex of the malate-aspartate shuttle in mitochondria is expressed at a lower level by astrocytes than neurones (Ramos *et al.*, 2003), and e) neuronal activity regulates many astrocytic genes, in particular there is an upregulation of genes associated with glycolysis but not mitochondrial oxidative metabolism suggesting a neuronal influence on the astrocytic transcriptome (Hasel *et al.*, 2017). Astrocytes not only show a preference for glycolysis, but this glycolytic metabolism results in lactate as the end product, which they can then release into the extracellular space, thus they are described as the lactate producers within the nervous system (Walz & Mukerji, 1988). During activation of the brain, glucose is incompletely oxidised, suggesting astrocytes produce lactate even in the presence of sufficient oxygen (Bouzier-Sore & Pellerin, 2013; Magistretti & Allaman, 2015).

This is known as the Warburg effect and refers to increase glucose uptake and subsequent preferential formation of lactate, a phenomenon indicative of cancer cells (Liberti & Locasale, 2016).

The differential preference for glycolysis and mitochondrial oxidative metabolism between astrocytes and neurones is an area of active debate. In response to increased neuronal activity, neuronal, not astrocytic, glycolysis has been shown to increase (Díaz-García *et al.*, 2017) with mitochondrial oxidative metabolism of both neurones and astrocytes also upregulated (Sonnay *et al.*, 2018). Furthermore, it has been suggested neurones take up more glucose than astrocytes (Lundgaard *et al.*, 2015). However, a recent study using *Drosophila* has revealed that this metabolic disparity between neurones and glia extends to invertebrates, showing glia are more dependent on glycolysis and neurones more dependent on mitochondrial oxidative metabolism (Volkenhoff *et al.*, 2015). This suggests metabolic compartmentalisation between neurones and glia has an evolutionary advantage and therefore it is most likely conserved in higher order mammals.

It has already been alluded to that the brain not only relies on glucose as its energy substrate but is also capable of efficiently metabolising other energy substrates, the most prominent being lactate. Whether lactate is the preferred energy substrate of the brain over glucose is still unclear. An *in vivo* study using enzyme biosensors to measure changes in the extracellular glucose and lactate of the rat striatum found stimulation of the midbrain, whose axons project to the striatum, caused a rise in extracellular glucose that peaked before that of the increase in extracellular lactate (Forderhase *et al.*, 2020). These concentration increases were found to be stimulus frequency dependent with the range of glucose concentrations much greater than that of lactate (Forderhase *et al.*, 2020). Lactate was also found to be consumed at a similar rate, in contrast to glucose consumption which increased with increased stimulus frequency, leading to the conclusion that glucose is the primary, and lactate the secondary, energy substrate

used by the brain under active conditions (Forderhase *et al.*, 2020). During the pre-weaning period of rats, the expression of transporters by the blood brain barrier for glucose or monocarboxylates e.g. lactate, are both high, but as the brain matures glucose transporters become the dominant metabolic transporter, suggesting glucose and lactate might be equally important energy substrates for the developing brain (Vannucci & Simpson, 2003). However, this does not exclude the use of lactate as an energy substrate in the adult brain, where the source is more likely from astrocytes than from the circulation. The brain is also able to use ketones as a source of energy, when there is a drop in glucose availability e.g. during fasting (Owen *et al.*, 1967). Ketogenic interventions are a potential therapy for neurodegenerative diseases such as Alzheimer's, conditions where the glucose metabolism of the brain is known to be reduced (Jensen *et al.*, 2020). Another energy substrate that can be used by the brain is fructose. Previously suggested to patients with mild diabetes as an alternative sweetener to glucose due to its reduced effects on blood glucose levels (Huttunen, 1971), fructose is able to cross the blood brain barrier (Mantych *et al.*, 1993) and is metabolised within the brain (Oppelt *et al.*, 2017). The ability of the nervous system to use different energy substrates suggests their primacy may change depending on the developmental state and metabolic circumstances.

The majority of research investigating the metabolic role of glia has focused on astrocytes. The metabolic complexity of the nervous system not only exists in its ability to metabolise different energy substrates, but also in the ability of different subtypes of glial cells, in particular astrocytes, oligodendrocytes and Schwann cells, to provide metabolic support to neurones. In addition, the different subtypes of glial cells may not just have independent metabolic roles, but may work together to maintain the energy homeostasis of the nervous system. The ability of different glial cells, in both the central and peripheral nervous systems, to supply energy substrates to neurones will now be discussed.

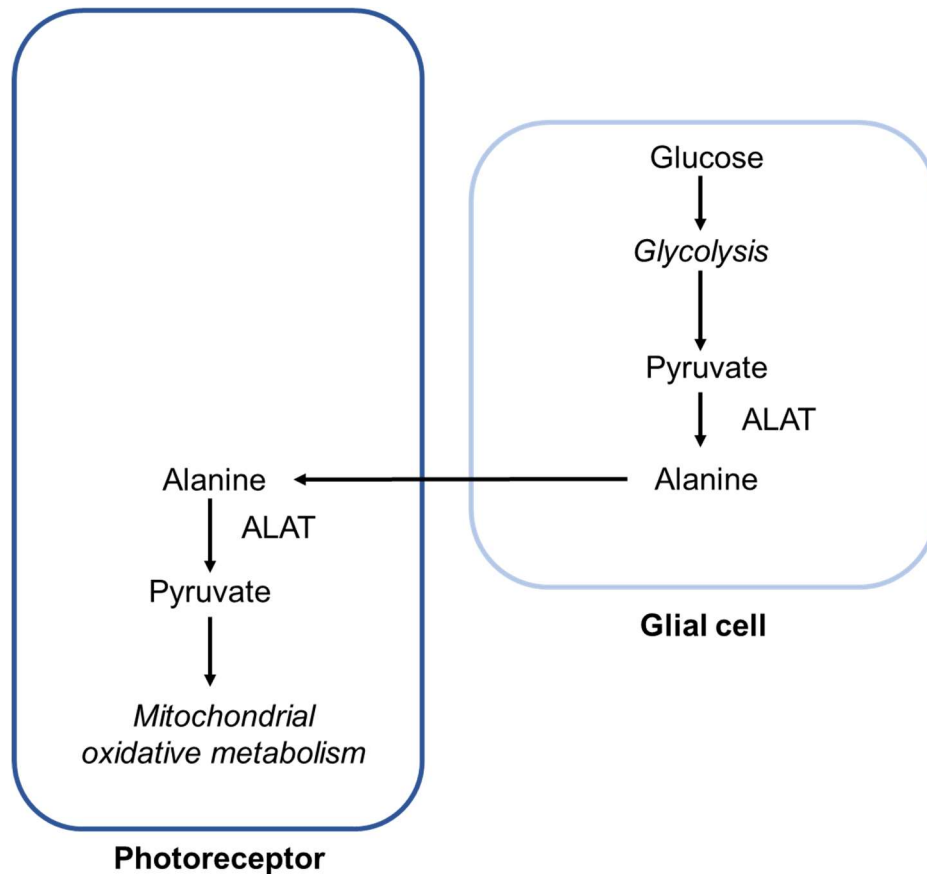


**Figure 1.4:** Glial cell-photoreceptor metabolic interactions of the honeybee drone retina. The glial cell glycolytically metabolises glucose to alanine which is supplied to the photoreceptor for mitochondrial oxidative metabolism. ALAT= alanine aminotransferase. (Tsacopoulos *et al.*, 1994).

### 1.3.1 Glucose

Cells must express the appropriate transporters and enzymes in order to access and utilise energy substrates such as glucose. In the CNS, energy substrates present in the systemic circulation must first cross the blood brain barrier into the extracellular space before they can access the cells. Due to the hydrophilic nature of energy substrates which prevents direct access to the brain, complementary transporters must be present on the blood brain barrier for them to cross (Bear *et al.*, 2007). Nerves of the PNS also comprise many barriers that substrates must be transported across; each axon and its associated Schwann cells are surrounded by the endoneurium, which are then bundled together into groups called fascicles surrounded by the perineurium, finally, the fascicles are bundled together into the nerve surrounded by

the epineurium (Pavelka & Roth, 2010; figure 1.5). The sciatic nerve, a peripheral nerve, is also supplied with blood via the vasa nervorum which runs longitudinally throughout the layers of the nerve (Mizisin & Weerasuriya, 2011). The perineurium and endoneurial microvessels make up the blood nerve barrier, the equivalent blood brain barrier of the PNS (Weerasuriya & Mizisin, 2011).

The isoforms of GLUTs are differentially expressed throughout the nervous system, with a similar pattern of expression seen between the central and peripheral nervous system, albeit more complex in the PNS. In the CNS, GLUT1 is expressed by endothelial cells of the blood brain barrier enabling glucose access into the extracellular space where it can be taken up by astrocytes (Vannucci *et al.*, 1997) and oligodendrocytes (Saab *et al.*, 2016) also via GLUT1, or via GLUT3 into neurones (Vannucci *et al.*, 1997). In the PNS glucose can diffuse from epineurial microvessels that lack a blood nerve barrier into the extracellular space of the epineurium (Allt & Lawrenson, 2000) then across the perineurium and endoneurium via GLUT1 (Magnani *et al.*, 1996). Glucose can also cross the endoneurial microvessels directly via GLUT1 into the extracellular space surrounding the axons (Magnani *et al.*, 1996). Glucose can then be taken up into Schwann cells via GLUT1 or into myelinated axons via GLUT3 (Magnani *et al.*, 1996).

Studies have shown that both neurones and astrocytes take up glucose and metabolise it efficiently (Nehlig *et al.*, 2004) with evidence to suggest neurones actually take up more glucose than astrocytes under both basal and increased neuronal activity conditions (Lundgaard *et al.*, 2015). The opposite has been suggested in terms of Schwann cells and axons in that Schwann cells take up ~75% of available glucose (Véga *et al.*, 2003).

A recent study investigating oligodendrocyte-axon metabolic interactions of the mouse corpus callosum, a white matter structure of the brain, has suggested that oligodendrocytes provide axons with glucose in order to maintain axon conduction (Meyer *et al.*, 2018).

Conduction was measured from the area of the compound action potential (CAP) since the CAP is the sum of the contributing axons, with a reduction in area reflecting a loss of contributing axons (Parker *et al.*, 2018). On exposure to aglycaemia the CAP was maintained for only 5 minutes at which point it rapidly fell but was fully restored by the reperfusion of 10mM glucose (Meyer *et al.*, 2018). To determine the role of oligodendrocytes in supporting axon conduction during aglycaemia the oligodendrocytes were preloaded with 20mM glucose by patch clamping onto individual cells (Meyer *et al.*, 2018). This still resulted in a drop in CAP area to ~50%, where it was maintained, however this was significantly better when compared to aglycaemia alone or when preloading astrocytes with 20mM glucose (Meyer *et al.*, 2018). Furthermore, blocking GLUT3, the glucose transporter expressed by axons not oligodendrocytes, in addition to loading oligodendrocytes with glucose during aglycaemia prevented any maintenance of the CAP suggesting oligodendrocytes supply axons with glucose (Meyer *et al.*, 2018).

Interestingly, rather than being lactate suppliers, like oligodendrocytes, astrocytes have been suggested as stores of free glucose. Cultured human foetal cortical astrocytes express endoplasmic reticulum glucose-6-phosphatase  $\beta$ , an enzyme that reverses the phosphorylation of glucose by hexokinase in the first step of glycolysis, resulting in production of free glucose (Müller *et al.*, 2018). Using knockout models, glucose-6-phosphatase was required by astrocytes for glucose uptake into the endoplasmic reticulum which led to the suggestion of two roles for astrocytic glucose-6-phosphatase  $\beta$ : 1) sequestering glucose-6-phosphate reduces hexokinase inhibition, therefore allowing sustained glucose uptake, and 2) it allows glucose to accumulate within the endoplasmic reticulum, acting as a store of free glucose. This glucose can then be transported, without being glycolytically metabolised, within the endoplasmic reticulum from the perivascular processes to an area of higher energy demand (Müller *et al.*, 2018). It is also likely that this glucose will be supplied to neurones in the form of glucose derived

lactate, in contrast to the direct transfer of glucose to axons by oligodendrocytes.

In addition to independent metabolic roles, an area of developing research is the cooperation between astrocytes and oligodendrocytes. Astrocytes and oligodendrocytes can be interconnected via gap junctions made up of connexin hemi-channels. In particular, astrocytes express connexin 26, 30 and 43 and can fuse with the oligodendrocyte connexin 32 and 47 (Nagy *et al.*, 2004). These gap junctions could act as routes for the transport of energy substrates between the different glial cells. A study using a fluorescent glucose analogue, 2-NBDG, and astrocyte-oligodendrocyte cell cultures showed that 2-NBDG loaded into oligodendrocytes was transferred to astrocytes (Niu *et al.*, 2016). This direction of transfer may be unexpected since it is the astrocytes that make contact with the blood supply, however gap junctions comprising connexin 47 and 43 display rectification for the transport of ions and large negatively charged proteins towards connexin 43 expressing cells (Fasciani *et al.*, 2018).

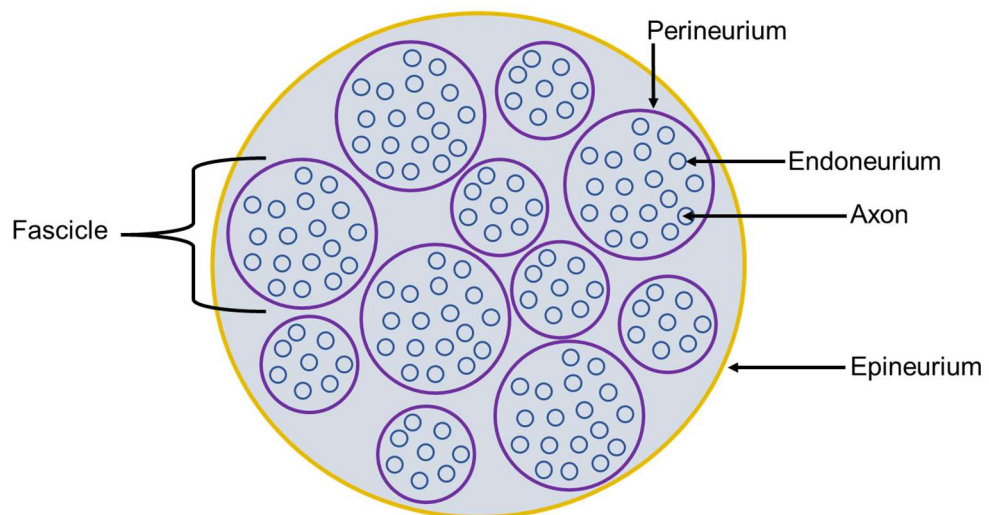


**Figure 1.5:** Peripheral nerve connective tissue layers. Individual axons are surrounded by the endoneurium, the perineurium bundles groups of axons into fascicles and the epineurium surrounds all the fascicles of the nerve. (Pavelka & Roth, 2010).

### 1.3.2 Glycogen

Glycogen is the storage form of glucose and one of the two major energy reserves of the body, the other being fat (Newsholme, 1981). The key enzyme involved in its synthesis (glycogenesis) is glycogen synthase, whereas glycogen phosphorylase (glycogenolysis) cleaves  $\alpha$ -1,4-glycosidic bonds releasing glucose-1-phosphate. Glucose-1-phosphate can then be converted to glucose-6-phosphate before entering glycolysis (Champe *et al.*, 2008). Glycogen is the short-term store of energy whilst fats are longer term stores of energy therefore glycogen metabolism is important for rapidly raising the blood glucose levels in response to temporary increases in energy demand, as occurs in the nervous system with rapid changes in the signalling activity of neurones (Newsholme, 1981).

Only in the last 20-30 years has research commenced into the role of glycogen as an energy source in the brain. This was in part due to the apparent low concentration of glycogen in the brain compared to other organs of the body: brain (8-12  $\mu\text{mol/g}$ ), muscle (30-100 $\mu\text{mol/g}$  tissue) and liver (100-500 $\mu\text{mol/g}$  tissue) (Shulman *et al.*, 1995; Cruz & Diemel, 2002). However, the optimisation and energy efficiency of the brain suggests glycogen would not have evolved to take up valuable space or energy if it was not going to be of use (Sterling & Laughlin, 2015).

Detailed analysis of the localisation of glycogen within the nervous system has revealed its presence within both the central and peripheral nervous systems, where glycogen is specifically localised to glial cells but not neurones. In the CNS glycogen is present in astrocytes (Cataldo & Broadwell, 1986) and tanycytes of the hypothalamus (Nilaweera *et al.*, 2011), and in the PNS myelinating, but not nonmyelinating, Schwann cells are the repository of glycogen (Brown *et al.*, 2012). Using improved methods (microwave fixation and immunohistochemistry) to investigate the distribution of glycogen throughout the brain, glycogen is localised the processes of astrocytes

(Oe *et al.*, 2016). This suggests a fundamental role of glial cells in controlling energy storage levels of the nervous system.

Rodent optic and sciatic nerves are well-used models to study the metabolic interactions between axons and glial cells in the central and peripheral nervous system, respectively. The optic nerve is the 2<sup>nd</sup> cranial nerve and a central white matter tract, thus comprises astrocytes, oligodendrocytes and axons (Ransom & Orkand, 1996). The sciatic nerve is the largest peripheral nerve, comprised of myelinating Schwann cells that myelinate the A fibre axons and non-myelinating Schwann cells that ensheath C fibre axons into Remak bundles (Kidd *et al.*, 2013). The optic nerve is a simplified model of the central white matter, consisting of one type of axon, astrocytes and oligodendrocytes (Ransom & Orkand, 1996), and since the two main fibres of the sciatic nerve can be selectively recruited due to their differences in thresholds (Rich & Brown, 2018a), studies using these tissues are able to make inferences in the metabolic interactions between the axons and the glia cells. Many of the studies involve recording the CAP *ex vivo*. Since nerves are a collection of axons the population response is recorded, known as the CAP (Parker *et al.*, 2018). In the case of the optic nerve the CAP refers to the entire nerve, whilst the A and C fibre CAP of the sciatic nerve can be recruited separately. The CAP acts as a measure of conduction, therefore studies involve changing the energy substrates supplied to the nerve and interfering with the metabolic pathways and cross talk between axons and glia to determine whether axons are able to obtain sufficient energy to maintain conduction under these conditions.

Glycogen is present in the rodent optic nerve (~10 (rat) and 7 (mouse) pmol glycogen/ $\mu$ g of protein) and mouse sciatic nerve (~9 pmol glycogen/ $\mu$ g of protein) specifically within the astrocytes and myelinating Schwann cells, respectively (Wender *et al.*, 2000; Brown *et al.*, 2003, 2012). These glial cells also express glycogen phosphorylase suggesting their ability to break down and metabolise glycogen (Pfeiffer-Guglielmi *et al.*, 2003, 2007; Brown *et al.*, 2012).

Since the purpose of glycogen is to provide short-term supply of glucose/lactate when glucose levels are low, this role of glycogen in the nervous system can be investigated by removal of the exogenous energy substrate supply to the nerve. Under these conditions the only remaining source of energy substrate will be glycogen, and thus the duration for which conduction is maintained indicates the duration for which sufficient energy can be obtained from glycogen. Removal of an exogenous energy substrate supply resulted in a latency to CAP failure of ~20 and 30 minutes in the mouse (Brown *et al.*, 2003, 2004) and rat (Wender *et al.*, 2000; Brown *et al.*, 2004) optic nerve, respectively, at which point the concentration of glycogen in the nerves had reached its minimum. A similar scenario occurred in the sciatic nerve in terms of the A fibres, however onset of CAP failure occurred after 2 hours of aglycaemia, ~4 times longer maintenance of conduction compared to optic nerve, but indicated glycogen exhaustion (Brown *et al.*, 2012). C fibre conduction declined after 30 minutes which did not coincide with complete glycogen metabolism (Brown *et al.*, 2012). The absence of glycogen present in the non-myelinating Schwann cells results in accelerated CAP failure of the C fibres compared to the A fibres (Brown *et al.*, 2012). This suggests that glycogen can act as a short-term supply of energy to axons of the CNS and A fibres, but not C fibres, of the PNS during reduced glucose supply. This was further demonstrated by incubating the nerves in varying concentrations of glucose, which increased and decreased the glycogen content (Brown *et al.*, 2003), respectively, before subjecting them to aglycaemia. This procedure increased the latency to CAP failure of the rat (Wender *et al.*, 2000; Brown *et al.*, 2004) and mouse (Brown *et al.*, 2003) optic nerve and A fibres of the sciatic nerve (Brown *et al.*, 2012) when preincubated in higher concentrations of glucose. The opposite was found for lower glucose i.e. lower glycogen concentrations (Brown *et al.*, 2003, 2012). As expected altering the glycogen content of the sciatic nerve had no effect on the C fibre latency to failure during aglycaemia (Brown *et al.*, 2012). In addition, the use of glycogen phosphorylase inhibitors (isofagomine and DAB) significantly reduced the latency to CAP failure

during aglycaemia in the mouse optic nerve (Brown *et al.*, 2005) and sciatic nerve A fibres, but not C fibres (Brown *et al.*, 2012). These findings demonstrate similarity between CNS axons and astrocytes and PNS A fibres, but not C fibres, and Schwann cells metabolic interactions.

These studies have tended to use young adult rodents and thus make the role and appearance of glycogen metabolism in the developing, adult and mature nervous system unclear. Glycogen metabolism can act as a marker of differentiation, with glycogen present at an almost negligible concentration in undifferentiated neural stem cells and different trophic factors required to induce the expression of glycogen and relevant glycogen metabolism enzymes of differentiating astrocytes (Brunet *et al.*, 2010). This suggests glycogen metabolism is performed efficiently once astrocytes are mature. The role of astrocytes in glycogen metabolism might not however, continue into old age. A recent study has found that with age, neurones show an increased ability to metabolise glycogen, with an increase in glycogen phosphorylase expression in the neurones of the hippocampus (Drulis-Fajdasz *et al.*, 2018). This led the authors to conclude that there is an age-related change in the dependence of hippocampal neurones on astrocyte glycogen (Drulis-Fajdasz *et al.*, 2018).

### 1.3.3 Lactate

Conventionally, lactate is described as a waste product of glycolysis that is harmful when present in the blood. A high concentration of blood lactate is associated with lactate acidosis, which results in a reduction in pH, which can ultimately lead to organ failure and in severe cases death (Foucher & Tubben, 2020). However, emerging insight into the metabolic interactions between axons and glial cells suggests lactate can be used as an effective energy substrate within the nervous system. Glial cells are considered lactate producers, glycolytically metabolising glucose and/or glycogen to lactate, which is then released and taken up by neurones (Powell *et al.*, 2020). Lactate appears to be

required by neurones under active conditions, but it is unclear whether this shuttling of lactate from glia to neurone occurs under resting conditions (Cali *et al.*, 2019).

Lactate is a metabolic dead-end, but conversion to pyruvate by the enzyme lactate dehydrogenase (LDH), in particular LDH1, allows its incorporation into metabolic pathways (Bittar *et al.*, 1996).

Monocarboxylate transporters (MCTs) facilitate cellular lactate uptake. The MCTs are a family of membrane transporters that co-transport monocarboxylates, e.g. lactate, with a proton ( $H^+$ ), therefore are electroneutral, with the direction of transport determined by the transmembrane gradients of the monocarboxylate as well as pH (Bröer *et al.*, 1998). MCT isoforms are differentially expressed by cells of the nervous system and have different affinities for lactate, a property which supports that glia cells release, whilst axons take up, lactate (Bergersen, 2007). MCT2 has the highest affinity for lactate ( $K_m$  of 0.7mM) followed by MCT1 ( $K_m$  of 3.5mM) and MCT4 ( $K_m$  of 35mM) (Bröer *et al.*, 1998, 1999; Bergersen, 2007). For lactate to access the CNS, MCT1 is expressed by the blood brain barrier (Halestrap & Price, 1999). Likewise, MCT1 and MCT4 are expressed on the perineurium of the blood nerve barrier and endoneurium of peripheral nerves (Takebe *et al.*, 2008; Domenech-Estevez *et al.*, 2015), enabling access of lactate to axons of the PNS. In the CNS, axons express MCT2 (Debernardi *et al.*, 2003), whilst oligodendrocytes and astrocytes express MCT1 (Debernardi *et al.*, 2003; Lee *et al.*, 2012). Astrocytes also express MCT4 (Bergersen, 2007). Expression of MCTs in the PNS is less clear but appears to show a similar pattern of expression as the CNS, where Schwann cells mirror the astrocytic expression of MCT1 and MCT4 (Domenech-Estevez *et al.*, 2015). MCT2 is also expressed in the PNS but its expression by specific cell types is unknown, thus it could be expressed by axons as in the CNS (Jha & Morrison, 2020), although there is evidence to suggest axons of the PNS express MCT1 (Domenech-Estevez *et al.*, 2015).

In addition to MCTs there is evidence to suggest lactate maybe released from astrocytes via a lactate permeable channel that is positively modulated by lactate itself (Sotelo-Hitschfeld *et al.*, 2015). In the CNS these channels may be the principal means of lactate release. A recent study has suggested pannexin hemichannels might mediate tonic lactate release, connexin hemichannels and MCTs mediate lactate release during hypoxia and connexin hemichannels mediate lactate release during increased neuronal activity (Karagiannis *et al.*, 2016). Myelinating glial cells, oligodendrocytes and Schwann cells, may also transport lactate in ways not requiring MCTs. Myelin consists of compact and non-compact regions (Philips & Rothstein, 2017). Non-compact myelinic channels run through the compact myelin, acting as transport channels, potentially for metabolites such as lactate, through the oligodendrocyte cytoplasm to the inner most layer of myelin abutting the sub-myelin space (Philips & Rothstein, 2017). Mice lacking CNP, a protein essential to establishing and maintaining these cytoplasmic channels, display axon degeneration suggesting these channels are important for oligodendrocytes to metabolically support axons (Lappe-Siefke *et al.*, 2003; Snaidero *et al.*, 2017). In the PNS, Schmidt-Lanterman Incisures (SLIs) are the equivalent cytoplasmic channels running through myelin. There is conflicting evidence as to whether SLIs can act as transport channels for metabolic substrates across the myelin to the axon (Ghabriel & Allt, 1981), however GLUT1 is expressed by the SLIs (Magnani *et al.*, 1996), suggesting a potential metabolic role. Altogether, this highlights the complexity of axon-glia metabolic interactions.

Since glia produce and release lactate whilst neurones take it up, research into the effective metabolism of lactate by neurones has been conducted. CAP electrophysiology studies using the rodent optic and sciatic nerves found replacing the exogenous supply of 10mM glucose with 20mM lactate resulted in the maintenance of conduction of both the mouse (Brown *et al.*, 2003) and rat (Wender *et al.*, 2000) optic nerve, and A and C fibres in the mouse sciatic nerve (Brown *et al.*,

2012) equally as well as 10mM glucose. It was also found that a loss of conduction, as a result of aglycaemia, of the mouse optic nerve (Brown *et al.*, 2012) and A and C fibres of the sciatic nerve (Brown *et al.*, 2012) could be recovered by 20mM lactate, as efficiently as 10mM glucose. Recovery of conduction requires more energy than simply maintaining conduction due to the restoration of transmembrane ion gradients, thus these findings suggest that lactate can be used efficiently by axons of both the central and peripheral nervous systems.

The use of lactate as an energy substrate by axons has been investigated under the condition of aglycaemia and has revealed the importance of glycogen as the source of lactate. However, glycogen is too large of molecule to be directly transferred from glia to axons and since glial cells possess the key glycogen metabolism enzymes it suggests they metabolise glycogen to a metabolic intermediate, which is then transferred to axons. Lactate is the metabolic intermediate. Preventing the uptake of astrocyte derived lactate through the addition of cinnamate (CIN), an MCT2 inhibitor, was found to accelerate the latency to failure of the mouse optic nerve CAP during substrate free conditions (Brown *et al.*, 2004), implying the use of astrocyte glycogen derived lactate by axons in the CNS when energy substrate availability is limited. Equivalent studies using the mouse sciatic nerve have been conducted in this thesis (see chapter 4) and reveal a similar response of reduced latency to failure of the A fibre CAP with the addition of CIN to substrate free conditions compared to substrate free alone. An earlier study that recorded lactate released from the mouse sciatic nerve showed that this extracellular lactate was rapidly depleted within 20 minutes of aglycaemia (Brown *et al.*, 2012). This, in combination with the delayed failure of the A fibre CAP, suggests A fibre axons rapidly take up and utilise Schwann cell glycogen derived lactate under substrate free conditions. This highlights the similarity in the metabolic interactions between glial cells and axons in the central and peripheral nervous systems. The link between glycogen derived lactate and a metabolic role for oligodendrocytes can be immediately ruled out due to

the absence of glycogen within oligodendrocytes. Despite this, oligodendrocytes are still capable of providing metabolic support to their associated axons in the form of lactate. Using mouse brain slices to record the CAP of the corpus callosum, preloading oligodendrocytes with 40mM lactate was found to prevent complete CAP failure during substrate free conditions (Meyer *et al.*, 2018). In addition, the maintenance of the CAP when oligodendrocytes were preloaded with 20mM glucose during aglycaemia was prevented with the addition of CIN, suggesting oligodendrocytes supply their associated axons with glucose derived lactate during substrate free conditions (Meyer *et al.*, 2018).

Glial cell lactate appears to be an essential energy substrate for axons during limited glucose availability, but also during increased neuronal activity under normoglycemic conditions. CAP electrophysiology studies are described in detail in chapter 4, but suggest Schwann cell and astrocyte lactate is used by axons as an energy substrate to meet their increased metabolic demands (Brown *et al.*, 2003, 2004, 2005). Studies utilising the technique of Forster Resonance Energy Transfer (FRET), where fluorescent nanosensors for particularly energy substrates are genetically encoded into specific cells (San Martín *et al.*, 2014), have provided further support for the metabolic role of astrocytes in providing lactate to axons in response to increased firing activity. In response to stimulation intracellular astrocytic lactate was rapidly depleted (Sotelo-Hitschfeld *et al.*, 2015; Ruminot *et al.*, 2019), accompanied by a reduction in intracellular glucose (Ruminot *et al.*, 2019). It was concluded that neuronal activity triggers an increase in astrocytic glycolysis resulting in increased glucose metabolism and subsequent lactate release for axonal use. This is supported by a modelling study that revealed an initial dip before a rapid rise in the extracellular lactate concentration in response to stimulation (Aubert *et al.*, 2005). This is likely the result of an initial rapid uptake of lactate by axons preceding the increased production of lactate by astrocytes, supporting the coupling of astrocyte glycolysis and lactate production to axonal lactate

metabolism to meet increased energy demands. So far these studies have only investigated the metabolic role of astrocytes, however oligodendrocytes and Schwann cells have been shown to respond to neuronal activity and thus imply their metabolic role under these conditions (Micu *et al.*, 2016, 2018; Saab *et al.*, 2016; Hu *et al.*, 2019).

Exercise is another condition which increases the activity and energy demand of neurones (Matsui *et al.*, 2017). During exercise blood lactate levels increase resulting in an increased uptake and subsequent metabolism in the brain (Dalsgaard *et al.*, 2004), suggesting circulating lactate is metabolised by neurones in order to meet their increased energy demand (Quistorff *et al.*, 2008). Within the brain astrocytic glycogen was found to decrease but was not fully depleted during exhaustive exercise (Matsui *et al.*, 2017). Neuronal MCT2 expression was increased and brain ATP levels maintained, leading to the conclusion that astrocyte glycogen derived lactate fuels the brain during exhaustive exercise and contributes to endurance (Matsui *et al.*, 2017). The importance of astrocyte glycogen derived lactate as an energy substrate in the CNS during exercise is supported by the finding that brain glycogen levels supercompensate i.e. recovery to a higher level than prior to the exercise training (Matsui *et al.*, 2012).

Although evidence suggests astrocytes supply lactate to axons as an energy substrate during increased neuronal activity, there is evidence to suggest otherwise. Firstly, it has been suggested that the time course of the increased lactate production is too slow to provide sufficient energy for neuronal use (Fillenz, 2005), and secondly, a modelling study using imaging data from the primary visual cortex during visual stimulation revealed a net flow of lactate from neurones to astrocytes (Mangia *et al.*, 2009). However, the high temporal resolution of recent FRET studies has revealed astrocytic glycolysis is triggered within seconds of neuronal activity (Bittner *et al.*, 2010) and the modelling study was unable to exclude local astrocyte to neurone lactate transfer that is likely to occur (Mangia *et al.*, 2009), therefore astrocyte derived

lactate can be considered a key energy substrate used by neurones during increased energy demand conditions.

Whether glial cell derived lactate is used by neurones as an energy substrate during resting conditions is still an area of debate. Recording extracellular lactate from the mouse optic (Yang *et al.*, 2014b) and sciatic nerve (Brown *et al.*, 2012; Rich & Brown, 2018b), using lactate biosensors, under baseline conditions of 10mM glucose and minimal stimulation, revealed a stable concentration of extracellular lactate, suggesting astrocytes and myelinating Schwann cells tonically release lactate which axons could use as an energy substrate. This is supported by a FRET study that has revealed a lactate gradient from astrocytes to neurones *in vivo* (Mächler *et al.*, 2016). However, the addition of CIN during baseline conditions has no effect on either the optic nerve (Brown *et al.*, 2003) or A fibre CAP (Rich & Brown, 2018b), suggesting under resting conditions central and peripheral nervous system axons do not necessarily require lactate as an energy substrate. Interestingly, downregulating the expression of oligodendrocyte specific MCT1 in the mouse optic nerve and corpus callosum *in vivo* resulted in axon degeneration (Lee *et al.*, 2012), suggesting axons utilise oligodendrocyte supplied lactate under physiological conditions (Lee *et al.*, 2012).

In addition to the role of lactate as an energy substrate, astrocyte derived lactate has also been shown to act as a signalling molecule. Consistent with its metabolic role, astrocyte derived lactate regulates cerebral blood flow. In response to neuronal activity the increase in astrocytic glycolysis and lactate production results in an increase in extracellular lactate. Although this lactate is metabolised by axons, it can also trigger vasodilation (Gordon *et al.*, 2008). This occurs via the prostaglandin transporter (PGT) which exchanges intracellular lactate for extracellular prostaglandin E<sub>2</sub> (PGE<sub>2</sub>; Chan et al 2002). This transporter is expressed by astrocytes and thus they have a role in the uptake of PGE<sub>2</sub> (Gordon *et al.*, 2008). However, the increase in extracellular lactate results in reduced uptake of PGE<sub>2</sub> by astrocytes

leading to an accumulation of PGE<sub>2</sub> in the extracellular space and vasodilation (Gordon *et al.*, 2008). This would enable increased oxygen and glucose supply to the active brain region. Whether Schwann cells and oligodendrocyte derived lactate also contributes to control of blood flow is unknown. Lactate acts as a signalling molecule via the hydroxycarboxylic acid receptor (HCAR1), a G-protein coupled receptor, highly expressed by neurones in the CNS (Bergersen, 2015). The HCAR1 is coupled to an inhibitory G protein, and when activated by lactate triggers a downstream pathway that reduces intracellular cyclic adenosine monophosphate (cAMP; Abrantes *et al.*, 2019). Lactate acts on the HCAR1 to reduce the activity of both GABAergic and glutamatergic primary cortical neurones (Bozzo *et al.*, 2013), an effect which has been linked to a 'glucose-saving' metabolic role (Morland *et al.*, 2015). Again, whether lactate signalling via HCAR1 occurs in the PNS is unknown.

#### *1.3.4 Physiological and pathophysiological importance*

Metabolic interactions between axons and glial cells are not only a means of energy substrate supply when axonal energy demands are increased but appear important in many physiological processes with disruption associated with pathophysiology (Bak *et al.*, 2018). Glial cell derived lactate is at the heart of many of these physiological processes, both within the central and peripheral nervous system, including pain and learning and memory, highlighting the translatability of this research to humans, with such metabolic interactions potential therapeutic targets

##### *1.3.4.i Learning and memory*

One of the most important functions of astrocyte lactate is the mediation of learning and memory. The hippocampus is a key brain structure involved in learning and memory and is one of the most glycogen rich brain areas (Sagar *et al.*, 1987) and as such astrocytic glycogenolysis has been implicated as key to learning and memory.

An early study using chicks revealed the importance of astrocytic glycogenolysis in memory formation (Gibbs *et al.*, 2006; Gibbs & Hertz, 2008) and prompted further investigations into the role of astrocyte-axon metabolic interactions in learning and memory, which revealed that astrocytic glycogen derived lactate is essential for long-term memory formation (Suzuki *et al.*, 2011). This study involved rat inhibitory avoidance behavioural experiments using the foot shock test in combination with *ex vivo* hippocampal slice electrophysiology to investigate the cellular process of memory formation, long-term potentiation (LTP). 1,4-dideoxy-1,4-imino-D-arabinitol (DAB), a glycogen phosphorylase inhibitor (Andersen & Westergaard, 2002), injected before training had no effect on short-term memory when rats were tested only 1 hour after training, but significantly reduced long-term memory, an effect which persisted for up to a week, but could be reversed by the delivery of 100nmol lactate in combination with DAB prior to training (Suzuki *et al.*, 2011). Knockdown of MCT1 or MCT4, expressed by astrocytes, using anti-sense oligodeoxynucleotides also had no effect on short-term memory formation, but disrupted long-term memory formation (Suzuki *et al.*, 2011). This disruption was reversed by the supply of exogenous lactate (Suzuki *et al.*, 2011). Knockdown of neuronal expressed MCT2 had no effect on short-term but reduced long-term memory (Suzuki *et al.*, 2011). This effect however was not reversed by lactate suggesting the importance of glycogen derived lactate transfer from astrocytes to neurones via MCTs during long-term memory formation. Interestingly, glucose was also not found to recover the long-term memory disruption as the result of MCT2 knockdown (Suzuki *et al.*, 2011), suggesting lactate is the primary energy substrate used by neurones to meet the increased energy demand during LTP. These behavioural results were supported by the finding that DAB injected to the CA1 region of hippocampal slices, prior to high frequency stimulation, prevented the maintenance, but not induction, of LTP, (Suzuki *et al.*, 2011). Supplying lactate in addition to DAB restored LTP, with induction and maintenance induced in response to high frequency stimulation (Suzuki *et al.*, 2011).

An example of the role of astrocytic glycogen derived lactate in memory that is translatable to humans is in memories that associate stimuli with effects. One study looked at the role of astrocytic lactate in the reconsolidation of memories associated with drugs of abuse. Using rats trained for cocaine induced conditioned place preference (cocaine induced CPP) injection of DAB after retrieval of the cocaine paired context or knockdown of MCT1 or MCT2 reduced the cocaine induced CPP score 24 hours later, indicating impairment in memory reconsolidation (Zhang *et al.*, 2016). This impairment was reversed by the additional delivery of 100nmol lactate (Zhang *et al.*, 2016). These mirror the initial study of Suzuki *et al.* (2011) and suggest that the transfer of astrocytic lactate to neurones could act as a therapeutic target for drug addiction.

Since the study by Suzuki *et al.* (2011) research has been conducted to unravel the mechanism of action of astrocytic lactate during long-term memory formation. Lactate promotes the expression of synaptic plasticity related genes in neurones (Yang *et al.*, 2014a). Lactate acts via neuronal N-methyl-D-aspartate (NMDA) receptors to potentiate the inward  $Ca^{2+}$  current following glutamate and glycine binding (Yang *et al.*, 2014a). This triggers the downstream extracellular signal-regulated kinase (Erk) 1/2 signalling cascade to increase the phosphorylation of Erk 1/2, a kinase involved in facilitating neuronal NMDA receptor mediated plasticity (Yang *et al.*, 2014a). In addition to NMDA receptor activity potentiation lactate increases Erk 1/2 phosphorylation as the result of increased intracellular NADH due to neuronal uptake of lactate and conversion to pyruvate, via lactate dehydrogenase, for mitochondrial oxidative metabolism (Yang *et al.*, 2014a). Altogether the increase in neuronal Erk 1/2 signalling cascade increases the expression of the immediate early genes, c-fos, arc and zif268, and the late response gene brain derived neurotrophic factor (BDNF), all of which are key plasticity related genes (Yang *et al.*, 2014a).

It is clear lactate is important for changes in synaptic strength during LTP, thus research has begun to investigate whether LTP is associated

with long-term changes in lactate dynamics. During high frequency stimulation the extracellular lactate response recorded was as expected with an initial dip followed by a rapid increase which reached a peak within ~7 seconds (Bingul *et al.*, 2020). After the induction of LTP, changes in the lactate dynamics were observed 24 hours later and lasted for the total 3 days of the study (Bingul *et al.*, 2020). Lactate dynamics were divided into 1) the acute response seen as an increase in the magnitude of the dip and peak, and 2) the chronic response seen as a rise in extracellular lactate (Bingul *et al.*, 2020). Altogether this suggests that an increase in synaptic strength is associated with potentiation of astrocytic glycolysis and lactate production.

Research into the mechanism of action of lactate has also revealed that varying aspects of lactate metabolism and signalling may be involved in different aspects of learning and memory. Firstly, differences in the roles of MCT isoforms in spatial memory have been suggested. Using specific hippocampal neuronal MCT2 or astrocytic MCT4 downregulated mice it was found that both are required for spatial memory learning and short-term memory formation, whilst only MCT2 is essential for long-term spatial memory formation (Netzahualcoyotzi & Pellerin, 2020). The disruption to long-term memory was explained by the reduction in hippocampal neurogenesis that was also observed in the neuronal MCT2 knock out mice (Netzahualcoyotzi & Pellerin, 2020). Overall, this suggests astrocyte derived lactate is required for neurogenesis and that neuronal and astrocytic MCTs have distinct roles in spatial learning and memory processes. Secondly, lactate metabolism and signalling, via HCAR1, is required differentially within learning and memory formation. This study utilised the lactate enantiomers, L and D-lactate. L-lactate is the enantiomer that is metabolised by cells, whilst D-lactate is the non-metabolisable form, but produced in low concentrations physiologically (Allaman *et al.*, 2015) and blocks the neuronal uptake of L-lactate via competition for MCTs (Flick & Konieczny, 2002). However, both enantiomers are able to act on the HCAR1 (Castillo *et al.*, 2015). Performing inhibitory avoidance

behavioural experiments with rats it was found only an agonist of HCAR1 or D-lactate, not L-lactate, were able to improve memory when injected after learning (Scavuzzo *et al.*, 2020). However, injection of the HCAR1 agonist or D-lactate prior to learning impaired memory, whilst prior injection of L-lactate improved memory (Scavuzzo *et al.*, 2020). Overall, this suggests lactate mitochondrial oxidative metabolism by neurones is required during learning whilst lactate signalling via HCAR1 expressed on neurones is required during consolidation (Scavuzzo *et al.*, 2020).

#### *1.3.4.ii Mental disorders*

The term mental health refers to an individual's state of well-being (WHO, 2018). Deviation from being able to cope with normal stresses, work productively or making contributions to the community is associated with mental disorders (WHO, 2018). There are a wide range of mental disorders with depression considered one of the main causes of disability in the world and stress a common contributing factor to the development of mental disorders (WHO, 2019). A variety of treatments are available from psychotherapy to pharmaceutical medications (WHO, 2019).

Much of the research into mental disorders has focused on the neurotransmitter serotonin (Lin *et al.*, 2014), however research is beginning to uncover a role for astrocytic lactate. Chronic stress shifts the balance of glycogen synthesis and metabolism towards metabolism within hippocampal astrocytes, resulting in a decrease in glycogen levels (Zhao *et al.*, 2017). This finding is supported by the increase in astrocytic lactate production in the medial prefrontal cortex seen in response to stress, an effect that appears to be regulated by both serotonin and glutamate (Uehara *et al.*, 2006, 2007). The association of stress with upregulation of astrocytic lactate production suggests a potential role of astrocyte lactate in mental disorders.

A key feature of major depressive disorder is the passive coping response, known as hopelessness in humans (Yin *et al.* 2020). A recent

study has investigated the role of astrocyte lactate in the passive coping response and involved subjecting mice to the force swim test, where a passive response is characterised by the inability of the mice to escape from the cylinder containing water (Yin *et al.*, 2020). As expected during the forced swim test extracellular lactate in the medial prefrontal cortex increased, with injection of DAB or knockdown of astrocytic MCT4 prior to the behavioural test reducing the passive coping response, seen as a decrease in the immobility time (Yin *et al.*, 2020). In addition, the application of DAB or knockdown of MCT4 resulted in an increase in excitability of neurones in medial prefrontal cortex brain slices (Yin *et al.*, 2020). Both the behavioural and electrophysiology responses were found to be reversed by the delivery of lactate (Yin *et al.*, 2020). This suggests that astrocytic glycolytic lactate production modulates the passive coping response. This may be considered a negative role of astrocytic lactate in that it promotes mental disorders rather than mental disorders being associated with dysregulated neurone-glia metabolic interactions. However, lactate administration produces antidepressant like effects. Peripheral administration of lactate to mouse models of depression has been associated with an increase in the concentration of lactate in the hippocampus as well as the regulation of downstream genes and signalling molecules associated with antidepressant effects including serotonin receptor trafficking, neurogenesis and cAMP (Carrard *et al.*, 2018). This is an exciting area of research with the potential for the development of therapeutic treatments of mental health disorders.

#### *1.3.4.iii Pain*

Pain is defined as ‘an unpleasant sensory and emotional experience associated with, or resembling that associated with, actual or potential tissue damage’ (IASP, 2020). With a third to one half of the UK population suffering from chronic pain (Fayaz *et al.*, 2016) it is clear that understanding of the mechanisms behind all aspects of pain is a clinical priority.

A recent study has suggested that increased lactate production by astrocytes in the dorsal spinal cord contributes to the mechanical hyperalgesia experienced in neuropathic pain. Firstly, reproducing the activation of dorsal horn spinal cord astrocytes, as seen in neuropathic pain, reduced the mechanical threshold of mice (Miyamoto *et al.*, 2019). A similar effect on mechanical threshold was observed in response to intrathecal injection of lactate (Miyamoto *et al.*, 2019). The reduction in threshold in either condition could be reversed by CIN suggesting astrocytic lactate production mediates the mechanical hypersensitivity (Miyamoto *et al.*, 2019). Further investigations to study the mechanism of action of lactate revealed increased extracellular lactate upregulated dorsal horn spinal cord neurone expression of activated neuronal markers including c-fos, a response which was also reversed by CIN (Miyamoto *et al.*, 2019). Overall, this suggests increased production of astrocytic lactate contributes to mechanical hyperalgesia by maintaining neuronal activity. Again, this study implies a negative physiological role of astrocytic lactate, however astrocytic lactate may be a potential therapeutic target of cognitive processing of chronic visceral pain (Wang *et al.*, 2017). Visceral pain is associated with cognitive deficits including impaired decision making (Cao *et al.*, 2016), which involves processing in the anterior cingulate cortex, an area of the brain also key to the processing and perception of visceral pain (Cao *et al.*, 2008). LTP, a physiological process that astrocytic lactate plays an important role in, is known to be disrupted in the anterior cingulate cortex of rats experiencing visceral hypersensitivity (Wang *et al.*, 2015), therefore investigations into the role of astrocytic lactate in the decision making impairments of visceral pain were conducted. Using a visceral hypersensitivity rat model, delivery of lactate to the anterior cingulate cortex improved decision making of rats during a gambling task and restored LTP in the anterior cingulate cortex (Wang *et al.*, 2017). This initially suggests a requirement for lactate in appropriate decision making processing, but to confirm astrocytes as the source of lactate optogenetic manipulation was used to activate astrocytes of the anterior cingulate cortex. Firstly, this resulted in an increase in the concentration

of lactate in the extracellular space and secondly, improved decision making of visceral hypersensitive rats, an effect that was prevented by prior infusion of CIN (Wang *et al.*, 2017). This study, in contrast to the Miyamoto *et al.* (2019) study, suggests a reduction in astrocytic lactate production is associated with cognitive impairments of visceral pain and therefore lactate could be a potential treatment. The contrasting findings from these two studies highlight the complexity of pain processing and may imply a differential role for astrocytic lactate in the different aspects of pain.

#### *1.3.4.iv Myelin and axon physiology*

Myelination is considered the key function of Schwann cells and oligodendrocytes in the peripheral and central nervous systems, respectively. However, the metabolic role of Schwann cells and oligodendrocytes is beginning to be unravelled, with this role potentially important to their ability to myelinate effectively and maintain axon physiology.

A recent study found that knockout of the Schwann cell specific MCT1 had no effect on peripheral nerve morphology or function in young mice, but did result in hypomyelination and reduced the conduction velocity of sensory, but not motor, axons of mature mice (Jha *et al.*, 2020*b*). This was associated with a reduction in Schwann cell glycolysis and mitochondrial oxidative metabolism, ultimately causing reduced lipid production and increased lipid metabolism, resulting in insufficient lipids for myelin production (Jha *et al.*, 2020*b*). Overall, this suggests a role of Schwann cell lactate in maintaining myelination of peripheral axons during aging. Similarly, oligodendrocyte lactate production appears important for the maintenance of myelin in the CNS.

Genetically preventing mitochondrial oxidative metabolism of mature oligodendrocytes of mice was found to have no effect on CNS myelin, inflammation or cause pathology (Fünfschilling *et al.*, 2012). An increase in brain lactate was also detected suggesting oligodendrocyte glycolysis and lactate production is sufficient to maintain myelination

(Fünfschilling *et al.*, 2012). In contrast this study found inhibiting Schwann cell mitochondrial oxidative metabolism did result in hypomyelination, reduced conduction velocity and peripheral neuropathy suggesting Schwann cell lactate is insufficient to maintain peripheral myelin (Fünfschilling *et al.*, 2012). Furthermore another study using mice with Schwann cell specific mitochondrial metabolism deficits found these mice displayed severe peripheral neuropathy with early loss of small non-myelinated fibres followed by larger diameter axons, whilst there was no effect on Schwann cell survival (Viader *et al.*, 2011). These studies imply that not only is Schwann cell glycolysis important but mitochondrial oxidative metabolism is also required.

The separate metabolic pathways of Schwann cells have been proposed to play distinct roles in physiological processes, with Schwann cell glycolysis and lactate production required to maintain axon physiology and function, whereas mitochondrial oxidative metabolism is required for the production and maintenance of myelin (Deck *et al.*, 2020). The importance of Schwann cell lactate in maintaining axon physiology rather than myelin is supported by a study that found knockout of Schwann cell specific MCT1 resulted in disrupted motor end plate innervation, but normal myelination of peripheral nerves (Bouçanova *et al.*, 2021). The findings from this study contradicts those of Jha *et al.* (2020b) and Viader *et al.* (2011), both in terms of myelination and the subtype of axons affected. A possible explanation for the discrepancies in results could be that Schwann cell lactate is required to maintain axon physiology and function during high energy demand processes and less so during normal physiological conditions. In support of this, downregulation of MCT1 expression in the mouse sciatic nerve had no effect on the physiology or morphology of uninjured nerves whilst injured nerves showed delayed regeneration (Morrison *et al.*, 2015).

Like Schwann cells, metabolic interactions between axons and oligodendrocytes also appear important in maintaining axon physiology and function. Nonspecific down regulation of MCT1 causes widespread

axonopathy in the CNS but has no effect on myelination or oligodendrocyte number (Lee *et al.*, 2012). This suggests oligodendrocyte lactate supply to axons is required for axon survival and was further confirmed by the axon degeneration observed in the corpus callosum and optic nerve, white matter tracts, of mice with oligodendrocytes which show reduced MCT1 expression (Lee *et al.*, 2012).

An interesting area of research into the metabolic role of glial cells in myelination is the potential cooperation between oligodendrocytes and astrocytes in the CNS. A recent study found inhibiting glycogen breakdown, i.e. reducing astrocytic lactate production, in a mouse model of remyelination, prevented myelin recovery and reduced the oligodendrocyte number without affecting astrocyte or microglia activation (Ichiara *et al.*, 2017). This initially suggests astrocyte glycogen metabolism contributes to remyelination and was further investigated using oligodendrocyte progenitor cell cultures. Supply of lactate, in addition to glucose, was found to increase axon survival and promote cell cycling and differentiation, an effect that was reduced by CIN (Ichiara *et al.*, 2017). These results suggest astrocyte glycogen derived lactate supports oligodendrocytes during remyelination.

#### 1.3.4.v Diabetes

In England in 2017/2018 £5.6 billion was spent on hospital care for diabetic patients (Stedman *et al.*, 2020). The cost to the National Health Service (NHS) and high prevalence highlights the importance of understanding this disease. The sciatic nerve is particularly vulnerable to diabetes with peripheral neuropathy the most common form of diabetic neuropathy (NIDDK, 2021). Since diabetes is a metabolic disorder, understanding metabolic interactions between axons and Schwann cells in this disease state could provide a novel therapeutic target. In particular MCT1 has been proposed as a potential therapeutic target of diabetic peripheral neuropathy. Streptozotocin (STZ) induced diabetic mice were found to display reduced MCT1 expression in the

sciatic nerve and dorsal root ganglia, immediately suggesting changes to Schwann cell to axon lactate transfer (Jha *et al.*, 2020a). This prompted experiments using mice with reduced MCT1 expression leading to the finding that inducing diabetes in these mice resulted in exacerbated diabetic peripheral neuropathy, with impaired sensory and motor conduction velocity, associated with the reduced g-ratio, and reduced mechanical sensitivity (Jha *et al.*, 2020a). It appears impairment in Schwann cell lactate supply to axons as the result of diabetes may contribute to the subsequent peripheral neuropathy.

Diabetes is not only associated with damage to peripheral nerves, but impairments within the CNS are also apparent. In particular memory impairments associated with hippocampal damage may be an early sign of diabetes (Gold *et al.*, 2007). The role of astrocyte glycogen derived lactate in memory formation triggered investigations into this role within diabetes. Using a rat model of human type 2 diabetes, these rats performed worse on the Morris water maze task compared to controls, indicating spatial memory impairment as expected (Shima *et al.*, 2017). Investigations into the metabolic role of astrocytes revealed increased hippocampal glycogen content but reduced neuronal MCT2 expression and astrocytic GLUT1 expression, suggesting a dysregulation of astrocytic glycogen metabolism (Shima *et al.*, 2017). Exercise is a suggested treatment for many type 2 diabetic patients; therefore the next stage of this study was to investigate the influence of exercise on cognition and astrocytic glycogen metabolism. Four weeks of moderate exercise improved behavioural test performance, restored MCT2 and GLUT1 expression as well as increased glycogen content (Shima *et al.*, 2017). These findings imply dysregulation of hippocampal astrocytic glycogen derived lactate to neurones contributes to memory impairments associated with diabetes. An interesting finding of this study was the increased hippocampal glycogen of diabetic rats, which was further increased with exercise. An increase in hippocampal glycogen is common in other disorders associated with memory impairments e.g. epilepsy (Dalsgaard *et al.*, 2007), thus may be a

common feature of hippocampal dysfunction and an adaptive process due to reduced glucose uptake (Shima *et al.*, 2017).

#### *1.3.4.vi Neurodegenerative diseases*

Neurodegenerative disease describes a group of disorders characterised by the progressive loss of neurones (Dugger & Dickson, 2017). The major neurodegenerative diseases include Alzheimer's disease, Parkinson's disease and amyotrophic lateral sclerosis (ALS) (Erkkinen *et al.*, 2018).

Alzheimer's disease is characterised by the formation of amyloid  $\beta$  plaques and neurofibrillary tangles, both of which accumulate in neurones of the hippocampus (Perl, 2010). Glial cell lipid droplet accumulation is also thought to occur in neurodegenerative diseases as the result of neuronal mitochondrial deficits and increased reactive oxygen species increasing neuronal lipid production, which is subsequently transferred to glial cells (Liu *et al.*, 2015). The importance of glial cell lipid droplet accumulation is unknown but suggests an association between neuronal metabolism and neurodegenerative diseases. This transfer of lipids between neurones and glial cells requires transporters known as apolipoproteins. A recent study has found that lactate, supplied by glial cells via MCTs, fuels neuronal lipid synthesis and that the transfer of lipids from neurones to astrocytes requires apolipoproteins (Liu *et al.*, 2017). The apolipoprotein E4 allele is considered a major risk factor of Alzheimer's disease (Farrer *et al.*, 1997). Interestingly, it was found that the expression of this transporter significantly reduced glial cell lipid droplet accumulation, suggesting glial cell lipid droplet accumulation, ultimately as the result of glial cells supply of lactate to neurones, acts as a neuroprotective agent (Liu *et al.*, 2017).

Communication, potentially metabolic, between astrocytes and oligodendrocytes could also be affected in the neurodegenerative diseases, ALS and multiple sclerosis. In both diseases the astrocyte connexin 43 is upregulated whilst the oligodendrocyte 32 and 47 is

downregulated (Markoullis *et al.*, 2012; Cui *et al.*, 2014). Further research is required to determine whether this is associated with a dysregulation in metabolic communication. More specifically, MCT1 expression is reduced in the motor cortex of ALS patients and reduced specifically in oligodendrocytes of mice models of ALS (Lee *et al.*, 2012). In both cases oligodendrocyte number was not found to decrease, suggesting disruption to the metabolic role of oligodendrocytes may contribute to the neurodegeneration seen in ALS (Lee *et al.*, 2012).

## 1.4 Axon-glia metabolic signalling

The literature described so far clearly illustrates the ability of glial cells to produce and supply energy substrate to their associated axons, particularly when the energy demand of the axons is increased. This means the glial cells require a mechanism by which they are able to detect changes in the energy demand of the axons to subsequently up and down regulate their metabolism. Therefore, a signal(s) must be released from axons that communicates the need for metabolic support to the glial cells. This raises the questions: 1) what signal(s) released from axons triggers glial cell metabolism, and 2) are these metabolic signals universal amongst the different subtypes of glial cells. Many different signals have been suggested including various neurotransmitters and neuropeptides (Zhou *et al.*, 2019), but the remainder of this chapter will focus on glutamate, ammonium and  $K^+$ .

For the signal(s) to be effective it must possess specific attributes including: 1) rapidly increases, 2) rapidly removed from the extracellular space to prevent over stimulation, 3) reflects the degree of neuronal activity, and 4) can be sensed by the glial cells.

### 1.4.1 Glutamate

Glutamate was the first signal to be suggested, particularly in terms of astrocyte-axon metabolic signalling, resulting in the astrocyte-neurone lactate shuttle hypothesis (ANLSH; Pellerin & Magistretti, 1994; Pellerin *et al.*, 1998; figure 1.6). At the synapse, astrocytes play a key role in the recycling of glutamate. Astrocytes take up extracellular glutamate, preventing over activation of the postsynaptic receptors, and convert it to glutamine, before it is shuttled back to the presynaptic neurones for the resynthesis to glutamate (Danbolt, 2001). The ability of astrocytes to respond to increases in extracellular glutamate not only enables glutamate shuttling back to neurones but has also been found to trigger astrocyte glycolysis i.e. pairing increased neuronal activity with increased astrocytic energy substrate supply. Utilising cultures of mouse cerebral cortex astrocytes the addition of glutamate increased

their uptake and phosphorylation of [<sup>3</sup>H]-2deoxyglucose (2DG), an analogue of glucose that is only metabolised by hexokinase before inhibiting the glycolytic pathway, in a dose-dependent manner (Pellerin & Magistretti, 1994). The addition of antagonists to glutamate receptors did not prevent this, nor did agonists produce comparable effects (Pellerin & Magistretti, 1994). The application of an inhibitor of the glutamate transporter, DL-threo-P-hydroxyaspartate (THA), did abolish the increased glucose uptake by astrocytes (Pellerin & Magistretti, 1994). Astrocytic glutamate uptake is facilitated by the Na<sup>+</sup> coupled excitatory amino acid transporter (EAAT). The EAAT co-transporters glutamate and Na<sup>+</sup> down their concentration gradients (Magi *et al.*, 2019). Under physiological conditions this is a net influx and this results in an increase in the concentration of intracellular Na<sup>+</sup>, which must be restored by the energy dependent Na<sup>+</sup>/K<sup>+</sup> ATPase (Bouvier *et al.*, 1992). Supporting evidence for a role for glutamate is that its uptake triggers astrocyte metabolism, where either removal of the bath Na<sup>+</sup> or inhibition of the Na<sup>+</sup>/K<sup>+</sup> ATPase with ouabain resulted in reduced glutamate stimulated glucose uptake (Pellerin & Magistretti, 1994). To confirm that glutamate triggers astrocyte glycolysis and increases the supply of lactate available to neurones, the levels of lactate and pyruvate were measured using enzymatic spectrophotometry (Pellerin & Magistretti, 1994). As expected, glutamate increased the release of both lactate and pyruvate which was prevented by THA and the GLUT inhibitor Cytochalasin B (CCB; Pellerin & Magistretti, 1994). Overall, astrocytes take up glutamate, released from active neurones, coupled to Na<sup>+</sup> uptake, which in turn activates the Na<sup>+</sup>/K<sup>+</sup> ATPase. The ATP demand of the Na<sup>+</sup>/K<sup>+</sup> ATPase is met by an increase in glucose uptake and glycolysis, resulting in increased production and release of lactate from astrocytes into the extracellular space. Thus glutamate is considered an effective activity dependent metabolic signal between astrocytes and neurones.

Although oligodendrocyte cell bodies are not present at the synapse, the main site of neurotransmitter release, there is evidence to suggest

glutamate acts as a metabolic signal at the axo-myelinic synapse (figure 1.7). However, a key difference is the action of glutamate on the receptors expressed by oligodendrocytes rather than its uptake. Activating NMDA and  $\alpha$ -Amino-3-hydroxy-5-methyl-4-isoxazolepropionic acid (AMPA) receptors expressed by oligodendrocytes of rodent optic nerves results in an increase in myelin  $\text{Ca}^{2+}$  (Micu *et al.*, 2016). Rather than influx, the rise in myelin  $\text{Ca}^{2+}$  is the result of voltage gated calcium channels on the intranodal axon membrane, which sense depolarisation and mediate ryanodine receptors to release  $\text{Ca}^{2+}$  from the internal axoplasmic reticulum (Micu *et al.*, 2016). The rise in myelin  $\text{Ca}^{2+}$  triggers increased oligodendrocyte expression of GLUT1, enabling increased glucose uptake and subsequent lactate production and release (Saab *et al.*, 2016). This indicates that glutamate released by axons acts on glutamate receptors on oligodendrocytes to increase glycolysis and subsequent lactate release, leading to the term axo-myelinic synapse (Micu *et al.*, 2018).

The axo-myelinic synapse in addition to the ANLSH highlights the efficiency of glutamate as a metabolic signal within the CNS, irrespective of its mechanism of action. Whether via EAAT uptake into astrocytes or binding to NMDA and AMPA receptors expressed by oligodendrocytes, axonally released glutamate ultimately triggers glial cells glycolysis and lactate efflux.

There is much less information available regarding glutamate as a metabolic signal within the PNS. However, its presence in the cell bodies, axons and terminals of sensory and motor neurones of peripheral nerves (Battaglia & Rustioni, 1988; De Biasi & Rustioni, 1988; Westlund *et al.*, 1989; Meister *et al.*, 1993; Malet & Brumovsky, 2015) raises the question, can Schwann cells respond to axonal released glutamate and if so, what is the mechanism of action of glutamate? In addition to the expression of functional NMDA, AMPA and kainate glutamate receptors, Schwann cells also express glutamate transporters (Carozzi *et al.*, 2008; Campana *et al.*, 2017). This implies the potential for glutamate to trigger Schwann cell glycolysis as the

result of uptake, as with astrocytes, but also as the result of increased intracellular  $\text{Ca}^{2+}$  via ionotropic glutamate receptors as occurs in oligodendrocyte myelin. Experiments conducted using squid giant axons provided the earliest evidence for glutamate signalling between Schwann cells and axons. Using sharp electrodes to measure the membrane potential of Schwann cells, it was found that Schwann cells respond to glutamate receptor agonists and electrical stimulation of the nerve with an initial depolarisation followed by hyperpolarisation, an effect that was blocked by glutamate receptor antagonists (Lieberman *et al.*, 1989). The depolarisation of the Schwann cell membrane potential was found to not trigger the subsequent hyperpolarisation but instead these were revealed to be separate events mediated by separate mechanisms. The depolarisation was shown to be the result of glutamate acting on tetrodotoxin (TTX)-sensitive  $\text{Na}^+$  permeable glutamate receptors, whilst hyperpolarisation was due to glutamate acting on kainate/quisqualate receptors causing an increase in intracellular  $\text{Ca}^{2+}$  (Lieberman & Sanzenbacher, 1992). The increase in intracellular  $\text{Ca}^{2+}$  subsequently triggers acetylcholine release, which then acts on nicotinic autoreceptors to reduce outward  $\text{Cl}^-$  conductance and hyperpolarise the membrane potential (Lieberman & Sanzenbacher, 1992). More recent evidence has shown that cultured Schwann cells release exosomes in response to increased intracellular  $\text{Ca}^{2+}$  as the result of glutamate exposure (Hu *et al.*, 2019). These Schwann cell derived exosomes were found to increase neuronal activity, suggesting not only can axons signal to Schwann cells, but that Schwann cells can positively feedback to axons (Hu *et al.*, 2019). Although more research is still required this initial data suggests Schwann cells respond to axonally released glutamate via glutamate receptors, similar to oligodendrocytes, rather than through uptake as occurs in astrocytes.

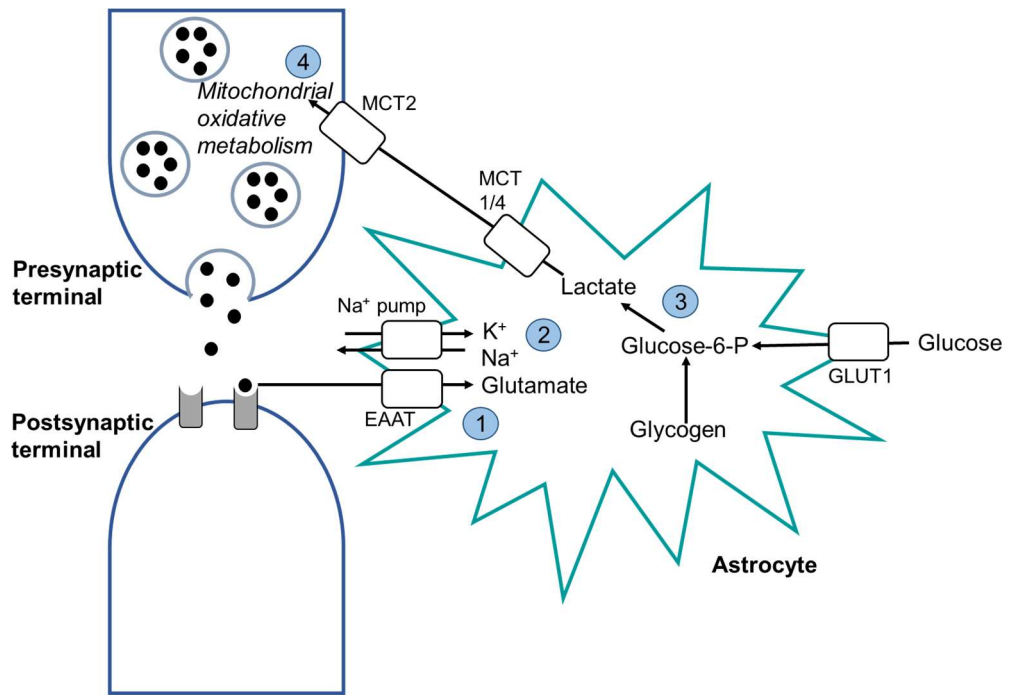


**Figure 1.6:** The astrocyte-neurone lactate shuttle hypothesis (ANLSH). Glutamate (filled circles) released at the synapse, is taken up by astrocytes along with Na<sup>+</sup> via the EAAT (1). The rise in intracellular Na<sup>+</sup> activates the Na<sup>+</sup>/K<sup>+</sup> ATPase (Na<sup>+</sup> pump, 2), which in turn triggers glycolysis (3) and lactate production. Astrocytes then release this lactate for neurones to use it as an energy substrate (4). GLUT= glucose transporter and MCT= monocarboxylate transporter. (Pellerin & Magistretti, 1994).

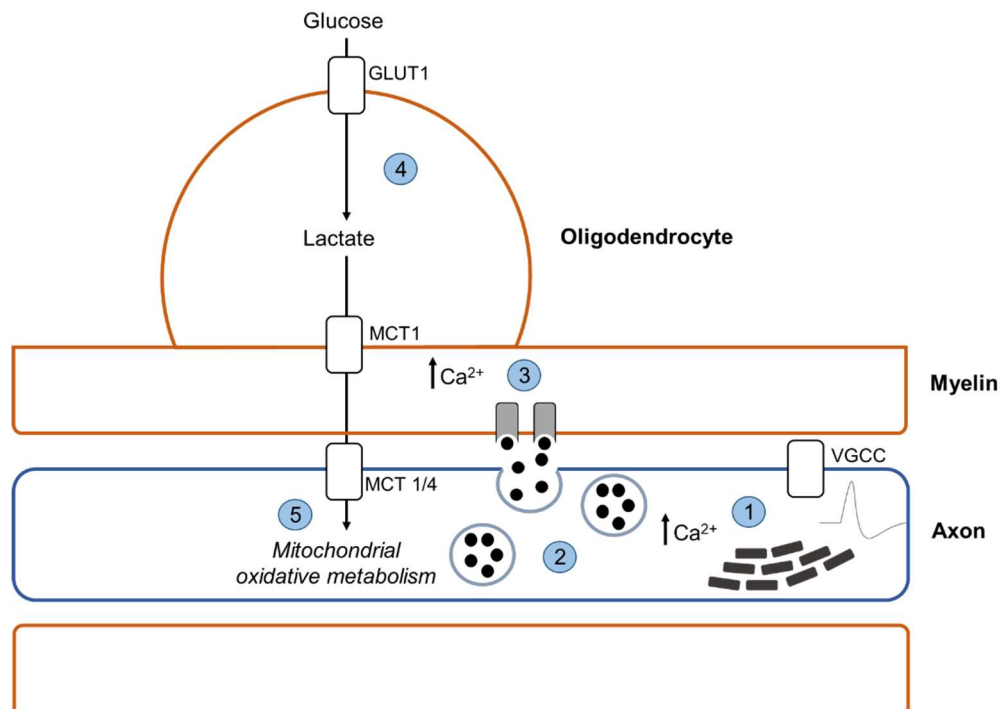


**Figure 1.7:** The axo-myelinic synapse. Voltage gated Ca<sup>2+</sup> channels (VGCC) sense depolarisation of the axon membrane potential and trigger Ca<sup>2+</sup> release from the axoplasmic reticulum (1). The increase in intracellular Ca<sup>2+</sup> triggers glutamate release from the internode (2), which then act on AMPA and NMDA receptors in overlying myelin causing a rise in Ca<sup>2+</sup> in the myelin cytoplasm (3). This stimulates increased glucose influx and glycolytic production of lactate by the oligodendrocyte (4). This lactate is then released, making it available for the associated axons to take up and use as a source of energy (5). GLUT= glucose transporter and MCT= monocarboxylate transporter. (Micu *et al.*, 2018).

### 1.4.2 Ammonium

Ammonium (NH<sub>4</sub><sup>+</sup>) has been proposed as a signalling compound. NH<sub>4</sub><sup>+</sup> is produced as a result of the glutamate-glutamine cycle when neurones convert glutamine back to glutamate and release it into the extracellular space during neuronal activation. Little is known about its role in PNS metabolic signalling, but it is released from frog sciatic nerve (Tashiro, 1922). More is known about its mechanism of action as a metabolic signal between astrocytes and axons of the CNS.

Genetically encoding cultured hippocampal astrocytes to express the lactate sensing FRET nanosensor Laconic demonstrated the presence of lactate in the cytosol of astrocytes, which increased with the addition of NH<sub>4</sub><sup>+</sup> (Lerchundi *et al.*, 2015). This increase was further enhanced by

an MCT blocker (1 $\mu$ M AR-C155858), suggesting that NH<sub>4</sub><sup>+</sup> stimulates astrocytic production and release of lactate (Lerchundi *et al.*, 2015). However, using cells genetically encoded with a glucose nanosensor it was revealed that glucose levels did not change in response to NH<sub>4</sub><sup>+</sup>, implying NH<sub>4</sub><sup>+</sup> does not stimulate astrocytic glycolysis, unlike glutamate (Lerchundi *et al.*, 2015). It was instead hypothesised that the lactate release was due to inhibition of mitochondrial pyruvate uptake. Pyruvate is co-transported into mitochondria with H<sup>+</sup>, thus H<sup>+</sup> must be at a higher concentration in the cytosol compared to the mitochondrial matrix (Lerchundi *et al.*, 2015). Genetically encoded FRET nanosensors for pH revealed that the matrix acidifies, but FRET nanosensors for pyruvate measured an increase in cytosolic pyruvate, implying that NH<sub>4</sub><sup>+</sup> is taken up into the mitochondria, increasing the H<sup>+</sup> concentration and preventing pyruvate uptake (Lerchundi *et al.*, 2015). The pyruvate is then converted to lactate and released from astrocytes for neuronal use (Lerchundi *et al.*, 2015; figure 1.8).

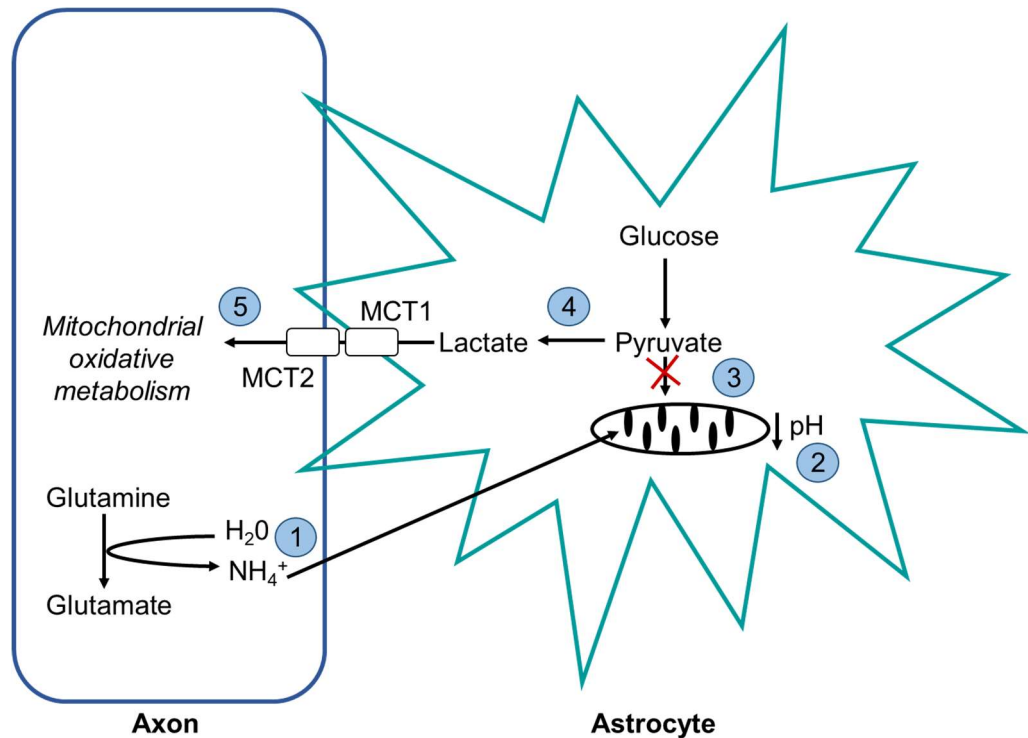


**Figure 1.8:**  $\text{NH}_4^+$  as a metabolic signal between axons and astrocytes.  $\text{NH}_4^+$ , produced as a by-product of glutamate synthesis, is released from neurones is taken up into the mitochondria of astrocytes (1). The increased  $\text{H}^+$  concentration and therefore acid conditions of the mitochondrial matrix (2) prevents  $\text{H}^+$  coupled pyruvate uptake via monocarboxylate transporters (3). Instead the pyruvate is converted to lactate (4) and released into the extracellular space for axons to use as an energy substrate (5). MCT= monocarboxylate transporter. (Lerchundi *et al.*, 2015).

### 1.4.3 Potassium

Although the evidence suggests glutamate acts an effective metabolic signal between axons and glial cells, its role is controversial. Firstly, a key aspect of the ANLSH is the preferential fuelling of the  $\text{Na}^+/\text{K}^+$  ATPase by glycolytic ATP. However, there is now evidence to suggest that ATP from mitochondrial oxidative metabolism mainly fuels the  $\text{Na}^+/\text{K}^+$  ATPase (Fernández-Moncada & Barros, 2014), potentially undermining the theory. Secondly, glutamate as the metabolic signal between glial cells and neurones can be applied to glutamatergic neurones but does not include for example inhibitory GABAergic neurones, therefore cannot be considered a universal metabolic signal.  $\text{K}^+$ , however is released by all axons during the repolarisation phase of the action potential, therefore  $\text{K}^+$  would make an ideal metabolic signal

due to its universality, but also because it is an ideal indicator of metabolic demand, where the accumulation of extracellular K<sup>+</sup> broadly represents the degree of neuronal activity (Baylor & Nicholls, 1969).

Glial cells, in particular astrocytes, are considered ideal sensors of extracellular K<sup>+</sup> due to their membrane potential determined solely by K<sup>+</sup> in a manner predicted by the Nernst equation (Kuffler *et al.*, 1966; eq 1.1).

**Eq 1.1:**

$$E_X = \frac{RT}{zF} \log_{10} \frac{[X]_o}{[X]_i}$$

Where E<sub>x</sub> is the reversal potential for a particular ion (X, concentration in mM), R is gas constant (8.315 J mol<sup>-1</sup> K<sup>-1</sup>), T is the temperature in Kelvin, Z is the valence of the ion and F is Faraday's constant (96,500 C mol<sup>-1</sup>). This can be simplified to:

$$E_X = 61.5 \log_{10} \frac{[X]_o}{[X]_i}$$

at 37°C and an ion valency of +1.

Kuffler is credited for the first membrane potential recordings of glial cells. From the invertebrate model, the leech, in 1964 where the large glial cell from ganglia of the CNS had resting membrane potentials of -60 to -75mV, did not fire an action potential in response to current injection but were electrically connected to each other (Kuffler & Potter, 1964).

Investigations then progressed on to a vertebrate model, the mud puppy optic nerve (Kuffler *et al.*, 1966). The membrane potential of the associated glial cells was recorded using intracellular sharp electrodes and revealed highly hyperpolarised potentials of ~-90mV (Kuffler *et al.*, 1966). Like the leech glial cells, mud puppy glial cells also showed a passive response to injected current as well as electrical connections to other glia (Kuffler *et al.*, 1966).

The match between the mud puppy optic nerve glial cell resting membrane potential and the estimated equilibrium potential of  $K^+$  led to investigations into the role of  $K^+$  in determining the membrane potential. Changing the concentration of  $K^+$  in the extracellular solution revealed that the membrane potential of the nerve changed by 59mV (59 not 61.5 due to recordings taking place at 23°C not 37°C) with a 10-fold change in  $K^+$ , as predicted by the Nernst equation (Kuffler *et al.*, 1966; eq 1.2 and figure 1.9).

**Eq 1.2:**

**A)  $[K]_o = 3mM$ ,  $[K]_i = 99mM$**

$$E_K = 59 \log_{10} \frac{3}{99}$$

$$E_K = -90mV$$

**B)  $[K]_o = 30mM$ ,  $[K]_i = 99mM$**

$$E_K = 59 \log_{10} \frac{30}{99}$$

$$E_K = -31mV$$

The difference in  $E_K$  between A and B = **59mV**

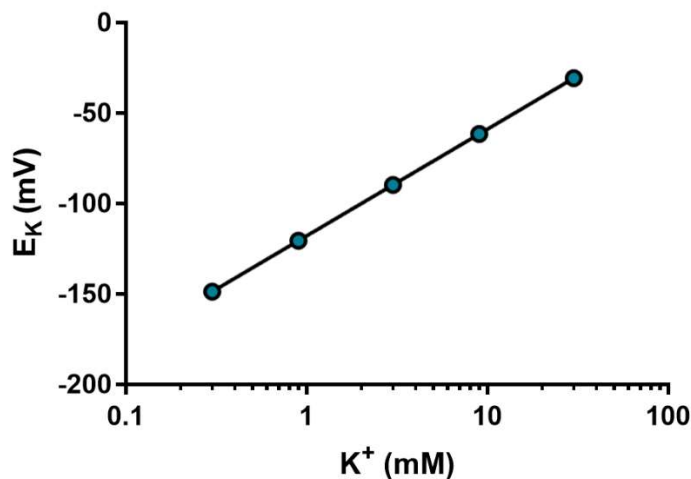


**Figure 1.9:** Nernstian relationship for K<sup>+</sup>. The Nernst equation ( $E_X = \frac{RT}{zF} \log_{10} \frac{[X]_o}{[X]_i}$ ) can be plotted as  $y=mx$  (equation of a straight line) on a log scale, where  $y$  is  $E_X$ ,  $m$  is  $\frac{RT}{zF}$  and  $x$  is  $\log_{10}[X_o]$  ( $[X_i]$  can be omitted since this remains unchanged). The line plotted here is for K<sup>+</sup> at 23°C, with a slope of 59mV i.e. for a 10 fold change in extracellular K<sup>+</sup> the reversal potential for K<sup>+</sup> ( $E_K$ ) changes by 59mV.

As a result of recording the membrane potential at a range of extracellular K<sup>+</sup> concentrations it was also possible to determine the intracellular K<sup>+</sup> concentration. When the membrane potential recorded is 0mV this indicates that the intracellular K<sup>+</sup> concentration is equal to that of the extracellular since  $\log_{10}(1) = 0$  and  $59 \times 0 = 0\text{mV}$ . Thus, at an extracellular K<sup>+</sup> concentration of 99mM the membrane potential was 0mV indicating the intracellular concentration of glial cells is 99mM (Kuffler *et al.*, 1966).

With the evidence clearly indicating the selectivity of glial cells to K<sup>+</sup> and axons a source of K<sup>+</sup> during neuronal activity investigations progressed towards the effects of nerve stimulation on the glial cell membrane potential. It was initially found that a single electrical stimulus to the *ex vivo* preparation or a flash of light into the eye of the *in vivo* preparation resulted in a transient depolarisation of glial membrane potential, whilst during a train of 3 stimuli, 1 second apart, the depolarisation is summed with each stimulus (Orkand *et al.*, 1966). If K<sup>+</sup>, released from axons, causes the depolarisation of the glial cell membrane potential, then an

increase in extracellular  $K^+$  will result in greater depolarisation at lower compared to higher extracellular concentrations i.e. the closer the extracellular/intracellular ratio is to 1 the smaller the change in membrane potential (Orkand *et al.*, 1966; eq 1.3).

**Eq 1.3:**

**A)**  $[K]_o = 3\text{mM}$ ,  $[K]_i = 99\text{mM}$

$$3/99 = \mathbf{0.03}$$

$$E_K = 59 \log_{10} \frac{3}{99}$$

$$E_K = -90\text{mV}$$

**B)**  $[K]_o = 8\text{mM}$ ,  $[K]_i = 99\text{mM}$

$$8/99 = \mathbf{0.08}$$

$$E_K = 59 \log_{10} \frac{8}{99}$$

$$E_K = -64\text{mV}$$

**C)**  $[K]_o = 13\text{mM}$ ,  $[K]_i = 99\text{mM}$

$$13/99 = \mathbf{0.13}$$

$$E_K = 59 \log_{10} \frac{13}{99}$$

$$E_K = -52\text{mV}$$

The difference in  $E_K$  between A and B = **26mV**

The difference in  $E_K$  between B and C = **12mV**

As predicted by the Nernst equation stimulating the nerve in the presence of 3mM  $K^+$  caused a depolarisation of ~12mV, but in the presence of 4.5mM  $K^+$  the depolarisation was only ~9mV whilst lowering the extracellular  $K^+$  to 1.5mM caused a depolarisation of 18.5mV during a single stimulation (Orkand *et al.*, 1966). This was further confirmed by calculating the increase in extracellular  $K^+$  required to produce the summated depolarisations of the glial membrane potential in response to a train of 9 stimuli. As predicted the amplitudes

of each summated depolarisation was successively reduced, but the increase in extracellular  $K^+$  was predicted to be 0.25mM with each stimulus (Orkand *et al.*, 1966).

The findings from Kuffler provide convincing evidence for the selective permeability of glial cells to  $K^+$ , however the mud puppy is a simple vertebrate model and thus reduces its translational value to humans. Studies progressed to investigating mammalian glial cells of the CNS, in particular the cat cortex. These experiments tended to be *in vivo* preparations in which the membrane potential of glial cells of the cortex is recorded using sharp microelectrodes from an anaesthetised cat. The resting membrane potential of these cells was found to vary between -50 and -95mV and slowly depolarise, but not generate impulses, in response to stimulation of the cortex, much like those of the leech and mud puppy (Pape & Katzman, 1972). In addition a change of 60mV for a 10-fold change in  $K^+$  was recorded and the intracellular concentration of  $K^+$  was calculated to be 200mM (Ransom & Goldring, 1973). This suggests mammalian glial cells are primarily permeable to  $K^+$ .

These studies do not definitively define the particular glial cell in which recordings were from, although astrocytes are the most likely candidate. A fairly recent study has recorded from astrocytes of adult mouse and rat optic nerves and revealed that astrocytes are a heterogenous population in that they can be divided into two groups with mean resting membrane potentials of -52 and -74mV (Bolton *et al.*, 2006). The fairly hyperpolarised nature suggests a dominant role of  $K^+$  in mediating the astrocyte membrane potential. Using a blocker of inwardly rectifying  $K^+$  (Kir) channels the membrane potential of astrocytes was found to depolarise resulting in a mean value of -30mV (Bolton *et al.*, 2006). The actions of Kir in determining the resting membrane potential is thought to occur through cAMP. Increasing cAMP using dbcAMP or activating adenylyl cyclase using forskolin resulted in a mean membrane potential of -70mV (Bolton *et al.*, 2006). Moreover, blocking protein kinase A (PKA) caused a similar effect as blocking Kir and resulted in a mean membrane potential of -40mV, that

was partially reversed by dbcAMP, suggesting cAMP acts via PKA dependent and independent pathways (Bolton *et al.*, 2006). Overall the membrane potential recorded when upregulating the pathway is comparable with the more hyperpolarised group, whilst downregulating the pathway results in membrane potentials similar to that of the less negative group, implying the strongly negative resting membrane potential group of astrocytes appears to depend on Kir channels (Bolton *et al.*, 2006).

The accepted sensitivity of the astrocyte membrane potential to  $K^+$  has prompted research into  $K^+$  as a metabolic signal between axons and astrocytes. The predominant paper in this area of research alluded to the mechanism of action of  $K^+$  as a metabolic signal. Soluble adenylyl cyclase (sAC) is sensitive to bicarbonate ( $HCO_3^-$ ) and is expressed by both rat cultured and hippocampal brain slice astrocytes (Choi *et al.*, 2012). sAC produces cAMP from ATP, a downstream molecule thought to stimulate glycogenolysis (Zhou *et al.*, 2019). Using cultured and hippocampal brain slice astrocytes genetically encoded with FRET nanosensors to detect cAMP, revealed that an increase in extracellular  $K^+$  increased intracellular cAMP, an effect which was blocked by 4,4'-Diisothiocyano-2,2'-stilbenedisulfonic acid (DIDs), a sodium bicarbonate cotransporter (NBC) inhibitor (Choi *et al.*, 2012). This suggests that a rise in extracellular  $K^+$  promotes  $HCO_3^-$  entry via the NBC, which in turn activates sAC to produce cAMP. To investigate whether this pathway stimulates astrocytic metabolism, the levels of NADH, formed during glycolysis resulting in pyruvate, were measured (Choi *et al.*, 2012). An increase in extracellular  $K^+$  was found to transiently increase NADH levels, an effect that was blocked by the sAC inhibitor, 2-OH, implying cAMP stimulates astrocytic glycolysis (Choi *et al.*, 2012). This mechanism was also studied under aglycemic conditions to determine the role of  $K^+$  in stimulating glycogen breakdown. As expected under such conditions intracellular cAMP was found to increase, a response that was blocked by 2-OH and DIDs (Choi *et al.*, 2012). Overall, an increase in the concentration of extracellular  $K^+$ , as the result of

increased axonal activity, depolarised the astrocyte membrane potential triggering an influx of  $\text{HCO}_3^-$ . This elevation in intracellular  $\text{HCO}_3^-$  increases the degree of alkalinisation thereby activating sAC, resulting in cAMP production, which stimulates astrocytic glycolysis and lactate production (figure 1.10).

The involvement of the NBC in  $\text{K}^+$  mediated metabolic signalling between axons and astrocytes is supported by the cooperative nature of the NBC and MCT1. Lactate transport via MCT1 was found to increase 2-fold when MCT1 was co-expressed with the NBC, likely the result of the pH buffering capacity of the NBC which enables MCT1 to keep functioning (Becker *et al.*, 2004). This finding supports the role of the NBC in triggering lactate production and release from astrocytes. Change in the intracellular pH appears key to the mechanism of action of  $\text{K}^+$  as a metabolic signal, an effect mediated by the NBC. This was further confirmed by a FRET study that found the intracellular pH of cultured astrocytes increased i.e. became more alkaline, whilst almost simultaneously the intracellular glucose concentration decreased (Ruminot *et al.*, 2011). Either knockout or inhibition of the NBC was found to prevent  $\text{K}^+$  induced alkalinisation and glycolysis by astrocytes, suggesting intracellular pH mediates  $\text{K}^+$  induced astrocytic glycolysis (Ruminot *et al.*, 2011).

A more recent study has provided further evidence for the metabolic role of  $\text{K}^+$  between axons and astrocytes, using FRET expressing mice to record from hippocampal brain slices. In response to increased extracellular  $\text{K}^+$  the astrocytic intracellular concentration of glucose was found to rapidly decrease whilst the intracellular concentration of pyruvate rapidly increased suggestive of increased astrocytic glycolysis (Ruminot *et al.*, 2019). The glucose response was coupled to an increase in intracellular pH when the brain slices were electrically stimulated, an effect which was blocked by the knockout of the NBC (Ruminot *et al.*, 2019). Astrocytic intracellular lactate concentration was also found to rapidly decrease in response to stimulation, suggesting an increased efflux of lactate from astrocytes into the extracellular space

(Ruminot *et al.*, 2019). Altogether, these findings confirm that  $K^+$  released from axons rapidly triggers astrocytes glycolysis via the NBC. Interestingly, a study combining FRET detection of intracellular ATP with real-time oxygen measurements has provided evidence to support the metabolic mechanism of action of  $K^+$ . In response to increased extracellular  $K^+$  astrocytic intracellular levels of ATP increased whilst oxygen consumption decreased, effects that were blocked by the inhibition of the NBC (Fernández-Moncada *et al.*, 2018). The decrease in astrocyte oxygen consumption was suggested to be the result of increased glycolytic ATP inhibiting mitochondrial oxidative phosphorylation, a phenomenon known as the crab tree effect (Fernández-Moncada *et al.*, 2018). This ultimately spares oxygen for neuronal mitochondrial oxidative metabolism of astrocyte derived lactate (Fernández-Moncada *et al.*, 2018). However, a rise in extracellular  $K^+$  has not been found to result in an increase in neuronal ATP levels, unlike that of astrocytes, therefore further research is still required to understand how an increase in astrocyte glycolytic ATP feeds back to active neurones, possibly through the expression of FRET nanosensor for a variety of metabolic intermediates by neurones as well as astrocytes (Lerchundi *et al.*, 2019).

Although little research is available with regard to  $K^+$  as a metabolic signal for Schwann cells and oligodendrocytes, myelinating glial cells may be considered ideally positioned as sensors for  $K^+$ , with channels responsible for the efflux of  $K^+$  from axons located at the juxtaparanode of the internode (Waxman & Ritchie, 1993; Stassart *et al.*, 2018). The Schwann cell membrane potential has been found to respond to axonal activity, possibly through depolarisation of the paranodal loops as the result of increased extracellular  $K^+$  (Lev-Ram & Ellisman, 1995). However, the Schwann cell membrane potential is thought to be more depolarised than the reversal potential of  $K^+$ , i.e. Schwann cells are unlikely to be Nernstian (Hargittai *et al.*, 1991). In addition to the large extracellular space of peripheral nerves (Hoppe *et al.*, 1991) this suggests Schwann cells membrane potential may be less sensitive to

changes in extracellular  $K^+$ . This is supported by the apparent slow passive uptake of extracellular  $K^+$  by Schwann cells in comparison to the active uptake by astrocytes (Ransom *et al.*, 2000). Interestingly, one study suggested that non-myelinating, but not myelinating, Schwann cells of the rabbit vagus nerve take up axonally released  $K^+$  via the  $Na/K^+$  ATPase i.e. active uptake (Robert & Jirounek, 1994). This contradicts the idea of  $K^+$  as a metabolic signal to trigger Schwann cell glycolysis, since the non-myelinating Schwann cells are not considered to provide metabolic support to their associated C fibres (Brown *et al.*, 2012). Despite this the Schwann cell membrane potential responds to changes in extracellular  $K^+$ , not  $Na^+$  (Hargittai *et al.*, 1991), therefore a role for  $K^+$  as a metabolic signal between axons and Schwann cells should not be dismissed.

The oligodendrocyte membrane potential is around -70mV and responds to changes in extracellular  $K^+$ , suggesting oligodendrocytes may also be Nernstian, like astrocytes (Kettenmann *et al.*, 1983). Furthermore, the oligodendrocyte resting membrane potential is mediated by both PKA dependent and independent pathways (Bolton & Butt, 2006), comparable to that of astrocytes, implying oligodendrocytes, like astrocytes, would be sufficiently sensitive to changes in extracellular  $K^+$ .

Based on the research to date glutamate, could be argued as the most universal metabolic signal amongst the different subtypes of glial cells. However, the research also implies that there is no single metabolic signal with the potential for a role of a combination of signals. In particular a FRET study using cultured mice astrocytes revealed a temporal difference in the astrocyte glycolytic response to glutamate and increased extracellular  $K^+$ . The presence of glutamate resulted in a 5 minute delayed increase in astrocyte glycolysis whilst exposure to increased extracellular  $K^+$  stimulated astrocytic glycolysis within seconds (Bittner *et al.*, 2011). Whether similar temporal differences in metabolic signals are evident for Schwann cells and oligodendrocytes is unknown.

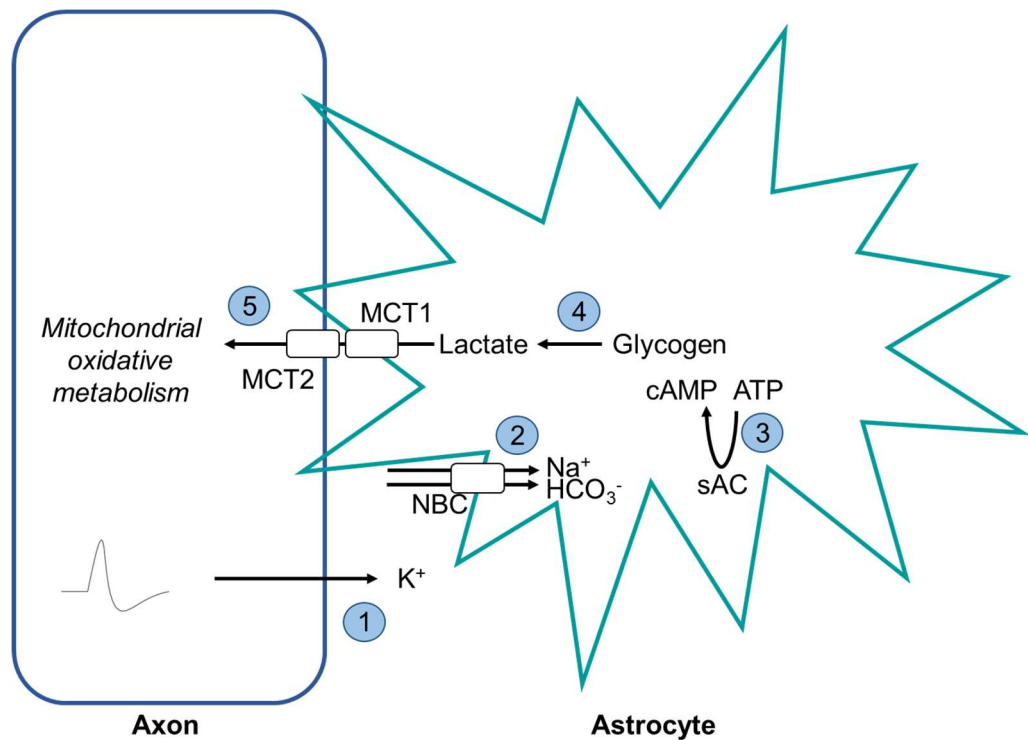


**Figure 1.10:**  $K^+$  as a metabolic signal between axons and astrocytes.  $K^+$  released from active axons depolarises the astrocyte membrane potential (1) enabling the influx of  $HCO_3^-$  via the NBC (2). The increased intracellular  $HCO_3^-$  stimulates soluble adenylyl cyclase (sAC) and therefore cAMP formation (3), which in turn triggers glycogen breakdown to lactate (4). Astrocytes then release this lactate into the extracellular space making it available for axons to take up and use as an energy substrate (5). MCT= monocarboxylate transporter. (Choi *et al.*, 2012).

## 1.5 Aim

The aim of this thesis was to investigate the role of Schwann cells in providing metabolic support to axons of the mouse sciatic nerve, a peripheral nerve. Conduction of fibre subtypes of the sciatic nerve was quantified using stimulus evoked CAP electrophysiology. Specific aims and background are stated in the introduction of each Results chapter.

The aim of my first results chapter was to adapt the suction electrode CAP electrophysiology method to record from paired, rather than single nerves. This increased efficiency and maintained statistical power, whilst reducing the number of animals required for subsequent experiments. This was achieved in two separate, but related, ways.  $N = 2$  from each animal, and reduced standard deviation in sample groups of data

Using the newly adapted CAP recording method the aim was to investigate the role of Schwann cells in providing lactate to A fibres of the mouse sciatic nerve during increased axonal activity. A fibres are known to benefit from Schwann cells, which provide glycogen derived lactate when energy substrate supply to the nerve is decreased (Brown et al 2012). Whether Schwann cells provide similar metabolic support to axons when their energy demand is increased is unknown.

The role of Schwann cells in supplying lactate as a source of energy to A fibres during increased axonal activity prompted further investigations into the role of  $K^+$  as a potential metabolic signal released from axons to communicate the need for metabolic support to Schwann cells. The aim was to incorporate lactate biosensors with CAP recordings to determine the effect of changes in the concentration of extracellular  $K^+$  on Schwann cell lactate production of the sciatic nerve.

The final Results chapter of this thesis aimed to further develop the understanding of the role of Schwann cells in fructose metabolism of the sciatic nerve. It has previously been shown that Schwann cells take up and metabolise fructose to lactate, which is released into the extracellular space for A fibres to use as an energy substrate to

maintain conduction (Rich & Brown 2018). Using molecular techniques, the expression of key fructose enzymes and transporters by Schwann cells, A fibres and C fibres of the mouse sciatic nerve was investigated.

# Chapter 2: Methodology

---

## 2.1 Mice

Male, CD-1, 28-32g (5 weeks) mice (total n= 193) (Charles River Laboratories International, Inc) were sacrificed by cervical dislocation with death confirmed by permanent cessation of the circulation in accordance with the UK Home Office guidelines of Schedule 1 (ASPA, 1986).

Dissections were performed to remove the optic and/or sciatic nerves depending on the experiment(s) to be performed. Nerves dissected from the mouse were then placed in a superfusion chamber for electrophysiology experiments, placed in an Eppendorf tube submerged in ice in for Western blot analysis or snap frozen in liquid nitrogen for immunohistochemistry.

Mice were chosen as the animal model for this research for several reasons: 1) the function of the nerve in mouse is the same as in humans, i.e. to conduct electrical signals, and no significant differences have been found in the cellular and subcellular components, i.e. axons, glial cells, myelin and ion channels, that facilitate conduction between the two species (Ten Asbroek *et al.*, 2006), 2) their genome is similar to that of humans, providing confidence in the translatability of the findings in mice to that of humans (Vandamme, 2014), 3) many genetically modified models of mice are available, which allows for the progression of research into various models of disease (Vandamme, 2014) and 4) due to their smaller size than that of rats, the issue of diffusion distance of energy substrate from the superfused bath solution into the centre of the dissected nerve is reduced.

### 2.1.1 Optic nerve dissection

When the optic nerves were to be used for the experiment they were removed prior to sciatic nerve dissection since the central nervous system (CNS) is more sensitive to ischaemia than the PNS (Kabat & Anderson, 1943). The head of the mouse was first removed, and an incision made along the midline of the top of the head using a scalpel to expose the skull. Incisions were made behind each eye to allow access

of surgical scissors to cut the optic nerve where it exits the eye. Cutting the skull along the midline then enables the brain to be exposed and flipped caudally to reveal the ventral side of the brain and optic nerves. Cutting at the optic chiasm liberates the optic nerves (figure 2.1).

The mouse optic nerve was used as a representative model of CNS white matter.

### *2.1.2 Sciatic nerve dissection*

The body was pinned out prone and incisions made in the skin overlying the spinal cord and hind legs to allow access to the underlying muscle. Incisions were made along the exposed muscle of the right hind leg and up along the spinal cord to reveal the sciatic nerve. The nerve was gently freed from surrounding tissue and cut as close to the spinal cord (L4-6) as possible and where it branches (peroneal, tibial, sural and cutaneous) close to the foot in order to liberate the longest length of nerve possible, taking care to avoid stretching the nerve. This was then repeated on the left hind leg (figure 2.2).

The mouse sciatic nerve was used as a representative model of the peripheral nervous system (PNS), chosen for several reasons: 1) dissection of the sciatic nerve from mice can be performed easily and quickly, reducing the likelihood of damage and duration of exposure to ischaemic conditions, 2) the length of nerve obtained from adult mice is sufficient to record both the faster A fibres as well as the slower conducting C fibres without merging of the stimulus artefact with the CAP (figure 2.4A and B), 3) it is a good model of the PNS, comprised of sensory, motor, myelinated and non-myelinated axons (Schmalbruch, 1986), and 4) it is exquisitely sensitive to the metabolic disruption that underlie type 2 diabetes, thus may act as a model for diabetic neuropathy (NIDDK, 2021).

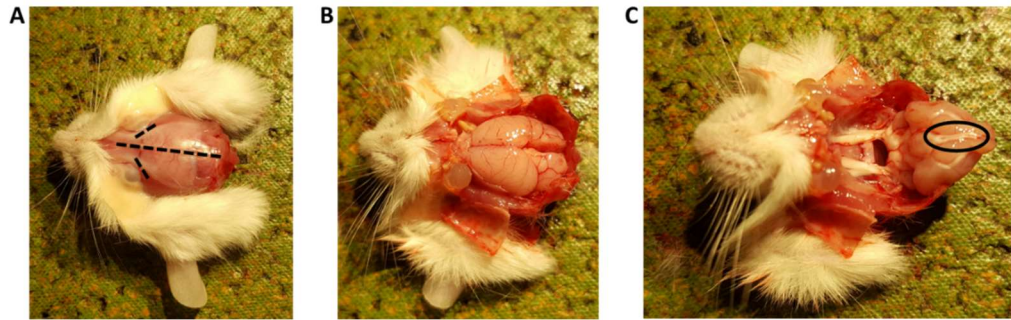


**Figure 2.1:** Mouse optic nerve dissection. **(A)** Cutting the skin along the midline of the head revealed the underlying skull. Incisions (--) were made behind the eyes, allowing access for scissors to cut the optic nerve, and along the midline of the skull. **(B)** The skull was peeled back to reveal the brain. **(C)** Gently lifting the brain back revealed the optic nerve (circled) on the caudal side of the brain. The optic nerve was then cut at the chiasm and dissected free.



**Figure 2.2:** Mouse sciatic nerve dissection. **(A)** The body of the mouse was pinned out belly down and the skin covering the lower end of the body removed. Incisions (--) were made up alongside the spinal cord and along the hind leg towards the foot revealing the sciatic nerve **(B)**. **(C)** The sciatic nerve was then cut at the level of the spinal cord and pulled out to create tension before cutting it just as it branches close to the foot.

## 2.2 Stimulus evoked CAP electrophysiology

For electrophysiological recordings once the nerves had been dissected, they were immediately placed in a superfusion chamber (Harvard Apparatus). The nerves were superfused, at a rate of ~2ml/min, with 10mM glucose (normoglycemic) artificial cerebral spinal fluid (aCSF; 126mM NaCl, 3mM KCl, 2mM MgSO<sub>4</sub>, 26mM NaHCO<sub>3</sub>, 1.25mM NaH<sub>2</sub>PO<sub>4</sub> and 2mM CaCl<sub>2</sub>), buffered at pH 7.45, maintained at 37°C with both the aCSF and chamber continuously bubbled with 95% O<sub>2</sub> and 5% CO<sub>2</sub> mixture.

The chamber also contained glass stimulating and recording suction electrodes (fabricated from thin-walled capillary with filament glass (OD/ID 1.5/1.12mm, TW150F-4, WPI) and chlorided silver (AgCl) wires) filled with substrate free aCSF, thus preventing a reservoir of energy substrate available to the nerve. After trimming each end of the nerve, one end of a single nerve was inserted into the recording electrode and the other end into the stimulating electrode (figure 2.3). A square electrical pulse of 30µs duration (Grass S88 double channel stimulator or Grass S44) was applied to the nerve, via a stimulus isolation unit (SIU5, Grass), in order to evoke a response. Since nerves are a collection of axons a population response is recorded known as the compound action potential (CAP; figure 2.4). The stimulus was applied at a strength greater than that required to recruit all axons i.e. a supramaximal stimulus (figure 2.5). This was determined by measuring the amplitude/area of the CAP; an increase in amplitude/area as a result of increased stimulus is related to an increase in axon recruitment with no further increase in amplitude/area the result of maximal axon recruitment (Bear *et al.*, 2007). The A fibre CAP was measured in terms of amplitude due to its narrow single peak profile whilst the wide triple peak profile of the optic nerve CAP meant area was the most suitable measurement. The evoked response was amplified x1000 and band pass filtered between 10Hz and 30kHz (Standford Research Systems preamplifier, SP560). PClamp 10.7 (Molecular Devices) software was used to generate the protocol to trigger the stimulus and record the

evoked response at a sampling frequency of 50kHz using a 16-bit Digidata 1440A A to D converter (A/D). Responses were saved as an average response every minute e.g. when stimulating at 1Hz, i.e. once a second, 60 responses were averaged together into one file. Averaging was implemented as a way of reducing the signal to noise ratio without resorting to excessive filtering (Dempster, 1993). The amplitude/area of the CAP was then monitored over the duration of the experiment as a measure of conduction.

Nerves were incubated in 10mM glucose aCSF and stimulated at 1Hz for a baseline period of at least 30 minutes in order to gain a stable CAP amplitude/area. Subsequent experimental conditions involved changes in energy substrate supply within the aCSF e.g. concentration and substrate type, the addition of inhibitors to the aCSF e.g. cinnamate (200 $\mu$ M CIN) and changes to the frequency of stimulation e.g. 100Hz (figure 2.6).

### 2.2.1 Data analysis

All data was initially analysed using Clampfit 10.7 (Molecular Device) and normalised from the beginning of the experimental period, before curve fitting (Boltzmann sigmoidal curve) to measure the latency to failure in Excel (Microsoft Office) or area under the curve (AUC) in Prism 7 (GraphPad Software). Latency to failure was defined as a fall in the CAP to 95% of its normalised baseline value (Wender *et al.*, 2000). AUC was used due to many of the experimental conditions failing to reduce the CAP amplitude, where latency to failure could not be calculated. Since the CAP was normalised to 1, complete maintenance of conduction for the 8-hour experimental should result in an AUC value of ~480 NCAP.mins (figure 2.7). All data are expressed as mean  $\pm$  standard deviation (SD) and statistical analysis was performed using Prism 7 (GraphPad Software).

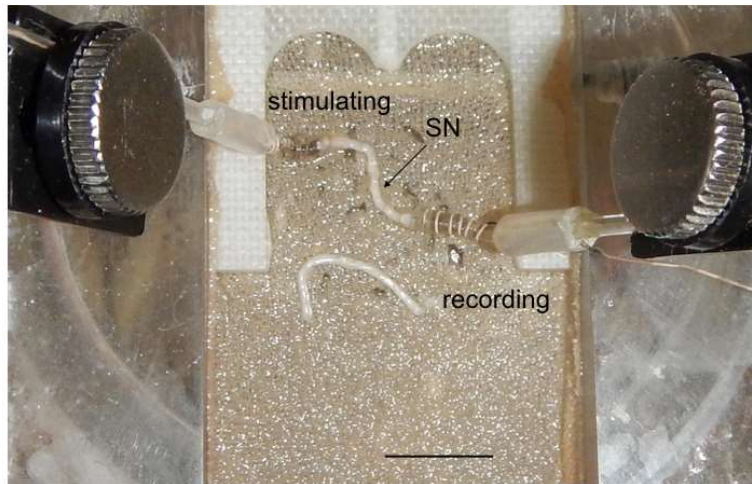


**Figure 2.3:** Stimulus evoked CAP setup. Once dissected the nerve e.g. sciatic nerve (SN) was placed in the superfusion chamber superfused with oxygenated aCSF and maintained at 37°C. One end of the nerve was inserted into the stimulating electrode and other into the recording electrode, both of which were filled with substrate free aCSF. This figure demonstrates the conventional method, recording from only one nerve. Chapter 3 describes the adaption of this method to record from a pair of nerves simultaneously. Scale bar = 1cm.

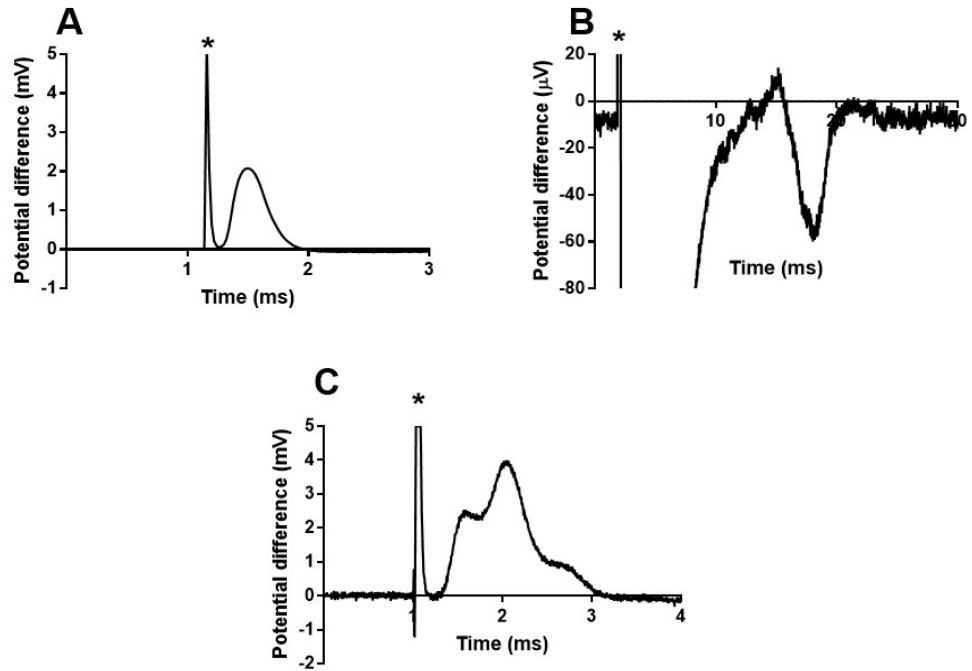


**Figure 2.4:** CAP characteristics. (A) Sciatic nerve A fibre CAP, seen as a large single peak. (B) Sciatic nerve C fibre CAP, seen as a smaller distinct peak occurring ~15ms after the stimulus artefact. (C) Optic nerve CAP, present as a triple peak profile representing 3 groups of axons with different conduction velocities. \*= stimulus artefact.

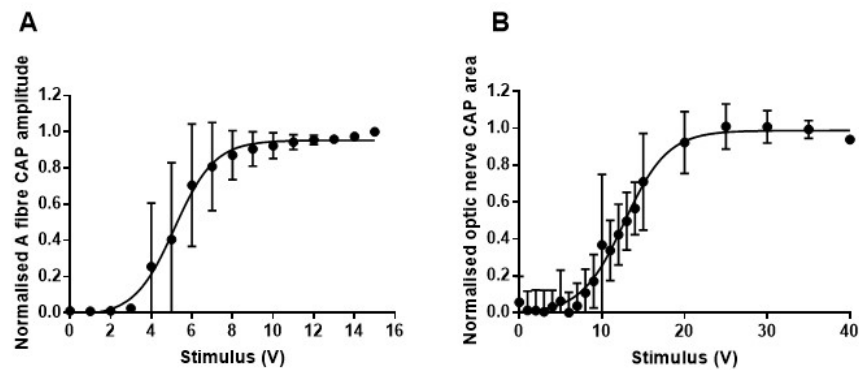


**Figure 2.5:** Stimulus response curves. (A) Voltage stimulus response curve for mouse sciatic nerve A fibres revealing a threshold of 4V and plateau after 10V (n= 5). The supramaximal stimulus used was 15V. (B) Voltage stimulus response curve for mouse optic nerve revealing a threshold of 8V and plateau after 25V (n= 6). The supramaximal stimulus used was 35V. Curves fitted with a Boltzmann sigmodal curve.

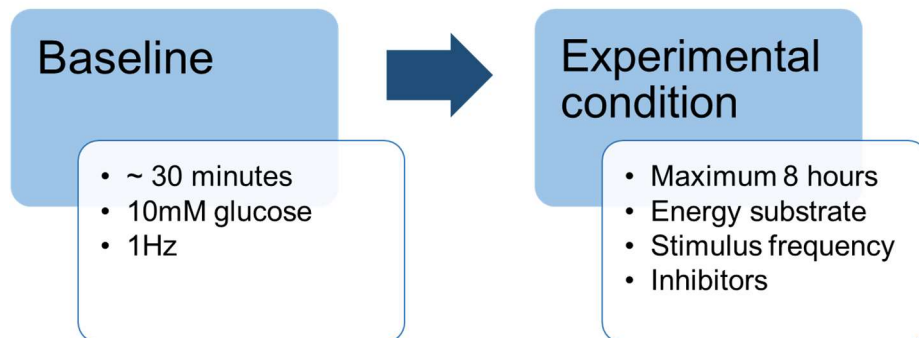


**Figure 2.6:** CAP electrophysiology protocol. Once the nerves have been dissected and inserted into the suction electrodes within the superfusion chamber superfused with 10mM glucose aCSF they are stimulated at 1Hz to record a stable baseline CAP for at least 30 minutes, after which the nerves are exposed to the specific experimental condition for a maximum of 8 hours.

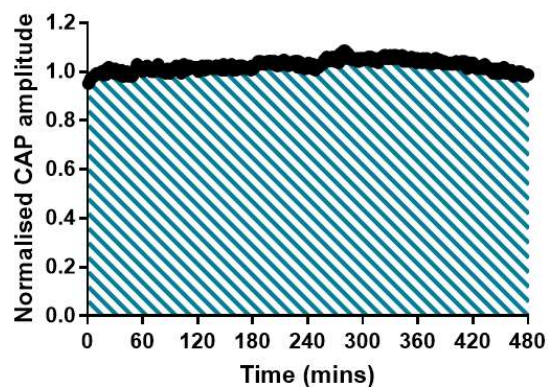
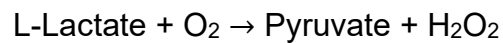


**Figure 2.7:** Analysis of the A fibre CAP. The area under the normalised CAP amplitude vs. time trace (blue shading) acts as an index of the maintenance of conduction over time. Conduction remains stable under control conditions (10mM glucose + 1Hz) with a maximum theoretical value of 480 NCAP.mins.

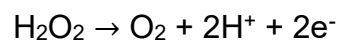
## 2.3 Lactate biosensors

Lactate biosensors are enzyme electrodes that enable real time detection of lactate. These are platinum electrodes selectively sensitive to lactate. When lactate crosses the selectively permeable layer it is oxidised by lactate oxidase to pyruvate and hydrogen peroxide (H<sub>2</sub>O<sub>2</sub>; eq 2.1). H<sub>2</sub>O<sub>2</sub> is subsequently oxidised at the platinum electrode producing a current recording that is linearly proportional to the concentration of lactate; eq 2.2 (Rathee *et al.*, 2016).

### Eq 2.1:



### Eq 2.2:



The largest electrodes available (2mm long and 50µm diameter; Sarissa Biomedical) were used in order to maximise the signal amplitude by exposing lactate to the largest variable surface area of enzyme in order to detect the small concentration of lactate released from the nerves. These experiments also took place in the superfusion chamber and could be performed simultaneously with stimulus evoked CAP electrophysiology or alone.

Before using an electrode to record lactate release from the nerve it was first calibrated in 0µM, 25µM, 50µM, 75µM and 100µM lactate aCSF; a fully functioning electrode should detect a greater signal (current) as the concentration of lactate increases (figure 2.8A). The calibration took place with the nerve absent from the chamber or with the nerve downstream of the electrode in order to prevent the interference of lactate released from the nerve. The signal recorded at each concentration then allowed extrapolation of the lactate concentration released from the nerve based on the lactate signal recorded. This full calibration only took place on the first day of use of each electrode, subsequent days involved a limited calibration in only

one of the lactate concentrations. A single electrode had the potential to be used for 5 consecutive days.

After calibration the chamber was perfused with 10mM glucose aCSF in order to gain a steady baseline recording of 0 before the nerve was then added. The nerve could either be inserted into the suction electrodes as described in 2.2 and then placed very close to, but not completely on top of, the lactate electrode to enable simultaneous stimulation, and if required recording, of the CAP and lactate (figure 2.8B). Care was taken to ensure the nerve was not completely covering the lactate biosensor since this might reduce the access of oxygen to the lactate oxidase enzymes. The lactate recorded from the nerve is defined as extracellular i.e. lactate released from the nerve into the surrounding bath solution and changes in the recorded signal is the result of changes in fluxes due to increased/decreased release/uptake. A baseline period was then recorded until both the CAP and lactate or just the lactate signal were stable. From here the experimental condition could be applied as described in 2.2 through changes in energy substrate, stimulus frequency and the addition of inhibitors.

### *2.3.1 Data analysis*

Lactate biosensors signals were recorded with Axoscope 10.7 (Molecular devices) acquired at sampling frequency of 1kHz using a 16-bit Minidigi 1B. 1kHz is the default sampling frequency of the Minidigi 1B, however this frequency is far too fast for these slow lactate biosensor recordings therefore the resulting trace was first filtered using a Bessel (8-pole), low pass filter, to remove high frequency noise, and then reduced by 1000 to a sampling frequency of 1Hz (Clampfit 10.7). This filtering and data reduction was found to remove noise sufficiently and reduce the size of the file without distorting the recording. Using Clampfit 10.7 the trace was then adjusted during the period of 0 $\mu$ M lactate, in order to get a true 0 baseline period, and saved as an axon text file to be subsequently opened in Excel (Microsoft Office Software). An average of the lactate signal recorded during the calibration was

then calculated and plotted against its corresponding calibration lactate concentration (figure 2.8A). Knowing the lactate signal equivalent to a known concentration of lactate allowed the rest of the trace to be converted to concentration ( $\mu\text{M}$ ). Once the lactate signal had been converted to a concentration, changes in the concentration of lactate released from the nerve during the experimental conditions, e.g. increased stimulus frequency, could be analysed. If the lactate response was found to plateau during the experimental condition, an average of the lactate concentration was measured otherwise the peak lactate concentration during the experimental condition was used.

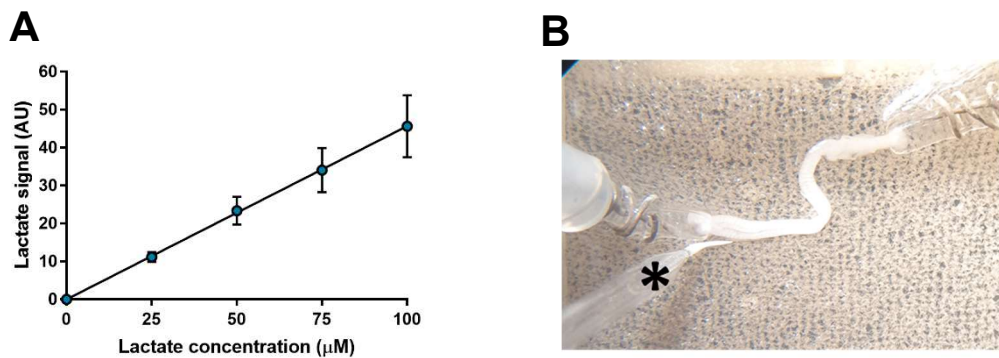


**Figure 2.8:** Lactate biosensor recording. **(A)** Lactate electrode response curve. Increasing the concentration of perfused lactate increased the lactate signal detected by lactate electrodes ( $n=6$ ). **(B)** To record lactate release from the nerve, the nerve was placed very close to the biosensor (\*). Placing the nerve upstream of the biosensor helped ensure the most stable recordings due to the downward direction of flow of the bath solution.

## 2.4 Western blot

Tissue used for protein detection using the Western blot technique was dissected and placed in Phosphate Buffered Saline (PBS, pH 7.4) on ice. Each tissue was weighed in order to calculate the volume of lysis buffer (radioimmunoprecipitation assay (RIPA) buffer) required (1ml per 100mg of tissue). In buffer, the samples were homogenised on ice using a sonic probe homogeniser and spun on a daisy spinner for 20 minutes at 4°C. This disrupts the tissue and cells enabling the release of intracellular proteins. Finally, the samples were spun on a bench top centrifuge for 5 minutes at 850 Relative Centrifugal Force (RCF) and 4°C before the supernatant was pipetted out (pellet discarded) and Sodium Dodecyl Sulfate (SDS) solubilisation buffer added (6x dilution). This process is known as subcellular fractionation and is performed to separate the cells into their integral parts; organelles, cytoplasm and membranes (Ruiz, 2021). The centrifugal speed is chosen based on the proteins required for Western blot (Ruiz, 2021). At 850 RCF the supernatant should contain cytoplasm, membrane and mitochondria and the pellet should contain nuclei (Abcam, 2021). The proteins we were interested in were either membrane bound or present in the cytoplasm, therefore this supernatant was sufficient.

To ensure parity of total protein concentration for each tissue type loaded on to the Western blot gel a standard protein concentration curve had first to be established allowing the total protein concentration of the tissues to be extrapolated. This is known as protein estimation and was conducted using the Lowry test (Lowry *et al.*, 1951). Bovine Serum Albumin (BSA) was used as the protein standard and made up in increasing dilutions with distilled water (11 dilutions made up to 200µl starting at the largest dilution: 0µl BSA and 200µl distilled water then to the smallest dilution of 100µl BSA and 100 µl distilled water, in 10µl BSA steps). Tissue dilutions (1:10, 1:50 and 1:100) were also made up. An equivalent volume (200µl) of Working Lowry reagent (0.5% copper sulphate pentahydrate, 2.7% potassium/sodium tartrate and anhydrous 10% sodium carbonate in 0.5M sodium hydroxide) was added to all

dilutions of tissue and BSA and left for 10 minutes at room temperature. Folin's reagent (100µl, 1:1 Folin's reagent and distilled water) was added for another 45 minutes at room temperature. This results in a colorometric change whose intensity is directly proportional to the protein concentration. All dilutions were performed twice to provide an average reading. Each dilution and repeat (100µl of each) was added to a 96-well plate, which was subsequently placed in a plate reader and the absorbance measured at 720nm. Absorbance could then be plotted against the known concentration of BSA enabling the protein concentration of each tissue to be extrapolated from the linear relationship between the concentration of BSA and the corresponding absorbance reading. The same total concentration of protein for each tissue can then be loaded into separate lanes of the gel. BSA was always added to the first of a set of lanes to act as the standard protein molecular weight marker. Before samples were loaded onto the gel, the samples were heated to 100°C for 5 minutes on a hot plate to denature the proteins. Once the gel was loaded 100V was then applied for 90 minutes via a power source. The process of electrophoresis causes protein displacement down the gel, the lightest proteins travelling the furthest distance. After the gel had run the proteins were transferred onto nitrocellulose membrane filters by electroblotting. This transfer is important as it ensures proteins are in a fixed location and allows easier access of the antibodies to the proteins for detection. The gel was first soaked in transfer buffer (1x dilution) and then placed on top of filter paper on a sponge. The nitrocellulose sheet was then added on top of the gel followed by a final piece of filter paper and sponge, avoiding the formation of bubbles between layers. The gel was then run at 100V for 60 minutes in transfer buffer (1x dilution).

Proteins bands were initially visualised using the Ponceau red stain, to ensure successful transfer of proteins to the membrane (reaction reversed with distilled water), before the nitrocellulose was blocked in blocking buffer (5% milk powder (blocking agent) in Tris-buffered saline with Tween 20 (TBST)) for 1 hour at room temperature by shaking

incubation. The nitrocellulose was then immunoprobed overnight at 4°C with gentle rocking, with a primary antibody (table 2.1) raised against the protein of interest. After incubation the nitrocellulose was rinsed in TBST (0.1% Tween-20 in 10x TBS) then washed 3 times for 15 minutes each in TBST on the orbital shaker. Appropriate Licor Odyssey secondary antibody was then added to the nitrocellulose and left to incubate in the dark for 1 hour at room temperature on the orbital shaker. Finally the nitrocellulose was washed 3 times in TBST for 15 minutes each in the dark before being dried between two pieces of filter paper. The nitrocellulose was then scanned on a Licor Odyssey reader and an image of the Western blot produced.

## 2.5 Fluorescence immunohistochemistry

Dissected tissues were snap frozen in liquid nitrogen or dry ice. Tissue was then embedded in OCT (Optimal cutting temperature compound) on dry ice and mounted onto a chuck to be and cut into sections on a cryostat at -80°C. During cutting the sections were thaw-mounted onto APES (3-aminopropyltriethoxysilane) slides, which were stored at -20°C until required.

For the application of a single primary antibody a standard 2-day protocol was performed in which the primary antibody was added on the first day and incubated overnight with its corresponding secondary antibody applied on the second day. For co-localisation staining where 2 primary antibodies were used a 3-day protocol was employed. Briefly this involved repeating the 2-day protocol with the second primary antibody after the addition of the secondary antibody to the first primary on day 2.

The slide was first removed from the freezer and allowed to warm to room temperature. Staining was carried out in a humidified chamber to prevent the slide drying out during incubations. To begin, tissue sections were fixed in 4% paraformaldehyde (PFA) for 10 minutes. Fixing immobilises antigens. PFA achieves this by crosslinking to maintain the cellular and subcellular structure. Slides were then washed 3 times for 5 minutes each in phosphate buffered saline (PBS) before 3 washes of 5 minutes each in buffer 1 (PBS, 1% BSA, 0.3% Triton-X). Washing in PBS helps maintain pH of the tissue, BSA is used to help block non-specific binding of the primary antibody and Triton-X is a detergent used to permeabilise cells to enable access of the antibodies to subcellular structures. The slides were then incubated in the appropriate normal serum blocker (buffer 1, 2% normal serum) determined by the species in which the secondary antibody was raised (goat and rabbit normal serum were used) for 1 hour at room temperature. After the blocker was tapped off, the slides were incubated in the primary antibody (table 2.1) overnight at 4°C. At this

stage a negative control could be performed in which the blocker was not removed for the overnight 4°C incubation i.e. a no primary negative control.

The following day the slides were processed in a dark, humidified chamber. They were first washed 3 times for 5 minutes each in buffer 1 before incubation in the corresponding secondary antibody for 1 hour at room temperature. At this point another negative control could be performed by omitting the secondary antibody, but keeping the slide incubated in buffer 1 i.e. a no secondary negative control. Afterwards slides were washed 3 times in buffer 1 then 3 times in PBS for 5 minutes each. If a 2-day protocol was being carried out the slides were briefly flooded with DAPI (4',6-diamidino-2-phenylindole) and washed in PBS before a cover slip, with DABCO (mounting media) applied, was placed on top. If a 3-day protocol was being performed the 2-day protocol was repeated, before cover slipping, starting with 3 washes in buffer 1 before the application of the second primary antibody. The protocol was then continued as before.

Negative controls were performed to ensure no non-specific binding occurs with either the secondary or primary antibody. Fluorescence should not be observed. The no primary negative control involved omitting the primary, but adding the secondary antibody to ensure the secondary antibody only binds to the epitopes present on the primary antibody, not those present in the tissue. The no secondary negative control involved adding the primary, but omitting the secondary antibody. This was done to ensure no fluorescent staining was present without the addition of a fluorescent secondary antibody.

Negative control slides were viewed under a fluorescence microscope, at 20x, and images taken using Spot Advanced (SPOT Imaging). Positive slides were first checked using a fluorescent microscope before being sealed with nail varnish and viewed using a confocal microscope (Zeiss L8M 880C), at 63x. Confocal images were acquired as Z-stacks and then combined to create maximum projections. The

maximum projection images were then processed using Fiji (Image J) to add scale bars and merge double staining.

Immunogen	Host species	Mono- or poly-clonal	Isotype	Protocol	Concentration	Source
Neurofilament 200	Mouse	Monoclonal	IgG1	IHC	1 in 200	Sigma-Aldrich, SAB4200705
Neurofilament 200	Rabbit	Polyclonal	IgG	IHC	1 in 200	Sigma-Aldrich, N4142
Peripherin	Mouse	Monoclonal	IgG1	IHC	1 in 200	Abcam, ab4653
S100 $\beta$	Rabbit	Polyclonal	IgG	IHC	1 in 200	Abcam, ab227914
GFAP	Mouse	Monoclonal	IgG1	IHC	1 in 200	Abcam, ab4648
Fructokinase	Chicken	Polyclonal	IgY	IHC WB	1 in 200 1 in 500	Sigma-Aldrich, GW22373
SLC2A5	Mouse	Monoclonal	IgG1	WB	1 in 500	ThermoFisher Scientific, MA1-036X
GLUT5	Rabbit	Polyclonal	IgG	IHC	1 in 100	Invitrogen, PA580024

**Table 2.1:** Primary antibody details. Specific details related to the primary antibodies used to investigate fructokinase and GLUT5 expression by different cell types of the sciatic nerve. Neurofilament 200 is a marker for A fibres, peripherin for C fibres and S100 $\beta$  for Schwann cells (Black *et al.*, 2012; Mata *et al.*, 1990). IHC= immunohistochemistry and WB= Western Blot.

# **Chapter 3: A statistically validated method for recording the stimulus evoked CAP that reduces animal use**

---

### 3.1 Introduction

Since the 1980's suction electrodes have been used as a robust method for stimulating and recording the compound action potential (CAP) from nerves and central fibre tracts (Raymond, 1979; Kocsis *et al.*, 1986). The electrodes are made from glass capillaries, heated to slight bend at one end and fashioned to a constricted opening that snugly fits the nerve when inserted into the capillary (Stys, 1992). Suction applied to the lumen of the electrode enables the nerve to be drawn into the capillary tube (Stys, 1992). Two electrodes are used for each nerve, one at either end, enabling the nerve to be stimulated at one end and the propagating CAP to be recorded at the other (Stys, 1992). Each suction electrode is fabricated with one silver chloride wire wrapped around the outside and one inserted inside (Stys, 1992). The external silver chloride wire enables the subtraction of the bath field potential from the potential difference recorded by the internal wire from the nerve, resulting in a recording of the CAP devoid of any electrical interference (Stys, 1992). This has proven to be an invaluable technique because dissection of each nerve ultimately results in the isolation of nerve trunks, free from synapses and cell bodies, allowing the CAP to be recorded in real time. The CAP can be used as a measure of conduction since its area represents the number of contributing axons; a reduction in area indicative of loss of conducting axons. As a result, this technique is ideal for assessing the pathological effects of metabolic insult on central nervous system (CNS; Wender *et al.*, 2000; Brown *et al.*, 2003), where the CAP acts as an index of the number of conducting axons. The degree of injury and the putative neuro-protective effects of various therapeutic interventions can be assessed when compared to the baseline CAP area (Brown *et al.*, 2019). The technique has recently been adapted to record from the mouse sciatic nerve to study the metabolic interactions between axons and Schwann cells (Brown *et al.*, 2012; Rich & Brown, 2018b).

Exposing a nerve to substrate free conditions, i.e. no glucose or other energy substrate added to the artificial cerebral spinal fluid (aCSF)

superfusing the nerve, results in a decline in the CAP area to zero as the axons metabolise existing available energy substrates. The use of suction electrodes to record from the optic and sciatic nerve during substrate free conditions provided functional evidence that astrocytes and myelinating Schwann cells provide metabolic support to their respective axons, in the form of glycogen derived lactate (Brown *et al.*, 2003, 2012). This has since been extended to fructose derived lactate from myelinating Schwann cells to A fibres of the sciatic nerve (Rich & Brown, 2018b). Under substrate free conditions the mouse optic nerve CAP remains stable for approximately 15 minutes before the rapid onset of failure, a latency which coincides with the minimum concentration of glycogen present in the nerve (Wender *et al.*, 2000; Brown *et al.*, 2003). A qualitatively similar phenomenon was found when measuring conduction in the A fibres of the mouse sciatic nerve, however the latency to A fibre CAP failure and glycogen depletion is prolonged to approximately 2 hours (Brown *et al.*, 2012). Imposing an increased energy demand by increasing the firing frequency of the nerves under substrate free conditions would result in an increased rate of glycogen metabolism and therefore reduce the latency to CAP failure.

There is no doubt about the important contribution these studies have added to this field of research, but with suitable optimisation their efficiency could be improved. This is simply due to the paired nature of nerves i.e. an optic nerve extends from the retina of each eye to join at the optic chiasm, and a sciatic nerve extends from each side of the dorsal spinal cord to innervate each leg. Rather than utilising the pair, a single nerve was historically used and the other likely discarded (Stys *et al.*, 1991). This is not only wasteful but halves the efficiency of the study. Furthermore, not only could one type of nerve be utilised, but duplication of the suction electrode setup could enable the use of both nerve types thus enabling 4 nerve recordings from one mouse, thereby complying with the reduction policy of the National Centre for the

## Replacement, Refinement & Reduction of Animals in Research (NC3Rs).

Adaptation of the suction electrode technique so that pairs of recording and stimulating electrodes are located in a single bath enables stimulation and recording of the CAP from both optic, or sciatic nerves simultaneously. Since pairs of nerves will be subjected to almost identical conditions the random variability in the data will be reduced and therefore the precision increased in that any differences seen are likely due to biological variability. In this study we aimed to provide mathematical evidence for this methodological improvement by comparing the latency to CAP failure of pairs or single nerve recordings under control (1Hz) and high frequency stimulation (HFS; 50Hz) substrate free conditions.

### *3.1.1 Statistics theory*

This section has been written using De Muth (2006) as a source unless stated otherwise and provides the mathematical justification for this adapted method.

Statistical analysis is an important component of scientific research, allowing conclusions about data to be made based on mathematical foundations. Descriptive statistics, i.e. measures of central tendency and dispersion, are universally recognised and enable data to be quantitatively summarised and displayed as tables and graphs. Inferential statistics are used to imply differences between data and incorporate aspects of descriptive statistics, such as the mean and standard deviation, into statistical tests e.g. Student's *t-test* and one-way ANOVA.

The statistical test(s) is chosen once the research question and hypotheses have been decided. Factors that influence the choice of statistical test(s) include the data type, i.e. discrete or continuous, the number of data groups and whether the population parameters are known. Once the test is chosen the data can then be collected. An important point to note is that in most research environments collecting

data from an entire population is not possible, thus a sample is used. Characteristics of a population are known as parameters whereas sample characteristics are known as statistics. The sample should not be biased but selected at random in order to be as representative of the population as possible. Sample data that represents the population is described as accurate. However, despite being randomly selected sample data can be influenced by two types of errors, systematic and random, which then affect how accurate the data is. Systematic errors tend to affect all the samples in the same way, are predictable and can be controlled by the experimental design e.g. incorrect calibration of equipment, whereas random errors result in fluctuations and are much more difficult to control e.g. changes in temperature throughout the day. Therefore, the way in which data is collected can influence how precise, accurate and powerful a study is.

Two hypotheses are applied based on the research question. The null hypothesis ( $H_0$ ) states there is no difference between either of the groups/conditions i.e. the mean from sample 1 ( $X_1$ ) or population 1 ( $\mu_1$ ) equals the mean from sample 2 ( $X_2$ ) or population 2 ( $\mu_2$ ). The alternative hypothesis ( $H_1$ ) broadly states there is a difference between the two sets of data i.e. the mean from sample 1 ( $X_1$ ) or population 1 ( $\mu_1$ ) does not equal the mean from sample 2 ( $X_2$ ) or population 2 ( $\mu_2$ ). This hypothesis can either be one-tailed in that the difference will only be present in one direction i.e. greater or smaller, or two-tailed in that the difference could occur in either direction. The statistical test ultimately determines whether the null hypothesis is rejected or not; this is known as hypothesis testing.

Just as the collection of sample data is affected by errors, inferences from sample data using statistical tests are also subject to two errors known as type 1 and type 2. Type 1 error ( $\alpha$ ) is the probability of rejecting a true null hypothesis i.e. a false positive conclusion, and type 2 error ( $\beta$ ) is the probability of accepting a false null hypothesis i.e. a false negative conclusion.  $\alpha$ , also known as the significance level, is generally pre-set to 5% before the statistical test is performed and is

related to the confidence level (1- $\alpha$ ), i.e. we can be 95% confident in the outcome that a true null hypothesis will be rejected only 5% of the time. As a result, the sample data is tested and conclusions are inferred whilst allowing for a degree of error.

The statistical test used to compare a sample to the population is the Z test and results in a Z score. If comparisons are made between 2 samples the statistical test used is the *t-test* (one-way ANOVA is used for comparisons amongst 3 or more sample groups), resulting in a calculated t score. The sample size is another key determinate of whether a Z or t test is used, with the Z test used when sample sizes are larger (usually  $n > 120$ ). Once calculated the Z or t score is then compared to the critical value. The critical value is a point on the normal standard distribution (Z distribution) or t distribution, determined by the significance level ( $\alpha$ ), which divides the distribution into an acceptance and rejection region of the null hypothesis. This comparison converts the Z or t score into a probability, known as the p value, which in turn determines the level of support given to the null hypothesis. In general, the larger the score the smaller the probability is returned. Since  $\alpha$  is the significance level and generally set to 5%, or a probability of 0.05, if  $p < 0.05$  the null hypothesis is rejected and the alternative hypothesis accepted, therefore a statistically significant difference exists between the two data sets.

### **Z-test:**

The Z test is used when the sample size is 120 or more, assumes the sample is normally distributed and uses the population mean ( $\mu$ ) and standard deviation ( $\sigma$ ) to infer whether a sample mean ( $X$ ) belongs to a population. The Z score is calculated using eq 3.1:

### **Eq 3.1:**

$$Z = \frac{X - \mu}{\sigma}$$

For hypothesis testing  $\sigma$  should be calculated as the standard error of the mean (SEM) (Lynch, 2013):

**Eq 3.2:**

$$SEM = \frac{\sigma}{\sqrt{n}}$$

Where n is the sample size. Therefore:

**Eq 3.3:**

$$Z = \frac{X - \mu}{\frac{\sigma}{\sqrt{n}}}$$

The Z critical value of a normal standard distribution at an  $\alpha$  value of 0.05 is 1.645 for a one-tailed hypothesis and 1.96 for a two-tailed hypothesis, i.e.  $\alpha/2$ . If the Z score is bigger than the critical value, then the null hypothesis is rejected. To give weight to this rejection the Z score is converted to a probability; the smaller the p value the more weight is given to the rejection.

***t-test:***

The *t-test* assumes samples are symmetrically distributed and is used when the population characteristics are unknown or the sample size is less than 30. To account for the sample size the t distribution is a modified version of the Z distribution, calculated using degrees of freedom, n-1, rather than n. Degrees of freedom is defined as the number of samples that are free to vary, with a larger sample size resulting in a higher degree of freedom.

**Eq 3.4:**

$$t = \frac{X_1 - X_2}{\sqrt{\frac{S^2p}{n_1} + \frac{S^2p}{n_2}}}$$

Where  $S^2p$  is the pooled sample variance and calculated using n-1.

The calculated t score (eq 3.4) is compared to the T critical value determined from the t distribution based on degrees of freedom (n-1) and confidence level (1- $\alpha$ ). Usually a one-tailed hypothesis has a confidence level of 0.95 (1- $\alpha$ ) whilst a two-tailed hypothesis has a

confidence level of 0.975 ( $1-\alpha/2$ ). If  $t$  is bigger than  $T$  or less than  $-T$ , the null hypothesis is rejected. As with the  $Z$  test, converting the  $t$  score to a probability gives weight to rejection of the null hypothesis; the smaller the  $p$  value the more weight is given to the rejection.

Common features of the  $Z$  and  $t$ -test include the difference between means, i.e.  $X - \mu$  and  $X_1 - X_2$ , and the critical value. This relationship is illustrated in figure 3.1A. This figure highlights the separation, by the critical value, into null hypothesis acceptance and rejection regions as well as the area defined as type 2 error ( $\beta$ ). From this it is clear that a  $p$  value less than  $\alpha$  results in the rejection of the null hypothesis but with a risk of making a type 1 error (area on the graph denoted  $\alpha$ ), whilst a  $p$  value greater than  $\alpha$  results in acceptance of the null hypothesis but with a risk of making a type 2 error.

The area associated with type 2 error ( $\beta$ ) is also related to the power of the study (eq 3.5). Statistical power is the probability of correctly rejecting a false null hypothesis. For example, a power of 80% (the accepted value used in most studies) means we can be confident that rejection of the null hypothesis will be correct 80% of the time.

**Eq 3.5:**

$$Power (\%) = (1 - \beta) * 100$$

Therefore, the smaller  $\beta$ , and hence a reduced risk of making a type 2 error, the larger the power is. Because the area of power corresponds to the rejection region, larger power means the null hypothesis is more likely to be rejected when it is false (due to smaller type 2 error area) and provides strength that a true difference exists.

Unlike  $\alpha$ ,  $\beta$  is not pre-set before the statistical test is carried out. Instead  $\beta$  is influenced by the difference between means ( $X_1 - X_2$ ), known as the effect size, dispersion of the data sets and  $n$  number. This is illustrated algebraically (for simplicity the equation relates to a  $t$ -test between two sample  $T$  distributions):

**Eq 3.6 (Displayed graphically in figure 3.1):**

$$X_1 - X_2 = (t_\alpha * S_1) + (t_\beta * S_2)$$

where  $t_\alpha$  and  $t_\beta$  are T critical values and  $S_1$  and  $S_2$  are the sample standard deviations of the first and second samples, respectively. This can be re-arranged to solve for  $t_\beta$  i.e. the area of  $\beta$ :

**Eq 3.7:**

$$t_\beta = \frac{(X_1 - X_2)}{S_1} - t_\alpha$$

From this equation a larger value of  $t_\beta$  and therefore the smaller the corresponding probability/area of  $\beta$  can result from a) larger effect size ( $X_1 - X_2$ ) and b) smaller sample standard deviation (dispersion). Since the equation for sample standard deviation (S) is:

**Eq 3.8:**

$$S = \sqrt{\frac{\sum(X_i - X)^2}{n-1}}$$

Where  $X_i$  is an individual data point, it is clear that dispersion is influenced by the sample size (n); increasing the sample size reduces the standard deviation and thus increases the value of  $t_\beta$ .

Overall, from equations 3.7 and 3.8 it is possible to investigate ways of reducing the likelihood of making an error during hypothesis testing. Since  $\alpha$  is fixed the area depicting the possibility of making a type 1 error remains constant. The area of  $\beta$  however is variable and can be affected by the three variables: effect size, standard deviation and n number. Increasing the effect size would pull the two distributions further apart therefore reducing overlap and the area of  $\beta$  (figure 3.1B). However, effect size for any particular comparison is constant and unaffected by methods of data collection, since the means of the data are based upon biological characteristics. The dispersion of data, on the other hand, can be reduced by decreasing random variation as the result of refined experimental techniques i.e. careful dissection of

nerves as well as by increasing the number of repeats. Reducing the spread of data would result in narrowing of the distributions and therefore reduce overlap and the area of  $\beta$  (figure 3.1C). A reduced area of  $\beta$  signifies increased power.

*Aim:*

The aim of this study was to demonstrate mathematically how a change in our experimental/data collection method, by recording from paired rather than single nerves, can maintain power, whilst reducing the number of animals used as the result of reducing the standard deviation of our sample data.

*Hypotheses:*

Null hypothesis 1: There will be no difference in latency to failure of the A fibre CAP of the sciatic nerve at 1Hz compared to 50Hz during substrate free conditions.

Alternative hypothesis 1: Increasing the energy demand on the sciatic nerve during substrate free conditions by increasing stimulus frequency to 50Hz will reduce the latency to failure of the A fibre CAP compared to 1Hz.

Null hypothesis 2: There will be no difference in the latency to failure of the optic nerve CAP during substrate free conditions after baseline incubation compared to prior glycogen depletion.

Alternative Hypothesis 2: Prior glycogen depletion will accelerate the latency to failure of the optic nerve CAP compared to baseline incubation before substrate free conditions.

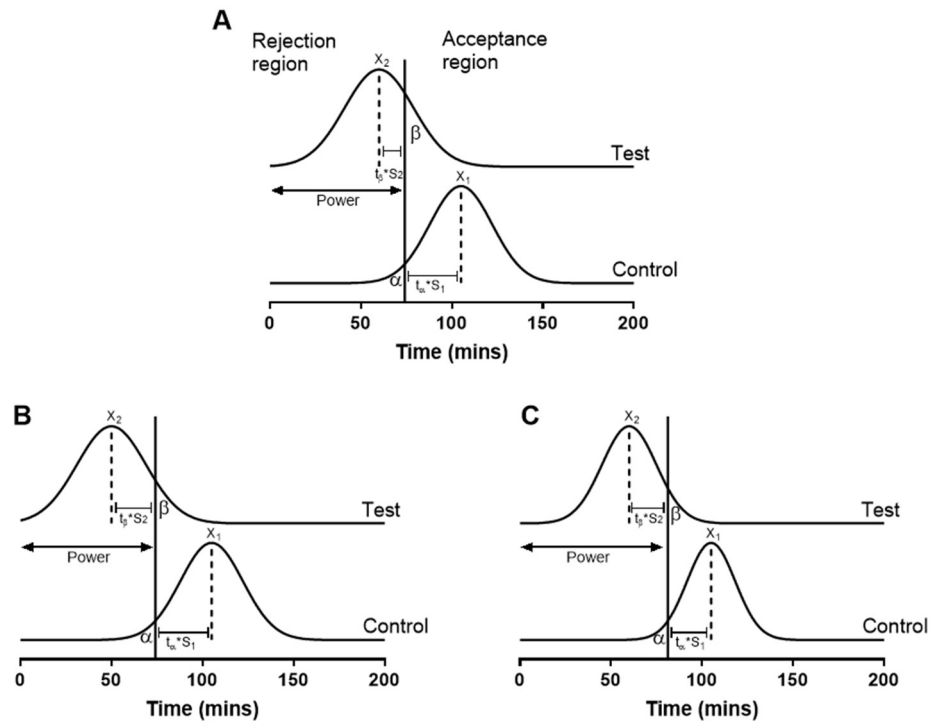


**Figure 3.1:** One-tailed statistical analysis between two sample distributions. **(A)** Each distribution represents the spread of data (standard deviation) about the mean ( $X_1$  and  $X_2$ ). Comparing the test to the control distribution based on the sample mean and variance ( $t$ -test) results in a  $t$  score that is compared to the  $T$  critical value ( $t_\alpha$ ). The  $T$  critical value can be converted to an absolute value through multiplication by the sample standard deviation ( $t_\alpha \cdot S$ ). The  $t$  score is then converted to a probability ( $p$  value), i.e. proportion of the control distribution in which the test mean may lie. A  $p$  value of 0.05 or less suggests the test mean lies somewhere to the left of the critical value and is significantly different to the control mean i.e. the null hypothesis is rejected. A  $p$  value of more than 0.05 suggests the test mean lies to the right of the critical value and is not significantly different from the control i.e. the null hypothesis is accepted. The critical value also determines the areas of type 1 and 2 errors. The area to the left of the critical value within the control distribution is known type 1 error or  $\alpha$  i.e. fixed at 0.05. The area to the right of the critical value within the test distribution denotes type 2 error or  $\beta$ . This area is not fixed and determines the power ( $1-\beta$ ) of the study. A small area of  $\beta$  results in greater power. In this illustration the value of  $\beta$  is 0.2131 **(B)** Increasing the effect size results in two distributions with their means further apart. The area of  $\alpha$  remains constant since it is pre-set to 0.05 whilst the area of  $\beta$  is reduced to 0.093. Consequently, the power of the study is increased from 78.7% (fig 3.1A) to 90.7%. **(C)** Reducing the standard deviation (but maintaining the effect size as in fig 3.1A) of the sample data results in narrower distributions. Again, the area of  $\alpha$  is fixed at 0.05 whilst the area of  $\beta$  is reduced from 0.2131 (fig 3.1A) to 0.068. Consequently, the power of the study is increased from 78.7% (fig 3.1A) to 93.2%. Solid vertical lines represent the critical value dividing the distribution into acceptance and rejection regions for the null hypothesis.

## 3.2 Methodology

### 3.2.1 Mice and tissue dissection

See chapter 2.1 for full details of the mice and nerve dissections.

A total of 72 mice were used for collection of the sciatic (mice= 36) and optic nerves (mice= 36) for use in stimulus evoked CAP electrophysiology.

### 3.2.2 Stimulus evoked CAP electrophysiology

The procedure for carrying out these electrophysiology recordings is described in chapter 2.2. However, this description relates to the original method of recording from a single nerve and thus adaptations to this method to enable recording from pairs of nerves are described here. The n number refers to the number of individual nerves recorded from.

It must first be realised that a nerve pair refers to both optic or both sciatic nerves being recorded from at the same time in the same bath, the bath did not contain a mixture of optic and sciatic nerves. Once the nerve pair had been dissected and had sufficient time to equilibrate in the bath they were inserted into the glass suction electrodes as described in chapter 2.2. Rather than a single stimulating and single recording electrode the setup was modified so that a pair of stimulating and a pair of recording electrodes could be added to the bath, enabling each nerve to be taken up by its own set of electrodes (figure 3.2). The nerves were placed side-by-side allowing for a small gap between them, to ensure sufficient flow of aCSF. Neither nerve was considered to be affected by the other for 3 reasons 1) since the concentration of lactate released (see chapter 5) from the upstream nerve is too low to influence the downstream nerve, 2) the temporal aspects of the recordings between pairs were found to be comparable (seen in comparability of latency to failure means between single and paired nerves; figure 3.4.Ai and Bi, and 3.5Ai and Bi), and 3) the CAP from each nerve was comparable (figure 3.3). The right sciatic nerve was

always inserted into the suction electrode pair closest to the back of the bath, with the proximal (spinal cord) end inserted into the recording electrode and the distal (leg) end into the stimulating electrode. The chiasmic end of the optic branches was also always inserted into the recording electrodes. The use of two stimulators (Grass S44 and Grass SD9 stimulator, Grass Medical Instruments) or a double channel stimulator (Grass S88 double channel stimulator, Grass Medical Instruments) enabled a stimulus to be delivered to each of the stimulating electrodes. Both stimulators were triggered by the same protocol enabling simultaneous delivery of pulses to each nerve. Therefore, both nerves were exposed to almost identical conditions. Each of the recording electrodes was connected to an amplifier, the output of each received by separate channels of the A/D converter enabling visualisation and recording of the individual nerve responses simultaneously.

Only the A fibre, not C fibre, CAP (figure 2.4A of chapter 2) was recorded for this study at a stimulus intensity of ~15V (figure 2.5A of chapter 2) and control frequency of 1Hz. The optic nerve was stimulated with ~35V pulses (figure 2.4C and 2.5B of chapter 2) at a control frequency of 1Hz. Nerves were first incubated in 10mM glucose and stimulated at 1Hz for a baseline period of 30 minutes before being subjected to the experimental condition. High frequency stimulation (HFS) was defined as 50Hz.

### *3.2.2.i Data analysis*

See chapter 2.2.1 for more detail of CAP data analysis.

The baseline area the optic nerve CAP and amplitude of the A fibre sciatic nerve CAP was normalised to 1 before curve fitting, using the Boltzmann sigmoidal equation, to measure the latency to failure in Excel (Microsoft Office). The latency to CAP failure, expressed as mean  $\pm$  SD, from two different conditions was statistically compared using a one tailed *t-test* with significance level of 0.05 (GraphPad Software). A *t-test* was chosen since sample sizes were less than 30.

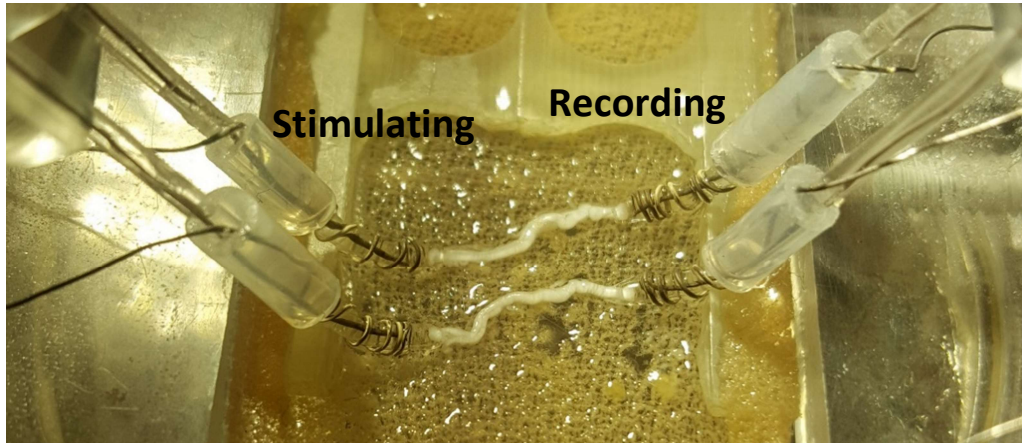


**Figure 3.2:** Paired stimulus evoked CAP setup. Both sciatic nerves, obtained from one animal, are placed in their own stimulating (left) and recording (right) electrodes enabling simultaneous recording of the CAPs.

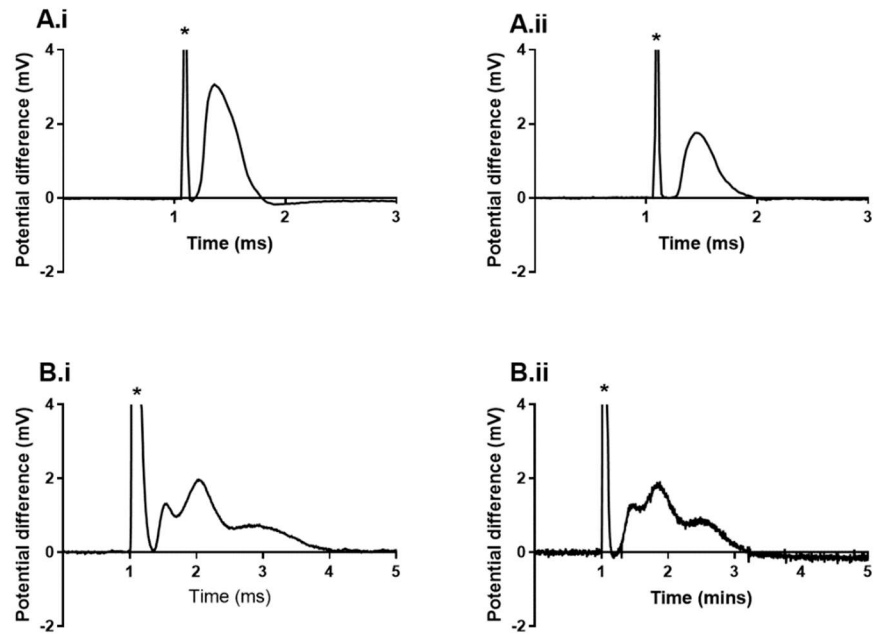


**Figure 3.3:** Paired stimulus evoked CAP profiles. **(A)** A fibre CAPs from a pair of sciatic nerves. **(i)** A fibre CAP from the first nerve of the pair. Seen as a large single peak at 1.5ms of ~3mV. **(ii)** A fibre CAP from the second nerve of the pair. Seen as a large single peak of ~2mV. **(B)** CAPs from an optic nerve pair. **(i)** CAP from the first optic nerve of the pair, present as a triple peak profile with the largest peak reaching ~2mV. **(ii)** CAP from the second optic nerve of the pair. Present as a triple peak profile with the largest peak reaching ~2mV. \*= stimulus artefact.

## 3.3 Results

### *3.3.1 HFS under substrate free conditions reduces the latency to failure of the mouse sciatic nerve A fibre CAP*

It has already been established that exposing the sciatic nerve to substrate free conditions results in the maintenance of the A fibre CAP for ~90 minutes before failure (Rich & Brown, 2018*b*). For this study, this condition was repeated using single and pairs of sciatic nerves as well as imposing an increased frequency of stimulation from 1Hz to 50Hz. Recordings from single sciatic nerves revealed a mean latency to A fibre CAP failure of  $99.4 \pm 28$  minutes vs.  $79.7 \pm 24.9$  minutes in the presence of substrate free aCSF and 1Hz or 50Hz, respectively (figure 3.4A.i). This reduced latency to failure, as the result of HFS, was found to be significantly different  $p=0.04$ . Comparable results were found when recording from pairs of sciatic nerves simultaneously;  $96.4 \pm 17.2$  minutes vs.  $80.1 \pm 18.9$  minutes and  $p=0.02$  (figure 3.4B.i). Although significance was implied between the conditions for both single and paired recordings, the standard deviation i.e. variation in the latency to failure values was reduced for paired nerves. This can be clearly seen in the narrowing of the latency to failure distributions under both conditions for the paired compared to single nerves (figure 3.4A.ii and 3.4B.ii). As a result, the area of  $\beta$  is reduced (from 85% to 79%) and subsequently the area of power increased (from 15% to 21%) for equivalent n values (n= 12 for each condition).

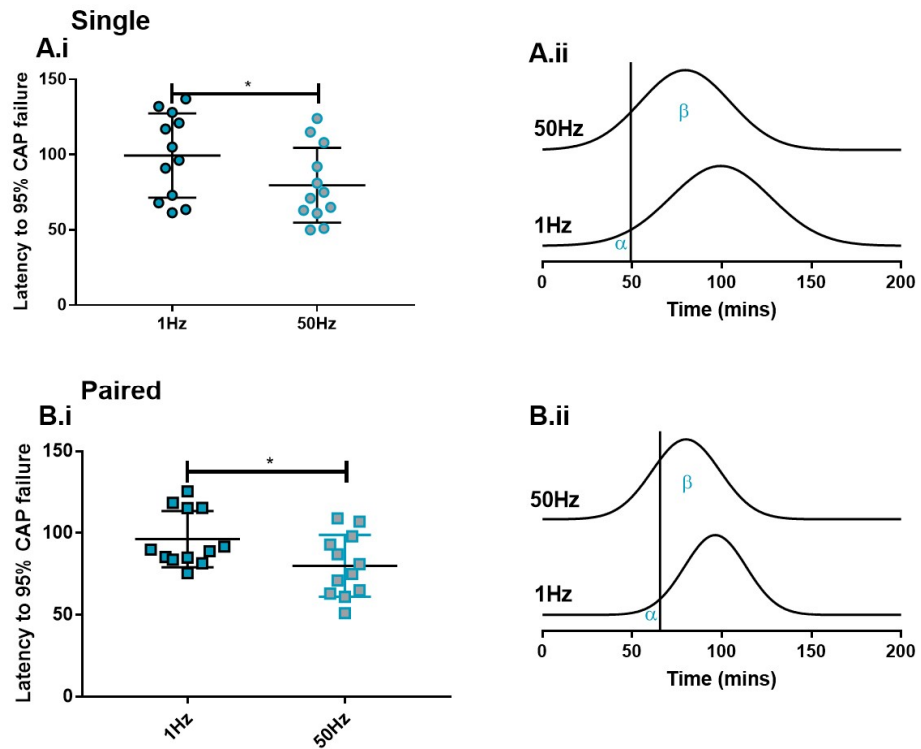


**Figure 3.4:** Latency to A fibre CAP failure of sciatic nerve during substrate free conditions. **(A)** Latency to A fibre CAP failure recorded from single nerves. **(i)** A fibre CAP maintenance in substrate free aCSF ( $n=12$ ) was further reduced by the addition of 50Hz stimulus ( $n=12$ ) **(ii)** shifting the distribution of latency to CAP failure to the left of the 1Hz distribution. **(B)** Latency to A fibre CAP failure recorded from pairs of nerves. **(i)** Latency to CAP failure was further reduced by imposing HFS ( $n=12$ ) during substrate free conditions ( $n=12$ ) **(ii)** shifting the distribution to the left. \* =  $p<0.05$ . Solid vertical lines in figures A.ii and B.ii represent the critical value.

### *3.3.2 Conditioning exposure reduces latency to failure of the mouse optic nerve CAP in subsequent substrate free conditions*

To ensure that our adapted method of recording from pairs of nerves reduced the variation in data irrespective of the experimental condition, we performed a different set of experiments with the mouse optic nerves compared to that of the sciatic nerves. The optic nerves were first exposed to substrate free aCSF (conditioning) but once the CAP had reached approximately 50% of its baseline area control 10mM glucose aCSF was supplied in order to recover the CAP. Soon after the CAP had recovered to the baseline area, a substrate free condition was then reimposed (post-conditioning). The latency to CAP failure was compared between conditioning and post-conditioning substrate free conditions for both single and pairs of optic nerves. Recordings from single optic nerves revealed a mean latency to CAP failure of  $14.2 \pm 3.1$  minutes vs.  $11.4 \pm 2.7$  minutes during conditioning and post-conditioning substrate free conditions, respectively (figure 3.5A.i). The mean latency to CAP failures from pairs of optic nerves during conditioning and post-conditioning substrate free conditions were  $14.9 \pm 2.1$  minutes and  $11.5 \pm 1.9$  minutes, respectively (figure 3.5B.i). The reduction in the latency to failure evident in the post-conditioning substrate free condition for both single and paired nerve recordings was found to be significant;  $p=0.02$  and  $p=0.0002$ , respectively. Again, the dispersion of data was reduced for the paired recordings (figure 3.5A.ii and 3.5B.ii), reducing the area of  $\beta$  (from 81% to 56%) and subsequently increasing the area of power (from 19% to 44%) for equivalent n values (n= 12 for each condition).

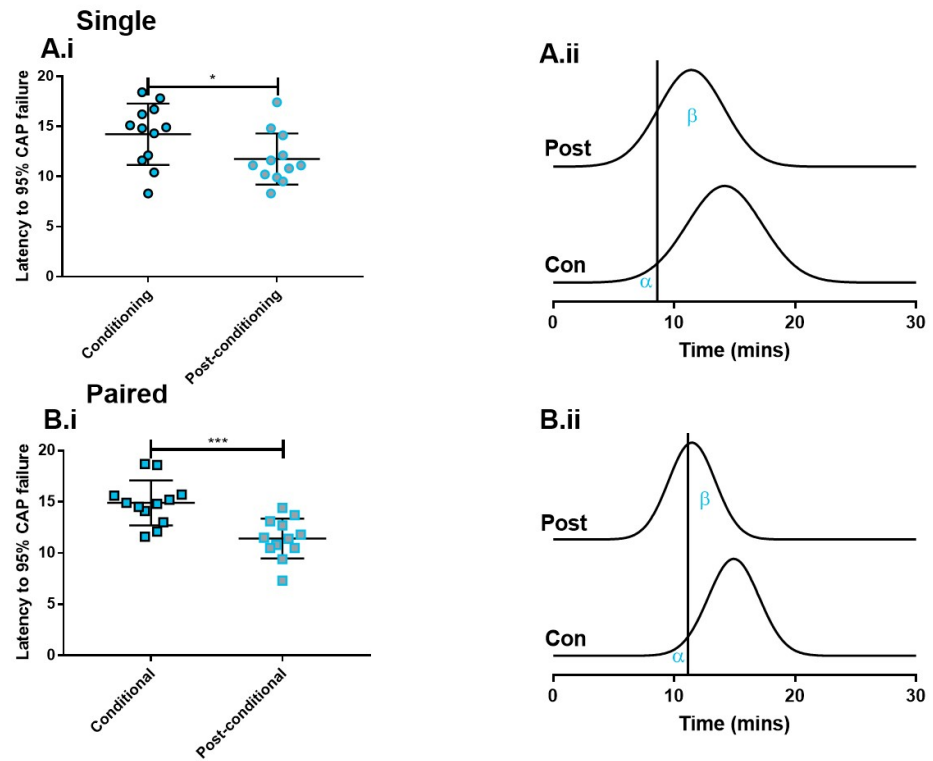


**Figure 3.5:** Latency to optic nerve CAP failure during substrate free conditions. **(A)** Latency to CAP failure recorded from single nerves. **(i)** Exposing the optic nerve to substrate free aCSF ( $n=12$ ) reduces the latency to failure in a subsequent period of substrate free ( $n=12$ ) **(ii)** shifting the post-conditioning distribution to the left of the conditioning distribution. **(B)** Latency to CAP failure recorded from pairs of nerves. **(i)** Maintenance of the optic nerve CAP is reduced during the second period of substrate free ( $n=12$  for each condition) **(ii)** shifting the latency to CAP failure distribution to the left. \* =  $p<0.05$ , \*\*\* =  $p<0.001$ . Solid vertical lines in figures A.ii and B.ii represent the critical value.

## 3.4 Discussion

The data from this study not only demonstrates the metabolic support role of glial cells within the central and peripheral nervous systems, but also reveals the mathematical justification of this adapted suction electrode CAP electrophysiology technique. By recording from two of the same nerve type simultaneously taken from a single animal, rather than the conventional single nerve, the variability in data was reduced. As a result, the power of the study could be maintained whilst reducing the number of required animals.

### *3.4.1 The role of glial cell glycogen in supporting axon conduction during insufficient energy substrate availability*

Myelinating Schwann cells of the sciatic nerve and astrocytes of the optic nerve possess glycogen which they can subsequently metabolise to lactate and pass to axons for oxidative metabolism (Wender *et al.*, 2000; Brown *et al.*, 2003, 2012). This metabolic cooperation is known to occur when these nerves are exposed to substrate free conditions. We expanded upon this by imposing an additional 50Hz stimulus (sciatic nerve) or conditioning substrate free period (optic nerve).

Stimulating the sciatic nerve at 50Hz increased A fibre activity and thus energy demand. As result the demand and supply of glycogen derived lactate would increase. Since glycogen is in finite supply this store would be metabolised sooner therefore reducing the duration of maintenance of A fibre conduction under this increased energy demand condition, as seen in figure 3.4A.i and 3.4B.i. p values of less than 0.05 allow null hypothesis 1 to be rejected and conclude that increased energy demand as the result of increased stimulus frequency reduced the latency to A fibre CAP failure due to an increased rate of glycogen metabolism.

The role of astrocytic glycogen to support axonal conduction during substrate free conditions was confirmed by exposing the optic nerve to a conditioning substrate free period. This conditioning period depleted the astrocytic glycogen stores. With little recovery time between the

conditioning and subsequent substrate free condition, glycogen stores would not have been replenished. The reduced latency to CAP failure in the post-conditioning substrate free condition (figure 3.5A.i and figure 3.5B.i) highlights the use of glycogen derived lactate by axons which would have been significantly reduced/no longer available. p values of less than 0.05 enable null hypothesis 2 to be rejected and conclude that conditioning exposure to substrate free aCSF reduces the latency to CAP failure of the optic nerve in post-conditioning substrate free aCSF as the result of prior glycogen depletion.

### *3.4.2 Statistical acceptance*

The adaptation of this electrophysiology method to record from pairs of nerves simultaneously dramatically reduced the variability of the data whilst resulting in mean values that were comparable to single nerve recordings of the same condition e.g. mean latency to A fibre CAP failure of 79.7 and 80.1 minutes during substrate free and 50Hz, from single and paired nerves respectively. Since the critical value for the test distribution ( $t_{\beta}$ , section 3.1.1) is influenced by the standard deviation it becomes apparent as to why the reduced data variability from this paired method reduces the area of  $\beta$  and thus maintains the power of the statistical test. Reducing the standard deviation of the distribution increases the value of  $t_{\beta}$  therefore shifting the critical value to right, reducing the area to the right of the critical value, which is denoted as  $\beta$  e.g. the critical value was 50 and 66 minutes for single and paired sciatic nerve recordings, respectively (see figure 3.4A.ii and 3.4B.ii). The reduction in  $\beta$  as the result of recording from pairs of nerves means we are less likely to accept a false null hypothesis during statistical testing (type 2 error).

Although the area of  $\alpha$  remains constant irrespective of whether the recordings were made from the single or pairs of nerves, the p value generated from the *t-test* was smaller with pairs of nerves e.g. significance was found at  $p=0.02$  and  $p=0.0002$  using single and paired optic nerves, respectively. Since the p value denotes the level of

support for the null hypothesis, the larger the p value the more support, the reduced p value when using the adapted electrophysiology technique implies even less support for the null hypothesis and we are less likely to reject a true null hypothesis (type 1 error).

Overall, for the same n number, but reduced number of animals (see section below), the risk of making type 1 and 2 errors is reduced therefore using this adapted method we are less likely to accept a false null hypothesis and more likely to find significance when there is a difference.

#### *3.4.2.i Reduced animal requirement*

To calculate the required n number of a study a power calculation is performed. This involves the known values of  $\alpha$  (0.05), power (most likely 80%), effect size and standard deviation. The smaller the standard deviation the fewer n numbers required. Since our paired nerve method clearly reduces the variability of the data fewer n numbers will be required for the same power and  $\alpha$  of 0.05 compared to the single nerve method (see power calculation below).

As with all previous studies using suction electrode CAP electrophysiology (Rich & Brown, 2018b), the n number refers to the number of individual nerves. This was maintained using the adapted method of recording from pairs of nerves i.e. 2 sciatic nerves are obtained from one animal therefore n=2. Therefore, the reduced n number requirement from the power calculation as the result of the reduced standard deviation, reduces the number of nerves and therefore animals used, but since 2 nerves are collected from one animal the paired recording technique halves the animal requirement (see power calculation below), complimenting the reduction requirement of the NC3Rs. Furthermore, if sufficient experimental equipment is available setups can be replicated enabling multiple paired nerve recordings from the one animal increasing efficiency (i.e. time take to obtain data) of data collection.

**Power calculation example** (calculated from [www.stat.ubc.ca](http://www.stat.ubc.ca)):

$X_1 = 98$ ,  $X_2 = 80$ ,  $\alpha = 0.05$  and power = 0.8

Single nerve recording:  $S = 27$

$n = 28$  (nerves = 28, animals = 28)

Paired nerve recording:  $S = 19$

$n = 14$  (nerves = 14, animals = 7)

However, in order to completely halve the number of animals required 100% of the paired nerve experiments are required to work. As with many experimental techniques, success rate is increased with practice. Careful dissection and control of *ex vivo* conditions not only increase the success rate but also help to reduce experimental variability and therefore dispersion of the data obtained.

#### 3.4.2.ii *The compromise*

Assigning the  $n$  number to each individual nerve rather than to the individual animal could be considered as pseudo-replication, since two of the same nerve are utilised from a single animal using the adapted technique. The topic of replication and pseudo-replication is one that has been intensely debated. Simply stated, replication increases the sample size,  $n$ , whilst pseudo-replication artificially increases it (Lazic *et al.*, 2018). By correctly identifying the experimental unit (EU) of the experiment, studies can be carried out in a manner that meets the three criteria for genuine replication (Lazic *et al.*, 2018). We define the nerve, sciatic or optic depending upon the hypothesis being tested, as the EU. Many *in vivo* studies assign the  $n$  number to the whole animal rather than individual tissue components. However, we use an in-bred strain of mice thus each mouse is engineered as a phenotypic, if not genotypic, clone; our mice also do not undergo behavioural testing neither is the experimental condition administered to the whole animal therefore all nerves should be physiologically equivalent between and within animals. Differences between the nerves can occur when *ex vivo*

e.g. in our dissection protocol the right sciatic nerve is always dissected out before the left meaning the left nerve is exposed to ischaemic conditions for slightly longer than the right, a variable that could have significant influence on metabolic studies. The differences in the nerves *ex vivo* in combination with the experimental condition being applied directly to the nerve rather than the whole animal suggests each nerve, regardless of whether they are from the same animal or not, can be considered as individual units.

Firstly, the EU should be independently and randomly allocated to the experimental condition. We do our best to achieve this through our tendency to perform a different experiment with each mouse out of the weekly order. Therefore although 2 recordings are made from each mouse, different mice, and therefore nerves, from different litters are randomly assigned to each experimental condition. The second criterion states the experimental condition should be applied to each individual EU and must not affect adjacent EUs. Although using our adapted technique two nerves are recorded from in a bath together, and strictly speaking to achieve true independence each nerve would ideally be recorded in a separate bath, they are exposed to slightly different conditions, e.g. stimulus voltage and suction electrode resistance, that is dependent on the individual nerve (seen in the slight differences in CAP profiles between the pairs in figure 3.3). Moreover, even though both nerves are exposed to the same perfused aCSF and are situated next to each other in the bath, neither nerve appears to influence the other since simultaneous recordings show them respond almost identically to the experimental condition (seen in the reduced variation the latency to failure data), satisfying the final criteria that EUs must not influence each other.

Recording from two nerves simultaneously reduces variability in the data. This is likely the result of reduced random variability between experiments. For example, aeration of the bath and aCSF and ambient room temperature, although controlled as much as possible, can vary between experiments (systematic error) thus act as confounding

variables. By reducing the number of setups required for each experimental condition random error is reduced. However, since double the number of nerves are exposed to very similar conditions compared to the original technique the effect of systematic errors e.g. incorrect make up of aCSF is increased. Similar to success rate, experience and diligence ensure systematic errors are prevented.

### 3.5 Conclusion

Our data shows adaption of the suction electrode CAP electrophysiology technique to record from pairs of nerves simultaneously minimises random errors seen in the reduced variability of data. As a result, the risk of making type 1 and 2 errors during statistical analysis is reduced and power maintained. Since sample size refers to the number of nerves recorded from, simultaneously recording from both nerves from a single animal halves the number of animals required for equivalent n numbers using single nerves assuming all nerves produce viable recordings.

The concern over pseudo-replication might inflict doubt with regards to validity of this updated technique. However, the opportunity scientists are given to carry out research using animals suggests they should accept a level of compromise in order to reduce the number of animals required. This, in addition to our estimated success rate of 90%, we believe justifies the use of this improved method in subsequent future experiments.

# **Chapter 4: Schwann cell metabolic support of A fibre conduction during high frequency stimulation in mouse sciatic nerve**

---

## 4.1 Introduction

Energy homeostasis in the nervous system requires the cooperation between neurones and glial cells to ensure maintenance of axon conduction. The vast majority of research investigating axon-glia metabolic interactions has simulated pathological conditions such as aglycaemia to unravel the metabolic compartmentalisation that exists between these cell types. Astrocytes and myelinating Schwann cells are the repository for glycogen within the central and peripheral nervous systems, respectively (Brown *et al.*, 2003; Brown *et al.*, 2012). Within astrocytes glycogen is glycolytically metabolised to lactate, which is subsequently released and made available for axonal uptake and oxidatively metabolised. Axons of the mouse optic nerve utilise astrocyte glycogen derived lactate when energy substrate supply is withdrawn, with the concentration of available glycogen an indicator of the duration of conduction during aglycaemia (Brown *et al.*, 2003). Myelinating Schwann cells of the mouse sciatic nerve also supply glycogen derived lactate to their associated A fibres during energy substrate deprived conditions (Brown *et al.*, 2012).

The convincing evidence for astrocyte glycogen providing energy for axons during pathological aglycemic conditions led to investigations into this role during the more physiological condition of increased axonal activity. This was achieved by stimulating the mouse optic nerve at high frequencies whilst monitoring the compound action potential (CAP) area and nerve glycogen content. 100Hz stimulation led to an initial increase then decline in the CAP area in 10mM glucose, whilst conduction was fully maintained with 30mM glucose, clearly implying that high frequency stimulation (HFS) increases energy demand (Brown *et al.*, 2003). Reducing the duration of HFS in 10mM glucose appeared to enable maintenance of the CAP area but depletion of the glycogen content of the optic nerve. However, the optic nerve CAP is comprised of 3 peaks, rather than a single peak, indicative of sub-populations of axons with different conduction velocities. Detailed analysis of the CAP under these conditions revealed that the first peak was unaffected

whilst the second and third reduced in amplitude and increased in duration, suggestive of conduction failure of the axons that make up these two peaks (Brown *et al.*, 2003). These results initially imply that glycogen acts as a source of additional energy for axons when exogenously supplied glucose alone is insufficient to support conduction. The addition of isofagomine (glycogen phosphorylase inhibitor) during HFS and 10mM glucose (Brown *et al.*, 2005) resulted in a rapid fall in the CAP area, further supporting the requirement of astrocytic glycogen by axons during increased axonal activity. A comparable rapid failure of the CAP was also seen with the addition of cinnamate (CIN) or quercetin (monocarboxylate transporter inhibitors) to 10mM glucose and HFS, suggesting axons of the mouse optic nerve benefit from astrocyte glycogen in the form of lactate as energy source during increased firing (Brown *et al.* 2003; Brown *et al.* 2004).

Whether Schwann cell glycogen is as beneficial to A fibres during increased axonal activity is yet to be established, however based on the similarities between the astrocytes and axons and myelinating Schwann cells and A fibres, it is reasonable to suggest a role of glycogen during HFS of the mouse sciatic nerve.

*Aim:*

To investigate the metabolic support of Schwann cells to A fibres during increased axonal firing.

*Objective:*

Using stimulus evoked CAP electrophysiology and the mouse sciatic nerve *ex vivo*, measure changes in the maintenance of conduction of A fibres in response to increased stimulus frequency and energy substrate supply.

*Hypothesis:*

A fibres utilise Schwann cell glycogen derived lactate during HFS when glucose alone is not sufficient.

## 4.2 Methods

### 4.2.1 Mice and tissue dissection

See chapter 2.1 for full details of the mice and nerve dissections.

A total of 78 mice were used for collection of sciatic nerves only (total n= 115) for use in stimulus evoked CAP electrophysiology.

### 4.2.2 Stimulus evoked CAP electrophysiology

The CAP was recorded using the paired nerve adaptation of this method, as described in chapter 3.2.2. For further details of this method see chapter 2.2. The n number refers to the number of individual nerves recorded from.

Only the A fibre, not C fibre, CAP (figure 2.4A of chapter 2) of the sciatic nerve was recruited for this study at a stimulus intensity of ~15V (figure 2.5A of chapter 2) and control frequency of 1Hz. C fibres were not recruited for this study since these slow conducting fibres would not be able to fire action potentials continuously during HFS (see below).

Nerves were first incubated in 10mM glucose and stimulated at 1Hz for a baseline period of 30 minutes before being subjected to a HFS experimental condition (figure 4.1) Different HFS protocols were used to investigate different aspects of Schwann cell-axon metabolic interactions during increased axonal activity.

#### 4.2.2.i High frequency stimulation

This study involved changing the stimulus protocol from a baseline frequency of 1Hz to HFS of 100Hz, in order to increase axonal activity and therefore energy demand of the sciatic nerve. 100Hz was chosen as the HFS for 2 reasons: 1) this was the frequency used in the mouse optic nerve experiments (Brown *et al.*, 2003) allowing comparisons between the two nerve types, and 2) this frequency allows sufficient time for the recovery of the voltage gated sodium channels from their inactivated state such that CAPs 'follow' with no loss of amplitude.

To ensure the stimulus frequency does not interfere with the refractory period of the A fibres, a double pulse protocol was carried out (figure 4.2A and B). This involved the delivery of an initial pulse (P1) followed by a second pulse (P2), at decreasing time intervals. The amplitude of the CAP evoked from P2 is compared to the CAP amplitude from P1; the amplitude should remain constant if the same axons are being recruited, whilst a drop in the P2 CAP amplitude suggests there was not sufficient time for the voltage gated sodium channels of all A fibres to recover from their inactivated state and return to rest.

#### *4.2.2.ii Data analysis*

See chapter 2.2.1 for more detail of CAP data analysis.

The amplitude of the A fibre CAP over time was normalised to 1, before curve fitting, using the Boltzmann sigmoidal equation, to measure the latency to failure in Excel (Microsoft Office) or area under the curve (AUC) in Prism 7 (GraphPad Software). Latency to failure was defined as a fall in the CAP to 95% of its normalised baseline value (Wender *et al.*, 2000). AUC was used due to many of the experimental conditions failing to reduce the CAP amplitude, therefore latency to failure could not be calculated (figure 2.7 of chapter 2). Since the CAP was normalised to 1, full maintenance of conduction for the 8-hour experimental should result in an AUC value of ~480 NCAP.mins. All data are expressed as mean  $\pm$  SD and statistical analysis was performed using Prism 7 (GraphPad Software), where  $p < 0.05$  was considered significant.

#### *4.2.3 Lactate biosensors*

See chapter 2.3 for a detailed explanation of lactate electrode implementation to the superfusion chamber and recording of lactate. The n number refers to the number of individual nerves recorded from.

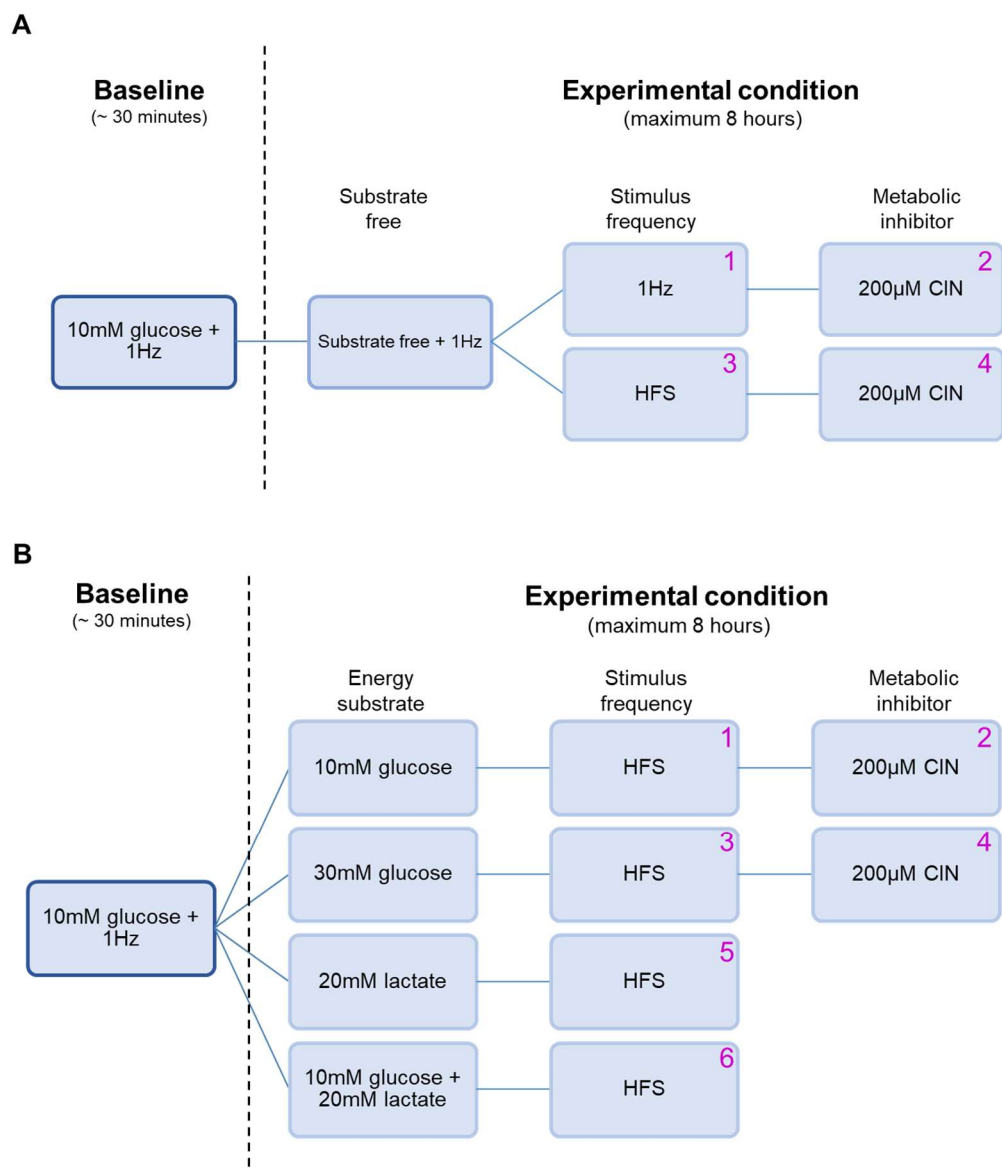
It should be borne in mind that the lactate was recorded at the border of the nerve, and is thus extracellular, and does not quantitatively reflect the concentration of lactate present in the extracellular space of the nerve. Although the concentration of lactate within the extracellular

space of nerve is likely to be higher than that recorded due to the dilution of lactate in the bath artificial cerebral spinal fluid (aCSF), it qualitatively reflects the extracellular concentration.

#### 4.2.3.i Data analysis

See chapter 2.3.i for more detail of lactate analysis.

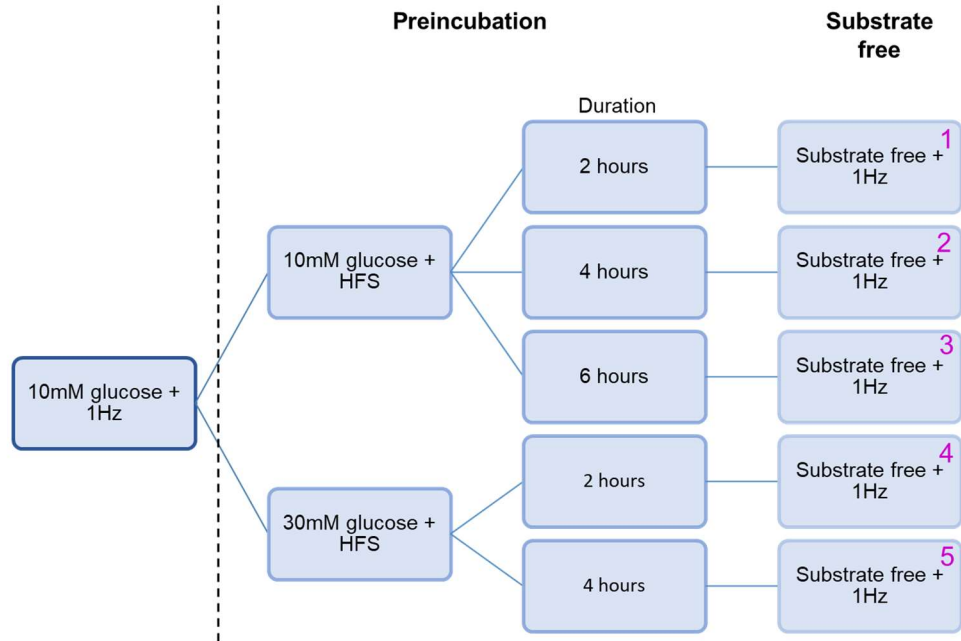
Lactate biosensor recordings were filtered (Clampfit 10.7) before being converted to a concentration based on the lactate calibration.



C

**Baseline**  
(~ 30 minutes)

**Experimental condition**  
(maximum 8 hours)



D

**Baseline**  
(~ 30 minutes)

**Experimental condition**  
(maximum 8 hours)

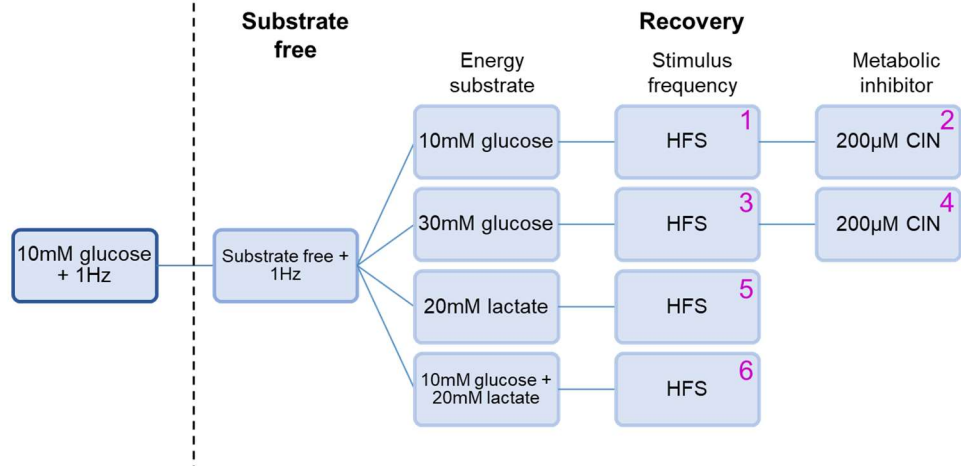


**Figure 4.1:** CAP electrophysiology HFS protocols. **(A)** Substrate free protocols. After 30 minutes of baseline the exogenous supply of energy substrate was removed whilst stimulating the nerves at 1Hz (1) or 100Hz (3). Substrate free conditions at 1Hz or 100Hz was also performed in the presence of CIN (2 and 4). This protocol was used to investigate the role of Schwann cell glycogen in supporting A fibre conduction. **(B)** Maintenance protocols. After 30 minutes of baseline the nerves were stimulated at 100Hz whilst supplied with 10mM glucose (1), 30mM glucose (3), 20mM lactate (5) or 10mM glucose and 20mM lactate (6). 10mM glucose and HFS, and 30mM glucose and HFS stimulus maintenance protocol could also be performed with the addition of CIN (2 and 4). These protocols were used to investigate the concentration and type of energy substrate required to maintain A fibre conduction during increased axonal activity. **(C)** Preincubation protocols. After 30 minutes of baseline the nerves were preincubated in 10mM glucose and stimulated at 100Hz for 2, 4 or 6 hours before the exogenous supply of energy substrate was removed and stimulated at 1Hz (1, 2 and 3). Nerves were also preincubated in 30mM glucose and stimulated at 100Hz for 2 or 4 hours before being exposed to substrate free conditions (4 and 5). This protocol was used to investigate the role of Schwann cell glycogen derived lactate to support A fibre conduction during increased axonal activity. **(D)** Recovery protocols. After 30 minutes of baseline the exogenous energy supply to the nerves was removed until the CAP fell to ~50% of its baseline amplitude. Energy substrate, in the form of 10mM glucose, 30mM glucose, 20mM lactate or 10mM glucose and 20mM lactate, was resupplied and the nerves stimulated at 100Hz (1, 3, 5 and 6). 10mM glucose and HFS, and 30mM glucose and HFS stimulus recovery protocols could also be performed with the addition of CIN (2 and 4). This protocol was used to investigate the role of Schwann cell glycogen derived lactate to support A fibre conduction during increased axonal activity.

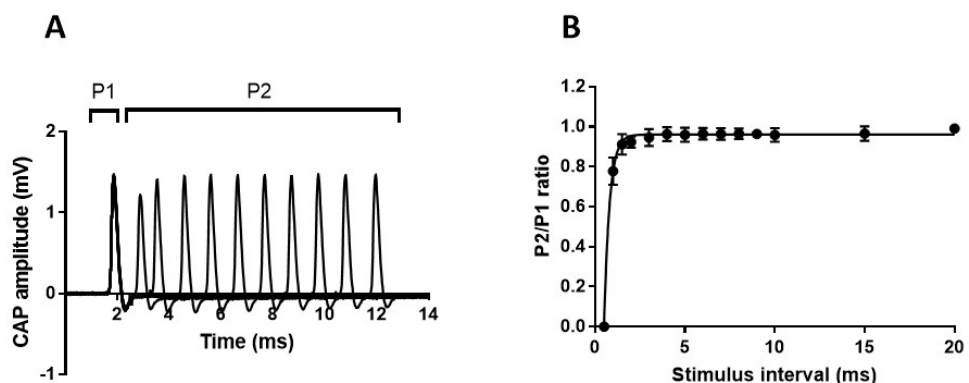


**Figure 4.2:** Mouse sciatic nerve A fibre CAP recording. **(A)** A double pulse protocol was used to **(B)** determine the maximum stimulus frequency that could be applied by calculating the ratio of the amplitude of the second with that of the first evoked CAP (n= 4). HFS is defined as 100Hz i.e. a stimulus frequency of 10ms.

## 4.3 Results

### 4.3.1 The role of Schwann cell glycogen during substrate free conditions

Removing the exogenous supply of energy substrate to the sciatic nerve puts it under metabolic stress to utilise any remaining endogenous sources of energy in order to maintain conduction, one of which is glycogen. Under substrate free conditions A fibres of the sciatic nerve maintained stable conduction for approximately 90 minutes (figure 4.3A and B) before the onset of failure, seen as the drop in the CAP amplitude (figure 4.3A). The 90 minutes of conduction is known to coincide with metabolism of available glycogen (Brown *et al.*, 2003), a feature we investigated further by increasing the energy demand on the tissue (HFS) and blocking lactate uptake into axons (CIN; figure 4.3C; the main effect of treatment was found to be significant  $F(3,23)31.27$ ,  $p<0.0001$ ). Individually, both protocols accelerated the latency to failure of A fibre conduction compared to substrate free (post-hoc multiple comparisons,  $p<0.0001$  and  $p<0.001$ , respectively; figure 4.3A and B), an affect that was slightly additive by the combination of HFS and CIN compared to substrate free ( $p<0.0001$ ; figure 4.3A and B). However, it was not significantly different from HFS or CIN alone ( $p=0.9$  and  $p=0.31$ , respectively).

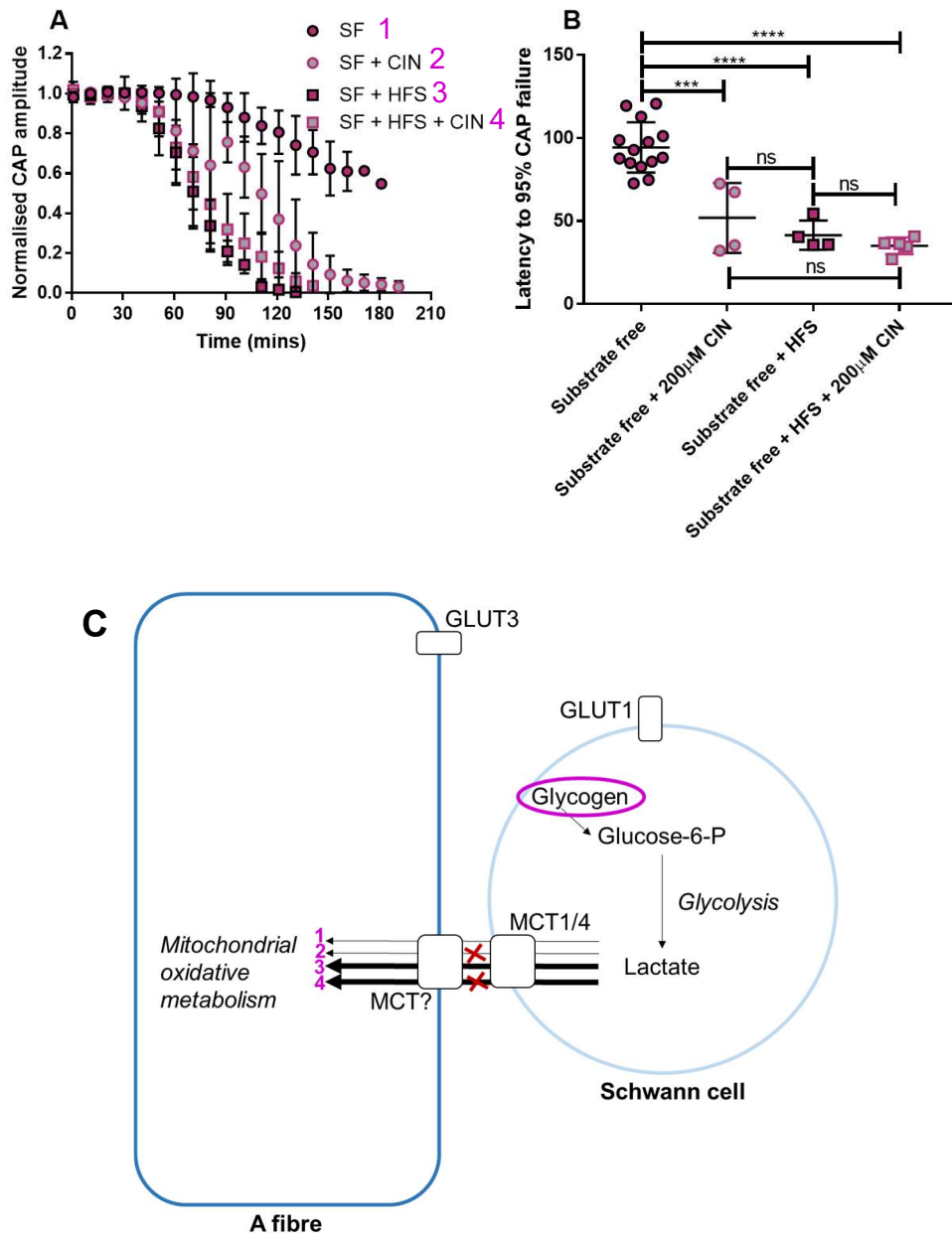


**Figure 4.3:** A fibre maintenance of conduction in the absence of exogenously supplied energy substrate. **(A)** Removal of supplied glucose to the mouse sciatic nerve resulted in A fibre conduction failure, an effect which was accelerated by the addition of 200µM cinnamate (CIN), HFS or both. **(B)** Under substrate free conditions A fibre conduction was maintained for  $94.3 \pm 15.1$  minutes ( $n=14$ ), which was further reduced as a result of the addition of CIN ( $51.9 \pm 21$  minutes,  $n=4$ ), HFS ( $41.5 \pm 8.8$  minutes,  $n=4$ ) and further with both ( $35.1 \pm 5$  minutes,  $n=5$ ). **(C)** Schematic of proposed cellular interactions. Under substrate free conditions Schwann cell glycogen derived lactate is released and taken up by A fibres via MCTs (1), which are blocked by CIN (2). During HFS glycogen is depleted faster (3), but in the presence of additional CIN A fibres are unable to benefit from lactate during this increased energy demand (4). One-way ANOVA with Tukey's post hoc test. \*\*\* =  $p < 0.001$ , \*\*\*\* =  $p < 0.0001$ . SF= substrate free, GLUT = glucose transporter and MCT= monocarboxylate transporter.

### *4.3.2 Energy supply vs. demand*

Investigations into the response of the sciatic nerve to HFS began with studies into the concentration of glucose required to meet this increased energy demand (figure 4.4C; the main effect of treatment was found to be significant  $F(2,19)13.46$ ,  $p=0.0002$ ). A fibre conduction remained stable for 8 hours under control, 10mM glucose and 1Hz conditions (figure 4.4A and B). Increasing the energy demand by raising the stimulus frequency to 100Hz under normoglycemic conditions reduced the maintenance of conduction (post-hoc multiple comparisons,  $p<0.001$ ; figure 4.4B), resulting in a steady decline in CAP amplitude after approximately 4 hours/240 minutes (figure 4.4A). Increasing the concentration of supplied glucose fully maintained conduction in the presence of HFS ( $p=0.02$ ; figure 4.4B), for 8 hours, similar to that of 10mM glucose and 1 Hz conditions (figure 4.4A).

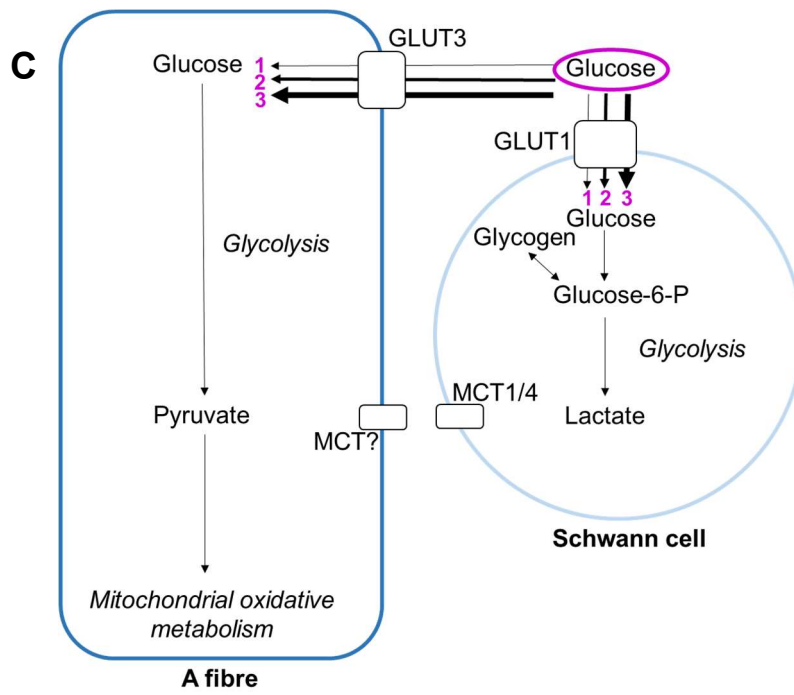
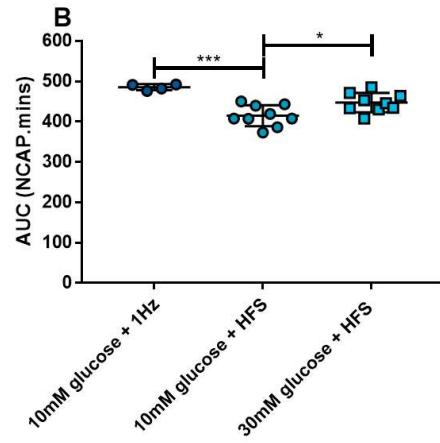
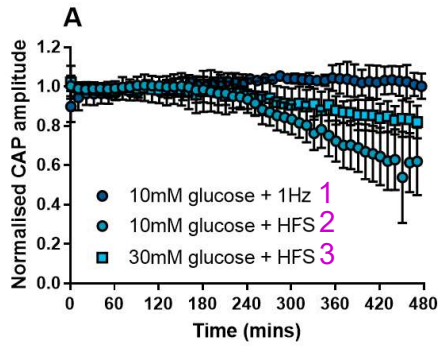


**Figure 4.4:** The increased energy demand placed on the sciatic nerve due to HFS was better met by increased energy substrate supply. **(A)** A fibre conduction was better supported during HFS when glucose supply is increased from 10mM to 30mM **(B)** Increasing the stimulus frequency under normoglycemic conditions reduced the maintenance of conduction ( $485.4 \pm 7.7$  NCAP.mins, n= 4 (+ 1Hz) vs.  $414.9 \pm 26.0$  NCAP.mins, n= 9 (+ HFS)). This reduction was mitigated by increasing the concentration of supplied glucose to 30mM ( $414.9 \pm 26.0$  NCAP.mins, n= 9 (10mM glucose) vs.  $447.2 \pm 23.8$  NCAP.mins, n= 9 (30mM glucose)). **(C)** Schematic of proposed cellular interactions. Under control conditions glucose is taken up by both cell types (1). Increasing the stimulus frequency (2) and availability of glucose (3) would result in increased uptake. One-way ANOVA with Sidak's post hoc test. \* =  $p < 0.05$ , \*\*\* =  $p < 0.001$ . GLUT= glucose transporter and MCT= monocarboxylate transporter.

### 4.3.3 The role of lactate during HFS

Since the normoglycemic concentration of glucose was unable to fully maintain A fibre conduction during HFS, the role of lactate was investigated (figure 4.5E; the main effect of treatment was found to be significant  $F(5,29)59.62$ ,  $p < 0.0001$ ). Blocking lactate uptake into A fibres with the addition of 200 $\mu$ M CIN in the presence of 10mM glucose and HFS significantly reduced the maintenance of conduction compared to 10mM glucose and HFS, resulting in complete failure after approximately 6.5 hours (post-hoc multiple comparisons,  $p < 0.0001$ ; figure 4.5A and D). The presence of CIN with 30mM glucose however, had no effect, with conduction almost fully maintained in either the presence or absence of CIN ( $p = 0.52$ ; figure 4.5B and D). Interestingly, supplying 20mM lactate instead of glucose to the nerve during HFS resulted in further reduced maintenance of conduction compared to 10mM glucose and HFS ( $p = 0.04$ ; figure 4.5C and D). Finally supplying 20mM lactate and 10mM glucose, in combination, resulted in sustained conduction for the 8 hours of HFS compared to the incomplete maintenance of conduction during 10mM glucose and HFS ( $p < 0.001$ ; figure 4.5C and D).

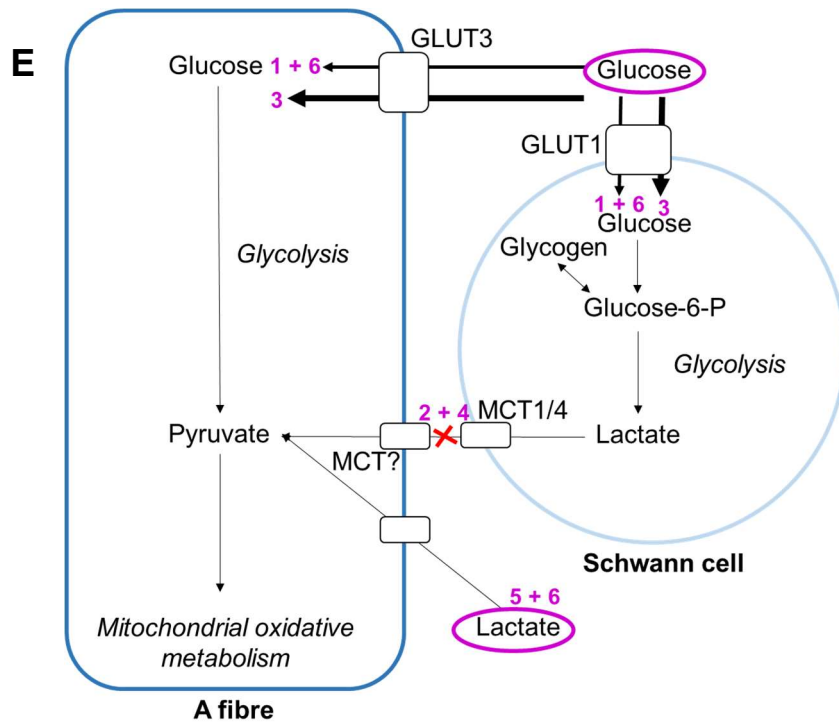
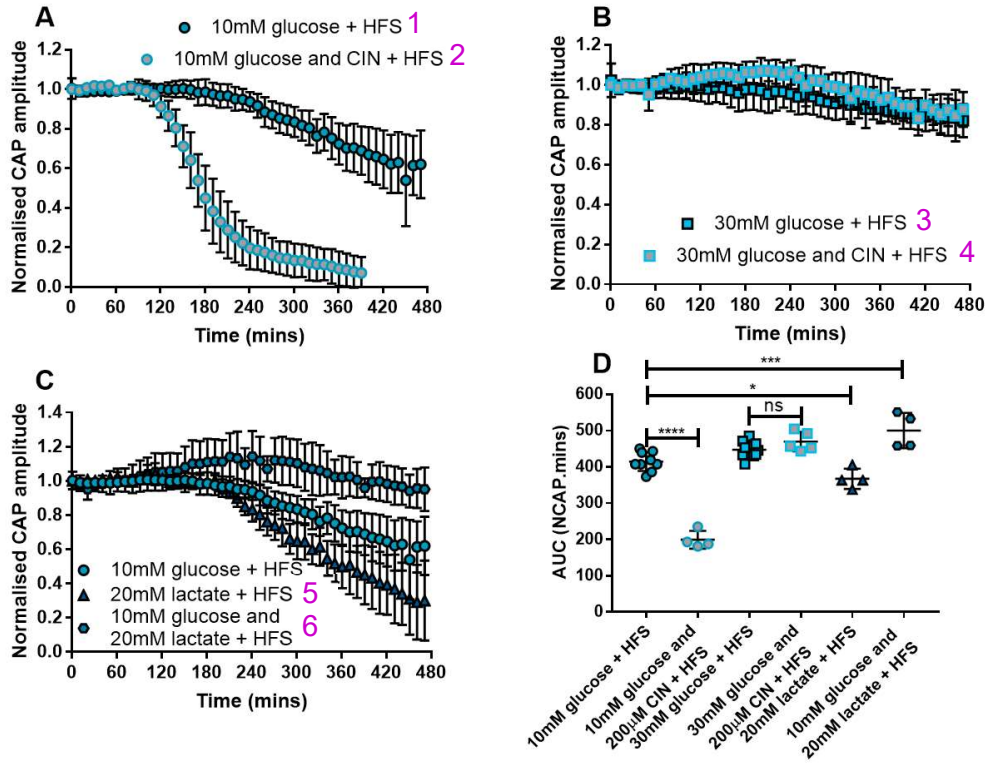


**Figure 4.5:** Lactate as an energy source for A fibres during HFS. **(A)** The addition of 200 $\mu$ M CIN during 10mM glucose and HFS resulted in accelerated failure of conduction with both reduced latency to failure onset (approximately 2 hours compared to 4 hours) and increased rate of conduction failure. **(B)** The A fibre CAP was fully maintained with 30mM glucose in the presence or absence of 200 $\mu$ M CIN. **(C)** Supply of 20mM lactate reduced the latency to, and slightly increased the rate of, failure compared to 10mM glucose and HFS. The combination of 10mM glucose and 20mM lactate enabled full maintenance of conduction. **(D)** The addition of 200 $\mu$ M CIN significantly reduced the maintenance of conduction of the A fibres in the presence of 10mM glucose and HFS ( $414.9 \pm 26.0$  NCAP.mins, n= 9 (10mM glucose) vs.  $199.3 \pm 24.5$  NCAP.mins, n= 4 (10mM glucose and 200 $\mu$ M CIN)) but had no effect when supplied with 30mM glucose ( $447.2 \pm 23.8$  NCAP.mins, n= 9 (30mM glucose) vs.  $469.9 \pm 27$  NCAP.mins, n= 5 (30mM glucose and 200 $\mu$ M CIN)). Supply of 20mM lactate during HFS resulted in reduced maintenance of conduction compared to 10mM glucose and HFS ( $414.9 \pm 26.0$  NCAP.mins, n= 9 (10mM glucose) vs.  $367.2 \pm 28$  NCAP.mins, n= 4 (20mM lactate)), whilst 10mM glucose and 20mM lactate supplied together increased the maintenance of conduction compared to 10mM glucose alone during HFS ( $414.9 \pm 26.0$  NCAP.mins, n= 9 (10mM glucose) vs.  $500.3 \pm 48.7$  NCAP.mins, n= 4 (10mM glucose and 20mM lactate)). **(E)** Schematic of proposed cellular interactions. Glucose is taken up by both cell types (1 and 6) with increased availability resulting in increased uptake (3). Any lactate produced by glycolytic metabolism of supplied glucose (or stored glycogen) within Schwann cells is prevented being taken by A fibres in the presence of CIN (2 and 4). Lactate is presumed to be taken up mainly by axons (5 and 6). One-way ANOVA with Sidak's post hoc test. \* = p<0.05, \*\*\* = p<0.001, \*\*\*\* = p<0.0001 and ns = not significant. GLUT= glucose transporter and MCT= monocarboxylate transporter.

#### *4.3.4 Glycogen as a potential source of lactate*

Since blocking lactate uptake into axons and supplying additional lactate in the presence of 10mM glucose and HFS had the most significant effect, decreasing and increasing the maintenance of A fibre conduction respectively, the source of this lactate was next investigated. Glycogen derived lactate is utilised by axons of the mouse optic nerve during HFS in 10mM glucose, thus its role in the PNS under the same conditions is presumed.

Determining the contribution of glycogen involves the knowledge that the latency to failure under substrate free conditions (figure 4.3) acts as an indicator of glycogen availability; increased latency to failure suggests increased glycogen content available at the onset of substrate free conditions and vice versa. This knowledge can be utilised in two ways. Firstly, the nerve can be exposed to substrate free conditions after preincubation, e.g. 10mM glucose and HFS, for varying lengths of time (figure 4.6E). Comparison of the latency to failure after preincubation compared to baseline preincubation (~ 30 mins of 10mM glucose + 1Hz) provides an indication as to whether glycogen is used, not used, or levels are increased during preincubation. Secondly, glycogen can be completely metabolised by subjecting the nerve to substrate free conditions, resulting in a reduction in the CAP amplitude, prior to the experimental condition of interest e.g. 10mM glucose and HFS (figure 4.7G). Under these conditions, recovery of the CAP amplitude would suggest glycogen is not needed.

Preincubation experiments involved exposing the sciatic nerve to 10mM glucose (the main effect of treatment was found to be significant  $F(3,23)27.05$ ,  $p<0.0001$ ) or 30mM glucose (the main effect of treatment was found to be significant  $F(3,22)5.6$ ,  $p=0.005$ ) and HFS for 2, 4 or 6 hours prior to removal of an exogenous supply of energy substrate. Increasing the time the sciatic nerve was exposed to 10mM glucose and HFS resulted in accelerated latency to failure in subsequent substrate free conditions (post-hoc multiple comparisons,  $p=0.002$ ,

$p < 0.0001$  and  $p < 0.0001$ , respectively; figure 4.6A and B). In comparison latency to failure increased with increased exposure to 30mM glucose and HFS ( $p = 0.94$  and  $p = 0.009$ , respectively; figure 4.6A and D).

The main effect of treatment was not found to be significant with regards to percentage of CAP recovery ( $F(4,33)2.41$ ,  $p = 0.07$ ), but significant with regards to latency to CAP recovery ( $F(4,33)3.42$ ,  $p = 0.02$ ). After removal of an exogenous supply of energy substrate, resulting in a drop in the CAP amplitude to approximately 50% of its baseline, glucose, at either concentration, or lactate, were able to recover the A fibre CAP (figure 4.7A-C) equally as well (post-hoc multiple comparisons,  $p = 0.13$  and  $p = 0.92$ , respectively; figure 4.7D), and as fast ( $p = 0.19$  and  $p = 0.46$ , respectively; figure 4.7E). Interestingly, although the presence of CIN with 10mM glucose did not prevent the recovery of the CAP, conduction after recovery could not be sustained, instead resulting in almost immediate reduction in the CAP amplitude (figure 4.7A). Simultaneously recording the lactate released from the sciatic nerve and the A fibre CAP revealed an initial rapid rise in extracellular lactate on introduction of 10mM glucose, CIN and HFS that preceded that of the CAP recovery (figure 4.7F). The extracellular lactate continued to slowly rise as the CAP started to recover (figure 4.7F).

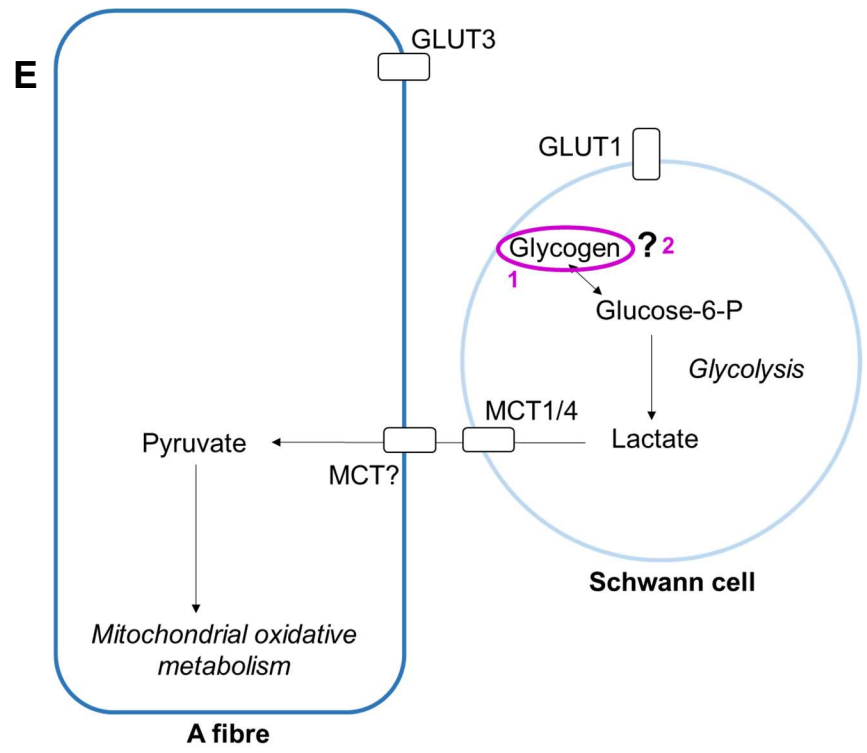
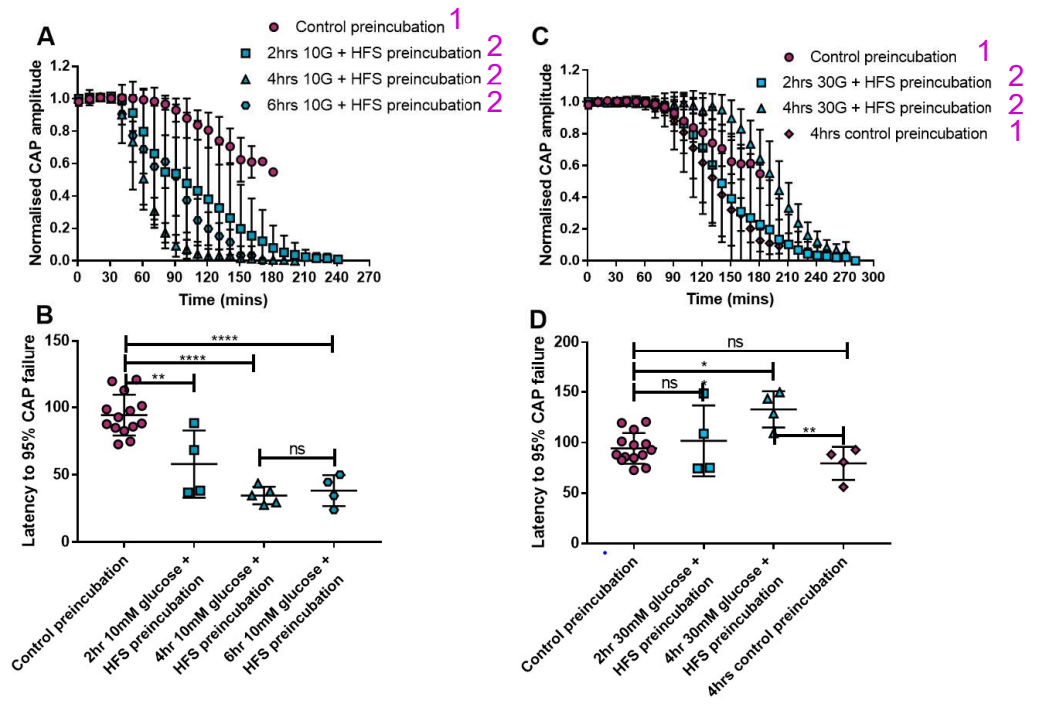


**Figure 4.6:** Glycogen is metabolised during normoglycaemia, but synthesised during increased glucose supply, and HFS. **(A)** Conduction failure during removal of exogenous energy substrate supply was accelerated as result of exposure to HFS when supplied with 10mM glucose compared to baseline conditions. **(B)** Preincubating the nerve in 10mM glucose and HFS for increasing durations reduced the latency to A fibre CAP failure during subsequent substrate free conditions until further exposure has no further effect on latency to CAP failure ( $58 \pm 24.9$  mins after 2hrs (n= 4),  $34.7 \pm 6.5$  mins after 4hrs (n= 5) and  $38.3 \pm 11.5$  mins after 6hrs (n= 4) compared to  $94.3 \pm 15.1$  mins after baseline incubation in 10mM glucose at 1Hz (n= 14)); a time which appears to coincide with the slow conduction failure during 10mM glucose and HFS (see Figure 2A). **(C)** Increased exposure to 30mM glucose during HFS prolonged the maintenance of conduction in subsequent substrate free conditions compared to baseline incubation. **(D)** Latency to A fibre CAP failure during substrate free conditions was increased as a result of preincubation in 30mM glucose during HFS ( $101.7 \pm 35.1$  mins after 2hrs (n= 4) and  $132.8 \pm 18.0$  mins after 4hrs (n= 4) compared to  $94.3 \pm 15.1$  mins after baseline incubation in 10mM glucose at 1Hz (n=14)). Increasing baseline incubation from 30 minutes to 4 hours did not influence the latency to failure in subsequent substrate free conditions ( $94.3 \pm 15.1$  mins (n= 14) vs.  $79.5 \pm 16.3$  mins (n= 4)). **(E)** Schematic of proposed cellular interactions. Under substrate free conditions Schwann cell glycogen derived lactate is released and taken up by A fibres via MCTs (1). The latency to CAP failure under substrate free conditions acts as an indirect measure of glycogen content after preincubation (2). One-way ANOVA with Sidak's post hoc test. \*\* =  $p < 0.01$ , \*\*\*\* =  $p < 0.0001$ , ns= not significant. GLUT= glucose transporter and MCT= monocarboxylate transporter.

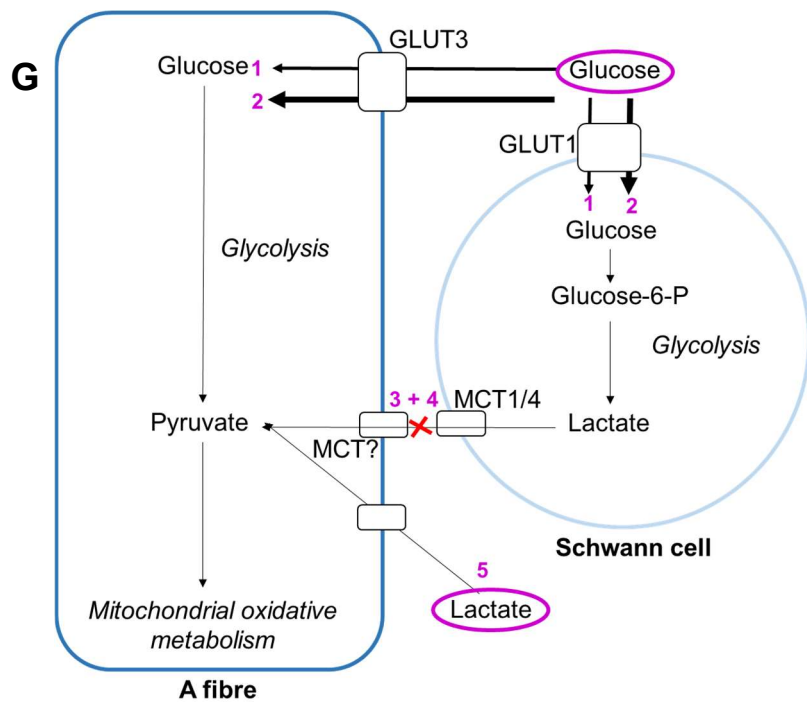
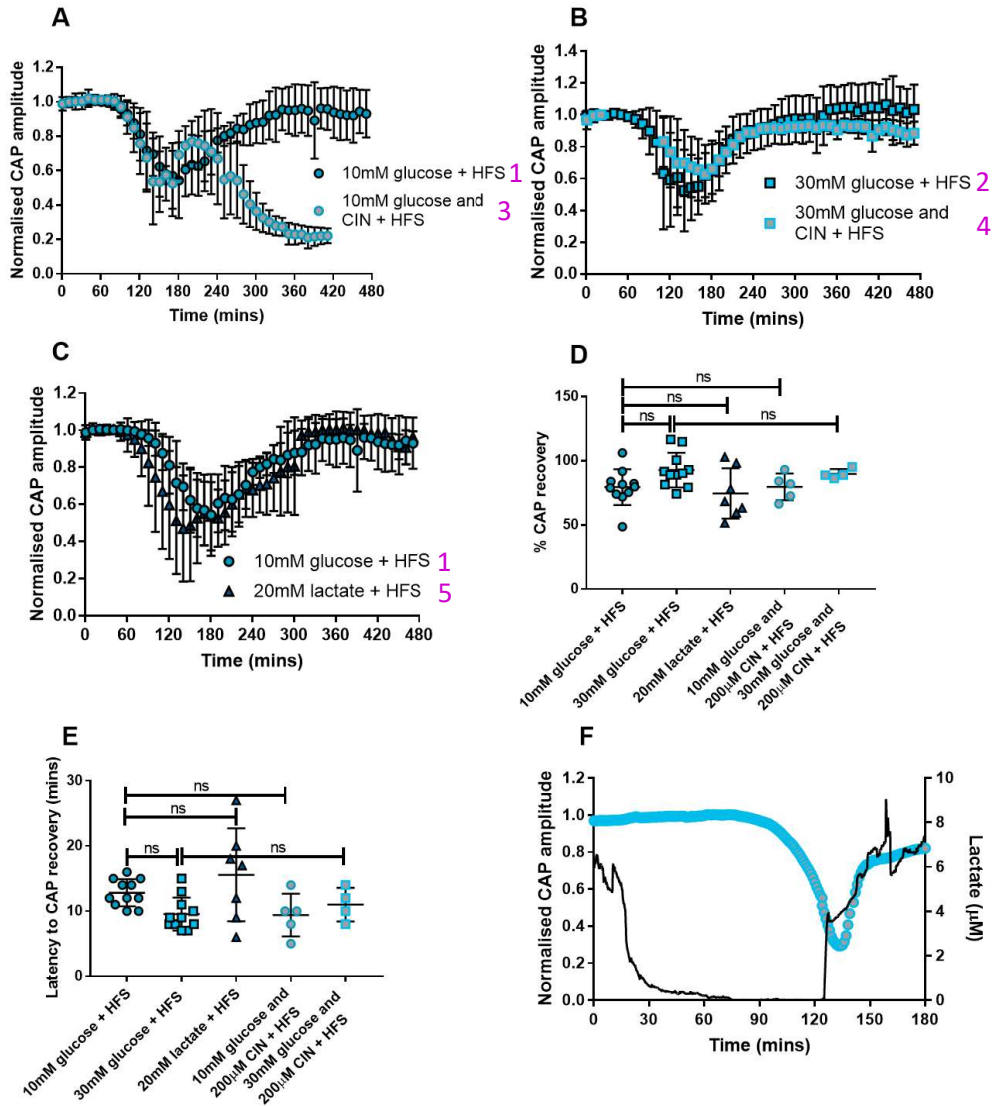


**Figure 4.7:** The A fibre CAP can be restored in the absence of glycogen. **(A)** After exposure to substrate free conditions resulting in a drop in amplitude, the A fibre CAP was restored by normoglycemic glucose and lactate during HFS. The recovery was not sustained with the addition of 200 $\mu$ M CIN. **(B)** The A fibre CAP was recovered in higher concentrations of glucose, even in the presence of 200 $\mu$ M CIN. **(C)** Exogenous supply of lactate was able to recover the A fibre CAP. **(D)** The A fibre CAP was restored to a similar level under all 5 conditions of HFS ( $79.5 \pm 14$ , n= 11 (10mM glucose) vs.  $92.8 \pm 13.4$ , n= 11 (30mM glucose),  $74.6 \pm 19.6$ , n= 7 (20mM lactate),  $79.7 \pm 10.4$ , n= 5 (10mM glucose and 200 $\mu$ M CIN) and  $89.8 \pm 3.7$ , n= 4 (30mM glucose and 200 $\mu$ M CIN)). **(E)** The time in which the A fibre CAP starts to recover during HFS after the onset of energy substrate supply was equal amongst all 5 conditions ( $12.8 \pm 2.1$ , n= 11 (10mM glucose) vs.  $9.5 \pm 2.5$ , n= 11 (30mM glucose),  $15.6 \pm 7.1$ , n= 7 (20mM lactate),  $9.4 \pm 3.3$ , n= 5 (10mM glucose and 200 $\mu$ M CIN) and  $11 \pm 2.6$ , n= 4 (30mM glucose and 200 $\mu$ M CIN)). **(F)** A trace of simultaneous lactate and CAP recording. During recovery of the A fibre in 10mM glucose, CIN and HFS, lactate in the extracellular space sharply increases before slowly rising as the CAP begins to recover (n= 1). **(G)** Schematic of proposed cellular interactions. Glucose is taken up by both cell types (1) with increased availability resulting in increased uptake (2). Any lactate produced by glycolytic metabolism of supplied glucose within Schwann cells is prevented being taken by A fibres in the presence of CIN (3 and 4). Lactate is presumed to be taken up mainly by axons (5). One-way ANOVA with Sidak's post hoc test. ns= not significant. GLUT= glucose transporter and MCT= monocarboxylate transporter.

## 4.4 Discussion

The data from this chapter extends the knowledge of established Schwann cell-axon metabolic interactions that occur during the pathological condition of aglycaemia to the more physiological condition of increased axonal firing. Firstly, A fibre conduction can be better maintained by simply increasing the supply of glucose. Schwann cell lactate, glycogen and/or glucose derived, acts as an additional source of energy when exogenous supplied 10mM glucose was insufficient to meet the increased energy demand of the A fibres

### *4.4.1 The low metabolic rate of the sciatic nerve in the absence of energy substrate supply*

Removal of the exogenous supply of energy substrate resulted in failure of A fibre conduction after an hour and a half (figure 4.3A and B), 6 times longer than that of the mouse optic nerve under equivalent conditions (Brown *et al.*, 2003). The energy source for this conduction is generally ascribed to glycogen, localised specifically to the Schwann cells and supplied to axons in the form of lactate (Brown *et al.*, 2012). Therefore, increasing the energy demand on the nerve further by HFS during substrate free conditions should result in an accelerated failure of conduction due to faster metabolism of the available glycogen. This was observed where latency to conduction failure was accelerated by approximately 50% when increasing the stimulus frequency from 1Hz to 100Hz (figure 4.3A and B). However, if glycogen derived lactate was the only source of energy at the onset of substrate free conditions, blocking the uptake (using CIN) and subsequent use of lactate by the axons should result in rapid failure of the A fibre CAP. Under substrate free and CIN conditions, A fibre conduction was maintained for approximately 50 minutes, which was further reduced to ~30 minutes in HFS conditions. Even with the addition of CIN to substrate free conditions conduction is still maintained for longer than that of the mouse optic nerve under substrate free conditions alone, suggesting the nerve slowly utilises any available glucose and glucose derived substrates that might be remaining at the onset of the substrate free

conditions. This highlights the lower metabolic rate of the sciatic compared to the optic nerve and reflects the difference in responses between the central and peripheral nervous system to ischaemia; occluded blood supply to peripheral nerves results in sensory and motor paralysis 15 minutes after the onset (Richards, 1951) whilst a comatose state is induced within minutes after restricted blood supply to the brain (Kabat & Anderson, 1943). However, it must be borne in mind that the optic nerve consists of far more axons than that of the sciatic nerve (100,000 vs 27,000 axons in the rat) and therefore could impact on the shorter latency to failure of the optic compared to sciatic nerve (Schmalbruch, 1986; Pazos *et al.*, 2015).

#### **4.4.2 Schwann cell metabolic support during increased firing of A fibres**

When the firing frequency of A fibres was increased, control (10mM) concentrations of glucose no longer provided sufficient energy to fully maintain conduction for the 8 hour experimental period. However, this was overcome by increasing the concentration of available glucose (figure 4.4A and B). The decline in the A fibre CAP after about 4 hours of HFS under normoglycemic conditions can be explained by a depletion of Schwann cell glycogen, and glucose at an insufficient concentration to meet the energy demands of both the A fibres and Schwann cells. The maintenance of the A fibre conduction in 30mM glucose during HFS therefore suggests glucose is available at a high enough concentration to support both the A fibres and Schwann cells and Schwann cell glycogen levels are unlikely to be reduced. To complement these findings future studies using techniques such as Periodic Acid-Schiff (PAS) staining, immunohistochemistry and glycogen assays, would enable direct measurement of changes in the glycogen content under these HFS conditions (Kong *et al.*, 2002; Evans *et al.*, 2013; Oe *et al.*, 2016). The response of the A fibres to the two concentrations of glucose and HFS is comparable to that of the mouse optic nerve, but once again the latency to A fibre CAP failure is much extended compared to optic nerve in the presence of 10mM glucose

and HFS (Brown *et al.*, 2003). A fibre conduction also failed much more gradually under this condition (complete failure does not occur within 8 hours) compared to the optic nerve in which conduction failure is very rapid (Brown *et al.*, 2003). This again highlights the sluggish, low metabolic rate of the sciatic nerve.

The metabolic support role of Schwann cells has been demonstrated during aglycaemia in that they provide glycogen derived lactate to the A fibres, which they myelinate (Brown *et al.*, 2012). Therefore, we wanted to investigate whether they play a similar role during the more physiological condition of increased axonal activity. Blocking lactate uptake into axons dramatically reduced the maintenance of conduction of A fibres when supplied with 10mM glucose, but had no effect in the presence of increased glucose (30mM) supply. The response of the A fibres to CIN with 10mM glucose and HFS is partially comparable to that of the optic nerve, however optic nerve CAP failure is almost instantaneous (Brown *et al.*, 2003, 2004) whilst the sciatic nerve CAP was maintained for a considerable period. Two main assumptions can be made from these findings: 1) A fibres directly take up glucose and metabolise glucose during HFS since conduction is maintained (fully in 30mM glucose and partially in 10mM glucose) when it is the only accessible energy substrate, and 2) under normoglycemic conditions A fibres require lactate as an energy source when energy demand is increased. This makes metabolic sense since lactate is converted to pyruvate which feeds the tricarboxylic acid (TCA) cycle, which is part of oxidative phosphorylation, the largest energy producing component of metabolism, and thus skipping the ATP-requiring glycolysis (Champe *et al.*, 2008). This is further supported by the full maintenance of conduction when 10mM glucose was supplied with additional lactate during HFS. Supplying lactate to the nerve alone, however, was less efficient than 10mM glucose at providing energy to maintain A fibre conduction during HFS. This may reflect a possible glycolytic requirement of either, or both the axons and Schwann cells. Overall,

under normoglycemic conditions of HFS Schwann cells provide metabolic support to A fibres in the form of lactate.

A potential source of the lactate is glycogen, however unlike during aglycaemia glucose is still being supplied to the sciatic nerve during HFS therefore glucose is another potential source of Schwann cell lactate. Since these are the only two energy substrates present under these experimental conditions, removing either one provides information about both, i.e. if conduction is maintained in the absence of glycogen it suggests glycogen is not required and under these specific conditions and glucose is the source of lactate. The preincubation experiments suggest that glycogen is metabolised when the nerve was subjected to HFS in the presence of 10mM glucose, seen in the reduction in latency to failure in subsequent substrate free conditions with increased preincubation (figure 4.6A and B). This suggests glycogen derived lactate is supplied by the Schwann cells to the A fibres during increased axonal activity. Furthermore, there appears to be no difference between the onset of conduction failure after 4 or 6 hours of 10mM glucose and HFS, suggesting glycogen is completely metabolised by 4 hours. Since glycogen appears to be metabolised under HFS conditions, the duration in which A fibre conduction was maintained for (~40 minutes) in the subsequent substrate free condition is again ascribed to the low metabolic rate and slow metabolism of remaining endogenous energy substrates.

Interestingly, 4 hours appears to coincide with the onset of the gradual decline in CAP amplitude during HFS in 10mM glucose (figure 4.4A), providing additional support to Schwann cell glycogen as the source of lactate. In comparison, when the sciatic nerve was exposed to increasing durations of 30mM glucose and HFS the maintenance of conduction in subsequent substrate free conditions was increased, suggesting glucose is being supplied in excess of demand and thus is stored as glycogen. We can be sure 30mM glucose exceeds the energy demand of the nerve during HFS, since preincubating the nerve for 4 hours under control, lower energy demand conditions did not increase

the latency to failure in subsequent substrate free conditions (figure 4.6C and D). This is another example highlighting the low metabolic rate of the sciatic, in that even whilst the A fibres are firing an action potential every 10ms (i.e. 100Hz), the nerve has the energy to synthesis glycogen from glucose.

Although the preincubation experiments suggest glycogen is metabolised under normoglycemic conditions and HFS, they do not differentiate between glycogen and glucose as the source of lactate since both are present, at least at the onset, during 10mM glucose and HFS. Therefore, completely depleting glycogen prior to the HFS experimental condition removes glycogen as a potential lactate source. In order to ensure glycogen is completely depleted, the sciatic nerve was exposed to substrate free conditions until the A fibre CAP amplitude reached approximately half its baseline value, at which point supply of energy substrate was resumed and HFS applied. Recovery of the CAP amplitude suggests these points: 1) loss of the CAP does not necessarily lead to axon damage, as long as substrate is appropriately resupplied, and 2) glycogen is not necessarily a source of energy to restore disrupted ion gradients whilst firing rate has increased, two processes that are of high energy demand. Surprisingly, A fibre conduction was recovered during HFS with the supply of either 10mM glucose, 30mM glucose or 20mM lactate (figure 4.7A-E). This is contrary to the preincubation experiments findings, but since the recovery experiments involve an additional energy requiring process, it suggests that glycogen is not a necessary source of energy for A fibres, but will be utilised if available under HFS conditions. Moreover, although the CAP is recovered, this restoration of conduction is transient when CIN was supplied in addition to 10mM glucose and HFS. The instant rise in extracellular lactate that occurs immediately with the introduction of the recovery condition (figure 4.7F) highlights the rapid production of lactate by Schwann cells and the likely requirement of this lactate as an energy source by A fibres. Due to the presence of CIN the A fibres were unable to take up and metabolise this lactate thus

resulting in the continuous gradual rise in lactate building up in the extracellular space. This further supports the importance of lactate as an energy substrate for A fibres during increased neuronal activity, and since only glucose, not glycogen, was available it suggests glucose is the potential source of lactate. This fits the earlier suggestion of a glycolytic nature of Schwann cells as well as the general concept that glial cells are preferentially glycolytic and produce lactate as the end product of glycolysis (Walz & Mukerji, 1988). The findings from these recovery experiments using the mouse sciatic nerve contrast with the predepletion experiments carried using the mouse optic nerve, which indicate astrocytic glycogen as the source of lactate (Brown *et al.*, 2003, 2004).

## 4.5 Conclusion

Altogether, Schwann cell supply of lactate appears to be an energy source for A fibres with increased firing rate. Both the A fibres and Schwann cells take up and metabolise the available glucose during HFS. However, under normoglycemic conditions A fibre glucose uptake alone is not sufficient to maintain conduction and they utilise Schwann cell derived lactate, most likely from glucose but also glycogen if it is available (figure 4.8). Even when glucose supply is increased it may be more energetically favourable for the A fibres to utilise lactate, potentially derived from the increasing stores of Schwann cell glycogen, rather than take up more glucose. This is in agreement with the suggestion that Schwann cells take up more of the available glucose than axons (Véga *et al.*, 2003).

Although the presence of glycogen appears beneficial to mouse optic nerve axons, but not to mouse sciatic nerve A fibres, axons of both nerve types display a requirement for metabolic support from their respective glial cell in the form of lactate during increased axonal firing. Therefore, our hypothesis is rejected, but our aim met. These findings provide support for a universal theory of glia-axon metabolic interactions between the central nervous system (CNS) and peripheral nervous system (PNS), despite evidence for differences in the way astrocytes and Schwann cells provide metabolic support (figure 4.8).

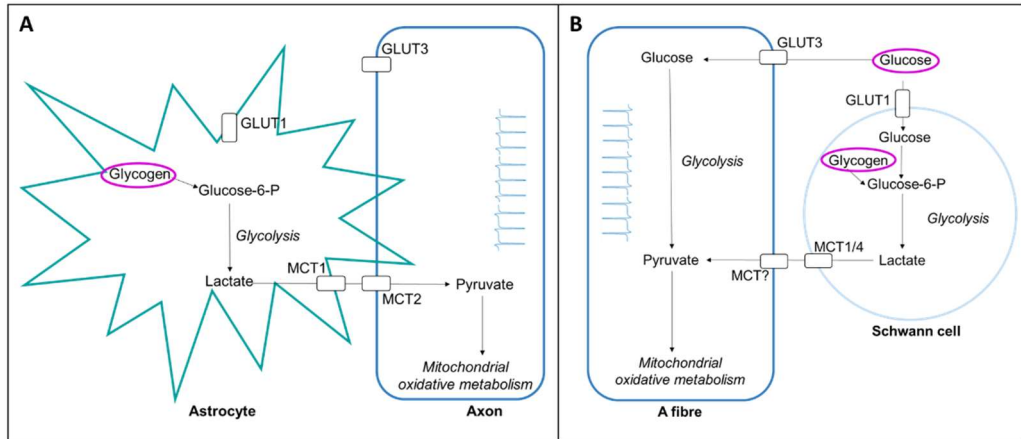


**Figure 4.8:** Glia-axon metabolic interactions during increased neuronal firing. **(A)** Astrocytes of the CNS provide glycogen derived lactate for axons to enable conduction to be maintained briefly. **(B)** Schwann cells of the PNS supply lactate, mostly likely derived from glucose but also glycogen if it is available, to maintain conduction for extended periods. GLUT= glucose transporter and MCT= monocarboxylate transporter.

# **Chapter 5: $K^+$ , a potential universal signal for axon-glia metabolic interactions**

---

## 5.1 Introduction

Metabolic interactions between axons and glia (both astrocytes (Bélanger *et al.*, 2011) and oligodendrocytes (Meyer *et al.*, 2018)) of the central nervous system (CNS) are widely recognised, with disruption of this metabolic cell-to-cell communication associated with many pathologies (Bak *et al.*, 2018). Such interactions are also becoming apparent within the peripheral nervous system (PNS; Rich & Brown, 2018b), with glycogen, glucose and lactate pivotal energy substrates in this metabolic cooperation. Whilst research has shown glia can metabolically support their associated axons, it is not fully understood how the glial cells recognise when to provide their supply of energy substrate. A signal(s) must first be released from axons, which communicates their increased energy demand and need for energy substrate to the glia. The glia then require a means by which they are capable of sensing this signal and a pathway that ensures changes in the levels of this signal regulates the glycolytic and glycogenolytic metabolism of the glial cells.

Glutamate was one of the first signals to be proposed with the introduction of the astrocyte-neurone lactate shuttle hypothesis (ANLSH; Pellerin & Magistretti, 1994). This model describes how the uptake of glutamate, released by CNS glutamatergic neurones, activates astrocytic glycolysis. Glutamate is taken up by astrocytes via the glutamate transporter which co-transportes glutamate with  $\text{Na}^+$ , resulting in a rise in both intracellular glutamate and  $\text{Na}^+$ . The rise in intracellular  $\text{Na}^+$  activates the glycolytic ATP dependent  $\text{Na}^+/\text{K}^+$  ATPase thus stimulating glucose uptake, glycolysis and subsequent lactate release. Recently, glutamate has been found to act as a metabolic signal between axons and oligodendrocytes, known as the axo-myelinic synapse (Micu *et al.*, 2018). Here glutamate released from the internodal axon acts on AMPA and NMDA receptors of overlying myelin of the oligodendrocytes increasing intracellular  $\text{Ca}^{2+}$  and ultimately leading to increased glucose influx and glycolytic production of lactate within oligodendrocytes (Micu *et al.*, 2016; Saab *et al.*, 2016). There is a

lot less information available regarding glutamate as a metabolic signal within the PNS, although its presence within axons of peripheral nerves provides promise for its role in axon-Schwann cell metabolic interactions (De Biasi & Rustioni, 1988; Westlund *et al.*, 1989; Meister *et al.*, 1993). Schwann cells also express glutamate transporters and functional glutamate receptors (Carozzi *et al.*, 2008; Campana *et al.*, 2017), suggesting the potential for glutamate to trigger Schwann cell lactate production as the result of uptake, as with astrocytes, but also as the result of increased intracellular  $\text{Ca}^{2+}$  via ionotropic glutamate receptors as occurs in oligodendrocyte myelin.

Although the evidence for glutamate as a metabolic signal in the CNS is compelling, its role is debated for a couple of reasons: 1) since the proposal of the ANLSH the evidence for the glycolytic preferential fuelling of the  $\text{Na}^+/\text{K}^+$  ATPase has been questioned (Fernández-Moncada & Barros, 2014), and 2) glutamate is not universally present throughout the nervous system i.e. it is only present in excitatory glutamatergic neurones. With universality in mind  $\text{K}^+$  has emerged to the forefront of this area of research. Released by all axons during the repolarisation phase of the action potential, the amount of  $\text{K}^+$  efflux is a direct indication of neuronal firing frequency and therefore energy demand (Baylor & Nicholls, 1969), making it an ideal activity dependent metabolic signal reflecting the degree of neuronal activity. Moreover, it is widely considered that the glial cell membrane potential, particularly astrocytes, is highly sensitive to  $\text{K}^+$ , with increases in extracellular  $\text{K}^+$  depolarising the membrane potential in a manner accurately predicted by the Nernst equation (Kuffler *et al.*, 1966; Ransom & Goldring, 1973), making them ideal sensors of changes of extracellular  $\text{K}^+$ . Increased extracellular  $\text{K}^+$ , produced by neuronal activity, is associated with increased astrocytic glycolysis (Ruminot *et al.*, 2019). The membrane depolarisation in response to elevations in extracellular  $\text{K}^+$  are thought to activate the sodium bicarbonate cotransporter (NBC) leading to intracellular alkalinisation, which stimulates soluble adenylyl cyclase resulting in increased cAMP and subsequent glycogenolysis (Choi *et*

*al.*, 2012). Research into  $K^+$  as a metabolic signal is ongoing with very little known about its metabolic role for myelinating glia. In particular, with regards to Schwann cells, their membrane potential in comparison to astrocytes, is thought to be more depolarised than the reversal potential for  $K^+$  and therefore not Nernstian (Hargittai *et al.*, 1991) implying they may be less sensitive to changes in extracellular  $K^+$ . Despite this, Schwann cells are ideally positioned to sense  $K^+$  released from axons, with  $K^+$  channels responsible for the extrusion of  $K^+$  from the axon located at the juxtaparanode of the internode (myelinated) region (Waxman & Ritchie, 1993; Stassart *et al.*, 2018), and have been found to respond to axonal conduction, possibly as the result of increased extracellular  $K^+$  depolarising the paranodal loops (Lev-Ram & Ellisman, 1995).

The research thus far suggests glutamate has the potential to act as an effective metabolic signal within both the central and peripheral nervous system. However, the insufficient evidence with regard to  $K^+$  as a metabolic signal within the PNS, implies further research is still required to unravel the metabolic communication pathways between axons and glia.

*Aim:*

To expand upon the role of  $K^+$  as a metabolic signal between axons and glia in the CNS and investigate its applicability with the PNS.

*Objective:*

Using lactate biosensors measure changes in lactate release, from both the mouse optic and sciatic nerve *ex vivo*, in response to changes in extracellular  $K^+$  concentration and high frequency stimulation (HFS).

*Hypothesis:*

1. Increased extracellular  $K^+$  will increase the concentration of lactate release by the optic nerve.

2. Increased extracellular  $K^+$  will have little effect on the concentration of lactate released by the sciatic nerve.

## 5.2 Methods

### 5.2.1 Mice and tissue dissection

See chapter 2.1 for full details of the mice and nerve dissections.

A total of 35 mice were used to collect sciatic (n= 47) and optic (n= 6) nerves for a mixture of compound action potential (CAP) electrophysiology and measurements of lactate using lactate biosensors.

### 5.2.2 Stimulus evoked CAP electrophysiology

Paired nerve CAP electrophysiology (see chapter 2.2 and 3.2.2 for more detail) was used with sciatic nerves, where only the A fibre CAP (figure 2.4A of chapter 2) was recruited using a stimulus intensity of ~15V (figure 2.5A of chapter 2) at control frequency of 1Hz. The n number refers to the number of individual nerves recorded from.

Nerves were first incubated in 10mM glucose and stimulated at 1Hz for a baseline period of 30 minutes before being subjected to the experimental condition. HFS was defined as 100Hz stimulus frequency. When used in combination with lactate biosensors (see below) only one nerve was stimulated.

#### 5.2.2.i Data analysis

See chapter 2.2.1 for more details of CAP data analysis. Specifically, the amplitude of the A fibre CAP was normalised to 1, before curve fitting using the Boltzmann sigmoidal equation to measure the latency to failure in Excel (Microsoft Office), or an average CAP amplitude at each extracellular K<sup>+</sup> concentration taken for each nerve. Latency to failure was calculated as a fall in the CAP to 95% of its normalised baseline value (Wender *et al.*, 2000). Data are expressed as mean  $\pm$  SD and statistical analysis was performed using Prism 7 (GraphPad Software), where p<0.05 was considered significant.

### *5.2.3 Lactate biosensors*

See chapter 2.3 for a detailed explanation of lactate electrode implementation to the superfusion chamber and recording of lactate. The n number refers to the number of individual nerves recorded from.

It should be borne in mind that the lactate was recorded at the border of the nerve, and is thus extracellular, and does not quantitatively reflect the concentration of lactate present in the extracellular space of the nerve. Although the concentration of lactate within the extracellular space of nerve is likely to be higher than that recorded due to the dilution of lactate in the bath artificial cerebral spinal fluid (aCSF), it qualitatively reflects the extracellular concentration.

#### *5.2.3.i Data analysis*

See chapter 2.3.i for more detail of lactate analysis.

Lactate biosensor recordings were filtered (Clampfit 10.7) before being converted to a concentration based on the lactate calibration. The concentration of lactate was taken at its peak or when it plateaued in response to changes in extracellular K<sup>+</sup> or stimulus frequency. Data are expressed as mean  $\pm$  SD.

## 5.3 Results

### *5.3.1 The relationship between extracellular K<sup>+</sup> and lactate concentration*

Lactate biosensors were used to estimate the change in the concentration of extracellular lactate in response to changes in the concentration of extracellular K<sup>+</sup>. This was achieved by superfusing the nerve with aCSF containing variable concentrations of K<sup>+</sup> in the presence of the lactate biosensor. Changes in aCSF K<sup>+</sup> were complemented by equimolar changes in Na<sup>+</sup>, e.g. control aCSF contains 3mM K<sup>+</sup> and 126mM Na<sup>+</sup>, thus an increase in K<sup>+</sup> to 9mM is balanced by a decrease in Na<sup>+</sup> to 120mM.

The optic and sciatic nerve displayed comparable responses to changes in extracellular K<sup>+</sup> (figures 5.1Ai and Bi, respectively), with extracellular K<sup>+</sup> above and below the normal 3mM increasing and decreasing, respectively, the steady state concentration of lactate recorded (figures 5.1Aii and Bii). This relationship was found to be logarithmic for both nerves (slope= 75.6 and 5.6  $\mu\text{M}$  lactate/mM K<sup>+</sup>, optic and sciatic respectively).

Further inspection of a complete lactate recording from either nerve reveals further details of the response to extracellular K<sup>+</sup> (figures 5.1Ai and Bi). On exposure to higher than 3mM extracellular K<sup>+</sup>, the concentration of extracellular lactate rose rapidly to a peak before slowly declining. In contrast, superfusion with aCSF containing 0.9 or 0.3mM K<sup>+</sup> resulted in an initial rapid decrease in extracellular lactate followed by a further gradual decrease to plateau.

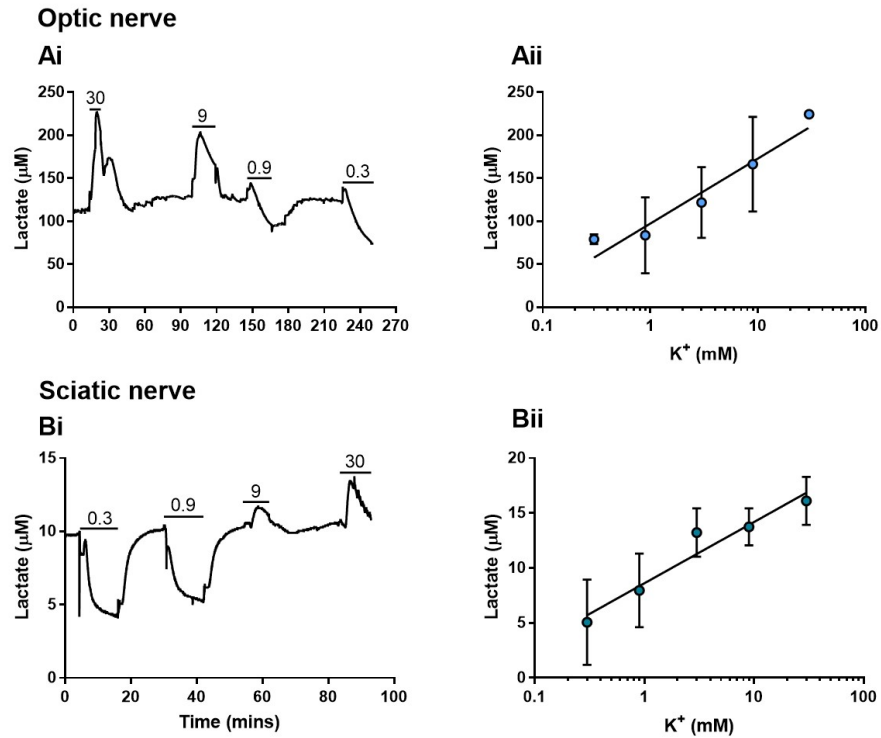


**Figure 5.1:** Lactate release is dependent upon extracellular  $\text{K}^+$  concentration. **(A)** Lactate release from astrocytes of the mouse optic nerve is dependent upon the concentration of extracellular  $\text{K}^+$ . **(i)** Representative trace of lactate biosensor recording during superfusion of the optic nerve with different concentrations of  $\text{K}^+$ . In between each concentration the nerve was superfused with control 3mM  $\text{K}^+$  to enable recovery and prevent axon damage. **(ii)** As the concentration of extracellular  $\text{K}^+$  increased, the concentration of extracellular  $\text{K}^+$  recorded increased ( $n=3$ ). **(B)** Lactate release from myelinating Schwann cells of the mouse sciatic nerve is influenced by the concentration of extracellular  $\text{K}^+$ . **(i)** Representative trace of lactate biosensor recording during superfusion of the sciatic nerve with different concentrations of  $\text{K}^+$ . In between each concentration the nerve was superfused with control 3mM  $\text{K}^+$  to enable recovery and prevent axon damage. **(ii)** As the concentration of extracellular  $\text{K}^+$  increased, the concentration of lactate released from the sciatic nerve increased ( $n=5$ ). Horizontal lines in Ai and Bi denote  $\text{K}^+$  in mM.

### 5.3.2 The effect of extracellular $K^+$ on sciatic nerve A fibre conduction

The ability of A fibres to maintain conduction in the presence of increasing and decreasing concentrations of extracellular  $K^+$  was investigated (figure 5.2A). Lowering the concentration of extracellular  $K^+$  below 3mM had no effect on the A fibre CAP amplitude, even at concentrations as low as 0.3mM (figure 5.2B). As the concentration of  $K^+$  rose to 12mM the CAP amplitude started to decrease, with concentrations of 20mM and above resulting in complete CAP failure (figure 5.2A and 3B).

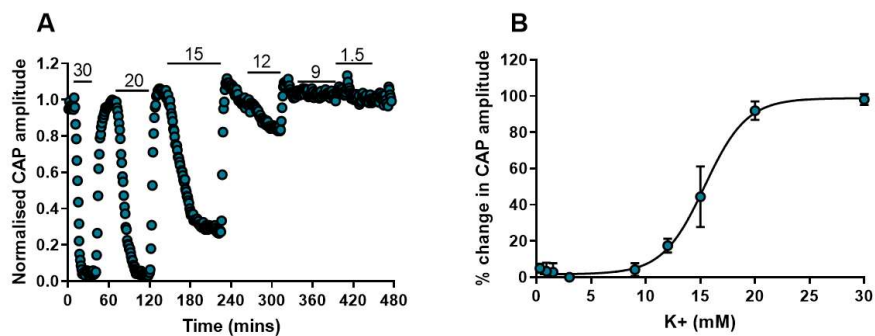


**Figure 5.2:** A fibre conduction during changes in extracellular  $K^+$ . **(A)** Representative trace of A fibre CAP amplitude during superfusion of the sciatic nerve with different concentrations of  $K^+$ . In between each concentration the nerve was superfused with control 3mM  $K^+$  to enable recovery and prevent axon damage. Horizontal lines denote  $K^+$  in mM. **(B)** As the concentration of extracellular  $K^+$  increased the reduction in the A fibre CAP amplitude increased with a  $V_{50}$  of  $13.7 \pm 2.1$  mM ( $n=9$ ).

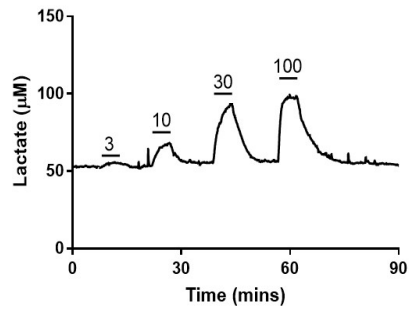
### *5.3.3 The effect of stimulus frequency on the extracellular lactate concentration*

Lactate release from the nerves was not just recorded in response to variable aCSF  $K^+$  concentration, but as the result of increased axonal release of  $K^+$ . This was achieved by increasing the frequency of stimulus applied to the nerve whilst simultaneously recording the extracellular lactate. An increase in action potential firing is directly related to an increase in the concentration of extracellular  $K^+$ .

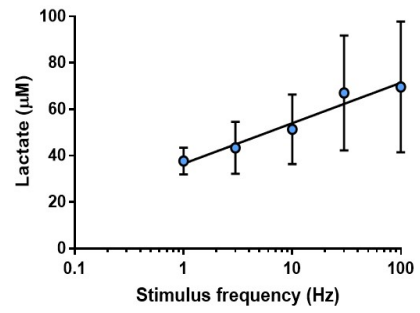
Increasing the frequency of stimulus applied to the mouse optic nerve resulted in obvious and substantial changes in the concentration of extracellular lactate recorded (figure 5.3Ai). Increasing the stimulus frequency slightly from 1Hz to 3Hz resulted in an approximately 20% increase in the concentration of extracellular  $K^+$ , with a stimulus frequency of 100Hz roughly doubling the concentration of lactate released from the optic nerve compared to baseline 1Hz stimulation. The magnitude of the lactate increase was related to the logarithm of the stimulus frequency (figure 5.3Aii). In comparison, when this stimulus protocol was applied to the mouse sciatic nerve, a stimulus frequency of 30Hz was required to increase the extracellular  $K^+$  by 10%, with 100Hz stimulus not even causing a 50% rise in extracellular lactate. As a result, this relationship was not found to be logarithmic (figure 5.3Bii). The increase in lactate released from the sciatic nerve during 100Hz stimulus appears equivalent to that produced in response to an increase in extracellular  $K^+$  to 6mM (figure 5.3Biii).

### Optic nerve

**Ai**

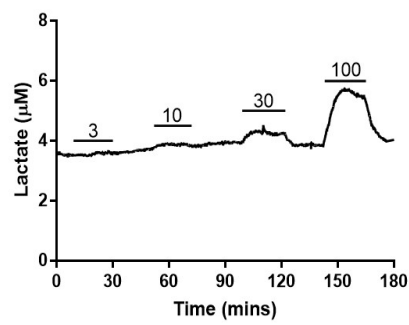


**Aii**

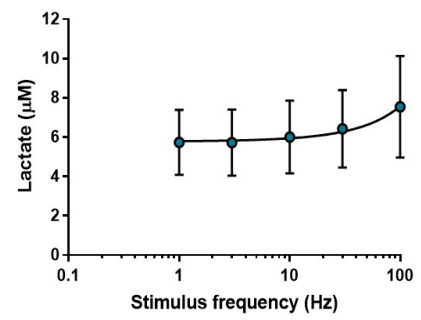


### Sciatic nerve

**Bi**



**Bii**



**Biii**

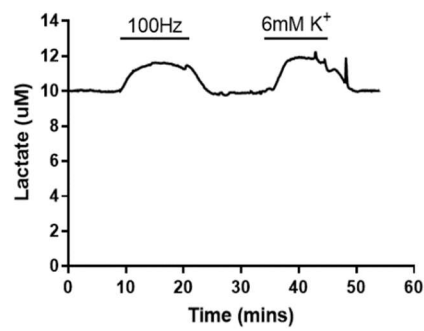


**Figure 5.3:** Lactate release from axons during increased firing frequency. **(A)** Lactate release from astrocytes of the mouse optic nerve is triggered by increased frequency of stimulation. **(i)** A representative trace of a lactate biosensor recording during increased frequency of stimulation of the optic nerve. In between each increasing stimulus frequency, the nerve was stimulated at control 1Hz to enable recovery. **(ii)** Increasing the frequency of stimulation increased the concentration of lactate detected by the biosensor (n= 3). **(B)** Lactate release from myelinating Schwann cells of the mouse sciatic nerve is stimulated by high frequency stimulation. **(i)** A representative trace of a lactate biosensor recording during increased frequency of stimulation of the sciatic nerve. In between each increasing stimulus frequency, the nerve was stimulated at control 1Hz to enable recovery. **(ii)** Stimulus frequencies above 30Hz resulted in an increase in the concentration of extracellular lactate (n= 6). **(iii)** A trace comparing the concentration of lactate released from the sciatic nerve during 100Hz and in the presence of 6mM K<sup>+</sup> aCSF. In between each condition the nerve was stimulated at 1Hz in 3mM K<sup>+</sup> aCSF (n= 1). Horizontal lines in Ai and Bi denote the stimulus frequency in Hz.

#### *5.3.4 The effect of BaCl<sub>2</sub> on the latency to A fibre CAP failure during substrate free conditions*

Since increases in extracellular K<sup>+</sup> were found to trigger increased production of lactate by astrocytes and myelinating Schwann cells of the mouse optic and sciatic nerve, respectively, the role of K<sup>+</sup> to trigger glycogen metabolism was investigated. Barium chloride (BaCl<sub>2</sub>) is used to block the inwardly rectifying K<sup>+</sup> channels expressed by glial cells as a result K<sup>+</sup> accumulates in the extracellular space (Bay & Butt, 2012; the main effect of treatment was found to be significant  $F(3,23)26.26$ ,  $p<0.0001$ ).

Exposing the sciatic nerve to substrate free conditions, when glycogen is considered the only source of energy, resulted in failure of the A fibre CAP within ~90 minutes (figure 5.4A and B). The addition of 100µM BaCl<sub>2</sub> accelerated this latency to failure (post-hoc multiple comparisons  $p=0.04$ ) but not to the same degree as imposing HFS (100Hz;  $p=0.008$ ) during substrate free (figure 5.4A and B). The combination of BaCl<sub>2</sub> and HFS during the removal of an exogenous supply of energy substrate to the sciatic was not found to give an additive affect but rather resulted in a similar latency to A fibre CAP failure to that during substrate free and HFS ( $p=0.93$ ; figure 5.4A and B).

Recording the lactate released from the sciatic nerve under baseline aCSF (10mM glucose) and stimulus frequency (1Hz) revealed an increase with the addition of 100µM BaCl<sub>2</sub> (figure 5.4C). Under these baseline conditions, increasing the stimulus frequency to 100Hz (HFS) was also found to increase the concentration of extracellular lactate, with the application of both HFS and BaCl<sub>2</sub> resulting in a further lactate release from the mouse sciatic nerve (figure 5.4D).

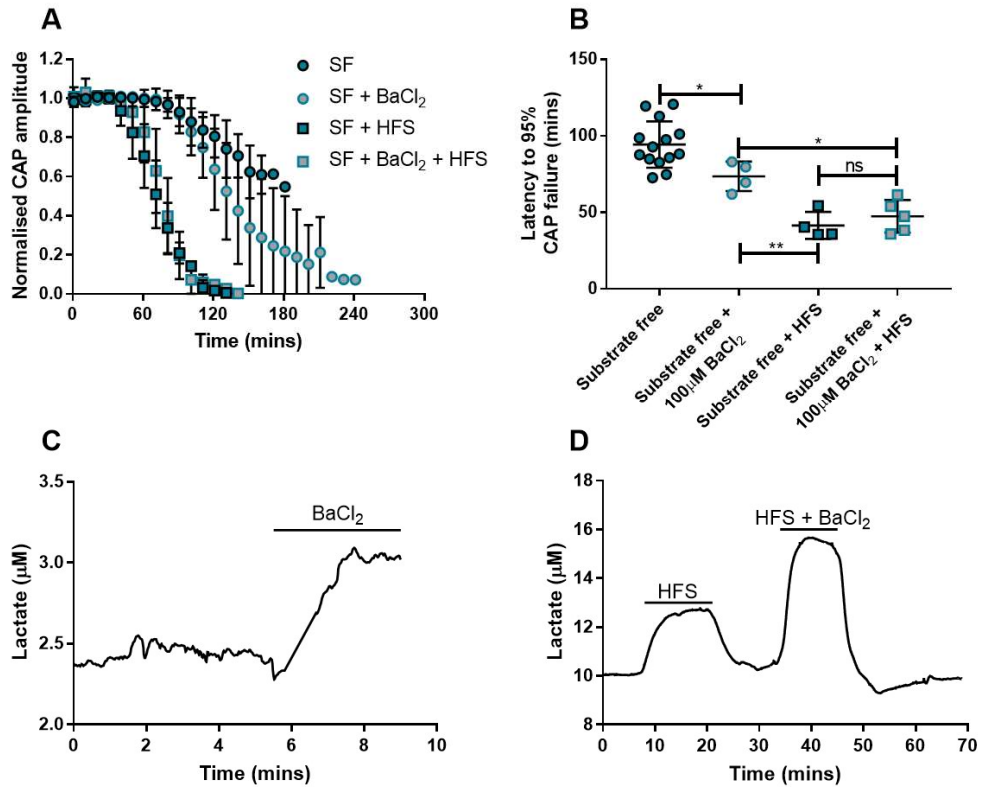


**Figure 5.4:** A fibre conduction during changes in extracellular K<sup>+</sup>. **(A)** Removal of an exogenous supply of glucose to the mouse sciatic nerve resulted in A fibre conduction failure, an effect which was accelerated by the addition of 100µM BaCl<sub>2</sub>, HFS or both. **(B)** Under substrate free conditions the latency to A fibre CAP failure was 94.3 ± 15.1 minutes (n= 14), which was further reduced by the addition of BaCl<sub>2</sub> (73.6 ± 9.6 minutes, n= 4), HFS (41.5 ± 8.8 minutes, n= 4) or both (47.4 ± 10.7 minutes, n= 5). **(C)** A trace of a lactate biosensor recording during the addition of 100µM BaCl<sub>2</sub> to the mouse sciatic nerve under control (10mM glucose and 1Hz) conditions (n= 1). **(D)** A trace of a lactate biosensor recording from the mouse sciatic nerve superfused with 10mM glucose during HFS and HFS and BaCl<sub>2</sub> (n= 1). One way ANOVA with Sidak's post hoc test. \* = p<0.05 and \*\* = p<0.01.

## 5.4 Discussion

The data from this study supports the role of  $K^+$  as a metabolic signal between axons and astrocytes in the CNS and provides insight into the role  $K^+$  might play as a metabolic signal within the PNS. To summarise, the results from this study show that the concentration of lactate produced by astrocytes of the mouse optic nerve was directly dependent upon the concentration of extracellular  $K^+$ . Although Schwann cell lactate production appears to be less sensitive to the concentration of extracellular  $K^+$ , requiring much higher concentrations to trigger a significant increase in lactate released from the mouse sciatic nerve, increased extracellular  $K^+$  was also found to accelerate the latency to failure under substrate free conditions.

### 5.4.1 Lactate profile

Recordings of lactate, using lactate biosensors, represent changes in lactate flux. The lactate recorded is the difference between the net efflux of lactate by glial cells and the net uptake of lactate in the entire nerve. Changes in lactate concentration recorded are indicative of changes in net flux, rather than absolute concentration.

In response to superfusion with supra-physiological concentrations of  $K^+$ , lactate recorded from the optic and sciatic nerve rapidly increased followed by a slower decrease (figure 5.1A and 5.1B, respectively). Since glia are considered the source of lactate (Walz & Mukerji, 1988) and increased extracellular  $K^+$  would have depolarised axons triggering action potential firing if threshold was reached, therefore increasing their energy demand, it is likely that the pattern of lactate recorded is due to the detection of  $K^+$  by the glial cell, rapidly increasing their production of lactate and subsequent release for axons to then take up and use as a source of energy to meet their increased energy demand. When taking into account the CAP (figure 5.2), a reduction in the amplitude and therefore contributing axons of the sciatic nerve A fibre CAP was observed at the ceiling concentration of  $K^+$  under physiological conditions (12mM), evident by the  $V_{50}$  value of  $\sim 13$ mM

K<sup>+</sup>, and supra-physiological concentrations (15mM and greater; Heinemann & Dieter Lux, 1977; Connors *et al.*, 1982). This was as expected since increased extracellular K<sup>+</sup> would depolarise the axon membrane potential resulting in Na<sup>+</sup> channel inactivation during prolonged depolarisation (Ulbricht, 2005).

Exposing the nerves to lower concentrations of K<sup>+</sup> resulted in an initial rapid fall in extracellular lactate (figure 5.1A and B). Since conduction of A fibres was maintained under such conditions (Figure 5.2) and glia are likely to respond rapidly to K<sup>+</sup>, the decrease in extracellular lactate was likely the result of reduced stimulation of glial cells to produce lactate, but an equivalent uptake of lactate by axons as in normal 3mM K<sup>+</sup>. The eventual plateau (figure 5.1A and B) suggests an equilibrium was reached between reduced glial cell lactate efflux and the concentration of lactate required by axons.

From figure 5.1 it is clear that changes in the concentration of extracellular K<sup>+</sup> influence glial cell lactate production and thus suggests K<sup>+</sup> acts as an activity dependent metabolic signal. However, changing the concentration of K<sup>+</sup> in the aCSF results in gross changes in the concentration of extracellular K<sup>+</sup> that could be considered unphysiological, therefore I progressed to determine whether more physiological changes in K<sup>+</sup> within the extracellular space of the nerves triggers a similar relationship with lactate. Increasing the frequency of stimulation of the nerves would result in more physiological increases in extracellular K<sup>+</sup> due to the proportional localised release of K<sup>+</sup> during the repolarisation phase of the action potential (Baylor & Nicholls, 1969).

Similar to the lactate recordings in response to changes in aCSF K<sup>+</sup>, the concentration of lactate recorded from the optic and sciatic nerve rapidly rose at the onset of the increased stimulus frequency (figure 5.3Ai and Bi, respectively), suggesting an increase in the production and release of lactate from astrocytes and Schwann cells, respectively. Rather than slowly falling, the concentration of lactate during increased

stimulus frequency then appeared to plateau suggesting an equilibrium between axon uptake and glial cell release of lactate was reached (figure 5.3Ai and Bi). The difference in lactate recordings between the two conditions likely reflects the global vs. local changes in extracellular  $K^+$ . When the  $K^+$  was increased as the result of imposing increased frequency of stimulus, the rises in extracellular  $K^+$  would have been more localised whereas when the  $K^+$  was increased via the aCSF the whole nerve would have been exposed to this increase in extracellular  $K^+$  thus depolarising the membrane potential of every axon and glial cell within the nerve. Not only are the  $K^+$  ion gradients changed but the depolarisation of the membrane potential would have also caused changes in the gradients of other ions such as  $Na^+$  (Thomas, 1972). As such the  $Na^+/K^+$  ATPase pump would have been working hard to try and restore these gradients and since many of the  $K^+$  concentrations used in this study were unphysiological, the system would have likely been overwhelmed and working at maximum capacity (Thomas, 1972). The rapid lactate responses recorded from both nerves during increased frequency of stimulation imply astrocyte and Schwann cell lactate production is triggered by physiological increases in the concentration of  $K^+$  in the extracellular space of the nerve as the result of increased axon firing. However, unlike the astrocytes, Schwann cells only appear to respond to higher stimulus frequencies of 30Hz and above, implying astrocytes maybe more responsive to changes in extracellular  $K^+$  as the result of increased axonal firing than Schwann cells.

Since the concentration of extracellular  $K^+$  increases with increased axonal firing frequency, it was possible to compare the concentration of lactate released from the sciatic nerve during increased stimulus frequency and an increase in the concentration of  $K^+$  in the aCSF. It was found that the concentration of lactate released from the sciatic nerve during 100Hz was equivalent to that when the extracellular  $K^+$  was increased from 3mM to just 6mM (figure 5.3Biii). This suggests that the lower stimulus frequencies used resulted in small rises in the

extracellular  $K^+$  and therefore explaining the small lactate response of the Schwann cells. A possible explanation for the small rise in extracellular  $K^+$  is the large extracellular space of the sciatic nerve (Hoppe *et al.*, 1991). This would dilute the  $K^+$  released from the axons and thus reduce the concentration of  $K^+$  the Schwann cells were exposed to. This is in comparison to the optic nerve where, the extracellular space is much smaller (Hoppe *et al.*, 1991), thus the astrocytes would be exposed to higher concentrations of  $K^+$  than Schwann cells for equivalent increases in axonal firing.

#### 5.4.2 Logarithmic relationship

The logarithmic relationship between the concentration of extracellular  $K^+$  and lactate, for both the optic and sciatic nerve (figure 1B and 2B), is as would be predicted by the Nernst equation (Kuffler *et al.*, 1966), therefore suggesting changes in glial cell membrane potential influences lactate efflux. However, although the logarithmic relationship looks comparable between the optic and sciatic nerve a difference was evident in the absolute magnitude in extracellular lactate concentration. Not only was the lactate recorded from the sciatic nerve much lower than that of the optic nerve ( $13 \pm 2\mu\text{M}$  vs.  $122 \pm 41\mu\text{M}$ , respectively) so was the change in concentration relative to extracellular  $K^+$ . For a 10-fold increase in extracellular  $K^+$ , from 3mM to 30mM, the concentration of lactate released from the optic nerve almost doubled to  $225 \pm 1\mu\text{M}$ , whereas the concentration released by the sciatic nerve only increased by  $3\mu\text{M}$  from  $13 \pm 2\mu\text{M}$  to  $16 \pm 2\mu\text{M}$ . This suggests the Schwann cell membrane potential may be less sensitive to  $K^+$  than astrocytes. Although there is significantly less data available regarding the membrane potential of Schwann cells compared to astrocytes, evidence suggests their resting membrane potential is around -45mV (Hargittai *et al.*, 1991), far more depolarised than the reversal potential for  $K^+$ ;  $\sim -80\text{mV}$  (Bear *et al.*, 2007). This, in addition to a change in their membrane potential of 27.5mV for a 10-fold change in  $K^+$ , suggests Schwann cells are not exclusively permeable to  $K^+$ , and likely permeable to  $\text{Na}^+$  and possible  $\text{Cl}^-$ . Therefore the Goldman-Hodgkin-

Katz equation describes the Schwann cell membrane potential in response to changes in  $K^+$  rather than the Nernst equation (Hargittai *et al.*, 1991; Powell *et al.*, 2020). The logarithmic relationship between stimulus frequency and lactate concentration for the mouse optic, but not sciatic, nerve (figure 5.3Aii and Bii), further supports the lower sensitivity of Schwann cells to  $K^+$  than that of astrocytes.

Although a logarithmic relationship was found between extracellular  $K^+$  and lactate and stimulus frequency and lactate for the optic nerve, the slope of the logarithmic relationship was much steeper with respect to changes in  $K^+$  in the aCSF compared to stimulus frequency; 75.6 $\mu$ M lactate/mM  $K^+$  and 17.5 $\mu$ M lactate/Hz, respectively. The lower concentrations of lactate produced by the astrocytes during more physiological changes in extracellular  $K^+$ , as the result of increased axonal firing, may further explain why the lactate plateaus during the stimulus frequency protocol whilst it falls when the nerve is superfused with aCSF containing higher concentrations of  $K^+$ . The lactate meets the increased metabolic demands of the axons, whilst exposing the nerve to very high concentrations of  $K^+$  might produce lactate in concentrations excess to demand. The more localised and physiological increases in extracellular  $K^+$ , as the result of axonal firing, means the system would unlikely be overwhelmed resulting in a balance between  $K^+$  buffering and energy substrate production.

#### *5.4.3 Increased extracellular $K^+$ increased glycogen metabolism of Schwann cells*

Removal of an exogenous energy supply forces the sciatic nerve to use any remaining energy substrate in order to maintain conduction. Glycogen, localised to the myelinating Schwann cells, is the main source of energy under substrate free conditions, with A fibres benefiting from Schwann cell derived lactate until this store is depleted (Brown *et al.*, 2012). The latency to failure of conduction, measured as a reduction in the A fibre CAP amplitude, therefore acts as an indirect measure of the rate of glycogen metabolism. A reduction in the latency to failure suggests glycogen is being metabolised at a higher rate. It

has previously been shown that within 10 minutes of exposing the sciatic nerve to substrate free conditions the extracellular lactate rapidly starts to fall to zero, preceding the fall in the A fibre CAP (Brown *et al.*, 2012). This illustrates axonal use of Schwann cell glycogen derived lactate on removal of exogenous energy substrate.

Under substrate free conditions the latency to failure of the A fibre CAP was ~90 minutes. This was accelerated by the addition of HFS or increasing the concentration of extracellular  $K^+$ , via  $BaCl_2$  blocking of the inwardly rectifying  $K^+$  channels (figure 5.4A and B). If the concentration of extracellular  $K^+$  acts as a measure of axonal energy demand, then increasing the extracellular  $K^+$  concentration should reduce the latency to failure, and this was found to be the case. This suggests glycogen was metabolised faster, and thus  $K^+$  acts as an effective metabolic signal to trigger Schwann cell glycogenolysis. This is supported by the further increase in lactate production under normoglycemic conditions when combining HFS and  $BaCl_2$  compared to HFS alone (figure 5.4D). However, this apparent increased rate of lactate production was not found to be reflected in the latency to failure of the A fibre CAP under substrate free conditions (figure 5.4B), potentially due to a limit to the rate of lactate metabolism by A fibres induced by HFS alone. The lack of effect of combining HFS with  $BaCl_2$  on the sciatic nerve A fibre CAP is in contrast to the exacerbated reduction in the optic nerve CAP amplitude seen under similar conditions, compared to HFS alone (Bay & Butt, 2012). The decline in the optic nerve CAP was explained by the requirement of astrocyte inwardly rectifying  $K^+$  channels in the clearance of increased extracellular  $K^+$ , as the result of increased axonal firing, which if left to accumulate leads to the suppression of axonal firing (Bay & Butt, 2012). The effect of blocking inwardly rectifying  $K^+$  channels on the CAP amplitude was only seen at higher stimulus frequencies i.e. higher extracellular  $K^+$  concentrations, with clearance of lower concentrations of  $K^+$ , as the result of lower levels of axonal firing, achieved by the  $Na^+/K^+$  ATPase pump (Bay & Butt, 2012). Since  $BaCl_2$  did not appear to have an

additive effect on the sciatic nerve A fibre CAP, it may suggest that although extracellular  $K^+$  increased, seen in the increased extracellular lactate, the clearance of this  $K^+$  was achieved by means other than that of Schwann cell inwardly rectifying  $K^+$  channels. Interestingly, nonmyelinating Schwann cells, those not associated with glycogen, have been proposed to play a role in the uptake of axonal released  $K^+$  via the  $Na^+/K^+$  ATPase (Robert & Jirounek, 1994), potentially implying a coordinated role of Schwann cell subtypes to buffer and respond to increased extracellular  $K^+$ .

Interestingly, from figures 5.4C and D it appears that under normoglycemic conditions,  $BaCl_2$  or HFS, increased the concentration of lactate released from the sciatic nerve by an equivalent amount (~20%). However, the reduction in latency to failure with the addition of  $BaCl_2$  was significantly less than with the addition of HFS, suggesting although the equilibrium between Schwann cell release and axon uptake of lactate appears similar under each condition, HFS stimulates faster Schwann cell glycogen metabolism and axonal metabolism of lactate. This could result from HFS increasing the concentration of extracellular  $K^+$  further than that of the addition of  $BaCl_2$  or due to the release of metabolic signals, in addition to  $K^+$  e.g. glutamate, during action potential firing that stimulates Schwann cell glycogen metabolism.

The rise in extracellular lactate recorded in this study is complementary to the depletion of intracellular lactate reservoirs recorded in astrocytes expressing Laconic (FRET lactate sensor) in response to the addition of  $BaCl_2$  (Sotelo-Hitschfeld *et al.*, 2015). This implies Schwann cells, like astrocytes, respond to increases in extracellular  $K^+$  by increasing their efflux of lactate into the extracellular space.

## 5.5 Conclusion

The compatibility of results between the optic and sciatic nerve, particularly with regards to the lactate profiles, suggests a universal role for  $K^+$  as an axon-glia metabolic signal within both the CNS and PNS. Furthermore, the logarithmic relationship observed between the concentration of  $K^+$  in the aCSF and the concentration of extracellular lactate implies changes in glial cell membrane potential influences lactate efflux. However, this logarithmic relationship was not carried through for the sciatic nerve in response to more physiological increases in the concentration of extracellular  $K^+$ . This, in addition to the smaller magnitude of lactate released from the sciatic nerve compared to the optic, as well as the significantly reduced latency to failure of the A fibre CAP with addition of HFS compared to the addition of  $BaCl_2$  under substrate free conditions, suggests Schwann cells might be less sensitive to  $K^+$  than astrocytes.

A recent study has suggested that different signals from neurones control glial cell metabolism at different time points (Barros *et al.*, 2020).  $K^+$ , as well as nitric oxide, are described as fast acting signals whilst glutamate is slow and produces a tonic response (Barros *et al.*, 2020). Although this study was focused on astrocytes the importance of other signals demonstrated here might explain why sciatic nerve lactate release only increases slightly and the latency to A fibre CAP failure is not as significant when  $K^+$  is the only upregulated signal.

Nevertheless, although a logarithmic relationship was not found between stimulus frequency and extracellular lactate concentration for the sciatic nerve, unlike the optic nerve, Schwann cells still responded to changes in extracellular  $K^+$  with an increase in the glycolytic production of lactate. Therefore  $K^+$  could be convincingly proposed as an effective metabolic signal to communicate the energy demand of axons to glial cells in both the central and peripheral nervous system, enabling hypothesis 1 to be accepted and hypothesis 2 to be rejected. Further research is still required to determine the mechanism in which

K<sup>+</sup> stimulates Schwann cell glycolysis and whether this is comparable to that of astrocytes via the NBC and soluble adenylyl cyclase (Choi *et al.*, 2012).

# **Chapter 6: The role of Schwann cells in fructose metabolism of the mouse sciatic nerve**

---

## 6.1 Introduction

Since the 1960's the intake of fructose in the diet has increased, with the average American's calorie intake now comprised 10% of fructose (54.6g/day) compared to 8% (37g/day) in the later 1970's (Vos *et al.*, 2008). Although fructose is a sugar found naturally in foods considered healthy such as fruit, it can be used as a sweetener in processed food mainly in the form of high-fructose corn syrup (HFCS) (Havel, 2005). The health effects of increased fructose intake have attracted interest due to the link with obesity, insulin resistance and hyperlipidemia all of which are associated with cardiovascular diseases and diabetes (Havel, 2005). Therefore, the importance of understanding fructose metabolism within the body seems evident.

The majority of ingested fructose is metabolised by the gut and released into the hepatic portal vein as glucose and lactate (Tappy & Rosset, 2019). Any unmetabolised fructose not metabolised next reaches the liver where it is also converted to, and released, as glucose and lactate into the circulation; some of this glucose is used to replenish liver glycogen stores (Tappy & Rosset, 2019). The ability of cells of the liver and gut to efficiently metabolise fructose is related to their expression of key fructolytic enzymes, fructokinase, aldolase and triokinase (figure 6.1, Tappy & Rosset, 2019). Consequently, it is generally considered that most fructose is metabolised by the gut and liver, leaving little remaining in the circulation, less than 0.5mM (Gonzalez & Betts, 2018). However, due to the increased dietary intake, fructose metabolism at the level of the gut maybe saturated and some fructose evades subsequent hepatic metabolism, thus the concentration in the circulation maybe higher than currently accepted (Tappy & Rosset, 2019). Therefore, research is needed to understand the ability and efficiency of fructose metabolism by cells other than those of the gut and liver e.g. cells of the nervous system. Recently many areas of the brain have been found to express fructokinase, with evidence to suggest the brain metabolises fructose at a higher rate (15-

150 times greater fructose oxidation rate) than liver (Oppelt *et al.*, 2017).

In addition to the potential for classically non-fructolytic organs to use the increased concentration of circulating fructose, a unique feature of the peripheral nervous system (PNS) is the potential ability of Schwann cells to convert glucose to fructose via the polyol pathway (figure 6.1, Champe *et al.*, 2008). This triggered investigations into the ability of fructose to maintain conduction of A and C fibres of the mouse sciatic nerve. Replacing glucose (10mM) in the artificial cerebral spinal fluid (aCSF) supplied to the nerve with fructose whilst recording the A and C fibre compound action potential (CAP) under baseline (1Hz) stimulation conditions resulted in maintenance of conduction of both the A and C fibre in a higher (20mM) concentration of fructose for extended periods of time (Rich & Brown, 2018b). Lowering the fructose concentration to 10mM fructose was able to sustain C fibre conduction but not A fibre conduction, with a latency to conduction failure similar to that under substrate free conditions, suggesting lower concentrations of fructose provided no additional energy, on top of that from Schwann cell glycogen derived lactate, to A fibres (Rich & Brown, 2018b). The requirement for a sufficient concentration of fructose to be present to maintain A fibre conduction was supported by the recovery of the CAP in 20mM, but not 10mM, fructose after glycogen depletion, where the C fibre CAP was recovered in both 10mM and 20mM fructose (Rich & Brown, 2018b). From these findings it initially appears that C fibres of the mouse sciatic nerve are capable of independent fructose metabolism, but a higher concentration is required to maintain A fibre conduction (Rich & Brown, 2018b). However, the addition of 200µM cinnamate (CIN), a MCT inhibitor, to 20mM fructose prevented the maintenance and recovery of the A fibre CAP, but had no effect on the C fibre CAP (Rich & Brown, 2018b). This suggests that even in higher concentrations of fructose A fibres rely on Schwann cells to provide lactate in order to meet their energy requirements. Overall, it was concluded that Schwann cells and C fibre directly take up and

metabolise fructose whilst A fibres benefit indirectly from fructose as an energy substrate in the form of fructose derived lactate.

Prior to investigations into the use of fructose as an energy substrate in the PNS, similar experiments had been conducted using central optic nerve tissue, where only smaller diameter axon conduction was maintained in both lower and higher concentrations of fructose (Allen *et al.*, 2006; Meakin *et al.*, 2007). The efficiency of fructose metabolism was related to the expression of fructokinase by the smaller, but not larger, diameter axons (Meakin *et al.*, 2007). Fructokinase is considered a key enzyme in fructose metabolism, substituting for hexokinase as the first enzyme in the glycolytic pathway (figure 6.1). The larger diameter axons express hexokinase, capable of metabolising fructose in addition to glucose, but due to its lower  $K_m$  (affinity) and higher  $V_{max}$  (maximum substrate production) for fructose requires a higher concentration of fructose for effective metabolism (Champe *et al.*, 2008). Thus fructose metabolism in central white matter tissue exhibits important differences when compared to the PNS tissue, with a smaller metabolic role for astrocytes, compared to Schwann cells, and axons' metabolic profile and ultimately physiological functions determined by the enzymes they express. Although the presence of fructose-1-phosphate has been detected in rat sciatic nerves (Poulsom *et al.*, 1983) the expression of fructokinase in the PNS is currently unknown. The apparent relationship between fructokinase expression and axon conduction in central nervous system (CNS) white matter has prompted this study to investigate the presence of fructokinase within the sciatic nerve and whether its localisation is linked to efficient fructose metabolism.

In addition to a means by which fructose can be metabolised, cells that utilise fructose need a way of accessing the energy substrate. GLUT5 is considered the main membrane bound transporter of fructose and is widely expressed in intestine, kidney and spermatozoa (Cura & Carruthers, 2012). GLUT5 is expressed in multiple areas of the CNS including axons of the optic nerve (Kojo *et al.*, 2016), supporting the

conclusion from optic nerve electrophysiology and immunohistochemistry data that axons directly take up and metabolise fructose. GLUT5 is expressed by axons and to a lesser extent Schwann cells of rat sciatic nerve (Asada *et al.*, 1998), however it is unclear whether there is a difference in GLUT5 expression by A fibres and C fibres.

*Aim:*

To determine the expression of fructokinase and GLUT5 by A fibres, C fibres and Schwann cells of the sciatic nerve.

*Objective:*

Using Western blot and fluorescent immunohistochemistry to determine the cellular localisation of fructokinase and GLUT5 in the mouse sciatic nerve. These data will complement the stimulus evoked CAP recordings from the mouse sciatic nerve *ex vivo* to form a more complete picture of the functional use of fructose to maintain axon conduction during high frequency stimulation (HFS).

*Hypothesis:*

Fructokinase and GLUT5 are expressed by Schwann cells and C fibres, not A fibres, of the mouse sciatic nerve.

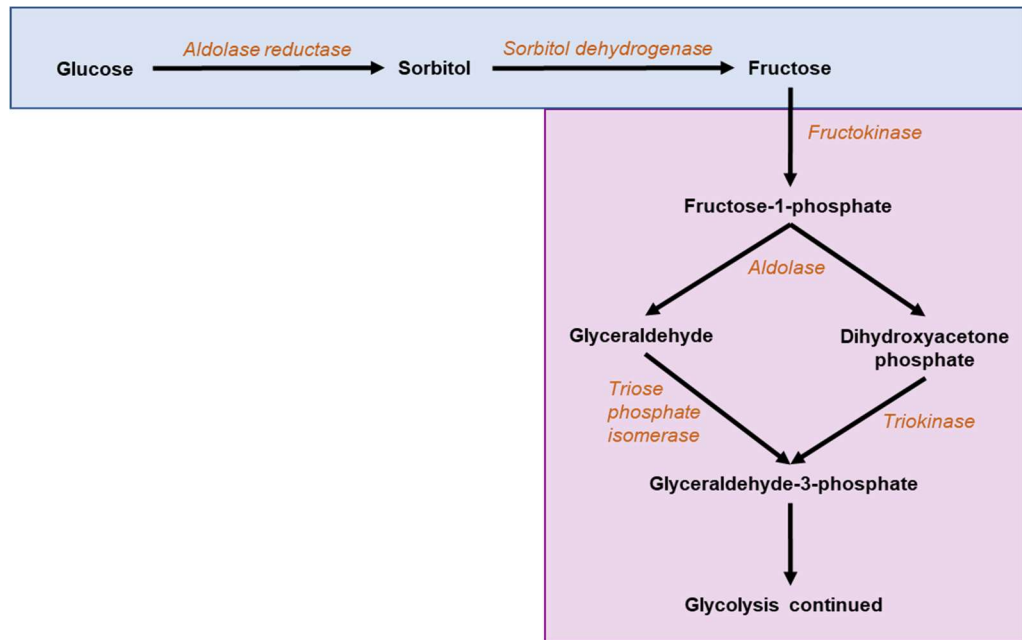


**Figure 6.1:** Key fructose metabolism pathways. The polyol pathway (blue) converts glucose to fructose. Glucose is reduced to sorbitol then oxidised to fructose. Fructolysis (purple) is the main pathway of fructose metabolism. Fructose is first converted to fructose-1-phosphate before it can be fed into the glycolytic pathway. Key fructose specific enzymes in orange and italics. (Nelson & Cox, 2009)

## 6.2 Methodology

### 6.2.1 Mice and tissue dissection

See chapter 2.1 for full details of the mice and nerve dissections.

A total of 20 mice were used to collect sciatic nerves (n= 24) as well as liver (n= 3) and small intestine (n= 3) for Western blot, fluorescence immunohistochemistry and CAP electrophysiology measurements.

Six mice were used to collect sciatic nerves (n= 6) as well as liver (n= 3) and small intestine (n= 3) for use in Western blot and fluorescent immunohistochemistry. After dissection of the sciatic nerves the body of the mouse was flipped over so that it was belly up and pinned out in a similar fashion to the sciatic nerve dissection. An incision of the skin was made up along the middle of the abdomen to reveal the abdominal muscle wall. A midline cut of the muscle using scissors, as far up as the lower rib cage, then revealed internal organs. The liver was clearly identified as the large dark red/brown organ and carefully removed using blunt forceps. Identification of the stomach preceded localisation and unravelling and removal of the intestine using forceps. The small intestine begins at the stomach and is divided into 3 parts; the duodenum, jejunum and ileum. The intestine was cut at the level of the ileum, just before the cecum, in order to obtain the longest length of tissue possible for Western blot. A smaller section of small intestine, of similar length to the sciatic nerve, was used for immunohistochemistry. On removal of the small intestine it was flushed through, using a 10ml syringe fitted with a yellow 1-200 $\mu$ l pipette tip, with distilled water to remove lumen content.

### 6.2.2 Western blot

For detail on the broad Western blot protocol used see chapter 2.4.

For this study sciatic nerve (n= 3), liver (n= 2) and small intestine (n= 2) were the tissues of interest. Liver was used as the positive control for fructokinase, whilst small intestine was used as the positive control for GLUT5.

After dissection and homogenisation (rather than using the sonic probe, the small intestine had to be homogenised by hand due to the presence of tough connective tissue), protein content of each tissue was determined using the Lowry test. This enabled the total protein concentration of each tissue to be calculated and therefore the appropriate volume of each tissue to be loaded onto the gel (gradient 4-20%) to ensure that the total protein concentration for each tissue was normalised to 50µg. Protein molecular weight marker was loaded into the first lane of the Western blot gel, in order to provide a reference for the bands of different sized proteins. Liver or small intestine and sciatic nerve were loaded into the second and third lanes, respectively.

The primary antibody used to immunoprobe the resulting nitrocellulose sheets was chicken anti-ketohexokinase (Sigma-Aldrich) to detect fructokinase (ketohexokinase and fructokinase are synonymous) or mouse anti-SLC2A5 (Thermo Fisher Scientific) to detect GLUT5 expression, both at a dilution of 1 in 500 in blocking buffer. The respective Licor Odyssey secondary antibodies (LI-COR Biosciences, Ltd) were IRDye 800CW donkey anti-chicken secondary IgG antibody and donkey anti-mouse secondary IgG antibody, at a dilution of 1 in 10,000 and 1 in 30,000, respectively, in blocking buffer.

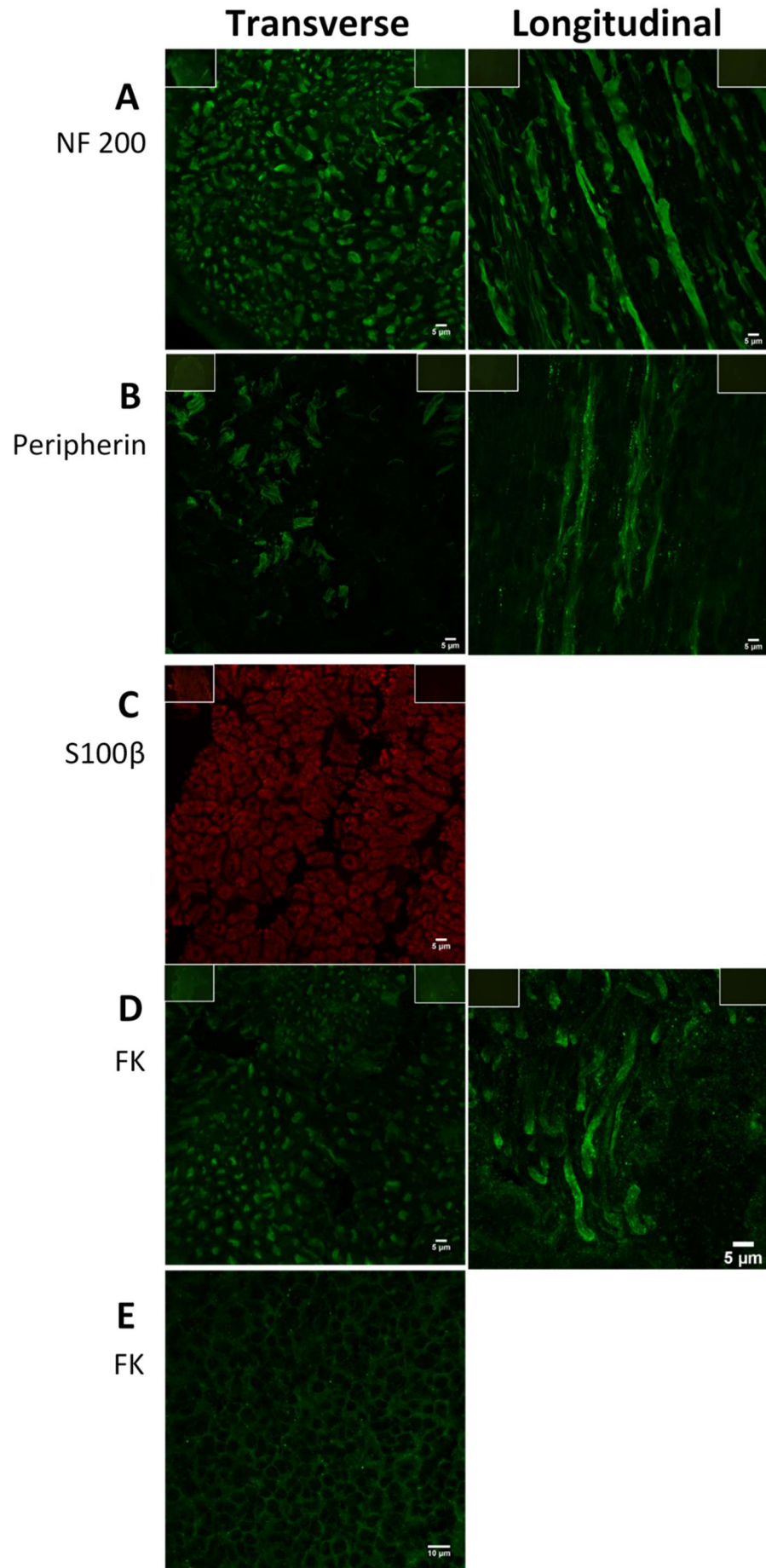
### *6.2.3 Fluorescence Immunohistochemistry*

Dissected sciatic nerves (n= 6) were placed on a plastic weighing boat in order to straighten the nerve before snap freezing in liquid nitrogen. Dissected liver (n= 1) and small intestine (n= 1) was also snap frozen on dry ice. Sciatic nerves were cut into both longitudinal and transverse 10µm thick sections. Liver was also cut into 10µm thick sections whilst small intestine was cut into 16µm thick sections.

For detail of the immunohistochemistry protocol see chapter 2.5. Specifically, the technique of fluorescence immunohistochemistry was used in this study to investigate the expression of fructokinase and GLUT5 by A fibres, C fibres and Schwann cells. This involved staining for specific markers of each cell type in combination with an antibody

against fructokinase or GLUT5. A and C fibres selectively express the intermediate filaments neurofilament 200 and peripherin, respectively, therefore these were used as markers to differentiate between the fibre subtypes (Black *et al.*, 2012), whilst S100 $\beta$ , a calcium binding protein, was used as a marker for Schwann cells (Mata *et al.*, 1990). Sections were stained with each antibody individually to act as positive controls for the cell type markers and reveal the true appearance of these markers in the absence of potential interactions from a second primary antibody (figure 6.2A-D and F). Liver was also used as a positive control for the fructokinase antibody, due to the abundant expression of fructokinase by hepatocytes (figure 6.2E, Champe *et al.*, 2008), whilst small intestine was used as the positive control for GLUT5 due to its apparent abundance (figure 6.2G, Douard & Ferraris, 2008). Combinations of these cell marker antibodies were then performed to determine the morphological arrangement among these cell types within the sciatic nerve. Using antibodies against neurofilament and peripherin revealed distinct fibre types that do not overlap, as expected (figure 6.3A and B). Staining for neurofilament and S100 $\beta$  revealed an axon surrounded by myelin (figure 6.3C), whilst S100 $\beta$  appeared to show no association with peripherin suggesting S100 $\beta$  is a marker for myelinating, but not non-myelinating, Schwann cells; in agreement with Mata *et al.* 1990 (figure 6.3D).

Primary antibodies (table 2.1 of chapter 2) were used at a 1:200 dilution in buffer 1, except anti-GLUT5 (1 in 100), whilst secondary antibodies were applied at a 1 in 500 dilution in buffer 1. When staining for GLUT5, Tween-20 rather than Triton-X (0.3%) was used as the detergent in buffer 1 and a biotinylated secondary antibody (1 in 200) and avidin tag (1 in 200) were required rather than a direct secondary. See table 6.1 for the combination of primary and secondary antibodies used for the co-localisation staining.



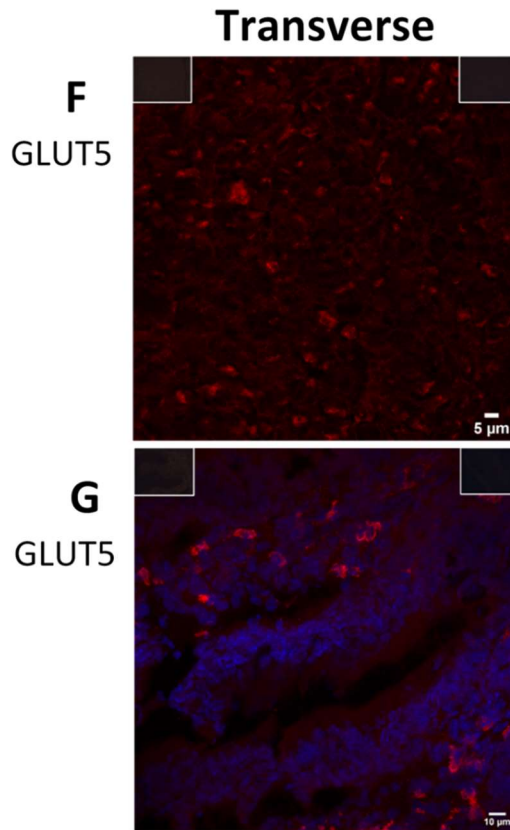


**Figure 6.2:** Positive controls. **(A)** Staining for neurofilament 200 as a marker for A fibres in both longitudinal (n= 1) and transverse (n= 1) sections. **(B)** Staining for peripherin as a marker for C fibres in both longitudinal (n= 1) and transverse (n= 1) sections. **(C)** Staining for S100 $\beta$  as a marker for Schwann cells in transverse sections (n= 1). **(D)** Staining for fructokinase in sciatic nerve transverse (n= 1) and longitudinal (2x zoom, n= 1) sections. **(E)** Staining for fructokinase expression in liver hepatocytes (n= 1). **(F)** Staining for GLUT5 expression in transverse sciatic nerve (n= 1). **(G)** Staining for GLUT5 expression (red) in small intestine, with DAPI in blue (n= 1). Corresponding negative controls in top left (no primary) and top right (no secondary) and show no significant staining. A-D and F scale bar= 5 $\mu$ M, E and G scale bar= 10 $\mu$ M. NF 200= neurofilament 200 and FK= fructokinase.

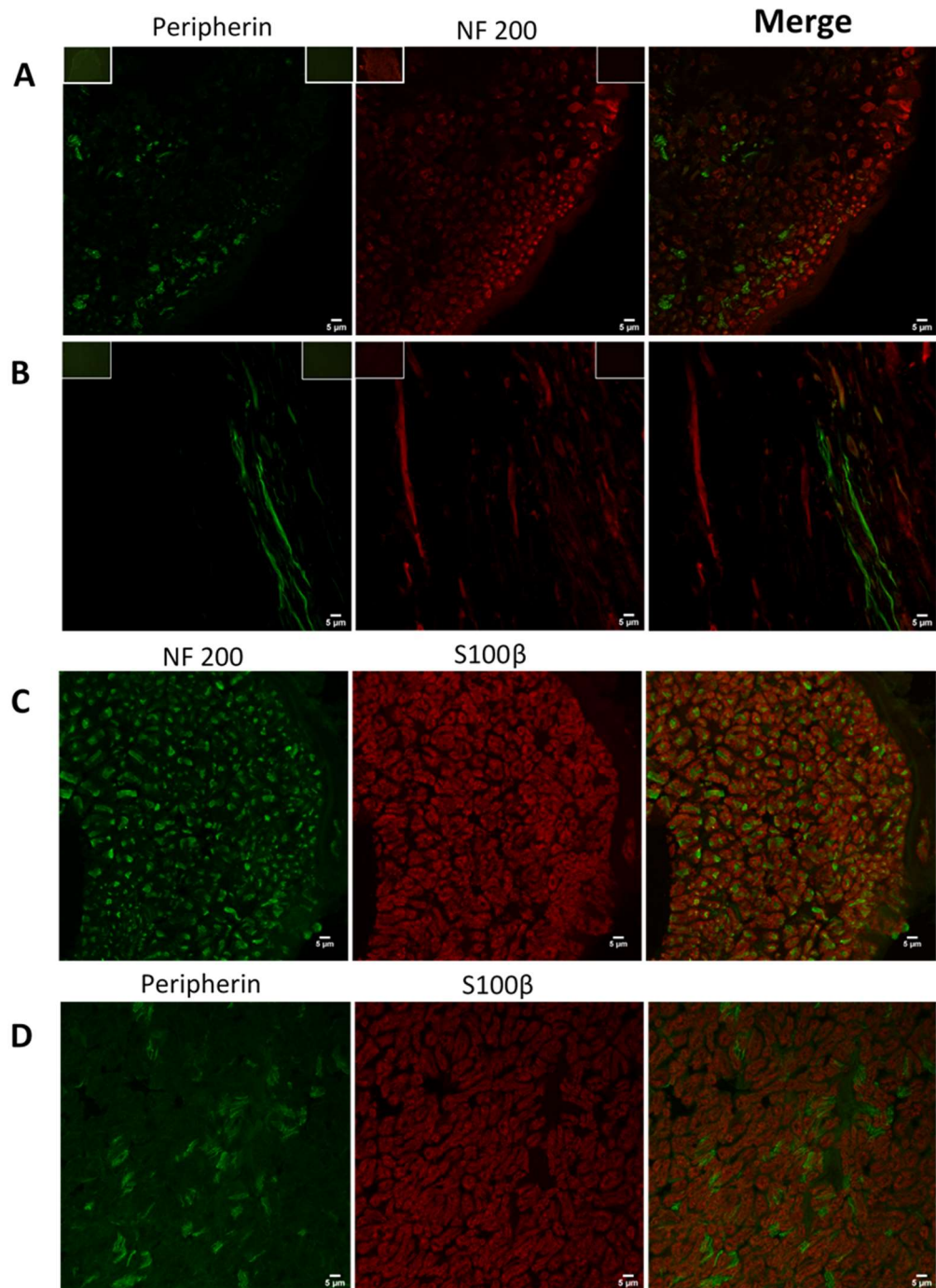


**Figure 6.3:** Cell types of the sciatic nerve. The first two columns display the staining of the individual cell types with the right column revealing the merged staining. Overlap in staining appears yellowish and suggests colocalisation. (**A and B**) Peripherin (green) selectively stains for C fibres and neurofilament 200 (red) selectively stains for A fibres, seen in both the transverse (**A**, n= 1) and longitudinal orientation (**B**, n= 1). (**C**) S100β (red) stains the myelinating Schwann cells that myelinate the A fibres (green, n= 1). (**D**) S100β (red) does not appear to stain the non-myelinating Schwann cells that ensheath the C fibres (green, n= 1). Corresponding negative controls in top left (no primary) and top right (no secondary). Scale bar= 5μM. NF 200= neurofilament 200.

Day 1	Day 2	Day 3	Normal serum
1. Mouse anti- <i>peripherin</i>	1. Goat anti-mouse (488nm) 2. Rabbit anti- <i>neurofilament 200</i>	2. Goat anti-rabbit (546nm)	NGS
1. Mouse anti- <i>neurofilament 200</i>	1. Goat anti-mouse (488nm) 2. Rabbit anti- <i>S100β</i>	2. Goat anti-rabbit (546nm)	NGS
1. Rabbit anti- <i>S100β</i>	1. Goat anti-rabbit (546nm) 2. Mouse anti- <i>peripherin</i>	2. Goat anti-mouse (488nm)	NGS
1. Mouse anti- <i>neurofilament 200</i>	1. Rabbit anti-mouse (568nm) 2. Chicken anti- <i>ketoheokinase</i>	2. Rabbit anti-chicken (488nm)	NRS
1. Mouse anti- <i>peripherin</i>	1. Rabbit anti-mouse (568nm) 2. Chicken anti- <i>ketoheokinase</i>	2. Rabbit anti-chicken (488nm)	NRS
1. Rabbit anti- <i>S100β</i>	1. Goat anti-rabbit (546nm) 2. Chicken anti- <i>ketoheokinase</i>	2. Rabbit anti-chicken (488nm)	NGS NRS
1. Rabbit anti- <i>GLUT5</i>	2. Biotinylated Goat anti-rabbit 3. Avidin Texas Red 1. Mouse anti- <i>neurofilament 200</i>	2. Goat anti-mouse (488nm)	NGS

**Table 6.1:** Antibody combinations for co-localisation staining. A 3-day protocol was used for co-localisation staining where the first primary and corresponding secondary were added on days 1 and 2 and the second primary and corresponding secondary were added on days 2 and 3. The final column shows the species of the normal blocking serum used for that combination in order to reduce non-specific binding of the secondary antibodies. NGS= normal goat serum, NRS= normal rabbit serum. Chicken anti-ketohexokinase and rabbit anti-GLUT5 are primary antibodies that bind to epitopes on fructokinase and GLUT5, respectively.

#### *6.2.4 Stimulus evoked CAP electrophysiology*

A total of 14 mice were used for the collection of sciatic nerves (n= 16), used to provide functional evidence for fructose metabolism by the sciatic nerve using stimulus evoked CAP electrophysiology (see methodology chapter 2.2 and 3.2.2). The n number refers to the number of individual nerves recorded from.

A stimulus of ~15V (figure 2.5A of chapter 2) was applied to the nerves in order to recruit the A fibre CAP only (figure 2.4A of chapter 2), at a control frequency of 1Hz. Nerves were first incubated in 10mM glucose and stimulated at 1Hz for a baseline period of 30 minutes before being subjected to the experimental condition. HFS was defined as 100Hz stimulus frequency. The C fibre CAP was not recruited for this study, unlike the previous study (Rich & Brown, 2018b), due to the slow conduction velocity and large stimulus artefact associated with the C fibres.

##### *6.2.4.i Data analysis*

See chapter 2.2.1 for more details of CAP data analysis.

The baseline CAP amplitude of the A fibre CAP was normalised to 1 and the area under the normalised CAP amplitude vs. time (NCAP.mins) was calculated using Prism 7 (GraphPad Software). AUC was used due to many of the experimental conditions failing to reduce the CAP amplitude; therefore latency to failure could not be calculated (figure 2.7 of chapter 2). Since the CAP was normalised to 1, full maintenance of conduction for the 8-hour experimental should result in an AUC value of ~480 NCAP.mins. All data are expressed as mean  $\pm$

SD and statistical analysis was performed using Prism 7 (GraphPad Software), where  $p < 0.05$  was considered significant.

## 6.3 Results

### 6.3.1 Fructokinase and GLUT5 are expressed within the mouse sciatic nerve

Fructokinase and GLUT5 expression within the sciatic nerve was first determined by Western blot. Immunoblotting for fructokinase revealed a band between 46 and 58kDa in the sciatic nerve which was consistent with the prominent band using liver (arrow in figure 6.4A), as well as a band at 58kDa. In comparison when using the liver a band was revealed at a lower molecular weight between 25 and 32kDa whilst a band of a higher molecular weight, between 75 and 100kDa, was revealed using the sciatic nerve (figure 6.4A). Performing a Western blot of GLUT5 expression, revealed a similar band pattern between the sciatic nerve and small intestine at ~58kDa, as expected, and 32kDa (figure 6.4B).

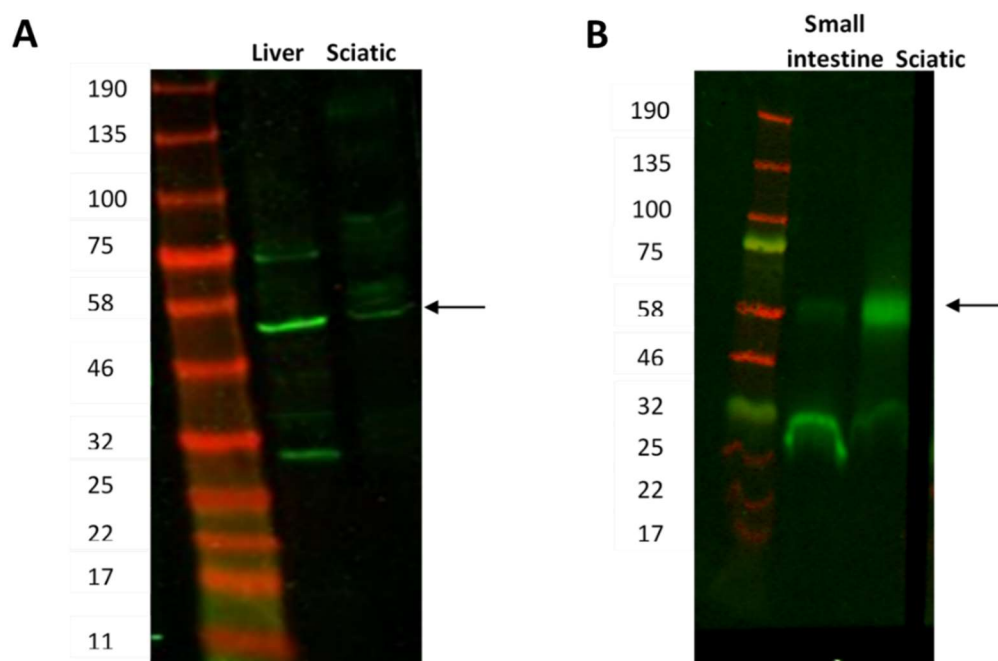


**Figure 6.4:** Fructokinase and GLUT5 expression. Protein molecular weight markers (kDa) seen in the left column. **(A)** Fructokinase is expressed in both the liver and the sciatic nerve particularly between the bands of 46 and 58kDa (arrow, n= 2). **(B)** GLUT5 is expressed in the small intestine and sciatic nerve with a molecular weight of ~60kDa (arrow, n= 2).

### *6.3.2 Fructokinase is only expressed by A fibres*

The presence of fructokinase within the whole sciatic nerve, determined by Western blot, prompted the investigation into the localisation of fructokinase to the 3 main cell types of the sciatic nerve, A fibres, C fibres and Schwann cells, using fluorescence immunohistochemistry. Co-staining for fructokinase along with a marker for each cell type revealed fructokinase to be clearly expressed by A fibres (figure 6.5), but not C fibres (figure 6.6) or Schwann cells (figure 6.7).

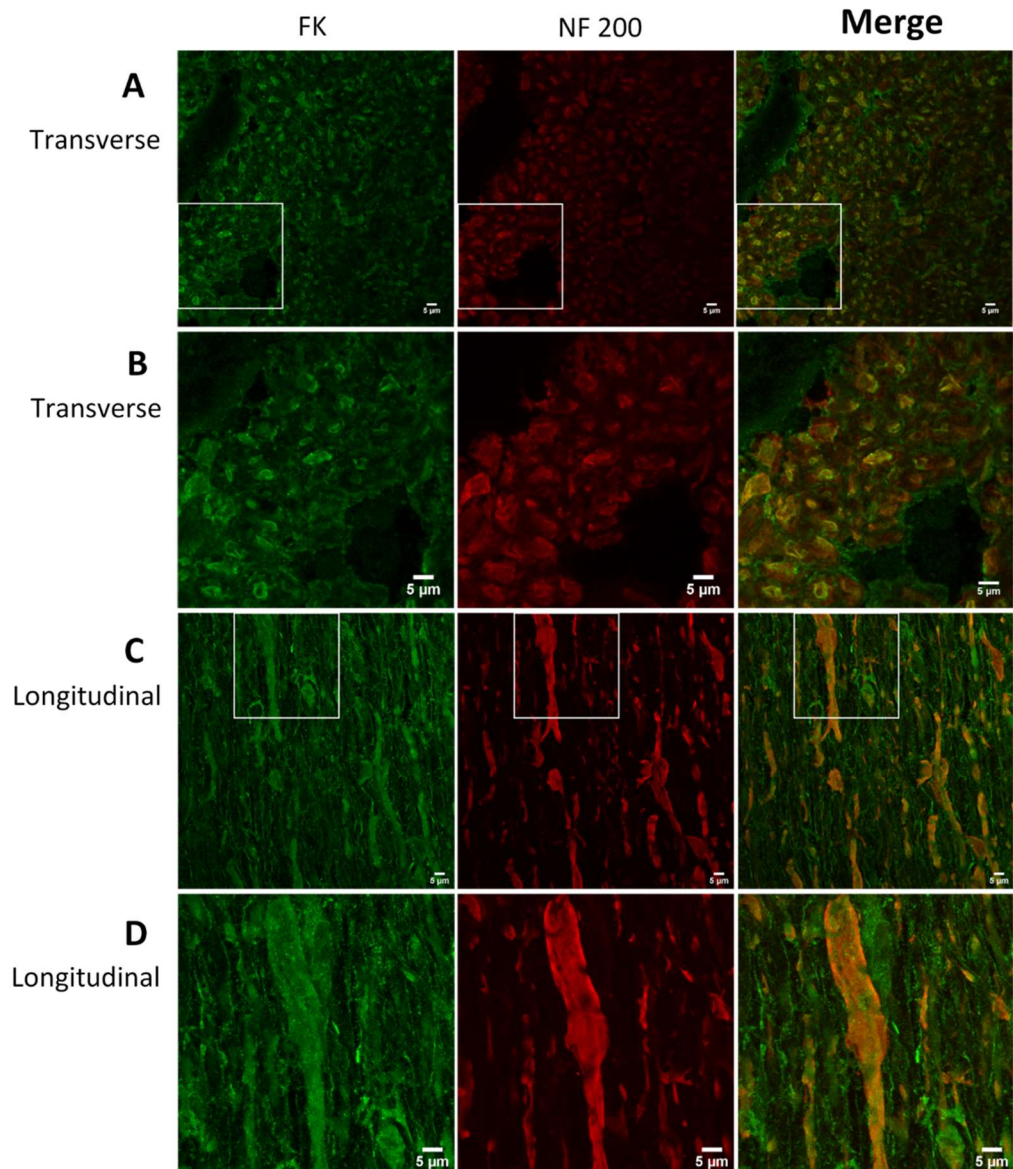


**Figure 6.5:** A fibres of the mouse sciatic nerve express fructokinase. The first two columns display the staining of the individual proteins with the right column revealing the merged staining. Overlap in staining would appear yellowish in colour and suggest colocalisation. (**A and C**) Fructokinase (green) expression colocalises with neurofilament (red), seen in both the transverse (**A**, n= 1) and longitudinal (**C**, n= 1) orientation. (**B and D**) Enlargements of the region of interest enclosed by white box in A and C, in the respective orientation. Scale bar= 5µM. NF 200= neurofilament 200 and FK= fructokinase.

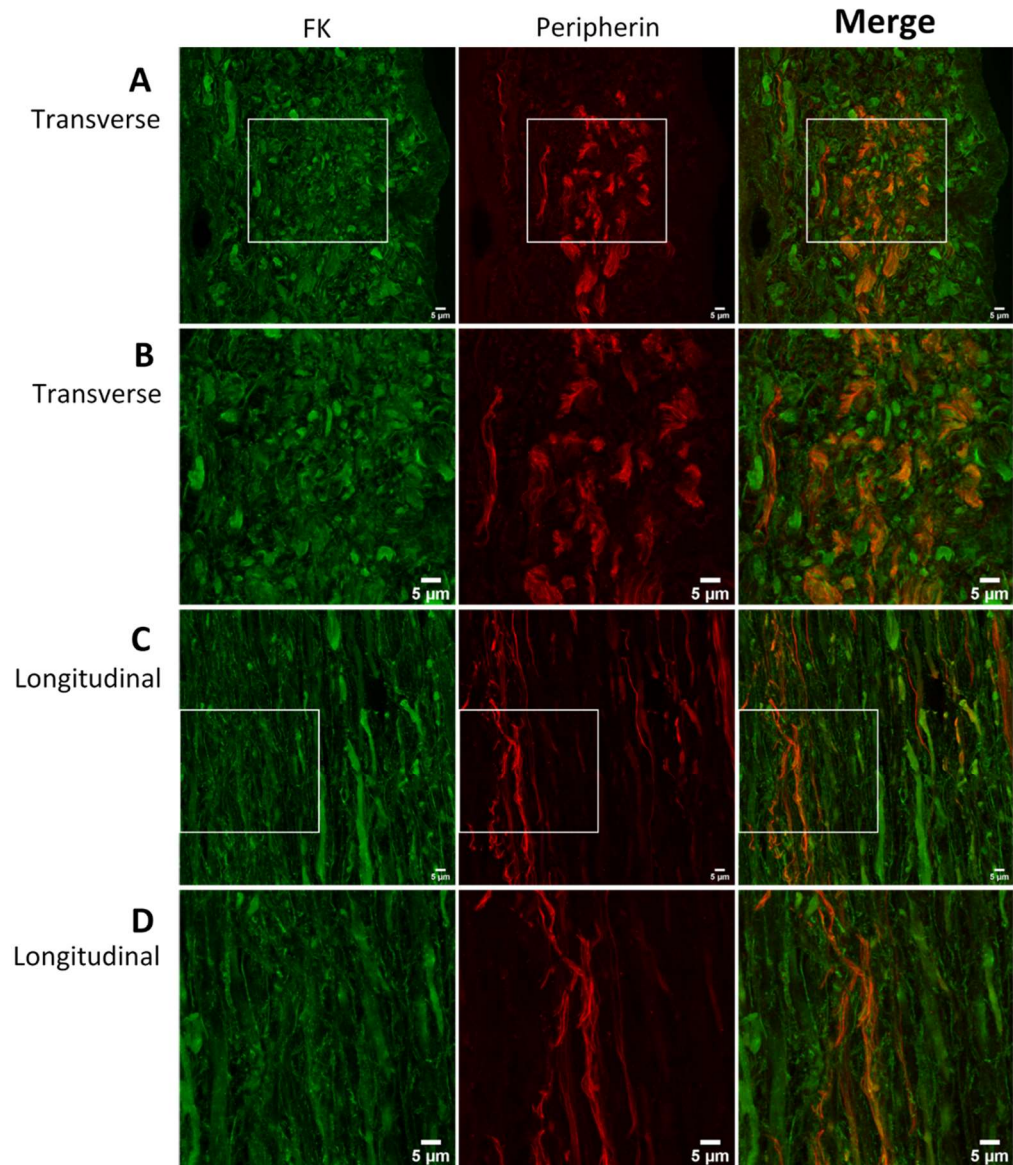


**Figure 6.6:** C fibres do not express fructokinase. The first two columns display the staining of the individual proteins with the right column revealing the merged staining. Overlap in staining would appear yellowish in colour and suggest colocalisation. (**A and C**) Fructokinase (green) expression does not colocalise with peripherin (red), seen in both the transverse (**A**, n= 1) and longitudinal (**C**, n= 1) orientation. (**B and D**) Enlargements of the region of interest enclosed by white box in A and C, in the respective orientation. Scale bar= 5μM. FK= fructokinase.

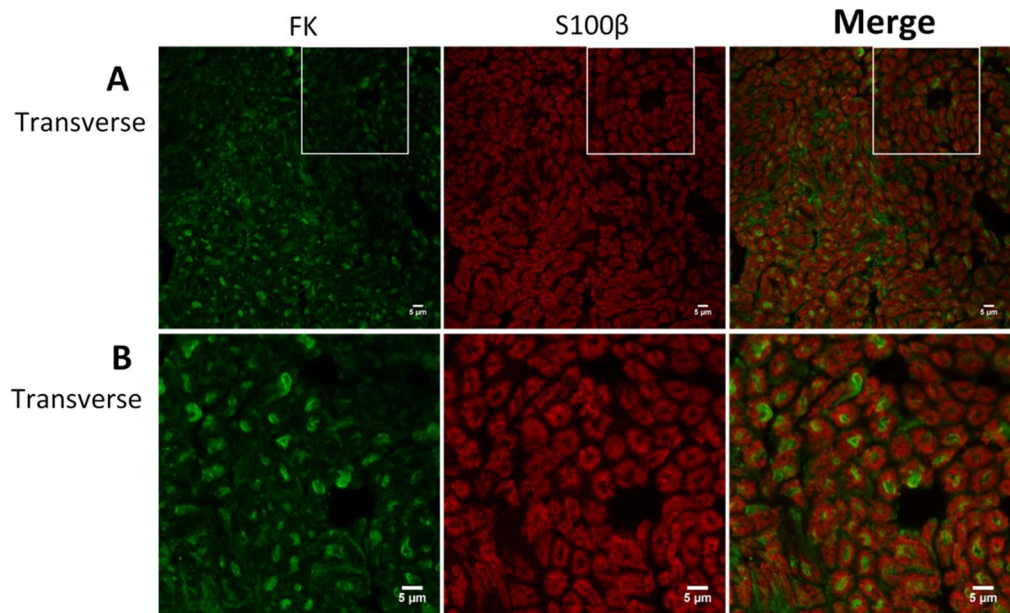


**Figure 6.7:** Myelinating Schwann cells do not express fructokinase. The first two columns display the staining of the individual proteins with the right column revealing the merged staining. Overlap in staining would appear yellowish in colour and suggest colocalisation. **(A)** Fructokinase (green) expression does not colocalise with S100β (red, n= 1). **(B)** Enlargements of the region of interest enclosed by white box in A. Scale bar= 5μM. FK= fructokinase.

### 6.3.3 GLUT5 is expressed by A fibres and Schwann cells

Using immunohistochemistry, the expression of GLUT5, initially confirmed by Western blot, was localised to specific cell types within the mouse sciatic nerve. Overlap of staining for GLUT5 with a cell specific marker appeared when GLUT5 was co-labelled with neurofilament 200, the A fibre marker (figure 6.8). It also appears that GLUT5 stains, although maybe to a lesser extent, the Schwann cell cytoplasm, seen as a ring of staining around the A fibre axon (see white arrows in figure 6.8B).

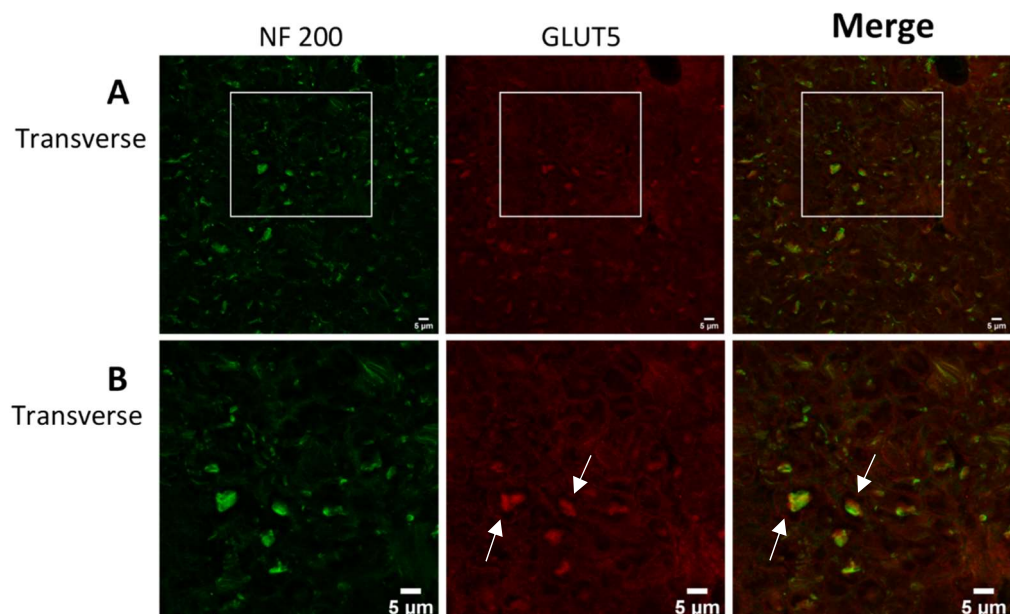


**Figure 6.8:** A fibres of the mouse sciatic nerve express GLUT5. The first two columns display the staining of the individual proteins with the right column revealing the merged staining. Overlap in staining would appear yellowish in colour and suggest colocalisation. **(A)** GLUT5 (red) expression colocalises with neurofilament 200 (green) in the transverse orientation (n= 1). **(B)** Enlargements of the region of interest enclosed by white box in A. Scale bar= 5μM. NF 200= neurofilament.

#### *6.3.4 Higher concentrations of fructose maintain A fibre conduction during HFS*

Electrophysiological techniques were used to provide functional insight into fructose metabolism in the sciatic nerve and complement molecular data from immunohistochemistry and Western blot.

For A fibre conduction to be maintained during HFS, fructose must be supplied at a sufficiently high concentration (the main effect of treatment was found to be significant  $F(3,12)175.6$ ,  $p<0.0001$ ); the A fibre CAP was almost fully maintained for the 8 hour duration of HFS in 20mM fructose aCSF superfusion whilst reducing the fructose concentration to 10mM resulted in conduction failure after ~50 minutes (post-hoc multiple comparisons,  $p<0.0001$ ). However, blocking lactate transport with the addition of cinnamate to the 20mM fructose aCSF prevented maintenance of conduction with the onset of failure occurring after ~90 minutes ( $p<0.0001$ ). Furthermore, maintenance of A fibre conduction appeared similar during HFS when the sciatic nerve was supplied with 10mM fructose or no exogenous energy substrate ( $p=0.94$ ; figure 6.9).

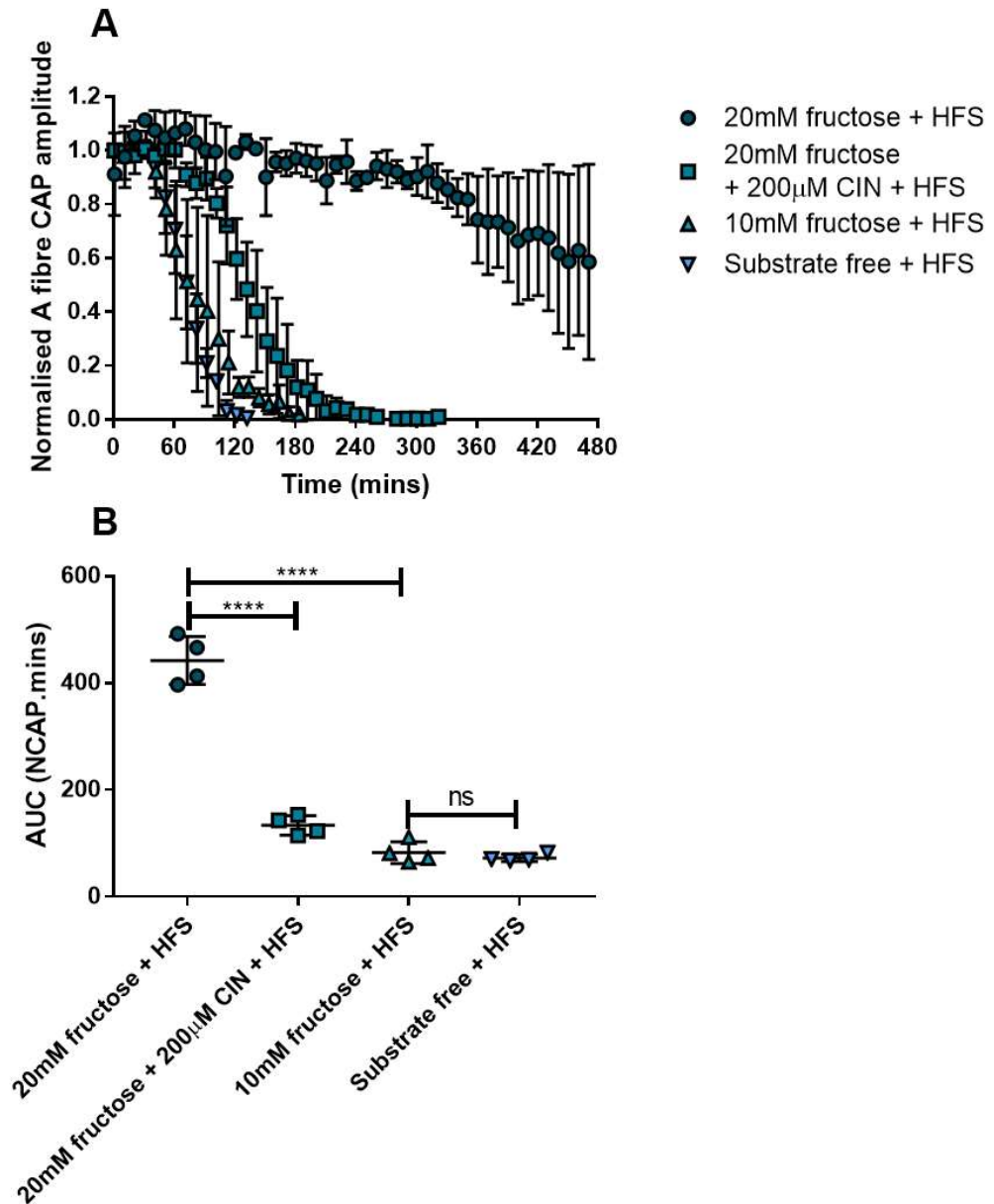


**Figure 6.9:** Sufficient fructose must be present for maintenance of A fibre conduction during HFS. **(A)** Higher concentrations of fructose (20mM) maintain A fibre conduction during HFS unless lactate transport is inhibited by the addition of 200 $\mu$ M CIN. Lower concentrations of fructose (10mM) or substrate free conditions result in conduction failure during HFS. **(B)** Maintenance of A fibre conduction is significantly decreased as a result of reducing the supplied fructose concentration ( $442 \pm 44.6$  NCAP.mins,  $n=4$  (20mM fructose) vs.  $82.4 \pm 20.4$  NCAP.mins,  $n=4$  (10mM fructose)). CAP maintenance in 20mM fructose during HFS is significantly reduced by the addition of 200 $\mu$ M CIN ( $442 \pm 44.6$  NCAP.mins,  $n=4$  (20mM fructose) vs.  $133.2 \pm 18$  NCAP.mins,  $n=4$  (20mM fructose + CIN)). The limited maintenance of A fibre conduction is comparable between 10mM fructose and substrate free conditions ( $82.4 \pm 20.4$  NCAP.mins,  $n=4$  (10mM fructose) vs.  $72.4 \pm 6.6$  NCAP.mins,  $n=4$  (substrate free)). One-way ANOVA with Sidak's post hoc test. \*\*\*\* =  $p < 0.0001$ , ns = non-significant.

## 6.4 Discussion

The data from this study extends and complements our previous finding of fibre subtype specific fructose metabolism of the mouse sciatic nerve (see Rich & Brown, 2018). Molecular techniques revealed fructokinase and GLUT5 expression within the sciatic nerve, specifically the A fibres, whilst electrophysiological techniques demonstrated the requirement of lactate to support A fibre conduction during HFS in the presence of sufficient exogenously supplied fructose.

### 6.4.1 *Sciatic nerve fructokinase expression*

Fructokinase exists in two isoforms, A and C, as a result of alternate splicing of the fructokinase gene (Diggle *et al.*, 2009). Isoform C is thought to be expressed by splanchnic organs including the liver and intestine, whilst isoform A is present in tissues outside of this region e.g. the brain (Tappy & Rosset, 2019).

Fructokinase A and C are 30kDa sized proteins, which is in agreement with ~30kDa band we found in the liver, (figure 6.4A, Diggle *et al.*, 2009). A predominant ~50kDa band is also observed in many tissues using N- or C-terminal fructokinase specific antibodies (Diggle *et al.*, 2009). Diggle *et al.* (2009) suggested that the 50kDa band represents nonspecific cross reactivity. However, both the 30kDa and 50kDa bands disappear when the fructokinase C isoform is not induced i.e. not present, whilst the 50kDa band remains in liver and brain devoid of fructokinase A suggesting the 50kDa band, as seen in the sciatic nerve and liver (figure 6.4A), represents fructokinase C (Diggle *et al.*, 2009). This is interesting since isoform C of fructokinase is considered to be expressed by the main fructolytic tissues i.e. liver (Tappy & Rosset, 2019).

### 6.4.2 *Fructokinase and GLUT5 expression does not determine efficient metabolism of exogenously supplied fructose by the mouse sciatic nerve*

Previously we showed that C fibres directly metabolise fructose whilst A fibres indirectly benefit from fructose in the form of Schwann cell lactate

(Rich & Brown, 2018*b*). Since C fibres and Schwann cells, but not A fibres, appear to metabolise fructose directly, this suggests that these 2 cell types would likely be the site of fructokinase and GLUT5 expression. However, based on the immunohistochemistry conducted for this study this hypothesis can be clearly rejected, where A fibres, not C fibres or Schwann cells, express fructokinase and GLUT5.

Results from molecular techniques such as immunohistochemistry should be interpreted with caution since the presence of an enzyme does not necessarily mean it is functional, therefore stimulus evoked CAP electrophysiology was conducted to provide functional evidence of fructose metabolism by the sciatic nerve. The results in figure 6.9 suggest that as long as fructose is supplied at a sufficiently high concentration A fibres will metabolise this fructose to maintain conduction for the 8 hours of HFS. However, if A fibres directly metabolised fructose, blocking lactate uptake should have no or little effect on the maintenance of conduction. Instead, conduction failure was evident in the presence of 20mM fructose and 200µM cinnamate, clearly implying a requirement for lactate by A fibres when fructose is present as the main energy substrate. Schwann cells are the source of lactate, suggesting they metabolise fructose directly through glycolysis, producing and releasing lactate, which is then available to be oxidatively metabolised by A fibres. The parity in conduction maintenance of A fibres in the presence of 10mM fructose and substrate free during HFS further highlights the requirement for Schwann cell supplied lactate by A fibres in the presence of fructose. Under substrate free conditions there is no exogenous supply of energy substrate meaning the only source of energy to maintain conduction is glycogen present in the myelinating Schwann cells. The fact that 10mM fructose provides no significant additional maintenance of conduction compared to substrate free would therefore imply A fibres benefit only from glycogen derived lactate in the presence of lower concentrations of fructose.

Combining the results from this study and our previous study (Rich & Brown, 2018b) initially suggests A fibres benefit the least from fructose despite being the main cell type of the sciatic nerve to express fructokinase and GLUT5, which could suggest fructokinase is not essential for efficient fructose metabolism by the sciatic nerve. However, several caveats must be borne in mind. Firstly, under our *ex vivo* conditions only fructose not a combination of fructose and glucose, as would more likely occur *in vivo*, was supplied to the sciatic nerve therefore there was no competition between fructose and glucose for hexokinase. Secondly, even the lowest concentration of fructose we supplied to the nerve was high compared to physiological concentrations and therefore is in plentiful supply. However, the maintenance of conduction under these experimental conditions does imply that the sciatic nerve can access and metabolise fructose.

An alternative and potentially more physiological explanation to the expression of fructokinase and GLUT5 within the sciatic nerve relates to the ability of Schwann cells to produce fructose from glucose via the polyol pathway. This pathway is upregulated during diabetes (Obrosova, 2009) therefore could provide a pathway to remove excess glucose. The glucose derived fructose may then be supplied directly to A fibres and efficiently metabolised by the fructose specific fructokinase rather than having to compete with glucose for hexokinase. If this Schwann cell to A fibre fructose transfer is more common *in vivo* than direct fructose uptake (as simulated under our *ex vivo* conditions) from the circulation, then this may explain fructokinase expression by A fibres only and GLUT5 expression by A fibres and Schwann cells, since this pattern of GLUT5 expression would enable the transfer of fructose from Schwann cells to A fibres which the A fibres can then efficiently metabolise via fructokinase.

#### **6.4.3. Central vs. peripheral nervous system fructose metabolism**

The findings from this study confirm a metabolic role of glia during fructose metabolism in the PNS, most obviously when fructose is

supplied to the tissue exogenously, where the metabolic role of glia is similar between the peripheral nervous system and grey matter structures of the CNS. Studies using hippocampal brain slices found that 10mM fructose was able to restore neuronal conduction but subsequent addition of either 50 $\mu$ M CCB, a GLUT inhibitor, or 200 $\mu$ M CIN, an MCT inhibitor, resulted in rapid failure and a reduction in ATP levels (Izumi & Zorumski, 2009). Oxygen was also required for fructose to provide sufficient energy for neurones (Izumi & Zorumski, 2009). Since oxygen and accessible MCTs are required by neurones for effective use of fructose as an energy substrate it suggests neurones oxidatively metabolise a derivative of fructose, most likely in the form of lactate, the source of which is astrocytes. The electrophysiology results from this study and Rich & Brown 2018 also imply A fibres of the PNS benefit indirectly from fructose in the form of lactate supplied by myelinating Schwann cells.

Interestingly, a contrasting scenario is apparent when comparing fructose metabolism in the PNS and white matter CNS tissue. Similar CAP electrophysiology experiments to those conducted in this study have been carried out using the mouse optic nerve, a CNS white matter tract. In the presence of 10mM fructose the mouse optic nerve CAP was found to gradually decline after ~30 minutes, a latency to the onset of failure slightly longer than that under substrate free conditions, whilst 20mM fructose resulted in complete maintenance of conduction (Allen et al 2006; Meakin et al 2007). Complete recovery of the mouse optic nerve CAP, after the depletion of glycogen, was also only possible by the supply of higher concentrations of fructose (Meakin et al 2007). The decline and only partial recovery of the optic nerve CAP in 10mM fructose was found to be due to the loss of the 1st peak of the CAP comprised of the larger diameter (>0.75 $\mu$ m) axons, but the smaller diameter axons of the 2<sup>nd</sup> and 3<sup>rd</sup> peaks were maintained/recovered (Allen et al 2006; Meakin et al 2007). This was found to agree with the expression of fructokinase by the smaller, but not larger, diameter axons meaning they are capable of metabolising lower concentrations

of fructose efficiently (Meakin et al 2007). There are 2 key conclusions that can be made from these findings. Firstly, glia of central white matter tissue appear to have a smaller metabolic role with regards to fructose metabolism than myelinating Schwann cells of the PNS. Secondly, the complementary immunohistochemistry and *ex vivo* electrophysiology findings of the optic nerve suggests axon uptake and metabolism of fructose from the extracellular space is the scenario likely to occur under more physiological conditions, supported by the known expression of GLUT5 by the blood brain barrier (Mantych *et al.*, 1993), suggesting fructose can enter the brain. Whilst the conflicting enzyme expression and electrophysiology results from the sciatic nerve suggest that although axons are capable of taking up fructose from the extracellular space, this may be unlikely to occur under more physiological conditions, where instead myelinating Schwann cells may be the source of fructose.

## 6.5 Conclusion

The expression of fructokinase by A fibres only and GLUT5 by A fibres and Schwann cells means our hypothesis can be rejected. These do not necessarily parallel the electrophysiology findings, however it is evident that myelinating Schwann cells of the mouse sciatic nerve have a metabolic role with regards to fructose metabolism, although this role may differ depending on the energy substrate availability. When fructose is the only substrate available Schwann cells can glycolytically metabolise it to lactate, which is then made available to the A fibres for oxidative metabolism. Alternatively, Schwann cells can convert glucose to fructose via the polyol pathway. This fructose can then be supplied to and metabolised by A fibres via GLUT5 and fructokinase (figure 6.10).

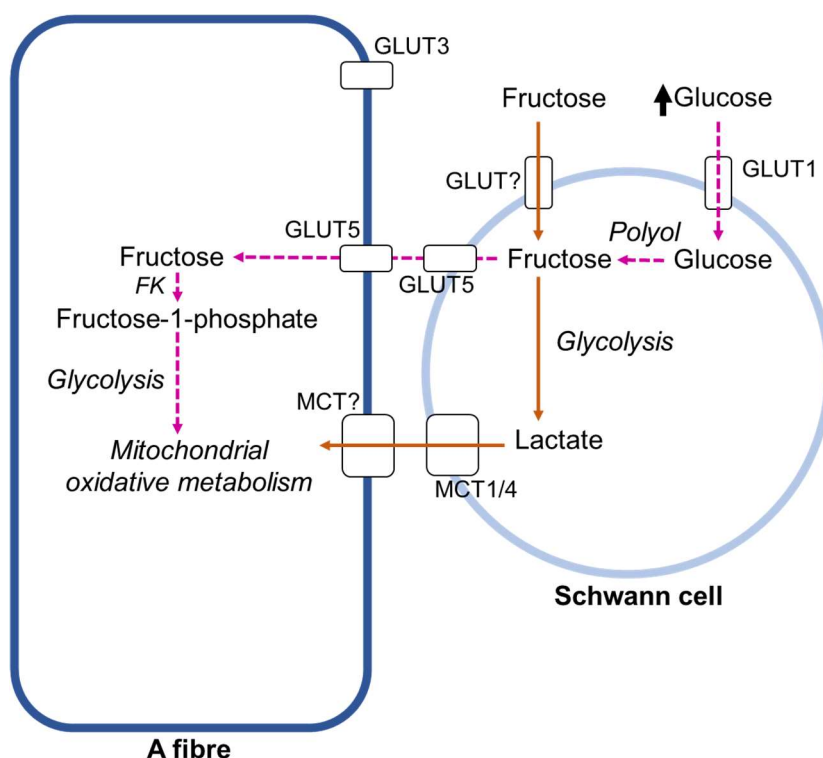


**Figure 6.10:** Schwann cell-A fibre fructose metabolism interactions. When fructose is available at sufficient concentration in the external environment, Schwann cells glycolytically metabolise this fructose to lactate which can then be supplied to A fibres for oxidative metabolism (solid, orange pathway). When the concentration of extracellular glucose is higher, i.e., during diabetes, Schwann cells can convert this glucose to fructose via the polyol pathway which is then subsequently supplied to A fibres for fructolysis and oxidative metabolism (dashed, purple pathway). FK= fructokinase, GLUT= glucose transporter and MCT= monocarboxylate transporter.

# Chapter 7: Summary

---

The studies that comprise this thesis demonstrate effective use of our improved method of stimulus evoked compound action potential (CAP) electrophysiology recordings and contribute to our understanding of the metabolic interactions between axons and Schwann cells of the peripheral nervous system (PNS). This summary will briefly collate these contributions and will focus on future directions for this field of research.

## **7.1 The importance of Schwann cell derived lactate as an energy substrate for A fibres of the mouse sciatic nerve**

Although research into the metabolic role of Schwann cells of the PNS has not received as much interest as research into the metabolic role of astrocytes of the central nervous system (CNS), previous research has revealed an important role of myelinating Schwann cells to provide glycogen derived lactate to their associated A fibre axons under conditions of decreased energy substrate availability (Brown *et al.*, 2012). This metabolic role of the myelinating Schwann cells is comparable to that of astrocytes under similar conditions (Brown *et al.*, 2003). Astrocytes are also known to provide lactate as an energy substrate to axons firing action potentials at increased frequencies where  $K^+$  released from the axons during the repolarisation phase of action potential triggers astrocytic production and supply of lactate (Ruminot *et al.*, 2019). The aim of this thesis was to expand upon the metabolic role of Schwann cells, to the more physiological condition of increased axonal energy demand as the result of increased firing activity, and begin to provide insight into the metabolic signal released from axons that communicates the need for metabolic support to the Schwann cells.

The results provided in chapter 4 demonstrate the role myelinating Schwann cells play in providing lactate to A fibre axons during increased axonal activity. The use of Schwann cell derived lactate as an energy substrate by A fibres was found to be particularly important when the concentration of glucose was not increased sufficiently to

meet their increased energy demand. This relationship is similar to that between astrocytes and axons during increased axonal energy demand, but interestingly the source of the Schwann cell lactate appears to be glucose as well as glycogen unlike astrocyte lactate which is glycogen derived (Brown *et al.*, 2005). The requirement for lactate by axons of the sciatic nerve during increased energy demand highlights an important similarity in the metabolic role between astrocytes and Schwann cells.

The ability of Schwann cells to provide lactate to A fibres during increased axonal firing prompted investigations into  $K^+$  as a metabolic signal released from A fibres that communicates their increased energy demand to Schwann cells. Schwann cell lactate production was found to be triggered by increased extracellular  $K^+$ , a response that was comparable to that of astrocytes of the mouse optic nerve. When the concentration of extracellular  $K^+$  was increased in the perfusate the relationship between the concentration of  $K^+$  and lactate was logarithmic implying changes in the glial cell membrane potential influences lactate production, supporting the theory that depolarisation of the glial cell membrane potential triggers glycolysis via the sodium bicarbonate cotransporter (NBC) and soluble adenylyl cyclase (Choi *et al.*, 2012). However, a logarithmic relationship was no longer evident for the sciatic nerve when the concentration of  $K^+$  increased on a local level achieved by imposing high frequency stimulation (HFS) in the nerve, in comparison to the optic nerve where a logarithmic relationship was still present. Irrespective of the logarithmic relationship, the results in chapter 5 reveal increased axonal firing triggers increased Schwann cell lactate production, a novel finding to this area of research.

## 7.2 The role of Schwann cells in fructose metabolism by the PNS

In addition to glucose, fructose is efficiently metabolised within the central and peripheral nervous systems, implicating a role for astrocytes and myelinating Schwann cells to provide fructose derived lactate to their associated axons (Izumi & Zorumski, 2009; Rich & Brown, 2018*b*). The expression of the fructose metabolism specific enzyme, fructokinase, explained the differential use of fructose by large and small diameter axons of the CNS optic nerve (Meakin *et al.*, 2007), therefore the expression of fructokinase within the PNS sciatic nerve was investigated. In contrast, the results presented in chapter 6 reveal the expression of fructokinase amongst the different types of sciatic nerve opposes the previous finding that A fibres are only the cell type not to directly benefit from exogenously supplied fructose (Rich & Brown, 2018*b*). However, this prompted investigations into the expression of the fructose specific transporter, GLUT5, revealing a potential shuttle of fructose from Schwann cells to A fibres. Whether these findings provide insight into a potential novel neuroprotective mechanism in which Schwann cells remove excess glucose, as occurs during diabetes, is an intriguing possibility.

## 7.3 Future directions

### 7.3.1 Metabolic signals

This thesis provides promising evidence that  $K^+$  acts as an effective metabolic signal between axons and Schwann cells of PNS, similar to that between axons and astrocytes of the CNS, but more studies should be conducted to further understand the relationship between extracellular  $K^+$  and lactate in the PNS. Firstly, to confirm and compare the change in the concentration of extracellular  $K^+$  with increased axonal firing  $K^+$  sensitive microelectrodes could be used to enable a more accurate measurement of the local rise in the concentration of extracellular  $K^+$  concentration during HFS, in comparison to the crude comparison I performed comparing the concentration of lactate released from the sciatic nerve during 100Hz and in the presence of 6mM  $K^+$ . Ideally lactate biosensors would also be used to simultaneously record changes in extracellular lactate and  $K^+$  in response to increased frequency of stimulation. Completing these experiments with both the optic and sciatic nerve would allow for the comparison between the changes in the  $K^+$  concentration, establishing whether or not the smaller increase in extracellular lactate of the sciatic nerve is related to the larger extracellular space diluting the change in extracellular  $K^+$  for equivalent stimulus frequencies. These experiments could also be carried out under substrate free conditions where the concentration of extracellular  $K^+$  increases due to reduced ATP availability required by the  $Na^+/K^+$  ATPase in order to restore ion gradients.

Due to the comparability in the metabolic role of astrocytes and Schwann cells it would be reasonable to assume that the mechanism of action of  $K^+$  as a metabolic signal would therefore be similar between the central and peripheral nervous system. With the current theory suggesting  $K^+$  acts as a metabolic signal via the NBC and soluble adenylyl cyclase, aspects of these pathways could be manipulated e.g. using inhibitors of soluble adenylyl cyclase or the NBC during HFS or

increased extracellular K<sup>+</sup> whilst recording lactate release from the sciatic nerve. If these findings proved promising this electrophysiology data could be supplemented with immunohistochemistry data staining for the expression of the NBC and soluble adenylyl cyclase within the mouse sciatic nerve.

The complexity of the nervous system implies it is also reasonable to suggest that there is no single metabolic signal that axon to glial cell metabolic interactions rely upon. Based on research into the metabolic role of myelinating counterpart of the CNS, oligodendrocytes (Micu *et al.*, 2018), glutamate likely assumes a metabolic role in the PNS. Similar to the experiments performed in chapter 5, lactate release from the sciatic nerve could be recorded in response to increases in the concentration of extracellular glutamate, representing increasing axonal activity. Since glutamate appears to act differentially between astrocytes and oligodendrocytes as a metabolic signal, experiments using the sciatic nerve could record changes in lactate release in response to inhibition/activation of the glutamate transporter and glutamate receptors, potentially providing insight into whether glutamate acts as a metabolic signal via its receptors, as with oligodendrocytes, or via its uptake, as with astrocytes.

### *7.3.2 Fructose metabolism of the sciatic nerve*

Due to technical difficulties faced the expression of GLUT5 by Schwann cells and C fibres still needs to be confirmed using immunohistochemistry. More interestingly, to provide insight into the role of Schwann cells in converting excess glucose into fructose, future experiments could involve streptozotocin (STZ) induced diabetic mice. GLUT5 expression has been shown to increase in the sciatic nerve of this diabetic model (Asada *et al.*, 1998), but more detail is required to determine the cell specific increase in expression. Whether fructokinase expression also increases is unknown. CAP recordings from the sciatic nerves of these diabetic mice could also be performed to determine

whether there is any difference in the efficiency of fructose metabolism compared to control mice.

# Bibliography

---

- Abcam (2021). Subcellular fractionation protocol. Available at: <https://www.abcam.com/protocols/subcellular-fractionation-protocol>.
- Abraham MA & Lam TKT (2016). Glucagon action in the brain. *Diabetologia* **59**, 1367–1371.
- Abrantes H de C, Briquet M, Schmuziger C, Restivo L, Puyal J, Rosenberg N, Rocher AB, Offermanns S & Chatton JY (2019). The lactate receptor HCAR1 modulates neuronal network activity through the activation of G $\alpha$  and G $\beta\gamma$  subunits. *J Neurosci* **39**, 4422–4433.
- Allaman I, Bélanger M & Magistretti PJ (2015). Methylglyoxal, the dark side of glycolysis. *Front Neurosci*; DOI: 10.3389/fnins.2015.00023.
- Allen L, Anderson S, Wender R, Meakin P, Ransom BR, Ray DE & Brown AM (2006). Fructose supports energy metabolism of some, but not all, axons in adult mouse optic nerve. *J Neurophysiol* **95**, 1917–1925.
- Allt G & Lawrenson JG (2000). The blood-nerve barrier: Enzymes, transporters and receptors - A comparison with the blood-brain barrier. *Brain Res Bull* **52**, 1–12.
- Andersen B & Westergaard N (2002). The effect of glucose on the potency of two distinct glycogen phosphorylase inhibitors. *Biochem J* **367**, 443–450.
- Asada T, Takakura S, Ogawa T, Iwai M & Kobayashi M (1998). Overexpression of glucose transporter protein 5 in sciatic nerve of streptozotocin-induced diabetic rats. *Neurosci Lett* **252**, 111–114.
- Ten Asbroek ALMA, Van Ruissen F, Ruijter JM & Baas F (2006). Comparison of Schwann cell and sciatic nerve transcriptomes indicates that mouse is a valid model for the human peripheral nervous system. *J Neurosci Res* **84**, 542–552.
- Attwell D & Laughlin SB (2001). An energy budget for signaling in the grey matter of the brain. *J Cereb Blood Flow Metab* **21**, 1133–1145.
- Aubert A, Costalat R, Magistretti PJ & Pellerin L (2005). Brain lactate kinetics: Modeling evidence for neuronal lactate uptake upon activation. *Proc Natl Acad Sci U S A* **102**, 16448–16453.
- Bak LK, Walls AB, Schousboe A & Waagepetersen HS (2018). Astrocytic glycogen metabolism in the healthy and diseased brain.

*J Biol Chem* **293**, 7108–7116.

Barros LF, Ruminot I, San Martín A, Lerchundi R, Fernández-Moncada I & Baeza-Lehnert F (2020). Aerobic Glycolysis in the Brain: Warburg and Crabtree Contra Pasteur. *Neurochem Res*; DOI: 10.1007/s11064-020-02964-w.

Battaglia G & Rustioni A (1988). Coexistence of glutamate and substance P in dorsal root ganglion neurons of the rat and monkey. *J Comp Neurol* **277**, 302–312.

Bay V & Butt AM (2012). Relationship between glial potassium regulation and axon excitability: A role for glial Kir4.1 channels. *Glia* **60**, 651–660.

Baylor DA & Nicholls JG (1969). Changes in extracellular potassium concentration produced by neuronal activity in the central nervous system of the leech. *J Physiol* **203**, 555–569.

Bear MF, Connors BW & Paradiso MA (2007). *Neuroscience: Exploring the brain*, Third edit.

Becker HM, Bröer S & Deitmer JW (2004). Facilitated Lactate Transport by MCT1 When Coexpressed with the Sodium Bicarbonate Cotransporter (NBC) in *Xenopus* Oocytes. *Biophys J* **86**, 235–247.

Bélanger M, Allaman I & Magistretti PJ (2011). Brain energy metabolism: Focus on astrocyte-neuron metabolic cooperation. *Cell Metab* **14**, 724–738.

Bender T & Martinou JC (2016). The mitochondrial pyruvate carrier in health and disease: To carry or not to carry? *Biochim Biophys Acta - Mol Cell Res* **1863**, 2436–2442.

Berg JM, Tymoczko JL & Stryer L (2002). *Biochemistry*, Fifth edit. W.H. Freeman and Company, New York.

Bergersen LH (2007). Is lactate food for neurons? Comparison of monocarboxylate transporter subtypes in brain and muscle. *Neuroscience* **145**, 11–19.

Bergersen LH (2015). Lactate transport and signaling in the brain: Potential therapeutic targets and roles in body-brain interaction. *J Cereb Blood Flow Metab* **35**, 176–185.

De Biasi S & Rustioni A (1988). Glutamate and substance P coexist in primary afferent terminals in the superficial laminae of spinal cord. *Proc Natl Acad Sci U S A* **85**, 7820–7824.

Bingul D, Kalra K, Murata EM, Belser A & Dash MB (2020). Persistent changes in extracellular lactate dynamics following synaptic potentiation. *Neurobiol Learn Mem*; DOI: 10.1016/j.nlm.2020.107314.

Bittar PG, Charnay Y, Pellerin L, Bouras C & Magistretti PJ (1996). Selective distribution of lactate dehydrogenase isoenzymes in

neurons and astrocytes of human brain. *J Cereb Blood Flow Metab* **16**, 1079–1089.

- Bittner CX, Loaiza A, Ruminot I, Larenas V, Sotelo-Hitschfeld T, Gutierrez R, Cordova A, Valdebenito R, Frommer WB & Barros LF (2010). High resolution measurement of the glycolytic rate. *Front Neuroenergetics*; DOI: 10.3389/fnene.2010.00026.
- Bittner CX, Valdebenito R, Ruminot I, Loaiza A, Larenas V, Sotelo-Hitschfeld T, Moldenhauer H, San Martín A, Gutiérrez R, Zambrano M & Barros LF (2011). Fast and reversible stimulation of astrocytic glycolysis by K<sup>+</sup> and a delayed and persistent effect of glutamate. *J Neurosci* **31**, 4709–4713.
- Black JA, Frézel N, Dib-Hajj SD & Waxman SG (2012). Expression of Nav1.7 in DRG neurons extends from peripheral terminals in the skin to central preterminal branches and terminals in the dorsal horn. *Mol Pain*; DOI: 10.1186/1744-8069-8-82.
- Bolton S & Butt AM (2006). Cyclic AMP-mediated regulation of the resting membrane potential in myelin-forming oligodendrocytes in the isolated intact rat optic nerve. *Exp Neurol* **202**, 36–43.
- Bolton S, Greenwood K, Hamilton N & Butt AM (2006). Regulation of the astrocyte resting membrane potential by cyclic AMP and protein kinase A. *Glia* **54**, 316–328.
- Boučanová F, Pollmeier G, Sandor K, Morado Urbina C, Nijssen J, Médard JJ, Bartesaghi L, Pellerin L, Svensson CI, Hedlund E & Chrast R (2021). Disrupted function of lactate transporter MCT1, but not MCT4, in Schwann cells affects the maintenance of motor end-plate innervation. *Glia* **69**, 124–136.
- Bouvier M, Szatkowski M, Amato A & Attwell D (1992). The glial cell glutamate uptake carrier countertransports pH-changing anions. *Nature* **360**, 471–474.
- Bouzier-Sore A-K & Pellerin L (2013). Unraveling the complex metabolic nature of astrocytes. *Front Cell Neurosci*; DOI: 10.3389/fncel.2013.00179.
- Bozzo L, Puyal J & Chatton JY (2013). Lactate Modulates the Activity of Primary Cortical Neurons through a Receptor-Mediated Pathway. *PLoS One*; DOI: 10.1371/journal.pone.0071721.
- Breasted JH (1930). *The Edwin Smith Surgical Papyrus: Published in Facsimile and Hieroglyphic Transliteration with Translation and Commentary in Two Volumes*. University of Chicago Press, Chicago.
- Bröer S, Bröer A, Schneider HP, Stegen C, Halestrap AP & Deitmer JW (1999). Characterization of the high-affinity monocarboxylate transporter MCT2 in *Xenopus laevis* oocytes. *Biochem J* **341**, 529–535.

- Bröer S, Schneider H-P, Bröer A, Rahman B, Hamprecht B & Deitmer JW (1998). Characterization of the monocarboxylate transporter 1 expressed in *Xenopus laevis* oocytes by changes in cytosolic pH. *Biochem J* **333**, 167–174.
- Brown AM, Evans RD, Black J & Ransom BR (2012). Schwann cell glycogen selectively supports myelinated axon function. *Ann Neurol* **72**, 406–418.
- Brown AM, Evans RD, Smith PA, Rich LR & Ransom BR (2019). Hypothermic neuroprotection during reperfusion following exposure to aglycemia in central white matter is mediated by acidification. *Physiol Rep*; DOI: 10.14814/phy2.14007.
- Brown AM, Sickmann HM, Fosgerau K, Lund TM, Schousboe A, Waagepetersen HS & Ransom BR (2005). Astrocyte glycogen metabolism is required for neural activity during aglycemia or intense stimulation in mouse white matter. *J Neurosci Res* **79**, 74–80.
- Brown AM, Tekkök SB & Ransom BR (2003). Glycogen regulation and functional role in mouse white matter. *J Physiol* **549**, 501–512.
- Brown AM, Tekkök SB & Ransom BR (2004). Energy transfer from astrocytes to axons: The role of CNS glycogen. *Neurochem Int* **45**, 529–536.
- Brunet JF, Allaman I, Magistretti PJ & Pellerin L (2010). Glycogen metabolism as a marker of astrocyte differentiation. *J Cereb Blood Flow Metab* **30**, 51–55.
- Cajal SRY (1888). Estructura de los centros nerviosos de las aves. *Rev Trimest Histol Norm y Patológica* **1**, 1–10.
- Calì C, Tauffenberger A & Magistretti P (2019). The strategic location of glycogen and lactate: From body energy reserve to brain plasticity. *Front Cell Neurosci*; DOI: 10.3389/fncel.2019.00082.
- Campana WM, Mantuano E, Azmoon P, Henry K, Banki MA, Kim JH, Pizzo DP & Gonias SL (2017). Ionotropic glutamate receptors activate cell signaling in response to glutamate in Schwann cells. *FASEB J* **31**, 1744–1755.
- Cao B, Wang J, Mu L, Poon DCH & Li Y (2016). Impairment of decision making associated with disruption of phase-locking in the anterior cingulate cortex in viscerally hypersensitive rats. *Exp Neurol* **286**, 21–31.
- Cao Z, Wu X, Chen S, Fan J, Zhang R, Owyang C & Li Y (2008). Anterior cingulate cortex modulates visceral pain as measured by visceromotor responses in viscerally hypersensitive rats. *Gastroenterology* **134**, 535–543.
- Carozzi VA, Canta A, Oggioni N, Ceresa C, Marmiroli P, Konvalinka J, Zoia C, Bossi M, Ferrarese C, Tredici G & Cavaletti G (2008).

Expression and distribution of 'high affinity' glutamate transporters GLT1, GLAST, EAAC1 and of GCP11 in the rat peripheral nervous system. *J Anat* **213**, 539–546.

Carrard A, Elsayed M, Margineanu M, Boury-Jamot B, Fragnière L, Meylan EM, Petit JM, Fiumelli H, Magistretti PJ & Martin JL (2018). Peripheral administration of lactate produces antidepressant-like effects. *Mol Psychiatry*; DOI: 10.1038/mp.2016.179.

Castillo X, Rosafio K, Wyss MT, Drandarov K, Buck A, Pellerin L, Weber B & Hirt L (2015). A probable dual mode of action for both L- and D-lactate neuroprotection in cerebral ischemia. *J Cereb Blood Flow Metab* **35**, 1561–1569.

Cataldo AM & Broadwell RD (1986). Cytochemical identification of cerebral glycogen and glucose-6-phosphatase activity under normal and experimental conditions. II. Choroid plexus and ependymal epithelia, endothelia and pericytes. *J Neurocytol* **15**, 511–524.

Champe P, Harvey R & Ferrier D (2008). *Biochemistry*. Lippincott Williams & Wilkins, London.

Choi HB, Gordon GRJ, Zhou N, Tai C, Rungta RL, Martinez J, Milner TA, Ryu JK, McLarnon JG, Tresguerres M, Levin LR, Buck J & MacVicar BA (2012). Metabolic communication between astrocytes and neurons via bicarbonate-responsive soluble adenylyl cyclase. *Neuron* **75**, 1094–1104.

Connors BW, Ransom BR, Kunis DM & Gutnick MJ (1982). Activity-dependent K<sup>+</sup> accumulation in the developing rat optic nerve. *Science (80- )* **216**, 1341–1343.

Cruz NF & Dienel GA (2002). High glycogen levels in brains of rats with minimal environmental stimuli: Implications for metabolic contributions of working astrocytes. *J Cereb Blood Flow Metab* **22**, 1476–1489.

Cui Y, Masaki K, Yamasaki R, Imamura S, Suzuki SO, Hayashi S, Sato S, Nagara Y, Kawamura MF & Kira J ichi (2014). Extensive dysregulations of oligodendrocytic and astrocytic connexins are associated with disease progression in an amyotrophic lateral sclerosis mouse model. *J Neuroinflammation*; DOI: 10.1186/1742-2094-11-42.

Cura AJ & Carruthers A (2012). Role of monosaccharide transport proteins in carbohydrate assimilation, distribution, metabolism, and homeostasis. *Compr Physiol* **2**, 863–914.

Dalsgaard MK, Madsen FF, Secher NH, Laursen H & Quistorff B (2007). High glycogen levels in the hippocampus of patients with epilepsy. *J Cereb Blood Flow Metab* **27**, 1137–1141.

Dalsgaard MK, Quistorff B, Danielsen ER, Selmer C, Vogelsang T & Secher NH (2004). A reduced cerebral metabolic ratio in exercise

reflects metabolism and not accumulation of lactate within the human brain. *J Physiol* **554**, 571–578.

- Danbolt NC (2001). Glutamate uptake. *Prog Neurobiol* **65**, 1–105.
- Debernardi R, Pierre K, Lengacher S, Magistretti PJ & Pellerin L (2003). Cell-specific expression pattern of monocarboxylate transporters in astrocytes and neurons observed in different mouse brain cortical cell cultures. *J Neurosci Res* **73**, 141–155.
- Deck M, Van Hameren G, Campbell G, Bernard-Marissal N, Devaux J, Berthelot J, Lattard A, Médard J-J, Gautier B, Quintana P, de la Barca JMC, Reynier P, Lenaers G, Chrast R & Tricaud N (2020). Myelinating Schwann cells use Warburg effect to sustain axonal physiology and function. *bioRxiv*2020.04.23.049056.
- Dempster J (1993). *Computer analysis of electrophysiological signals*. Academic Press, London.
- Diabetes UK (2021). Diabetes statistics. Available at: <https://www.diabetes.org.uk/professionals/position-statements-reports/statistics>.
- Díaz-García CM, Mongeon R, Lahmann C, Koveal D, Zucker H & Yellen G (2017). Neuronal stimulation triggers neuronal glycolysis and not lactate uptake. *Cell Metab* **26**, 361–374.
- Dienel GA (2019). Brain glucose metabolism: Integration of energetics with function. *Physiol Rev* **99**, 949–1045.
- Diggie CP, Shires M, Leitch D, Brooke D, Carr IM, Markham AF, Hayward BE, Asipu A & Bonthron DT (2009). Ketohexokinase: Expression and localization of the principal fructose-metabolizing enzyme. *J Histochem Cytochem* **57**, 763–774.
- Domenech-Estevez E, Baloui H, Repond C, Rosafio K, Médard J-J, Tricaud N, Pellerin L & Chrast R (2015). Distribution of monocarboxylate transporters in the peripheral nervous system suggests putative roles in lactate shuttling and myelination. *J Neurosci* **35**, 4151–4156.
- Douard V & Ferraris RP (2008). Regulation of the fructose transporter GLUT5 in health and disease. *Am J Physiol - Endocrinol Metab* **295**, 227–237.
- Drulis-Fajdasz D, Gizak A, Wójtowicz T, Wiśniewski JR & Rakus D (2018). Aging-associated changes in hippocampal glycogen metabolism in mice. Evidence for and against astrocyte-to-neuron lactate shuttle. *Glia* **66**, 1481–1495.
- Dugger BN & Dickson DW (2017). Pathology of neurodegenerative diseases. *Cold Spring Harb Perspect Biol*; DOI: 10.1101/cshperspect.a028035.
- Erkinen MG, Kim MO & Geschwind MD (2018). Clinical neurology and epidemiology of the major neurodegenerative diseases. *Cold*

*Spring Harb Perspect Biol*; DOI: 10.1101/cshperspect.a033118.

- Evans RD, Brown AM & Ransom BR (2013). Glycogen function in adult central and peripheral nerves. *J Neurosci Res* **91**, 1044–1049.
- Farrer LA, Cupples LA, Haines JL, Hyman B, Kukull WA, Mayeux R, Myers RH, Pericak-Vance MA, Risch N & Van Duijn CM (1997). Effects of age, sex, and ethnicity on the association between apolipoprotein E genotype and Alzheimer disease: A meta-analysis. *J Am Med Assoc* **278**, 1349–1356.
- Fasciani I, Pluta P, González-Nieto D, Martínez-Montero P, Molano J, Paíno CL, Millet O & Barrio LC (2018). Directional coupling of oligodendrocyte connexin-47 and astrocyte connexin-43 gap junctions. *Glia* **66**, 2340–2352.
- Fayaz A, Croft P, Langford RM, Donaldson LJ & Jones GT (2016). Prevalence of chronic pain in the UK: A systematic review and meta-analysis of population studies. *BMJ Open*; DOI: 10.1136/bmjopen-2015-010364.
- Fernández-Moncada I & Barros LF (2014). Non-preferential fuelling of the Na(+)/K(+)-ATPase pump. *Biochem J* **460**, 353–361.
- Fernández-Moncada I, Ruminot I, Robles-Maldonado D, Alegría K, Deitmer JW & Barros LF (2018). Neuronal control of astrocytic respiration through a variant of the Crabtree effect. *Proc Natl Acad Sci U S A* **115**, 1623–1628.
- Fillenz M (2005). The role of lactate in brain metabolism. *Neurochem Int* **47**, 413–417.
- Finger S (2010). *Minds behind the brain: A history of the pioneers and their discoveries*.
- Flick MJ & Konieczny SF (2002). Identification of putative mammalian D-lactate dehydrogenase enzymes. *Biochem Biophys Res Commun* **295**, 910–916.
- Forderhase AG, Styers HC, Lee CA & Sombers LA (2020). Simultaneous voltammetric detection of glucose and lactate fluctuations in rat striatum evoked by electrical stimulation of the midbrain. *Anal Bioanal Chem* **412**, 6611–6624.
- Foucher CD & Tubben RE (2020). *Lactic acidosis*. StatPearls.
- Fünfschilling U, Supplie LM, Mahad D, Boretius S, Saab AS, Edgar J, Brinkmann BG, Kassmann CM, Tzvetanova ID, Möbius W, Diaz F, Meijer D, Suter U, Hamprecht B, Sereda MW, Moraes CT, Frahm J, Goebbels S & Nave KA (2012). Glycolytic oligodendrocytes maintain myelin and long-term axonal integrity. *Nature* **485**, 517–521.
- García-Cáceres C et al. (2016). Astrocytic insulin signaling couples brain glucose uptake with nutrient availability. *Cell* **166**, 867–880.

- Ghabriel MN & Allt G (1981). Incisures of Schmidt-Lanterman. *Prog Neurobiol* **17**, 25–58.
- Gibbs ME, Anderson DG & Hertz L (2006). Inhibition of glycogenolysis in astrocytes interrupts memory consolidation in young chickens. *Glia* **54**, 214–222.
- Gibbs ME & Hertz L (2008). Inhibition of astrocytic energy metabolism by d-lactate exposure impairs memory. *Neurochem Int* **52**, 1012–1018.
- Gold SM, Dziobek I, Sweat V, Tirsi A, Rogers K, Bruehl H, Tsui W, Richardson S, Javier E & Convit A (2007). Hippocampal damage and memory impairments as possible early brain complications of type 2 diabetes. *Diabetologia* **50**, 711–719.
- Golgi C (1886). *Sulla fina anatomia degli organi centrali del sistema nervoso*. Hoepli, Milano.
- Gonzalez JT & Betts JA (2018). Dietary Fructose Metabolism By Splanchnic Organs: Size Matters. *Cell Metab* **27**, 483–485.
- Gordon GRJ, Choi HB, Rungta RL, Ellis-Davies GCR & MacVicar BA (2008). Brain metabolism dictates the polarity of astrocyte control over arterioles. *Nature* **456**, 745–749.
- Gould GW & Holman GD (1993). The glucose transporter family: Structure, function and tissue-specific expression. *Biochem J* **295**, 329–341.
- Halestrap AP & Price NT (1999). The proton-linked monocarboxylate transporter (MCT) family: structure, function and regulation. *Biochem J* **343**, 281–299.
- Halim ND, Mcfate T, Mohyeldin A, Okagaki P, Korotchkina LG, Patel MS, Jeoung NH, Harris RA, Schell MJ & Verma A (2010). Phosphorylation status of pyruvate dehydrogenase distinguishes metabolic phenotypes of cultured rat brain astrocytes and neurons. *Glia* **58**, 1168–1176.
- Hargittai PT, Youmans SJ & Lieberman EM (1991). Determination of the membrane potential of cultured mammalian schwann cells and its sensitivity to potassium using a thiocarbocyanine fluorescent dye. *Glia* **4**, 611–616.
- Hartley T, Lever C, Burgess N & O'Keefe J (2014). Space in the brain: How the hippocampal formation supports spatial cognition. *Philos Trans R Soc B Biol Sci*; DOI: 10.1098/rstb.2012.0510.
- Hasel P et al. (2017). Neurons and neuronal activity control gene expression in astrocytes to regulate their development and metabolism. *Nat Commun*; DOI: 10.1038/ncomms15132.
- Havel PJ (2005). Dietary fructose: Implications for dysregulation of energy homeostasis and lipid/carbohydrate metabolism. *Nutr Rev* **63**, 133–157.

- Havrankova J, Schmechel D, Roth J & Brownstein M (1978). Identification of insulin in rat brain. *Proc Natl Acad Sci U S A* **75**, 5737–5741.
- Heinemann U & Dieter Lux H (1977). Ceiling of stimulus induced rises in extracellular potassium concentration in the cerebral cortex of cat. *Brain Res* **120**, 231–249.
- Herrero-Mendez A, Almeida A, Fernandez E, Maestre C, Moncada S & Bolanos J (2009). The bioenergetic and antioxidant status of neurons is controlled by continuous degradation of a key glycolytic enzyme by APC/C-Cdh1. *Nat Cell Biol* **11**, 747–752.
- Hoosein NM & Gurd RS (1984). Identification of glucagon receptors in rat brain. *Proc Natl Acad Sci U S A* **81**, 4368–4372.
- Hoppe D, Chvatal A, Kettenmann H, Orkand RK & Ransom BR (1991). Characteristics of activity-dependent potassium accumulation in mammalian peripheral nerve in vitro. *Brain Res* **552**, 106–112.
- Hu M, Hong L, Liu C, Hong S, He S, Zhou M, Huang G & Chen Q (2019). Electrical stimulation enhances neuronal cell activity mediated by Schwann cell derived exosomes. *Sci Rep*; DOI: 10.1038/s41598-019-41007-5.
- Huttunen JK (1971). Fructose in medicine: A review with particular reference to diabetes mellitus. *Postgrad Med J* **47**, 654–659.
- IASP (2020). IASP announces revised definition of pain. *Int Assoc Study Pain*. Available at: <https://www.iasp-pain.org/publications/iasp-news/iasp-announces-revised-definition-of-pain/?ItemNumber=10475>.
- Ichihara Y, Doi T, Ryu Y, Nagao M, Sawada Y & Ogata T (2017). Oligodendrocyte progenitor cells directly utilize lactate for promoting cell cycling and differentiation. *J Cell Physiol* **232**, 986–995.
- Izumi Y & Zorumski CF (2009). Glial-neuronal interactions underlying fructose utilization in rat hippocampal slices. *Neuroscience* **161**, 847–854.
- Jensen NJ, Wodschow HZ, Nilsson M & Rungby J (2020). Effects of ketone bodies on brain metabolism and function in neurodegenerative diseases. *Int J Mol Sci*; DOI: 10.3390/ijms21228767.
- Jha MK, Ament XH, Yang F, Liu Y, Polydefkis MJ, Pellerin L & Morrison BM (2020a). Reducing monocarboxylate transporter MCT1 worsens experimental diabetic peripheral neuropathy. *Exp Neurol*; DOI: 10.1016/j.expneurol.2020.113415.
- Jha MK, Lee Y, Russell KA, Yang F, Dastgheyb RM, Deme P, Ament XH, Chen W, Liu Y, Guan Y, Polydefkis MJ, Hoke A, Haughey NJ, Rothstein JD & Morrison BM (2020b). Monocarboxylate transporter

1 in Schwann cells contributes to maintenance of sensory nerve myelination during aging. *Glia* **68**, 161–177.

Jha MK & Morrison BM (2020). Lactate transporters mediate glia-neuron metabolic crosstalk in homeostasis and disease. *Front Cell Neurosci*; DOI: 10.3389/fncel.2020.589582.

Jones EG (1994). The Neuron Doctrine 1891. *J Hist Neurosci* **3**, 3–20.

Kabat H & Anderson JP (1943). Acute arrest of cerebral circulation in man. *Arch Neurol Psychiatry* **50**, 510–528.

Karagiannis A, Sylantyev S, Hadjihambi A, Hosford PS, Kasparov S & Gourine A V. (2016). Hemichannel-mediated release of lactate. *J Cereb Blood Flow Metab* **36**, 1202–1211.

Kettenmann H, Sonnhof U & Schachner M (1983). Exclusive potassium dependence of the membrane potential in cultured mouse oligodendrocytes. *J Neurosci* **3**, 500–505.

Kidd G, Ohno N & Trapp B (2013). *Handbook of Clinical Neurology*. Elsevier Science Inc, United States.

Kmieć Z (2001). *Cooperation of liver cells in health and disease*.

Kocsis JD, Gordon TR & Waxman SG (1986). Mammalian optic nerve fibers display two pharmacologically distinct potassium channels. *Brain Res* **383**, 357–361.

Kojo A, Yamada K & Yamamoto T (2016). Glucose transporter 5 (GLUT5)-like immunoreactivity is localized in subsets of neurons and glia in the rat brain. *J Chem Neuroanat* **74**, 55–70.

Kong J, Shepel PN, Holden CP, Mackiewicz M, Pack AI & Geiger JD (2002). Brain glycogen decreases with increased periods of wakefulness: Implications for homeostatic drive to sleep. *J Neurosci* **22**, 5581–5587.

Kuffler SW, Nicholls JG & Orkand RK (1966). Physiological properties of glial cells in the central nervous system of amphibia. *J Neurophysiol* **29**, 768–787.

Kuffler SW & Potter DD (1964). Glia in the leech central nervous system: Physiological properties and neuron-glia relationship. *Journal of Neurophysiology*. *J Neurophysiol* **27**, 290–320.

Kuzawa CW, Chugani HT, Grossman LI, Lipovich L, Muzik O, Hof PR, Wildman DE, Sherwood CC, Leonard WR & Lange N (2014). Metabolic costs and evolutionary implications of human brain development. *Proc Natl Acad Sci U S A* **111**, 13010–13015.

Lappe-Siefke C, Goebbels S, Gravel M, Nicksch E, Lee J, Braun PE, Griffiths IR & Navel KA (2003). Disruption of *Cnp1* uncouples oligodendroglial functions in axonal support and myelination. *Nat Genet* **33**, 366–374.

- Lazic SE, Clarke-Williams CJ & Munafò MR (2018). What exactly is 'N' in cell culture and animal experiments? *PLoS Biol*; DOI: 10.1371/journal.pbio.2005282.
- Lee Y, Morrison BM, Li Y, Lengacher S, Farah MH, Hoffman PN, Liu Y, Tsingalia A, Jin L, Zhang PW, Pellerin L, Magistretti PJ & Rothstein JD (2012). Oligodendroglia metabolically support axons and contribute to neurodegeneration. *Nature* **487**, 443–448.
- Lerchundi R, Fernández-Moncada I, Contreras-Baeza Y, Sotelo-Hitschfeld T, Mächler P, Wyss MT, Stobart J, Baeza-Lehnert F, Alegría K, Weber B & Barros LF (2015). NH<sub>4</sub><sup>+</sup> triggers the release of astrocytic lactate via mitochondrial pyruvate shunting. *Proc Natl Acad Sci* **112**, 11090–11095.
- Lerchundi R, Kafitz KW, Winkler U, Färfers M, Hirrlinger J & Rose CR (2019). FRET-based imaging of intracellular ATP in organotypic brain slices. *J Neurosci Res* **97**, 933–945.
- Lev-Ram V & Ellisman MH (1995). Axonal activation-induced calcium transients in myelinating Schwann cells, sources, and mechanisms. *J Neurosci* **15**, 2628–2637.
- Liberti M V. & Locasale JW (2016). The Warburg effect: How does it benefit cancer cells? *Trends Biochem Sci* **41**, 211–218.
- Lieberman EM, Abbott NJ & Hassan S (1989). Evidence that glutamate mediates Axon-to-Schwann cell signaling in the squid. *Glia* **2**, 94–102.
- Lieberman EM & Sanzenbacher E (1992). Mechanisms of glutamate activation of axon-to-Schwann cell signaling in the squid. *Neuroscience* **47**, 931–939.
- Lin SH, Lee LT & Yang YK (2014). Serotonin and mental disorders: A concise review on molecular neuroimaging evidence. *Clin Psychopharmacol Neurosci* **12**, 196–202.
- Liu L, MacKenzie KR, Putluri N, Maletić-Savatić M & Bellen HJ (2017). The glia-neuron lactate shuttle and elevated ROS promote lipid synthesis in neurons and lipid droplet accumulation in glia via APOE/D. *Cell Metab* **26**, 719–737.
- Liu L, Zhang K, Sandoval H, Yamamoto S, Jaiswal M, Sanz E, Li Z, Hui J, Graham BH, Quintana A & Bellen HJ (2015). Glial lipid droplets and ROS induced by mitochondrial defects promote neurodegeneration. *Cell* **160**, 177–190.
- Lowry OH, Rosebrough NJ, Farr AL & Randall RJ (1951). Protein measurement with the Folin phenol reagent. *J Biol Chem* **193**, 265–275.
- Lundgaard I, Li B, Xie L, Kang H, Sanggaard S, Haswell JDR, Sun W, Goldman S, Blekot S, Nielsen M, Takano T, Deane R & Nedergaard M (2015). Direct neuronal glucose uptake heralds

activity-dependent increases in cerebral metabolism. *Nat Commun*; DOI: 10.1038/ncomms7807.

- Lynch SM (2013). *Using statistics in social research: A concise approach*.
- Mächler P, Wyss MT, Elsayed M, Stobart J, Gutierrez R, Von Faber-Castell A, Kaelin V, Zuend M, San Martín A, Romero-Gómez I, Baeza-Lehnert F, Lengacher S, Schneider BL, Aebischer P, Magistretti PJ, Barros LF & Weber B (2016). In vivo evidence for a lactate gradient from astrocytes to neurons. *Cell Metab* **23**, 94–102.
- Magi S, Piccirillo S, Amoroso S & Lariccia V (2019). Excitatory amino acid transporters (EAATs): Glutamate transport and beyond. *Int J Mol Sci*; DOI: 10.3390/ijms20225674.
- Magistretti PJ & Allaman I (2015). A cellular perspective on brain energy metabolism and functional imaging. *Neuron* **86**, 883–901.
- Magnani P, Varghese Cherian P, Gould GW, Greene DA, Sima AAF & Brosius FC (1996). Glucose transporters in rat peripheral nerve: Paranodal expression of GLUT1 and GLUT3. *Metabolism* **45**, 1466–1473.
- Malet M & Brumovsky PR (2015). VGLUTs and glutamate synthesis—focus on DRG neurons and pain. *Biomolecules* **5**, 3416–3437.
- Mangia S, Simpson IA, Vannucci SJ & Carruthers A (2009). The in vivo neuron-to-astrocyte lactate shuttle in human brain: Evidence from modeling of measured lactate levels during visual stimulation. *J Neurochem* **109**, 55–62.
- Mantych GJ, James DE & Devaskar SU (1993). Jejunal/kidney glucose transporter isoform (Glut-5) is expressed in the human blood-brain barrier. *Endocrinology* **132**, 35–40.
- Markoullis K, Sargiannidou I, Schiza N, Hadjisavvas A, Roncaroli F, Reynolds R & Kleopa KA (2012). Gap junction pathology in multiple sclerosis lesions and normal-appearing white matter. *Acta Neuropathol* **123**, 873–886.
- Mata M, Alessi D & Fink DJ (1990). S100 is preferentially distributed in myelin-forming Schwann cells. *J Neurocytol* **19**, 432–442.
- Matsui T, Ishikawa T, Ito H, Okamoto M, Inoue K, Lee M chul, Fujikawa T, Ichitani Y, Kawanaka K & Soya H (2012). Brain glycogen supercompensation following exhaustive exercise. *J Physiol* **590**, 607–616.
- Matsui T, Omuro H, Liu YF, Soya M, Shima T, Mcewen BS & Soya H (2017). Astrocytic glycogen-derived lactate fuels the brain during exhaustive exercise to maintain endurance capacity. *Proc Natl Acad Sci U S A* **114**, 6358–6363.
- Meakin PJ, Fowler MJ, Rathbone AJ, Allen LM, Ransom BR, Ray DE &

- Brown AM (2007). Fructose metabolism in the adult mouse optic nerve, a central white matter tract. *J Cereb Blood Flow Metab* **27**, 86–99.
- Meister B, Arvidsson U, Zhang X, Jacobsson G, Villar MJ & H&E;kfelt T (1993). Glutamate transporter mRNA and glutamate-like immunoreactivity in spinal motoneurons. *Neuroreport* **5**, 337–340.
- Meyer N, Richter N, Fan Z, Siemonsmeier G, Pivneva T, Jordan P, Steinhäuser C, Semtner M, Nolte C & Kettenmann H (2018). Oligodendrocytes in the mouse corpus callosum maintain axonal function by delivery of glucose. *Cell Rep* **22**, 2383–2394.
- Micu I, Plemel JR, Caprariello A V., Nave KA & Stys PK (2018). Axo-myelinic neurotransmission: A novel mode of cell signalling in the central nervous system. *Nat Rev Neurosci* **19**, 49–57.
- Micu I, Plemel JR, Lachance C, Proft J, Jansen AJ, Cummins K, van Minnen J & Stys PK (2016). The molecular physiology of the axo-myelinic synapse. *Exp Neurol* **276**, 41–50.
- Miyamoto K, Ishikura K ichiro, Kume K & Ohsawa M (2019). Astrocyte-neuron lactate shuttle sensitizes nociceptive transmission in the spinal cord. *Glia* **67**, 27–36.
- Mizisin AP & Weerasuriya A (2011). Homeostatic regulation of the endoneurial microenvironment during development, aging and in response to trauma, disease and toxic insult. *Acta Neuropathol* **121**, 291–312.
- Morland C, Lauritzen KH, Puchades M, Holm-Hansen S, Andersson K, Gjedde A, Attramadal H, Storm-Mathisen J & Bergersen LH (2015). The lactate receptor, G-protein-coupled receptor 81/hydroxycarboxylic acid receptor 1: Expression and action in brain. *J Neurosci Res* **93**, 1045–1055.
- Morrison BM, Tsingalia A, Vidensky S, Lee Y, Jin L, Farah MH, Lengacher S, Magistretti PJ, Pellerin L & Rothstein JD (2015). Deficiency in monocarboxylate transporter 1 (MCT1) in mice delays regeneration of peripheral nerves following sciatic nerve crush. *Exp Neurol* **263**, 325–338.
- Müller MS, Fouyssac M & Taylor CW (2018). Effective glucose uptake by human astrocytes requires its sequestration in the endoplasmic reticulum by glucose-6-phosphatase- $\beta$ . *Curr Biol* **28**, 3481–3486.
- Nagy JI, Dudek FE & Rash JE (2004). Update on connexins and gap junctions in neurons and glia in the mammalian nervous system. *Brain Res Rev* **47**, 191–215.
- Nakrani MN, Wineland RH & Anjum F (2020). *Physiology, Glucose Metabolism*. StatPearls.
- Nehlig A, Wittendorp-Rechenmann E & Lam CD (2004). Selective uptake of [ $^{14}$ C]2-deoxyglucose by neurons and astrocytes: High-

resolution microautoradiographic imaging by cellular<sup>14</sup>C-trajectography combined with immunohistochemistry. *J Cereb Blood Flow Metab* **24**, 1004–1014.

Nelson DL & Cox MM (2009). *Lehninger principles of biochemistry*, Fifth edit. W.H. Freeman and Company, New York.

Netzahualcoyotzi C & Pellerin L (2020). Neuronal and astroglial monocarboxylate transporters play key but distinct roles in hippocampus-dependent learning and memory formation. *Prog Neurobiol*; DOI: 10.1016/j.pneurobio.2020.101888.

Newsholme EA (1981). The glucose/fatty acid cycle and physical exhaustion. *Ciba Found Symp* **82**, 89–101.

Nicholson C & Syková E (1998). Extracellular space structure revealed by diffusion analysis. *Trends Neurosci* **21**, 207–215.

NIDDK (2021). Diabetic Neuropathy. *Natl Inst Diabetes Dig Kidney Dis*. Available at: <https://www.niddk.nih.gov/health-information/diabetes/overview/preventing-problems/nerve-damage-diabetic-neuropathies>.

Nilaweera K, Herwig A, Bolborea M, Campbell G, Mayer CD, Morgan PJ, Ebling FJP & Barrett P (2011). Photoperiodic regulation of glycogen metabolism, glycolysis, and glutamine synthesis in tanycytes of the Siberian hamster suggests novel roles of tanycytes in hypothalamic function. *Glia* **59**, 1695–1705.

Niu J, Li T, Yi C, Huang N, Koulakoff A, Weng C, Li C, Zhao CJ, Giaume C & Xiao L (2016). Connexin-based channels contribute to metabolic pathways in the oligodendroglial lineage. *J Cell Sci* **129**, 1902–1914.

Nortley R & Attwell D (2017). Control of brain energy supply by astrocytes. *Curr Opin Neurobiol* **47**, 80–85.

Obrosova IG (2009). Diabetes and the peripheral nerve. *Biochim Biophys Acta - Mol Basis Dis* **1792**, 931–940.

Oe Y, Baba O, Ashida H, Nakamura KC & Hirase H (2016). Glycogen distribution in the microwave-fixed mouse brain reveals heterogeneous astrocytic patterns. *Glia* **64**, 1532–1545.

Oppelt SA, Zhang W & Tolan DR (2017). Specific regions of the brain are capable of fructose metabolism. *Brain Res* **1657**, 312–322.

Orkand RK, Nicholls JG & Kuffler SW (1966). Effect of nerve impulses on the membrane potential of glial cells in the central nervous system of amphibia. *J Neurophysiol* **29**, 788–806.

Owen OE, Morgan AP, Kemp HG, Sullivan JM, Herrera MG & Cahill GF (1967). Brain metabolism during fasting. *J Clin Invest* **46**, 1589–1595.

Pape LG & Katzman R (1972). Response of glia in cat sensorimotor

- cortex to increased extracellular potassium. *Brain Res* **38**, 71–92.
- Parker JL, Shariati NH & Karantonis DM (2018). Electrically evoked compound action potential recording in peripheral nerves. *Bioelectron Med* **1**, 71–83.
- Pavelka M & Roth J (2010). Peripheral Nerve: Connective Tissue Components. In *Functional Ultrastructure*.
- Pazos M, Yang H, Gardiner SK, Cepurna WO, Johnson EC, Morrison JC & Burgoyne CF (2015). Rat optic nerve head anatomy within 3D histomorphometric reconstructions of normal control eyes. *Exp Eye Res* **139**, 1–12.
- Pellerin L & Magistretti PJ (1994). Glutamate uptake into astrocytes stimulates aerobic glycolysis: a mechanism coupling neuronal activity to glucose utilization. *Proc Natl Acad Sci* **91**, 10625–10629.
- Pellerin L & Magistretti PJ (2013). The central role of astrocytes in neuroenergetics. In *Neuroglia*.
- Pellerin L, Pellegrini G, Bittar PG, Charnay Y, Bouras C, Martin JL, Stella N & Magistretti PJ (1998). Evidence supporting the existence of an activity-dependent astrocyte-neuron lactate shuttle. *Dev Neurosci* **20**, 291–299.
- Perl DP (2010). Neuropathology of Alzheimer's disease. *Mt Sinai J Med* **77**, 32–42.
- Petersmann A, Müller-Wieland D, Müller UA, Landgraf R, Nauck M, Freckmann G, Heinemann L & Schleicher E (2019). Definition, Classification and Diagnosis of Diabetes Mellitus. *Exp Clin Endocrinol Diabetes*; DOI: 10.1055/a-1018-9078.
- Pfeiffer-Guglielmi B, Fleckenstein B, Jung G & Hamprecht B (2003). Immunocytochemical localization of glycogen phosphorylase isozymes in rat nervous tissues by using isozyme-specific antibodies. *J Neurochem* **85**, 73–81.
- Pfeiffer-Guglielmi B, Francke M, Reichenbach A & Hamprecht B (2007). Glycogen phosphorylase isozymes and energy metabolism in the rat peripheral nervous system-An immunocytochemical study. *Brain Res* **1136**, 20–27.
- Philips T & Rothstein JD (2017). Oligodendroglia: Metabolic supporters of neurons. *J Clin Invest* **127**, 3271–3280.
- Poulsom R, Mirrlees DJ, Earl DCN & Heath H (1983). The effects of an aldose reductase inhibitor upon the sorbitol pathway, fructose-1-phosphate and lactate in the retina and nerve of streptozotocin-diabetic rats. *Exp Eye Res* **36**, 751–760.
- Powell CL, Davidson AR & Brown AM (2020). Universal glia to neurone lactate transfer in the nervous system: Physiological functions and pathological consequences. *Biosensors* **10**, 183–201.

- Purves D, Augustine GJ, Fitzpatrick D, Hall WC, LaMantia A-S & E WL (2012). *Neuroscience*, Fifth edit. USA.
- Quistorff B, Secher NH & Van Lieshout JJ (2008). Lactate fuels the human brain during exercise. *FASEB J* **22**, 3443–3449.
- Ramos M, del Arco A, Pardo B, Martínez-Serrano A, Martínez-Morales J, Kobayashi K, Yasuda T, Bogóñez E, Bovolenta P, Saheki T & Satrústegui J (2003). Mitochondrial aspartate-glutamate carrier aralar1 in brain and prominent expression in the spinal cord. *Brain Res Dev Brain Res* **143**, 33–46.
- Ransom B & Goldring S (1973). Ionic determinants of membrane potential of cells presumed to be glia in cerebral cortex of cat. *J Neurophysiol* **36**, 855–868.
- Ransom BR & Orkand RK (1996). Glial-neuronal interactions in non-synaptic areas of the brain: Studies in the optic nerve. *Trends Neurosci* **19**, 352–358.
- Ransom CB, Ransom BR & Sontheimer H (2000). Activity-dependent extracellular K<sup>+</sup> accumulation in rat optic nerve: The role of glial and axonal Na<sup>+</sup> pumps. *J Physiol* **522**, 427–442.
- Rathee K, Dhull V, Dhull R & Singh S (2016). Biosensors based on electrochemical lactate detection: A comprehensive review. *Biochem Biophys Reports* **5**, 35–54.
- Raymond SA (1979). Effects of nerve impulses on threshold of frog sciatic nerve fibres. *J Physiol* **190**, 273–303.
- Rich LR & Brown AM (2018a). Comparisons of the metabolic interactions between neurones and glia in the central and peripheral nervous system. *Curr Trends Neurol* **12**, 65–74.
- Rich LR & Brown AM (2018b). Fibre sub-type specific conduction reveals metabolic function in mouse sciatic nerve. *J Physiol*; DOI: 10.1113/JP275680.
- Richards RL (1951). Ischaemic lesions of peripheral nerves. *J Neurol Neurosurg Psychiatry* **14**, 76–87.
- Robert A & Jirounek P (1994). Uptake of potassium by nonmyelinating Schwann cells induced by axonal activity. *J Neurophysiol* **72**, 2570–2579.
- Röder P V, Wu B, Liu Y & Han W (2016). Pancreatic regulation of glucose homeostasis. *Exp Mol Med*; DOI: 10.1038/emm.2016.6.
- Rogatzki MJ, Ferguson BS, Goodwin ML & Gladden LB (2015). Lactate is always the end product of glycolysis. *Front Neurosci*; DOI: 10.3389/fnins.2015.00022.
- Ruiz F (2021). How to prepare protein samples for Western blot. Available at: <https://www.goldbio.com/articles/article/Preparation-of-protein-samples-for-Western-Blot>.

- Ruminot I, Gutiérrez R, Peña-Münzenmayer G, Añazco C, Sotelo-Hitschfeld T, Lerchundi R, Niemeyer MI, Shull GE & Barros LF (2011). NBCe1 mediates the acute stimulation of astrocytic glycolysis by extracellular K<sup>+</sup>. *J Neurosci* **31**, 14264–14271.
- Ruminot I, Schmälzle J, Leyton B, Barros LF & Deitmer JW (2019). Tight coupling of astrocyte energy metabolism to synaptic activity revealed by genetically encoded FRET nanosensors in hippocampal tissue. *J Cereb Blood Flow Metab* **39**, 513–523.
- Saab AS et al. (2016). Oligodendroglial NMDA receptors regulate glucose import and axonal energy metabolism. *Neuron* **91**, 119–132.
- Sagar SM, Sharp FR & Swanson RA (1987). The regional distribution of glycogen in rat brain fixed by microwave irradiation. *Brain Res* **417**, 172–174.
- San Martín A, Sotelo-Hitschfeld T, Lerchundi R, Fernández-Moncada I, Ceballo S, Valdebenito R, Baeza-Lehnert F, Alegría K, Contreras-Baeza Y, Garrido-Gerter P, Romero-Gómez I & Barros LF (2014). Single-cell imaging tools for brain energy metabolism: A review. *Neurophotonics*; DOI: 10.1117/1.nph.1.1.011004.
- Scavuzzo CJ, Rakotavao I & Dickson CT (2020). Differential effects of L- and D-lactate on memory encoding and consolidation: Potential role of HCAR1 signaling. *Neurobiol Learn Mem*; DOI: 10.1016/j.nlm.2019.107151.
- Schmalbruch H (1986). Fiber composition of the rat sciatic nerve. *Anat Rec* **215**, 71–81.
- Shima T, Matsui T, Jesmin S, Okamoto M, Soya M, Inoue K, Liu YF, Torres-Aleman I, McEwen BS & Soya H (2017). Moderate exercise ameliorates dysregulated hippocampal glycometabolism and memory function in a rat model of type 2 diabetes. *Diabetologia* **60**, 597–606.
- Shulman RG, Bloch G & Rothman DL (1995). In vivo regulation of muscle glycogen synthase and the control of glycogen synthesis. *Proc Natl Acad Sci U S A* **92**, 8535–8542.
- Snaidero N, Velte C, Myllykoski M, Raasakka A, Ignatev A, Werner HB, Erwig MS, Möbius W, Kursula P, Nave KA & Simons M (2017). Antagonistic functions of MBP and CNP establish cytosolic channels in CNS myelin. *Cell Rep* **18**, 314–323.
- Sonnay S, Poirot J, Just N, Clerc AC, Gruetter R, Rainer G & Duarte JMN (2018). Astrocytic and neuronal oxidative metabolism are coupled to the rate of glutamate–glutamine cycle in the tree shrew visual cortex. *Glia* **66**, 477–491.
- Sotelo-Hitschfeld T et al. (2015). Channel-mediated lactate release by K<sup>+</sup>-stimulated astrocytes. *J Neurosci* **35**, 4168–4178.

- Stassart RM, Möbius W, Nave KA & Edgar JM (2018). The Axon-Myelin unit in development and degenerative disease. *Front Neurosci*; DOI: 10.3389/fnins.2018.00467.
- Stedman M, Lunt M, Davies M, Livingston M, Duff C, Fryer A, Anderson SG, Gadsby R, Gibson M, Rayman G & Heald A (2020). Cost of hospital treatment of type 1 diabetes (T1DM) and type 2 diabetes (T2DM) compared to the non-diabetes population: A detailed economic evaluation. *BMJ Open*; DOI: 10.1136/bmjopen-2019-033231.
- Sterling P & Laughlin S (2015). *Principles of neural design*. The MIT Press.
- Stino AM & Smith AG (2017). Peripheral neuropathy in prediabetes and the metabolic syndrome. *J Diabetes Investig* **8**, 646–655.
- Stys PK (1992). Suction electrode recording from nerves and fiber tracts. In *Practical Electrophysiological methods: A guide for in vitro studies in vertebrate neurobiology*. Wiley-Liss.
- Stys PK, Ransom BR & Waxman SG (1991). Compound action potential of nerve recorded by suction electrode: A theoretical and experimental analysis. *Brain Res* **546**, 18–32.
- Suzuki A, Stern SA, Bozdagi O, Huntley GW, Walker RH, Magistretti PJ & Alberini CM (2011). Astrocyte-neuron lactate transport is required for long-term memory formation. *Cell* **144**, 810–823.
- Takebe K, Nio-Kobayashi J, Takahashi-Iwanaga H & Iwanaga T (2008). Histochemical demonstration of a monocarboxylate transporter in the mouse perineurium with special reference to GLUT1. *Biomed Res* **29**, 297–306.
- Tappy L & Rosset R (2019). Health outcomes of a high fructose intake: the importance of physical activity. *J Physiol* **597**, 3561–3571.
- Tashiro S (1922). Studies on Alkaligenesis in tissues. *Am J Physiol Content* **60**, 519–543.
- Thomas RC (1972). Intracellular sodium activity and the sodium pump in snail neurones. *J Physiol* **220**, 55–71.
- Tsacopoulos M, Veuthey a L, Saravelos SG, Perrottet P & Tsoupras G (1994). Glial cells transform glucose to alanine, which fuels the neurons in the honeybee retina. *J Neurosci* **14**, 1339–1351.
- Uehara T, Sumiyoshi T, Itoh H & Kurachi M (2007). Role of glutamate transporters in the modulation of stress-induced lactate metabolism in the rat brain. *Psychopharmacology (Berl)* **195**, 297–302.
- Uehara T, Sumiyoshi T, Matsuoka T, Itoh H & Kurachi M (2006). Role of 5-HT1A receptors in the modulation of stress-induced lactate metabolism in the medial prefrontal cortex and basolateral amygdala. *Psychopharmacology (Berl)* **186**, 218–225.

- Ulbricht W (2005). Sodium channel inactivation: Molecular determinants and modulation. *Physiol Rev* **85**, 1271–1301.
- Vandamme T (2014). Use of rodents as models of human diseases. *J Pharm Bioallied Sci* **6**, 2–9.
- Vannucci SJ, Maher F & Simpson IA (1997). Glucose transporter proteins in brain: Delivery of glucose to neurons and glia. *Glia* **21**, 2–21.
- Vannucci SJ & Simpson IA (2003). Developmental switch in brain nutrient transporter expression in the rat. *Am J Physiol - Endocrinol Metab*; DOI: 10.1152/ajpendo.00187.2003.
- Véga C, Martiel JL, Drouhault D, Burckhart MF & Coles JA (2003). Uptake of locally applied deoxyglucose, glucose and lactate by axons and Schwann cells of rat vagus nerve. *J Physiol* **546**, 551–564.
- Viader A, Golden JP, Baloh RH, Schmidt RE, Hunter DA & Milbrandt J (2011). Schwann cell mitochondrial metabolism supports long-term axonal survival and peripheral nerve function. *J Neurosci* **31**, 10128–10140.
- Vijilar-Palasi C & Guinovart JJ (1997). The role of glucose 6-phosphate in the control of glycogen synthase. *FASEB J* **11**, 544–558.
- Virchow R (1856). *Gesammelte Abhandlungen zur wissenschaftlichen Medicin*. Frankfurt.
- Voet D & Voet JG (2011). *Biochemistry*, Fourth edi. Wiley.
- Volkenhoff A, Weiler A, Letzel M, Stehling M, Klämbt C & Schirmeier S (2015). Glial glycolysis is essential for neuronal survival in drosophila. *Cell Metab* **22**, 437–447.
- Vos MB, Kimmons JE, Gillespie C, Welsh J & Blank HM (2008). Dietary fructose consumption among US children and adults: The Third National Health and Nutrition Examination Survey CME. *MedGenMed Medscape Gen Med* **10**, 160.
- Walz W & Mukerji S (1988). Lactate release from cultured astrocytes and neurons: A comparison. *Glia* **1**, 366–370.
- Wang J, Tu J, Cao B, Mu L, Yang X, Cong M, Ramkrishnan AS, Chan RHM, Wang L & Li Y (2017). Astrocytic L-Lactate signaling facilitates amygdala-anterior cingulate cortex synchrony and decision making in rats. *Cell Rep* **21**, 2407–2418.
- Wang J, Zhang X, Cao B, Liu J & Li Y (2015). Facilitation of synaptic transmission in the anterior cingulate cortex in viscerally hypersensitive rats. *Cereb Cortex* **25**, 859–868.
- Waxman SG & Ritchie JM (1993). Molecular dissection of the myelinated axon. *Ann Neurol* **33**, 121–136.

- Weerasuriya A & Mizisin AP (2011). The blood-nerve barrier: structure and functional significance. *Methods Mol Biol* **686**, 149–173.
- Wender R, Brown AM, Fern R, Swanson RA, Farrell K & Ransom BR (2000). Astrocytic glycogen influences axon function and survival during glucose deprivation in central white matter. *J Neurosci* **20**, 6804–6810.
- Westlund KN, McNeill DL & Coggeshall RE (1989). Glutamate immunoreactivity in rat dorsal root axons. *Neurosci Lett* **96**, 13–17.
- WHO (2018). Mental health: strengthening our response. *World Heal Organ*. Available at: <https://www.who.int/news-room/fact-sheets/detail/mental-health-strengthening-our-response>.
- WHO (2019). Mental disorders. *World Heal Organ*. Available at: <https://www.who.int/news-room/fact-sheets/detail/mental-disorders>.
- Williams LR & Leggett RW (1989). Reference values for resting blood flow to organs of man. *Clin Phys Physiol Meas* **10**, 187–217.
- Yang J, Ruchti E, Petit JM, Jourdain P, Grenningloh G, Allaman I & Magistretti PJ (2014a). Lactate promotes plasticity gene expression by potentiating NMDA signaling in neurons. *Proc Natl Acad Sci U S A* **111**, 12228–12233.
- Yang X, Hamner MA, Brown AM, Evans RD, Ye ZC, Chen S & Ransom BR (2014b). Novel hypoglycemic injury mechanism: N-methyl-D-aspartate receptor-mediated white matter damage. *Ann Neurol* **75**, 492–507.
- Yin YN, Hu J, Wei YL, Li ZL, Luo ZC, Wang RQ, Yang KX, Li SJ, Li XW, Yang JM & Gao TM (2020). Astrocyte-derived lactate modulates the passive coping response to behavioral challenge in male mice. *Neurosci Bull* **37**, 1–14.
- Zhang Y, Xue Y, Meng S, Luo Y, Liang J, Li J, Ai S, Sun C, Shen H, Zhu W, Wu P, Lu L & Shi J (2016). Inhibition of lactate transport erases drug memory and prevents drug relapse. *Biol Psychiatry* **79**, 928–939.
- Zhao Y, Zhang Q, Shao X, Ouyang L, Wang X, Zhu K & Chen L (2017). Decreased glycogen content might contribute to chronic stress-induced atrophy of hippocampal astrocyte volume and depression-like behavior in rats. *Sci Rep*; DOI: 10.1038/srep43192.
- Zhou Z, Ikegaya Y & Koyama R (2019). The astrocytic cAMP pathway in health and disease. *Int J Mol Sci*; DOI: 10.3390/ijms20030779.

# Publications

---

## Peer reviewed papers

Rich LR & Brown AM. Fibre sub-type specific conduction reveals metabolic function in mouse sciatic nerve. *The Journal of Physiology* (2018) 596.10 p.1975-1812

Brown AM, Evans RD, Smith P S, Rich LR & Ransom BR. Hypothermic neuroprotection during reperfusion following exposure to aglycemia in central white matter is mediated by acidification. *Physiological Reports* 7 (2019) e14007 p.1-13

Rich LR, Patrick JA, Hamner MA, Ransom BR & Brown AM. A method for reducing animal use whilst maintaining statistical power in electrophysiological recordings from rodent nerves. *Heliyon* 6 (2020) e04143

## Book Chapters

Brown AM, Rich LR & Ransom BR. Metabolism of glycogen in the brain white matter. Brain Glycogen Metabolism. *Advances in Neurobiology* (2019) 23 p.187-207

## Reviews and Articles

Rich LR & Brown AM. Glycogen: Multiple roles in the CNS. *The Neuroscientist* 23(4) (2017) p.356-363 (IF 7.391)

Rich LR. Publishing my first paper in The Journal of Physiology. *Physiology News* 110 (2018) p.

Rich LR & Brown AM. Comparisons of the metabolic interactions between neurones and glia in the central and peripheral nervous system. *Current Trends in Neurology* (2019) 12 p.65-74

Rich LR, Harris W & Brown AM. The role of brain glycogen in supporting physiological function. *Frontiers in Neuroscience* (2019) 13 Article 1176

Rich LR & Brown AM. More than myelin: metabolic interactions between myelinating glia and axons in the central and peripheral nervous system. *Current Trends in Neurology* (2020) 14 p.89-101

## Presentations at Conferences

Brown AM & Rich LR. An improved method that allows simultaneous recording of stimulus evoked A and C fibre conduction in mouse sciatic nerve. Proc Physiol Soc 2017 39 PC11

Brown AM & Rich LR. The role of interstitial K<sup>+</sup> in stimulating lactate release from adult mouse optic nerve. Proc Physiol Soc 2018 41 PCB269

Brown AM & Rich LR. Stimulus induced elevations in lactate in mouse optic nerve are fuelled by glucose, not glycogen. Proc Physiol Soc 2018 41

Rich LR & Brown AM. Sciatic nerve C fibres utilise fructose directly to support conduction whereas A fibre conduction is maintained by Schwann cell fructose-derived lactate. Proc Physiol Soc 2018 41 PCA268

Brown AM & Rich LR. A method for increasing experimental efficiency whilst maintaining statistical power: application to electrophysiological recordings from rodent optic nerve. Proc Physiol Soc 2019 43 PC221

Rich LR & Brown AM. Schwann cell glycogen: a potential role in supporting A fibre conduction during high frequency stimulation in sciatic nerve. Proc Physiol Soc 2019 43 PC212

Rich LR, McMullan L & Brown AM. Fructokinase expression does not determine efficient fructose metabolism in the mouse sciatic nerve. Proc Physiol Soc 2019 45 PC31

# Covid-19 impact statement

---

Covid-19 prevented access to the lab between March 2020 and September 2020. On returning in September access to the lab was incomplete. I was unable to access my own lab and therefore unable to perform electrophysiology experiments until December 2020. The molecular biology lab I was able to access in September was on a restricted shift working pattern basis. This meant I had access to the lab for fewer than normal working hours which on many occasions was insufficient to progress with immunohistochemistry experiments sufficiently. Delays to the ordering and delivery of antibodies required for immunohistochemistry also prevented the intended progression of GLUT5 immunohistochemistry studies resulting in reduced data in chapter 6.

Time lost due to closure of laboratory facilities during the first lockdown in addition to the social distancing restrictions implemented on return my electrophysiology lab resulted in a change to my project plan. The initial plan was to learn and implement  $K^+$  sensitive microelectrode recordings from the mouse sciatic nerve for chapter 5. The restrictions made this an unfeasible task and therefore I devised an alternative plan using lactate biosensors and inhibitors to investigate the mechanism of action of  $K^+$  as a metabolic signal between axons and Schwann cells. However, the company that produces the lactate biosensors went bust shortly after this plan was decided. I used the remaining biosensors to collect as much data as I could at the time but unfortunately this was insufficient to collect the amount of data originally intended.